SYNTHESIS AND CHARACTERISATION OF DITHIOLATO COMPLEXES WITH PLATINUM GROUP METALS

Brian Morton-Fernández

A Thesis Submitted for the Degree of PhD
at the
University of St Andrews

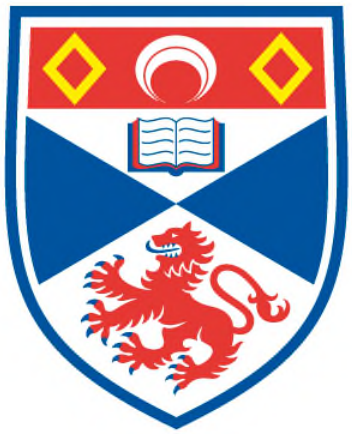

2013

Synthesis and Characterisation of Dithiolato Complexes with Platinum Group Metals

by

Brian Morton-Fernández

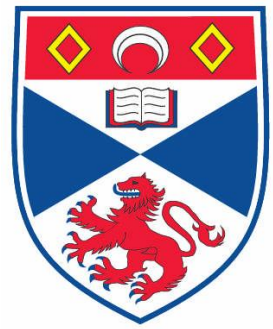

Thesis submitted in partial fulfilment for the degree of

Doctor of Philosophy

The University of St Andrews

May 2013

Declaration

I, Brian Morton-Fernández, hereby certify that this thesis, which is approximately 38,000 words in length, has been written by me, that it is the record of work carried out by me and that it has not been submitted in any previous application for a higher degree.

I was admitted as a research student in September 2008 and as a candidate for the degree of Ph.D. in June 2009; the higher study for which this is a record was carried out in the University of St Andrews between 2008 and 2012.

Date ….. Signature of Candidate ……..

I hereby certify that the candidate has fulfilled the conditions of the Resolution and Regulations appropriate for the degree of Ph. D. in the University of St Andrews and that the candidate is qualified to submit this thesis in application for that degree.

Date ….. Signature of Supervisor ……..

In submitting this thesis to the University of St Andrews I understand that I am giving permission for it to be made available for use in accordance with the regulations of the University Library for the time being in force, subject to any copyright vested in the work not being affected thereby. I also understand that the title and the abstract will be published, and that a copy of the work may be made and supplied to any bona fide library or research worker, that my thesis will be electronically accessible for personal or research use unless exempt by award of an embargo as requested below, and that the library has the right to migrate my thesis into new electronic forms as required to ensure continued access to the thesis. I have obtained any third-party copyright permissions that may be required in order to allow such access and migration, or have requested the appropriate embargo below.

The following is an agreed request by candidate and supervisor regarding the electronic publication of this thesis:

Embargo on both all of printed copy and electronic copy for a period of two years on the following grounds:

Publication would preclude future publication

Date …….. Signature of Candidate ……..

Signature of Supervisor ……..

Abstract

The interest into biosensors can be attributed to the first described enzyme containing sensor used to detect levels of glucose in 1962. Although research into biosensors was initially slow to pick up, the field has become increasingly popular and research has been widespread for the last 20 years.[1] The continuing research into biosensors is crucial as this will improve current devices to become smaller, faster and more economical and yield new biosensors. This thesis is mostly concerned with the development of an integral component of a biosensor, the redox mediator. Complexes of ruthenium incorporating electron rich sulfur-donor ligands such as naphthalenedithiol should possess interesting redox qualities which could be used to produce better mediators. A second area covered in this thesis is in the structural studies of a series of iridium and rhodium complexes.

Two classes of ruthenium complexes with sulfur-donor ligands have been prepared. The first class incorporates the ruthenium *bis*-bipyridine moiety while the second contains pentamethylcyclopentadienyl ruthenium. Most complexes synthesised exhibited reversible oxidation waves in the region of -0.1 to 0.2 V vs. Ag/Ag^{+}. Their possible use as redox mediators was hindered by several factors, particularly difficulties in purification. They also exhibited oxygen sensitivity and low stability when in solution.

The second area covered in this thesis is to further understand the bonding of the ligands used in the above study. A series of pentamethylcyclopentadienyl iridium and rhodium complexes were synthesised with three different dithiolato ligands. Two of the three ligands studies produced structures that included more than one metal centre leading to straining of the ligand. In order to study the monomeric form, the clusters were opened with a neutral phosphine ligand. Both the Ir…S and Rh…S bond lengths of all the complexes were within expected parameters.

Acknowledgements

I would like to give my sincerest gratitude to the people that have guided, helped and assisted me throughout my time in St Andrews.

Thanks in particular go to my supervisors Prof. Derek Woollins and Dr. Joe Crayston for their guidance and tutelage through my four years and for giving me the chance to carry out this project. Thanks are also due to both Ceimig Ltd and the Scottish Funding Council's SPIRIT scheme for their support.

I am grateful towards a few people that have provided me with invaluable crystallographic data. First and foremost, Prof. Alex Slawin for her work on many of my crystal structures, somehow achieving what seemed impossible from frequently questionable crystals. Thanks to Amy Fuller for teaching me the basics

A special thanks in particular goes to Brian, Ken, Upu, Matt and Jacks. All of whom have not only helped me understand and learn the new techniques required but also for making my time in St Andrews a memorable experience and for all the good *craic*. Thanks also goes to other members of The Woollins/Killian/Slawin greater group, both current and past, of which there are too many to name individually.

Thanks to both Caroline Horsburgh and the EPSRC National Mass Spectrometry Service for my numerous mass spectra and Stephen Boyer of London Metropolitan University for my elemental analyses

Lastly, to my parents and family, thank you. Your support throughout the many years of my studies have made me who I am today and to my wife Caitriona who single-handedly contributed to global warming and kept Ryan Air afloat over the last four years along with her various proof-reads.

Contents

List of Figures

List of Schemes

List of Tables

Abbreviations

The following is a list of common abbreviations and symbols used throughout this thesis.

Å	angstroms, 10^{-10} m
$AcenaphS_2$	5,6-dihydroacenaphtho[5,6-*cd*]-1,2-dithiol
aq.	Aqueous
BDMT	benzene-1,2-dimethanethiol
$BenzS_2$	benzene-1,2-dithiol
$BiphenS_2$	dibenzo[c,e]-2,2'-dithiol
BuLi	*n*-butyllithium
°C	degree Celsius
cm	centimetre, 10^{-2} m
Cp	cyclopentadienyl, η^5-C_5H_5
Cp*	pentamethylcyclopentadienyl, η^5-C_5Me_5
DCM	dichloromethane
equiv.	equivalents
η	multidenticity
Et	ethyl
g	grams
h	hour
J	coupling constant, Hz
L	neutral 2-electron ligand
	litre
M	molar, $molL^{-1}$
Me	methyl
mg	milligram, 10^{-3} g
Min	minute
mL	millilitre, 10^{-3} L
mmol	millimol, 10^{-3} mol
mol	mole, Avogadro number of molecules
μ	prefix micro, 10^{-6}
	bridging ligand
$NaphS_2$	naphthalene-1,2-dithiol
NaphNS	8-aminonaphthalene-1-thiol
N	infrared frequerncy, cm^{-1}
TMEDA	tetramethylethylenediamine
R	alkyl chain
THF	tetrahydrofuran
X	anionic 1-electron ligand
	halide

1 INTRODUCTION

A sensor is a device that is tuned to a specific external stimulus. When a sensor comes in contact with its sensing substrate, it is devised to give a response to the physical or chemical property of the material and then record, indicate or respond to it. Sensors are required in virtually all aspects of daily life and are used to prevent diseases, contaminants, poisons or toxins. They make sure food, water, medicines and other consumables are safe for human and animal consumption. Sensors are also used to track changes and can be programmed to take appropriate actions when abnormalities or defects are detected.

Modern day sensors are composed of three main components that when used together produce an appropriate signal from the substance being analysed. The first component is the recognition element which senses for the substance or material which is to be studied. After the analyte has been recognised, the transducer incorporates the recognition element and measures a change, for example, in the concentration of a substance. Finally, the signal processor which measures the transducer's response to its substrate and exports that information to a recording device in an analogue or digital format. Sensors can have different recognition elements according to their uses and are generally specific to a process. There are many types of transducers, each tuned to measure different changes in the analyte from concentration to another associated effect.

Sensors generally fall into one of two categories; those that are comprised entirely of mechanical or electronic parts and those that include biological molecules as part of one of their components. The latter are known as biosensors. Biosensors must operate with a high throughput and in a continuous manner. They must also have a high selectivity for the analyte being sensed, and must be sensitive enough to measure concentrations of an analyte material

up to the parts-per-million (ppm, 10^{-6}) range, and in some cases, in the parts-per-billion (ppb, 10^{-9}) range.

Research on biosensors is vital for managing diseases such as anaemia and diabetes. They are also an invaluable tool in allowing other illnesses caused by poisons e.g. food poisoning toxins, heavy metals etc., to be identified and hopefully, subsequently cured.

1.1 Biosensors

The history of biosensors begins with the invention of the first described enzyme based sensor for the measurement of glucose concentration by L.C. Clark.[2] Since then, many different kinds of biosensors have been produced, all catering for a different and specific use.

Clark's initial biosensor incorporated the enzyme glucose oxidase (GOx, **Figure 1-1**). This enzyme is known to catalyse the breakdown of D-glucose into D-glucono-1,5-lactone, along with production of H_2O_2 from the reduction of O_2. D-glucono-1,5-lactone then hydrolyses into gluconic acid. For GOx to function, it requires the cofactor flavin adenine dinucleotide (FAD). FAD is responsible for the redox properties of GOx. The latest studies have found that this co-factor is bound, but not covalently bonded to GOx.[3] Dioxygen is used in the system to transport electrons from glucose to GOx.

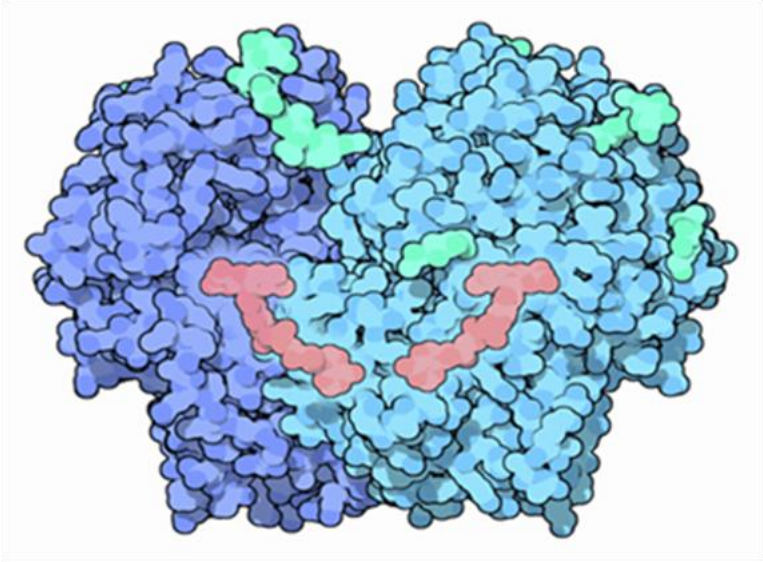

Figure 1-1 Glucose Oxidase (The cofactor FAD is shown in the middle).

Source: RCSB Protein Data Bank

Clark found that by measuring the concentration of O_2 amperometrically with a Pt electrode coated with a gas-permeable membrane (to eliminate other redox-active interfering species) (**Figure 1-2**), the concentration of glucose could be determined.

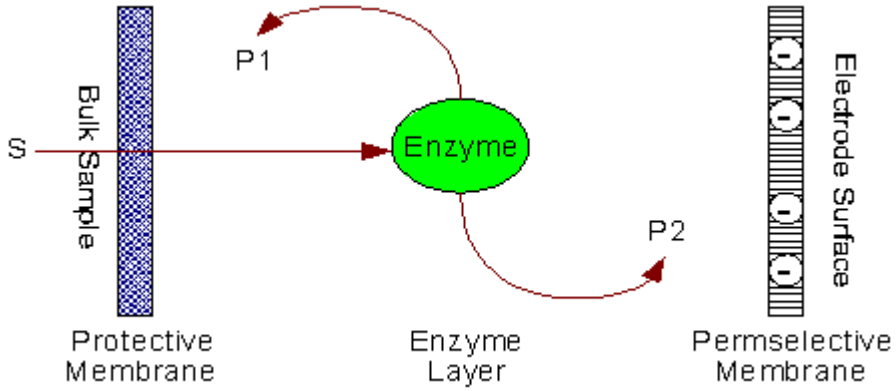

Figure 1-2 Schematic representation of an amperometric enzyme electrode.

S: substrate, P1 & P2: products

There can however be many problems associated with using the concentration of O_2 to find the amount of glucose in a sample. The most problematic of these is that this method is significantly affected by the fluctuating amounts of dissolved oxygen in the sample to be analysed.

Since their invention, biosensors have found important roles in many applications ranging from industry to personal health and wellbeing. The original biosensor set out by Clark was used for monitoring of the concentration of glucose in people suffering from diabetes. Other uses of biosensors include:

- Environmental applications – detecting levels of pesticides, herbicides and other pollutants
- Detection of toxins in water and foods in products for human consumption
- Drug discovery
- Monitoring drug residue in food (e.g. antibiotic and growth hormones in meat)
- Remote sensing of bacteria
- Routine quantification of milk components such as folic acid.

In order for a biosensor to be scientifically and commercially viable, the biosensors must be able to selectively identify the target molecule and react with an appropriate response. There must also be an appropriate biological recognition element available by which the sensing and measurement is carried out. The potential for the biosensor to be miniaturised is one of the main goals as this will allow the biosensor to be adopted for domestic use.

Biosensors (**Figure 1-3**) incorporate a biological component as part of their sensing element. This is the part of the sensor that recognises the substrate which is to be measured in the analyte. Sensing elements can be classed into two different groupings; the biocatalyst, which includes enzymes,[4] micro-organisms[5] and tissue material; and the bioligands, which include antibodies, nucleic acids, lectins etc.[6]

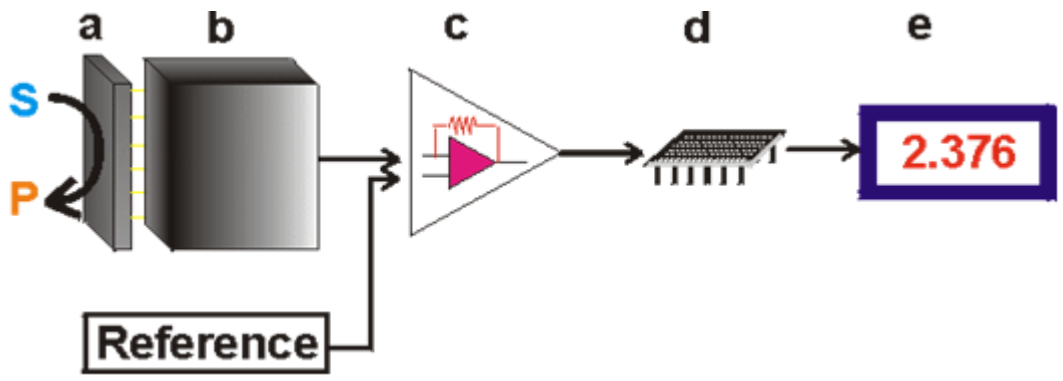

Figure 1-3 Schematic diagram showing the main components of a biosensor.

The biocatalyst (a) converts the substrate to product. This reaction is determined by the transducer (b) which converts it to an electrical signal. The output from the transducer is amplified (c), processed (d) and displayed (e).

Source: London South Bank University

The second main component of a biosensor is the transducer. This device converts the response of the sensing elements recognition to the target substrate's increasing, decreasing or continuous concentration. It then quantifies that response to generate a signal which is then relayed to a recording device.

There are several effects that are incurred upon the transducer when the sensing element responds to a change in its environment. The following are the most common responses utilised in transducers:[7]

- Electrochemical
    - Potentiometric – measurement of the potential at zero current. Potential is proportional to the logarithm of the concentration.
    - Voltammetric – increasing/decreasing potential until oxidation/reduction of substance occurs with a consequent rise/fall in the current.
    - Amperometric – same as voltammetric, but without sweeping the potential. The redox potential must be known.
    - Conductimetric – change in composition of solution leads to a change in electrical conductivity
- Calorimetric – measuring the heat absorbed/produced by the reaction.
- Optical – light absorbance/emission difference between substrate and product.

Some of the latest generation transducers now incorporate piezoelectric and magnetic components along with the traditional kinds to produce faster and more sensitive readings.[8] The selectivity of the biosensor for the target substrate is therefore determined by the biorecognition element, while the sensitivity of the sensor is due to the transducer. In the case of Clark's device, GOx was the sensing element, and the electrode operating in an amperometric mode was the transducer. The most widely used biosensors use enzymes as their sensing element, specifically the oxidase family, coupled with an amperometric transducer.[9]

While there can be a wide range of combinations of biosensors incorporating different biorecognition elements and transducers, biosensors incorporating enzymes or cells coupled with an electrochemical transducer as the bioelement have given the best and most reproducible results thus far.[10]

In order for these biosensors to function properly and reduce the possibility of electrochemical interference, the presence of an intermediary compound known as a redox mediator is required.

The rate of electron transfer (k_{ET}) is one of the most important factors in a biosensor system. Increasing the rate of transfer leads to a faster response time and improved results. The rate of electron transfer in an electrochemical system utilising enzymes as the recognition element is governed by several factors which were established by Marcus-Hush theory:[11,12]

- The distance between the electrode surface and the redox centre of the enzyme
- The potential (voltage) difference
- The reorganisation energy
- The nature of the intervening atoms and groups

Ideally, the numerical value of all of the first three factors influencing electron transfer should be as low as possible. A small distance between the enzyme redox centre and electrode will lower the potential needed to bring about oxidation or reduction. The lowest possible potential difference is required in order to avoid interference. Reorganisation energy according to Marcus theory "is the energy required for all structural adjustments (in the reactants and in the surrounding solvent molecules) which are needed in order that A and D assume the configuration required for the transfer of the electron".[13] The lower the reorganisation energy, the lower the amount of energy is required to bring about an electron transfer between the donor and acceptor.

Improving the rate of electron transfer between the electrode and the redox centre, which is often deep within the enzyme to avoid large solvent contributions to the reorganisation energy is one of the key research areas in the development of better biosensors.

For systems incorporating enzymes such as GOx, the electrode itself cannot directly reduce the GOx-FAD pair due to the FAD moiety being located deep within the enzyme (**Figure 1-1**) with a pocket size of ~10 Å.[14] This distance is too great for an electron to be able to cross efficiently. In order to bring about oxidation/reduction of the enzyme, the potential difference must therefore be increased. This increases the rate of the redox reaction and gives a better response. However, as the potential is increased, there is an increased possibility of electrochemical interference. Instead, the problem is solved by incorporating a soluble redox mediator into the electrochemical system to transport electrons.[15]

Redox mediating compounds are used to 'shuttle' electrons back and forth from the surface of the working electrode (the transducer) to the redox centre of the enzyme (the recognition element) (**Figure 1-4**). As a result, the operating potential required to bring about catalysed redox reactions is decreased and interference from electro-oxidisable species is avoided or minimised. Mediators can range from organic molecules to metal complexes containing organic or inorganic ligands. An example of such a mediator is ferrocene. The metal at the centre of the complex is the single most important component of the redox mediator. The metal itself is the 'bus' that 'shuttles' the electron back and forth. It also gives the mediator the ability to be chemically inert when oxidised or reduced.

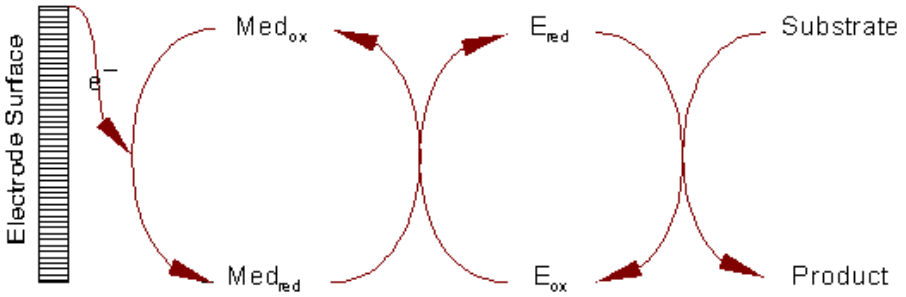

Figure 1-4 Electron Transfer Pathway using a Redox Mediator.

E: enzyme, Med: mediator, ox: oxidised, red: reduced

1.2 Redox Mediators

There are several criteria that must be met in order for a compound to be utilised as a mediator. Firstly, the mediator must be of low molecular mass incorporating a transition metal centre. The small size aids the mediator to access the redox centre deep within the enzyme. The mediator must also possess a low redox potential close to that of the redox enzyme: for GOx this is between -100 to 0 mV versus a saturated calomel electrode (SCE). This minimises the possibility of electrochemical reactive compounds that could cause interference giving rise to false readings. The mediator must also be oxygen stable in order to avoid interference or decomposition and must possess stable oxidised and reduced forms.[16] A low reorganisation energy is also essential in order to facilitate the rapid transfer electrons across the required distance, both from electrode to mediator and from mediator to enzyme centre.[17,18] Finally, the molecule must possess a high electrochemical rate constant to ensure that the mediator is not limited by electrode kinetics and oxygen interference.

Ferrocene along with aqueous soluble derivatives (**Figure 1-5**) have been extensively studied for their use as mediating compounds.[19] These class of compounds fulfil the majority of the criteria (small molecular size, low redox potential and stable oxidised form) required for their use as redox mediators. However, due to their instability to H_2O, they have found limited practical use.

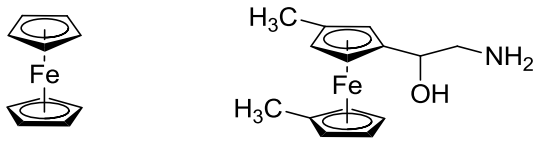

a **b**

Figure 1-5 Ferrocene (**a**) and an example of a ferrocene derivative (**b**) used in MediSense ExacTech and Precision QID blood glucose meters

Depending on the mediator's chemistry, and the method by which the sensing element has been immobilised, biosensors can be classed into three different generations:[9]

- 1st generation

  No artificial redox mediator is involved. Dioxygen is the natural co-substrate of oxidases, the most common family of enzymes used in biosensors. The O_2 is converted to H_2O_2 during the catalytic reaction of the enzyme. By reducing the molecular oxygen, or oxidising the peroxide, the current recorded is proportional to the substrate concentration. There are several limitations to this method. The selectivity, and hence the sensitivity, is compromised by the large voltage applied.

- 2nd generation

  Redox mediators replace the natural co-substrates and minimise the potential that has to be applied. This generation uses mediators that are not immobilised, but are freely diffused throughout the analyte solution.

- 3rd generation

  This is when the analyte cannot be contaminated by any foreign material, such as in the food or pharmaceutical industry. In this generation the enzyme is immobilised onto the surface of the electrode.

The immobilisation of the enzyme can be achieved by several methods. Some methods confine the enzyme behind a membrane using cellulose acetate.[20] The enzyme can also be reticulated (binding though cross-linkages) to glutaraldehyde or bovine serum albumen.[21] Other methods include covalent bonding to the gel, entrapment in a porous matrix, or coating behind a porous membrane.[22,23,24] A final protective layer is then added to protect the enzyme layer from contamination or harsh chemicals (**Figure 1-6**). The protective layer can also serve as a permselective barrier, blocking certain molecules, such as proteins or competing substances from entering the enzyme layer. Leakage of the enzyme into the liquid sample is also prevented by this barrier.

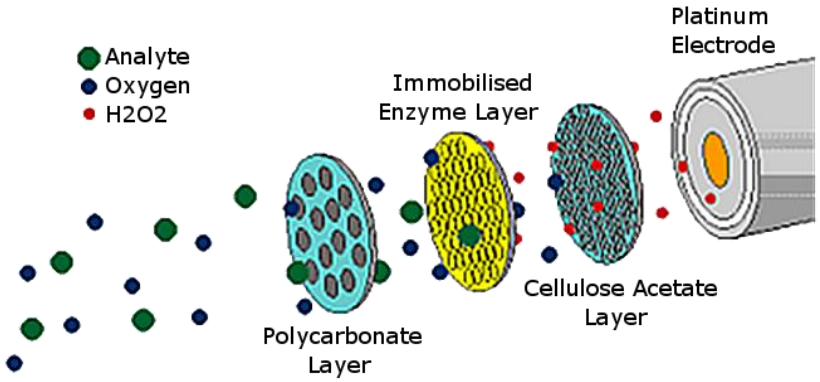

Figure 1-6 Example of Enzyme Immobilisation

Source: YSI Life Sciences

1.3 Chemistry of Redox Mediators

Mediator molecules can be either an organic or inorganic compound. The first molecule that was found to possess most of the essential qualities needed to be a good mediator was ferrocene.[9] This inorganic molecule has an iron atom in the middle of the complex sandwiched by two cyclopentadienyl rings. Ferrocene was first synthesised by T. J. Kealy and P. L. Pauson in Duqesne University. They found that the molecule possessed remarkable stability, and unlike the majority of organic molecules, underwent reversible one-electron oxidation at the low potential of 210 mV vs. SCE. It also exhibited a relatively high

electron exchange rate in the region of 2 $\times 10^5$ $M^{-1}s^{-1}$ for oxidation of the reduced GOx[25] and 5 $\times 10^5$ $M^{-1}s^{-1}$ for reduction of oxidised GOx.[26] Many analogues of ferrocene have since been created for use as mediators. Other iron redox mediators studies were much simpler in structure, such as the homoleptic ferricyanide (**c**).[27]

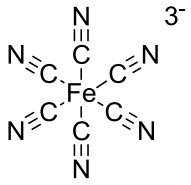

c

Figure 1-7 Iron Based Redox Mediator

As mentioned above, redox mediators are not solely found as inorganic complexes, but can also be found as organic molecules. Organic mediators, including benzoquinone (**d**),[28] methylene blue (**e**),[7] promazine (**f**),[7] and Meldola blue (**g**),[29] are less commonly used than their inorganic counterparts. This is due to their auto-oxidisability, lower stability when oxidised or reduced and because they possess far slower electron transfer rates when compared to metal complexes.[30] In order for an organic molecule to behave as an electron acceptor/donator, and thus a redox mediator, these compounds must be electron rich. This severely limits the organic class of mediators to hydrocarbons with extensive conjugation. Electron rich elements such as nitrogen and sulfur will also need to be incorporated. While these can act well when oxidised, when they become reduced they are short lived species due to their high reactivity. This limits the available number of organic redox mediators and so are rarely used except in specific applications.[31] Another problem that affects organic redox mediators is that they exhibit high sensitivity towards changes in pH, giving different readings according to the pH of the solution.[30]

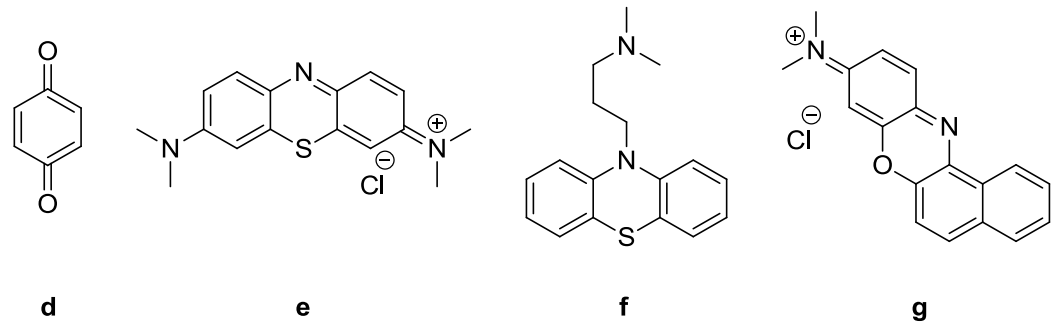

d **e** **f** **g**

Figure 1-8 Organic Based Redox Mediators

Inorganic complexes are best suited as mediators since the presence of the metal in the mediator gives rise to stable oxidised and reduced forms. Metals also promote fast electron transfer rates. Transition metal complexes of iron, ruthenium, and osmium are most commonly used as mediators. This is because the group 8 metals are relatively stable in their oxidised and reduced forms as they all possess more than one stable oxidation state and the M^{II} d^6 and M^{III} d^5 low-spin forms are kinetically labile with high-field ligands. This group of metals also exhibit a fast k_{ET}, the second-order rate constant for electron transfer to an enzyme or other substrate. A high k_{ET} is desirable in order to minimize the effect of dioxygen which can act as a competing electron mediator.

1.4 Ru and Os Redox Mediators

Although Fe, Ru and Os are in Group 8 of the periodic table, the chemistry of Fe is very different to that of Ru and Os.[33]

The electron configurations of Ru ($4d^7$ $5s^1$) and Os ($4f^{14}$ $5d^6$ $6s^2$) makes them special in that they both exhibit the widest range in oxidation states of all elements.[32] Ruthenium possesses 10 possible oxidation states from Ru^{-II} in $[Ru(CO)_4]^{2-}$ and [Ru(1,2-bis(diphenylphosphino)ethane)] to Ru^{+VIII} in $[RuO_4]$. Osmium possesses nine possible oxidation states from Os^0 in $[Os(CO)_5]$ to Os^{+VIII} in the well-known oxidising and poisonous compound $[OsO_4]$. The most common and stable oxidation states for both are +2, +3, +4 and +8.[33] The lower oxidation states are the most familiar, often stabilised by π-acceptor ligands such as CO

in $[Ru(CO)_4]^{2-}$ and PR_3 in $[Ru/Os^{II}Cl_2(PPh_3)_3]$ and π-bonding ligands such as Cp in the dimeric $[CpRu^{I}(CO)_2]_2$. Conversely, the higher oxidation states are stabilised by small π-donor ligands such as F^- in $[Ru/Os^{VI}F_6]$, and O^{2-} in $[Ru/Os^{VIII}O_4]$. Ligands such as H_2O and NH_3, which are good σ-donors, but which show no substantial π-acceptor/donor properties are associated with $Ru^{II/III}$ metal centres.[34,35]

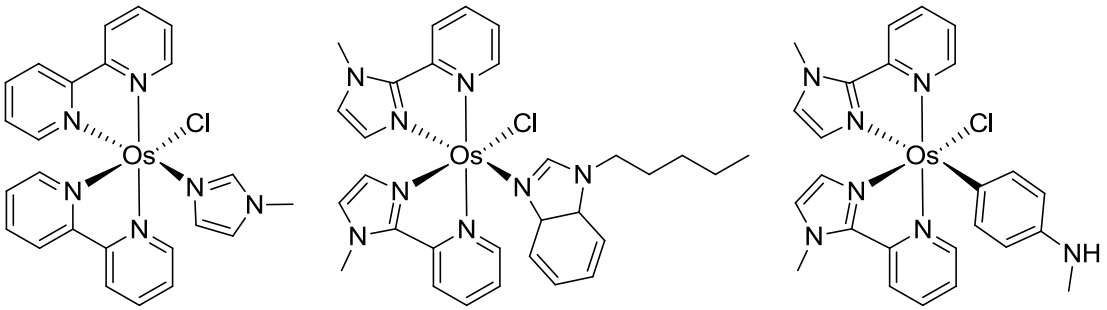

Figure 1-9 Original (left), 2nd Generation (centre) and Current (right)

Redox Mediators Used by the FreeStyle System

The property that makes complexes of ruthenium particularly well adapted to act as redox mediators is that ruthenium possesses relatively high rate of electron transfer.[36] Complexes of ruthenium are therefore commonly used in applications that require high k_{ET} such as photolysis and photochemistry. This property is particularly sought after in the area of dye-sensitised solar cells because dyes that have higher k_{ET} produce more efficient cells.[37] Although osmium possesses many of the vital traits that ruthenium exhibits, research into osmium-based redox mediators is not as intensive due to the higher cost of osmium.

Most of the original inorganic redox mediators were made of Ru complexes with heterocyclic N-donor (polypyridine) ligands.[38] These complexes have received much attention owing to their interesting spectroscopic and electrochemical properties. These aromatic amine ligands with π-systems have quite different characteristics from that of amine complexes. These complexes posses high electron transfer rates and low redox potentials of ~-100 mV vs SCE, both key traits sought after in redox mediators. Complexes of 2,2'-bipyridine (**h**) and 1,10'-phenathroline (**i**), along with their substitutions, are the most common used for redox mediators.

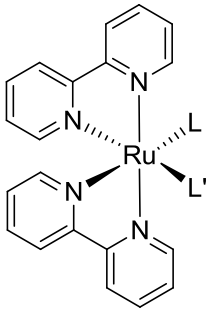

h

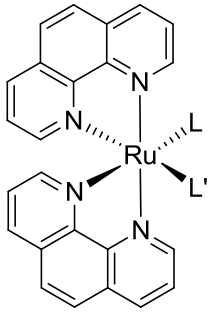

i

The redox potentials of these complexes can be changed by substituting the polypyridyl hydrogens with electron withdrawing (EW) or electron donating (ED) groups.[30] Since these complexes generally have high redox potentials these studies showed that ED groups produce better enzyme redox mediator properties, enhancing the electron transfer rate by lowering the redox potentials yielding redox mediators that are more sensitive with faster response times along with less interference from electrochemically oxidisable species.

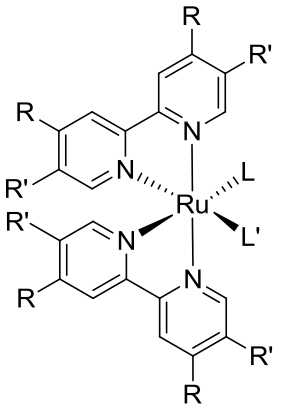

R & R' = H, EWG or EDG

Figure 1-10 Substitution Positions for bis(bipyridine) Complex

Owing to their convenient properties, research into polypyridyl ruthenium and osmium complexes acting as redox mediators has been ongoing. Many thousands of polypyridyl ruthenium/osmium complexes have been synthesised and their electrochemistry explored.[39,40,41] Interestingly, and serendipitously, the properties of these complexes are not

significantly altered by the substitution of auxiliary ligands L (**Figure 1-10**). The bulk of the chemistry that is sought after is due to the polypyridyl ligands themselves, and the substitution of L is only done to enhance or fine-tune the characteristics of the complexes. In fact, most of complexes with polypyridyl ligands substitute L with simple ligands such as thiocyanide, carbon monoxide or chloride. Recent research has mostly been focused on the 4-4' functionalisation of the 2,2'-bipyridine backbone. This makes bipyridine one of the most well studied compounds.[42] A few of the different types of polypyridine ligands recently studied are shown below in **Figure 1-11**.

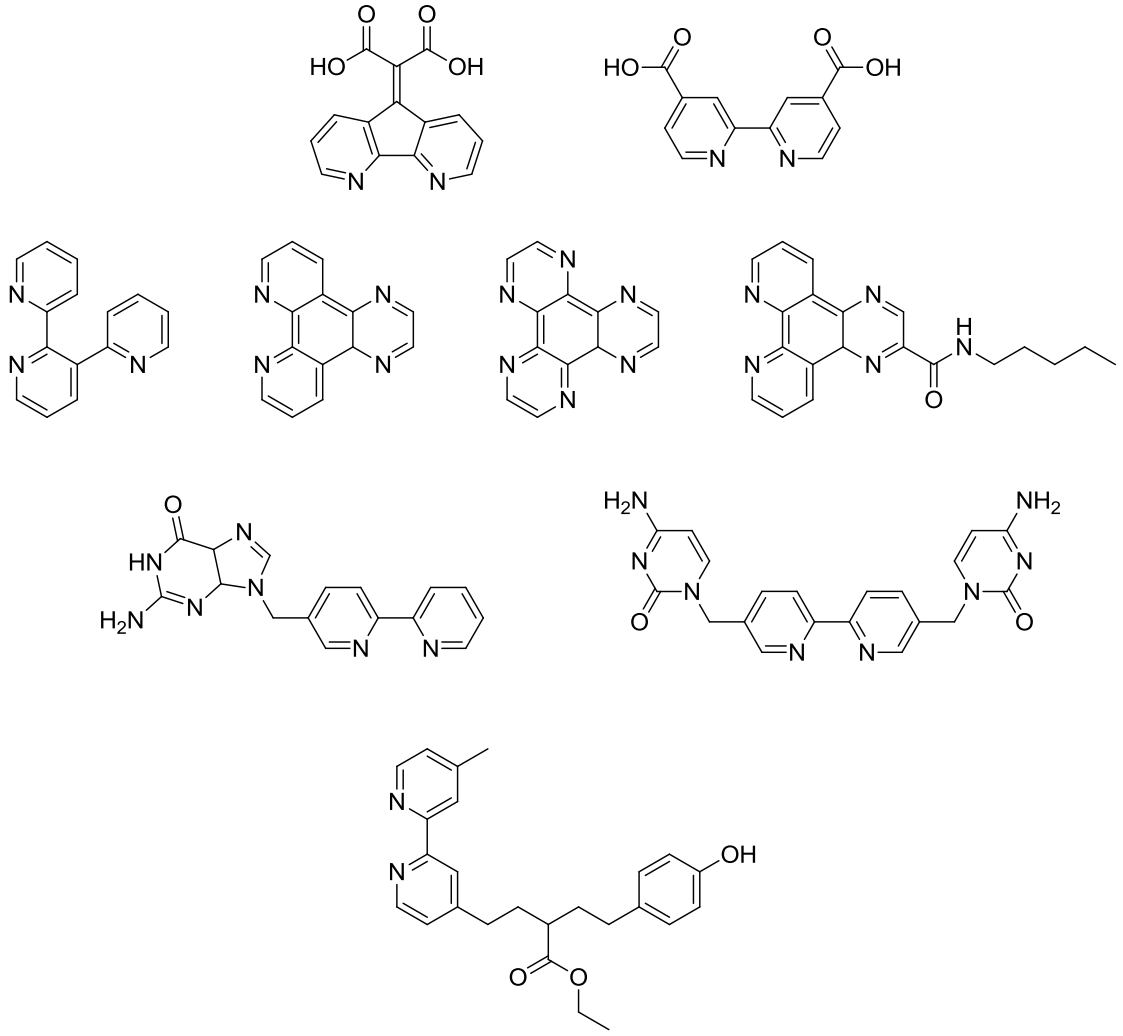

Figure 1-11 Recently Studied Polypyridine Ligands[41,43,44,45]

Recently, the emphasis into redox mediators has shifted from the traditional biosensors that have been used to since the 1970s. This biosensor technology is based on the redox mediator supported in a medium shuttling electrons back and forth between the electrode and the enzyme centre i.e. 2nd generation. This technology is somewhat outdated. These devices are prone to leakage of the mediator which contaminates the electrolyte and rapidly decreases the efficiency of the device giving erroneous results.[46] These devices are quite obstructive in the daily life of people with diabetes. For example, it is suggested that for people suffering from Type 1 diabetes that it is necessary to measure glucose levels four times daily. If done correctly, people affected by Type 1 diabetes can see a 60% lower risk of suffering from diabetes-related ailments such as kidney failure and heart disease.[47] In reality however, most people only measure their levels twice daily. This is in part due to the cost of the test strips (ca. €300 p.a.) and the inconvenience associated with drawing blood and, if necessary, administering the insulin. The miniaturisation and subcutaneous implantation of a measuring system would allow people to control their glucose levels without the associated shortcomings of traditional test strip devices.

The continued research into redox mediators has been focused on making biosensor systems smaller, faster and more accurate from smaller samples.[48] These improvements, together with the immobilisation of the mediators has given way to 3rd generation biosensors. Whereas the 2nd generation devices are based on redox mediators that are not immobilised but able to diffuse freely throughout the whole system leading to possible leakage and a decrease in biosensor response, 3rd generation devices are focused on the immobilisation of the mediators onto a surface such as the electrode itself. This would allow the biosensor devices to be implanted subcutaneously into a person's body without leeching of any poisonous material into the blood stream. The miniaturisation of these devices not only improves the accuracy and speed of the results, but also the quality and life expectancy of people affected with diseases such as diabetes. These also allow the continuous monitoring of glucose levels, allowing the user to track their changes and to take appropriate action if required.

There are several ways by which the redox mediator can be immobilised onto the electrode surface. These include affinity binding of the enzymes to the electrode surface,[49] by linking using hydrophobic/hydrophilic interaction,[50] or the covalent linking of the material to the electrode surface.[51] The latter option is most commonly used as this gives the strongest interaction and hence higher stability and longer product life. An example of one method of covalent linking is that based on Self-Assembled Monolayers (SAMs) on gold surfaces. SAMs are formed from long-chain thiols (e.g. hexadecanethiol) which behave much like surfactant molecules. They both have head and tail groups that exhibit different chemistry with one end preferring a different environment or chemistry to the other. This allows them to arrange themselves in an organised array. In the case of SAMs based on thiols, the thiol group is deprotonated and the sulfur head-group forms a covalent bond to the gold atoms on the surface.

SAMs have been applied quite successfully in a biosensor system for GOx.[52] In the paper, Willner and colleagues described the manufacturing of SAMs mediating to GOx that had a derivative of ferrocene (N-(2-methylferrocene)caproic acid) (**j**) that had been bonded directly on to the enzyme.

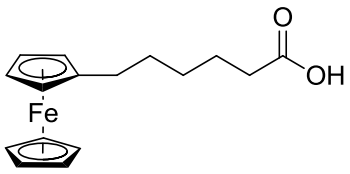

j

This yielded a ferrocene-GOx multilayer system directly connected to the gold electrode (**Figure 1-12**). By doing this, the potential required to bring about enzyme redox reaction had been lowered, significantly improving both the accuracy of the results and the speed with which they were obtained. This setup, however good, requires the modification of the protein, and by doing this alters the chemical qualities of the protein and often results in the denaturing of the protein.[53]

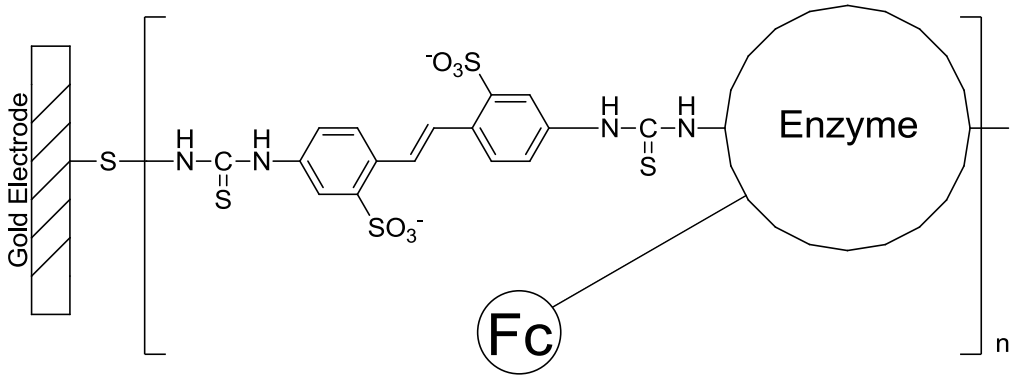

Figure 1-12 Tethered System by Willner

In the field of biosensors, the gold-thiol interaction is exploited producing a semi-covalent bond between the thiol and the gold. Long fatty alkane chains with a terminal thiol (S-H) group are projected from a substitution on one of the ligands of the Ru/Os complex. The thiols adsorb onto a gold electrode producing an organised array of mediators (**Figure 1-13**). These mediators are able to partially penetrate into the enzyme centre, while still tethered to the electrode surface.

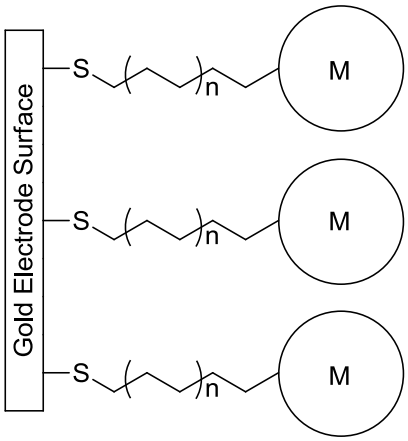

Figure 1-13 Thiol Bearing Mediators Bound to a Gold Surface

where M is a Metal Complex

The first practical system that exploited the gold-thiol system was that reported by Rubin *et al*.[51] They were able to grow monolayers of a ferrocene derivative and bond it directly to the gold electrode surface without modification of the enzyme. They employed ferrocenylhexadecanethiol (**k**) as the redox mediator using the 16-carbon chain to connect the mediator to the electrode. The 16-carbon long tether is ~20 Å long, and was it thought that this length would be able to penetrate partially into the enzyme.

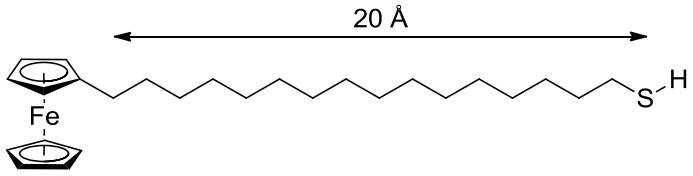

k

Although the technique proved to be unsuccessful, producing a response from the ferrocene moiety and not that of an amperometric response due to the enzyme, this method has led the way into the development of several other gold-thiol systems such as ones employing colloidal gold.[53]

A new and emerging method for the immobilisation of redox mediators is one termed a "wired" system. This method does not use the convenient gold-thiol interaction, but instead turns an insulator into an electronically conductive material by decorating the insulator with a conductive material.

Research into these "wired" systems began with Adam Heller at the renowned Bell Laboratories where through the chemical modification of a protein, a number of electron relaying centres were attached to the surface of the enzyme.[54] This allowed the electrons to travel efficiently, without the use of a high potential, from the enzyme centre to the electrode, relayed by ferrocene. This paper was the first to demonstrate direct communication between the FAD/$FADH_2$ centre of GOx and the electrode. Their modification involved the covalent bonding of an average of 12 molecules of ferrocenecarboxylic acid per GOx molecule. Their system, in order to work, had to be kept at a slightly basic pH of 7.2, but nevertheless brought about the oxidation of the enzyme at +0.44 V vs. SCE. This system allowed the electro-

oxidation of glucose without the use of a redox mediator shutting electron back and forth between enzyme and electrode. In essence, what the researchers achieved was turning the electronically insulating enzyme into a conductor by coating the surface of the enzyme with conducting materials.

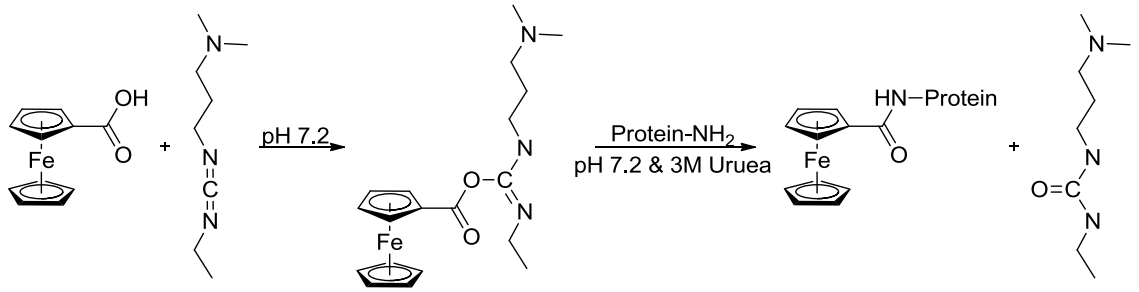

Figure 1-14 Steps Involved in Attaching the Ferrocene Derivative to the Protein

Although this example was not commercially successful as it caused the denaturing of the protein, this paper showed that it was possible to bind a redox mediator onto the surface of an insulating enzyme, turning it into an electronically conducting material.

These wired systems have become popular due to their ease of construction, fast response times and because they have the potential to be minimised, allowing *in vivo* continuous determination of glucose levels.[48] These types of sensors are known as redox hydrogel-based sensors and are so termed because they produce a network of hydrophilic polymers in which the liquid component, the solvent, is water.[55]

Current systems commonly employ polymers as the anchoring site for the conductive material. This method produces an array of metal complexes that act as wires, where the electron from the reduced enzyme, via an amine, is relayed by hopping from wire to wire (complex to complex) (**Figure 1-15**) eventually leading to the electrode.[48] It has been shown that this electron hopping can be characterised by an electron, or charge transport, diffusion coefficient, D_{CT}. Redox hydrogels are unique in that they possess both good electron diffusion coefficients but are also water soluble, allowing them to operate in aqueous environments.[56]

Figure 1-15 Relay System Employed by Wired Mediators

Source: ACS[57]

These polymer backbones vary in structure, although not significantly. They all consist of a polymerised chain of hydrocarbons with N-heterocyclic groups attached to the polymer e.g. 4-vinylpyridine or 1-vinylimidazole (**Figure 1-16**). Nitrogen-containing groups are chosen as these bind to the Ru/Os centre without change in oxidation number, i.e. are neutral, and due to the strong binding affinity of Ru/Os for nitrogen.

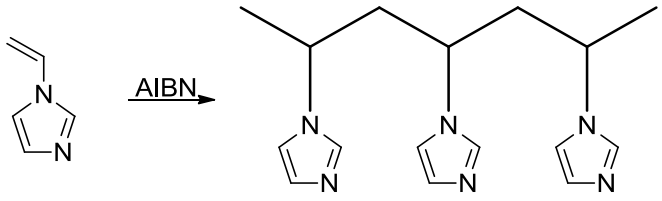

Figure 1-16 Poly(1-vinylimidazole)

Reacting the polymerised material with a Ru or Os complex, such as $[Os(bpy)_2Cl_2]$[56] (**Figure 1-17**), a hydrogel is created that is able to relay electrons through the collision of the complexes all the way to the electrode.

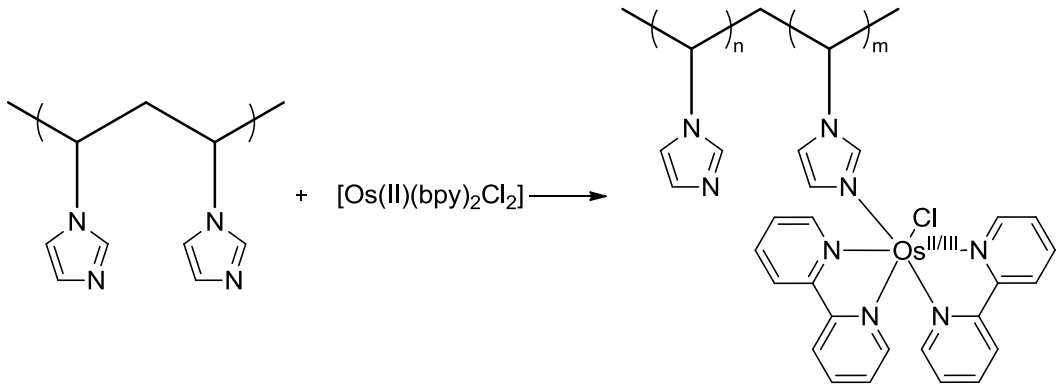

Figure 1-17 Reaction of Os Complex with Polymer

This technology has proven very successful. In a paper by Mao *et al.*,[58] a system of a *tris*-biimidazole osmium complex with a 13-atom long flexible tether showed great promise (**Figure 1-18**). They observed an electrooxidation of glucose at 40 mV vs.Ag/AgCl with excellent D_{CT} of 5.8×10^{-6} cm^2s^{-1}.

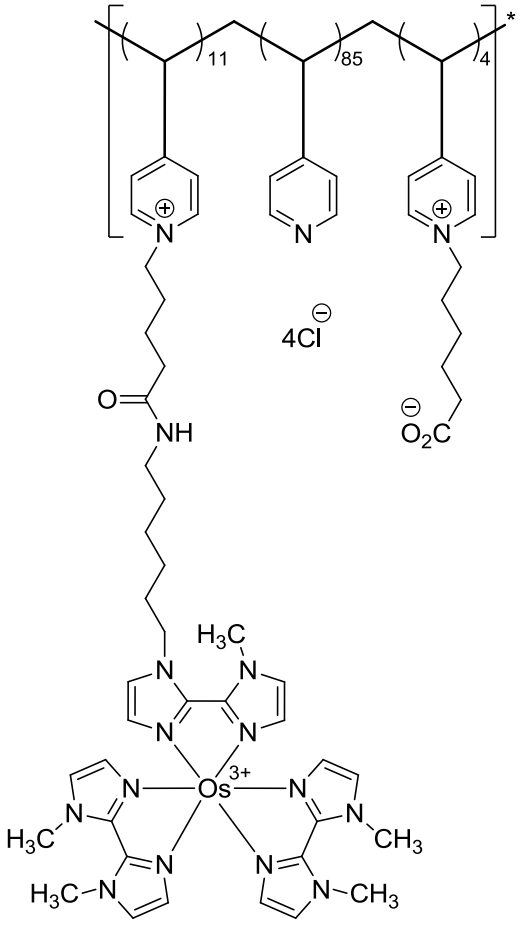

Figure 1-18 Wired System Made by Mao *et al*.[58]

This redox-hydrogel biosensor system has been put to practical and commercial use by Abbot Diabetes Care. The *FreeStyle Navigator* obtained regulatory approval and was released in Europe in 2007. The FreeStyle Navigator is a continuous glucose monitoring system that measures the concentration of glucose using a monitor implanted subcutaneously. It is a three part system and includes a transmitter and a monitor that shows the current glycemic concentration along with a directional arrow that shows if the concentration is increasing or decreasing. The second generation of the system negated the use for a separate monitoring device and instead the reading was shown on a sports watch which doubled as the monitoring system making the whole system even more inconspicuous.

There are several other promising possibilities for these tethered wired redox hydrogels. In a recent paper,[59] the viability for the production of biofuels was explored. In total, five different systems were tested for their ability to efficiently wire an enzyme to graphite electrodes. It was found that when the enzyme oxidoreductase pyranose dehydrogenase was wired to the Os complex, no appreciable change was recorded in the potential from that of the unwired natural enzyme, making such biofuel producing systems conceivable.

The possibility for these kind of systems to split water has also been explored.[60] The immobilisation of Photosystem II (water-plastoquinone oxidoreductase), an enzyme involved in light-dependent reactions that naturally splits water was explored. In the setup, the PSII was entrapped within the Os polymer (**Figure 1-19**). Their setup showed that it was possible to wire the PSII enzyme to split water using the Os polymer wires as both the immobilisation matrix and the electron carriers, and exhibited better properties to previously studied examples.

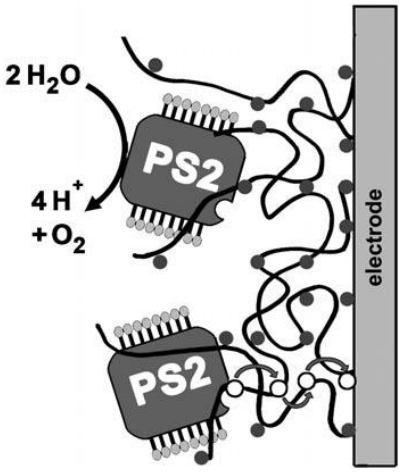

Figure 1-19 Entrapment of PSII by an Os-Based Redox Polymer

Source: Wiley InterScience[60]

1.5 Sulfur Ligands

Sulfur-donor ligands have the ability to bind to a wide range of transition metals. These soft ligands bind particularly well to Class B in the second and third row. Sulfur-donor ligands are able to form mononuclear, polynuclear and cluster compounds. Various S-donors,

such as sulfides, thiolates (**l**) and dithiolenes (**m**) are generally regarded as strong σ- and π-donors. Sulfur containing ligands like RS^-, dithiocarbamates (**n**), dithiochelates, etc., have been shown to exhibit novel redox properties because of the sulfur d-orbitals and the donating nature of sulfur.[61]

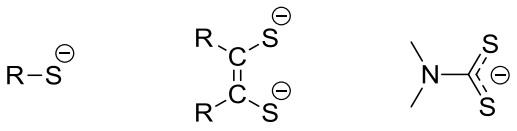

l **m** **n**

Sulfide, S^{2-}, and disulfide ligands, S_2^{2-}, are also noted for having strong electron donating properties and have also shown to lower the redox potential of compounds. Polysulfide ligands (S_x^{2-}, $x \geq 2$) to transition metals exhibit remarkably strong electron donating properties.[61]

Bidentate dithiolene ligands form complexes which are redox active in square planar [ML_2] and *tris*-chelate [ML_3] complexes. In the latter case, the complex forms trigonal prismatic geometry, rather than octahedral, thought to be due to S-S interactions. In dithiolene complexes it can be difficult to definitively describe the electron transfer processes as based on the metal or on the ligand. The problem arises from the facile electron transfer of the dithiolene ligands and the delocalisation of charge density across metal and ligand centres (**Figure 1-20**).[62]

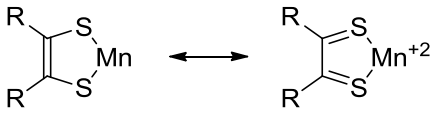

Figure 1-20 Resonance Structure of Metal-Dithiolene Ring

The [$Ru(bpy)_2mnt$] (mnt = maleonitriledithiolate, $(S_2C_2(CN)_2)^{2-}$) (**o**) complex was synthesised with the belief that the complex would hold promising uses as electron donors in photo-induced electron transfer reactions (redox mediators) and photosensitisers in energy conversion reactions.[63] It was found that by incorporating the mnt ligand on to the metal-

polyimmine complex, ligand-to-ligand CT occurred due to the differences in the redox potentials of the two ligands upon electronic excitation.

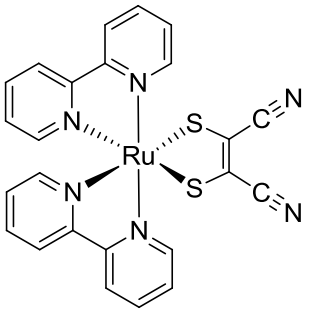

o

The electrochemistry of ruthenium *bis*-bipyridine complexes with different simple benzene ligands has been studied by Lever *et al*. in a series of papers over the past two decades.[64] The complexes of $[Ru(bpy)_2LL]$ studied consist of a benzene backbone with varying ortho-substituents (**p** – **t**).

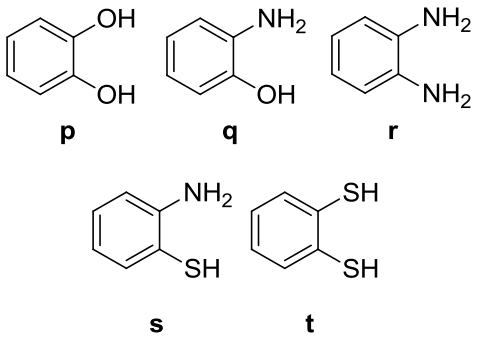

p **q** **r**

s **t**

The various studies found that such species possessed many one- and two-electron transitions. The complex $[Ru(bpy)_2(O{\cdot}O)]$ (**p**) was shown to exhibit multiple one-electron redox couples centred at the metal, bipyridine ligands and benzene ligand. It was also found that the electrochemical data for the species with ligands (**q** & **r**) were similar to those of ligand (**p**). From the spectroelectrochemical results, it was possible to assign each of the eight processes of the cyclic voltammogram to a specific chemical process. In aprotic and dry solvents containing the deprotonated quinoid ligand (**p** to **r**) the ligands showed two reversible couples,

while in protic or wet solvents, the ligands displayed two-electron irreversible waves due to the loss of hydrogen from the quinonoid nitrogen atoms. It was anticipated that the $[Ru(bpy)_2(NH{\cdot}S)]$ species (**s**) would behave much like those of $[Ru(bpy)_2(NH{\cdot}O)]$, with perhaps only a slight shift in potential due to the electron rich character of the sulfur. It was found, however, that the electrochemistry of the species was notably solvent dependent, and thus behaved differently in different organic solvents.

The latest paper published by Lever *et al.* studied the electrochemical behaviour of benzene-1,2-dithiol (**t**).[65] Initially, Lever noted that through literature research this simple dithiolate had never previously been synthesised and studied. This was surprising since the 1,2-dihydroxybenzene and 1,2-diaminobenzene analogues were well known. Through the study of this complex, Lever discovered that the complex exhibited oxygen sensitivity in air while in solution forming the metal-sulfur bound sulfhydryl monosulfinate and disulfinate products. It was found that the sulfhydryl monosulfinate ($S{\cdot}SO_2$) species possessed one reversible oxidation at +0.42 V versus NHE and two reversible waves at -1.34 and -1.61 V versus NHE. Lever was able to identify the waves using his previous results from the study of the oxygen and nitrogen analogues of the dithiol species and concluded that the +0.42 V oxidation was due to the $E_{1/2}[Ru^{III/II}]$ and the latter two waves due to the reduction of the $E_{1/2}[bpy/bpy^-]$. For the sulfhydryl disulfinate species ($SO_2{\cdot}SO_2$), the results showed the same trend. The $E_{1/2}[Ru^{III/II}]$ had shifted to +1.41 V versus NHE, and the reduction waves $E_{1/2}[bpy/bpy^-]$ were -1.28 and -1.54 V versus NHE.

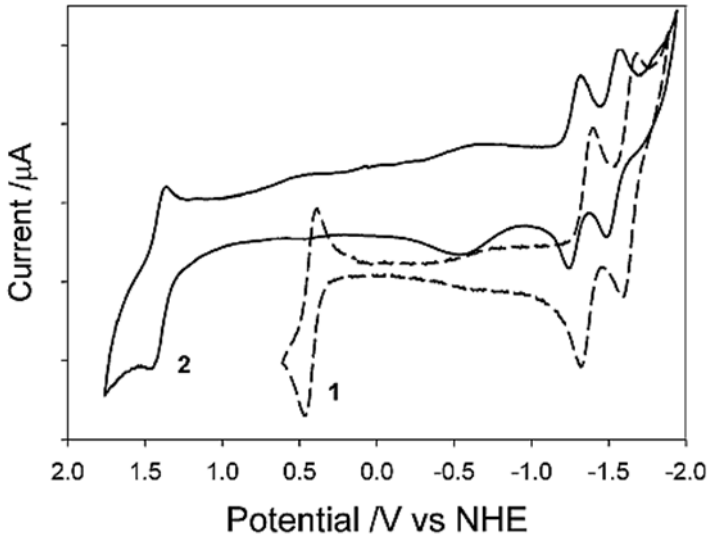

Figure 1-21 Cyclic Voltmmogram of $[Ru(bpy)_2(S{\cdot}SO_2)]$ (1) and $[Ru(bpy)_2(SO_2{\cdot}SO_2)]$ (2)[65]

It is clearly visible from the results of the benzene-1,2-dithiol complex that as the oxidation level of the chemically-oxidised complex increases, firstly to the sulfhydryl monosulfinate ($S{\cdot}SO_2$), then to the sulfhydryl disulfinate ($SO_2{\cdot}SO_2$), cyclic voltammetry shows that the corresponding $E_{1/2}[Ru^{III/II}]$ increases.

Due to the polarisable characteristics of S-donor ligands, these ligands can form a range of complexes in which the sulfur can bridge between one or two metal centres.[66] This bridging works particularly well if gold or silver are used to bridge the structures since both have a great affinity for sulfur. For example, work carried out with $[Pt(PPh_3)_2(\eta^2\text{-L})]$ (η^2-L = bidentate sulfur ligand) with gold has led to a gold-bridge structure (**Figure 1-22**), with the gold being inserted in between the sulfur ligands, joining two of the platinum structures.[67]

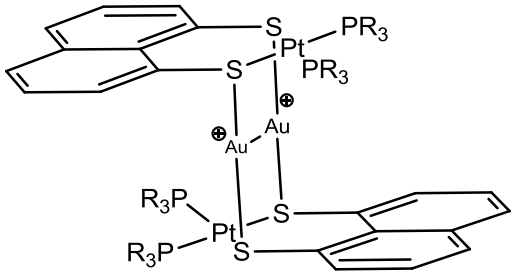

Figure 1-22 Gold-Gold Bridged Dimer
Perchlorate Anions Omitted

This bridging process is also possible by substituting gold with silver, but where two platinum complexes are bridged by one silver atom (**Figure 1-23**).[67]

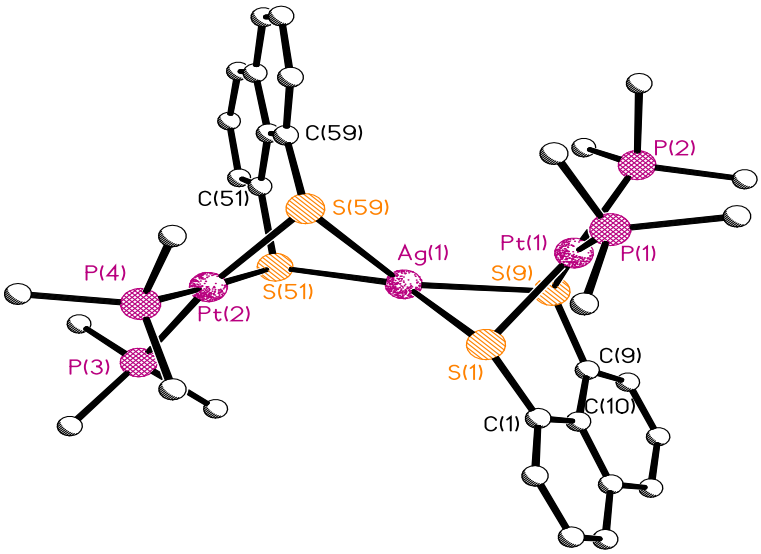

Figure 1-23 Crystal Structure $Ag[(PPh_3)_2Pt(S_2C_{10}H_6)]_2^+ ClO_4^-$

Anion omitted

1.6 Aims

The aims of this project is to synthesise a number of novel ruthenium complexes incorporating electron rich bidentate dithiolato ligands which have been previously synthesised or developed in our lab. These ligands will be coordinated onto an electron rich

ruthenium backbone such as ruthenium *bis*-bipyridine. Each complex will be characterised utilising the most common techniques used (MS, IR, NMR, etc.). Furthermore, each complex will be electrochemically studied using cyclic voltammetry to determine the redox potential of the complex. This will assess the viability and suitability of a complex to act as a redox mediator for glucose sensors.

The ability for these complexes to form multinuclear complexes will also be explored. This interaction through the lone pairs of the sulfur atoms with transition metals such as Pt, Ag, Au will test the ability for these complexes to bind onto a stationary or macromolecular entity giving a 3rd generation redox mediator.

2 PENTAMETHYLCYCLOPENTADIENYL IRIDIUM & RHODIUM COMPLEXES WITH DITHIOLATO LIGANDS

2.1 Introduction

Cp* or 1,2,3,4,5-pentamethylcyclopentadiene (**Figure 2-1**) is a cyclic non-aromatic hydrocarbon with the molecular formula C_5Me_5H. It is an analogue of its less substituted derivative cyclopentadiene.

Figure 2-1 Cyclopentadiene (left) and Pentamethylcyclopentadiene (right)

Cyclopentadienyl (Cp), the anion of cyclopentadiene, is one of the most documented ligands in organometallic chemistry.[68] The ligand can be used in two different ways. The ligand can either donate one electron to a metal centre yielding a single σ-bond (η^1), type X in the CBC method,[69] or can be used as a 6π-electron donor yielding 3 π-bonds to a metal centre (η^3). It is an anionic ligand, Cyclopentadiene with a pK_a of 16 is highly acidic for a non-polar, unsubstituted hydrocarbon. It can be deprotonated by a number of bases, typically simple metal hydrides such as sodium hydride. The loss of the hydrogen is promoted by the high stability of the conjugate base. The ligand, once deprotonated to Cp^-, is highly stable. The stability of this anionic compound is accounted for by the aromatisation of the conjugate base. This leads to the ring becoming planar, and possessing 4*n*+2 π-electrons. The ligand donates

the extra pair of electrons to a metal centre, becoming coordinated as a result. The M-C bond is not solely attributed to a single M-C bond, but to a share between all five carbon atoms. As a result, the metal centre is known to have become capped or half-sandwiched when one Cp ligand is bonded, or sandwiched when two Cp ligands are bonded (Figure 2-2).

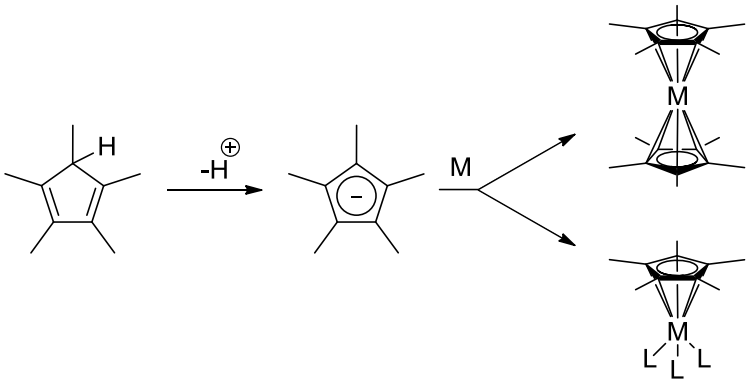

Figure 2-2 Sandwiched and Half-Sandwiched Metallocenes

The stability of these π-complexes is due to the favourable bonding interactions between the ligand and metal orbitals. The lowest energy orbital of the ligand (a_1) does not overlap with any of the metal d-orbitals as the ligand p-orbitals lie on the d_{z^2} plane and thus has little interactions with the metal d_{z^2}. Consequently, the e_1 set of degenerate orbitals overlap favourably with the metal d_{xz} and d_{yz} orbitals forming the π-bonds. Furthermore, the interaction between the e_{1u} and the metal p_x and p_y orbitals overlap leading to some added stabilisation effect. The metal's d_{xy} and $d_{x^2-y^2}$ orbitals play little part in the stabilisation as the degree of overlap with the e_{2g} orbital is minimal. The MO diagram of general metallocenes is shown below in **Figure 2-3**.

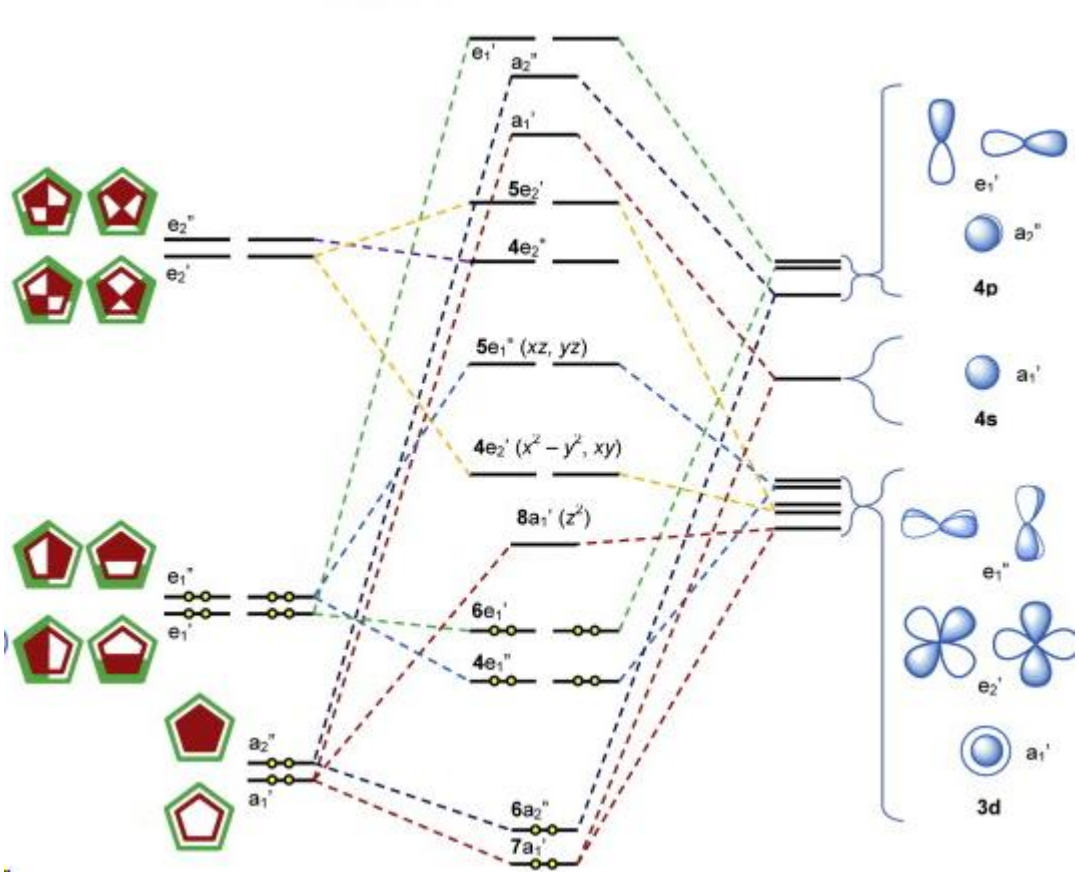

Figure 2-3 Generalised MO Bonding Diagram for Metallocenes[70]

The most well known compound with Cp ligands is ferrocene, (*bis*(η^5-cyclopentadienyl)iron(II)). Ferrocene was first synthesised unintentional by Kealy and Pauson in the attempt to synthesise fulvalene.[71] Instead, an orange powder was obtained, noting its "remarkable stability" towards acids and bases along with decomposition above 400 °C. The stability arises from the overlap of the ligand π-orbitals with the partially empty metal d-orbitals forming metal-carbon π-bonds. The discovery of these metallocenes, originally by Kealy and Pauson and expanded upon greatly by Fischer and Wilkinson, led to an explosion of interest into the synthesis, structure and reactivity of transition metal organometallic complexes with π-bonds, known as π-complexes.

Virtually all transition metals can be found in sandwich or half-sandwiched complexes. Hundreds of different sandwiched and half-sandwiched complexes are known for both Cp and Cp* along with their derivatives.[72,73,74,75,76] Many other associated derivative π-ligands, such as 1-methylcyclopentadiene and *p*-cymene (1-methyl-4-isopropyl-cyclohexadiene) are also known.

Although both Cp and Cp* are very similar, the latter is often favoured due to a few advantageous electronic and structural properties. Electronically, the methyl substituents on the Cp* offer a ligand that is more electron rich, and thus a stronger donor to the metal centre. This leads to a larger bond energy; a stronger metal–ligand bond that is less easily replaced by other ligands and resists decomposition as well as increased thermal stability. Structurally, Cp* is a much bulkier ligand, giving it greater steric effects. This steric bulk is best seen in that the Cp* starting material does not have to be 'cracked' prior to its usage, unlike Cp (**Figure 2-4**). The methyl groups prevent the dimerisation of the ligand through steric effects. The methyl groups of Cp* provide more steric bulk which can aid in the isolation of complexes for which the Cp analogues are unobtainable due to lower kinetic stability. This property is often prized in the design of organometallic catalysts, directly influencing catalytic behaviour. Moreover, the methyl groups increase the solubility of the complexes in organic solvents. This helps to isolate more of the compound. This is especially important since many Cp* complexes employ platinum group metals (PGM) as their metal centre, and maximum recovery is vital.

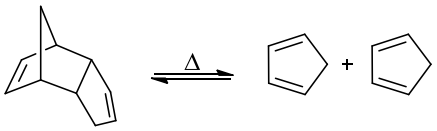

Figure 2-4 Cracking of Dicyclopentadiene to Cyclopentadiene

Platinum group metals, or PGMs as they are commonly abbreviated, are a group of six metallic elements. PGMs consist of Ru, Rh, Pd, Os, Ir, and of course Pt itself. They are so termed because they are all commonly found in the mineral deposits from which platinum is extracted, and are usually found with Au, Ag and Cu. They are amongst the rarest elements in terms of abundance with platinum having an average abundance of 5 μg/kg of ore, whilst the concentration of the least abundant member, Os, is that of 1.5 μg/kg of ore.[77]

They are further subdivided into the iridium-group PGMs (Ru, Os and Ir) and the palladium-group PGMs (Rh, Pd, and Pt). They are amongst the elements with the highest melting points, from 1552° for Pd to 3045° C. for Os. They have varied and important uses. They are used as circuit contacts in printed circuitry due to their high conductivity and as alloying agents to increase the strength and stability and corrosion resistance of their alloys.

The atoms themselves are large and so are able to bond large and complex ligands. This is most important as they are most commonly use as catalysts in the chemical and petrochemical industry. PGM catalysts used can vary wildly in structure and reactivity. Example of such catalysts are from the simple Adams' catalyst (PtO_2) used in the reduction of organic compounds (the catalytic activity of Adams' catalyst is due to the macromolecular structure of the lattice, rather than by single molecular interactions),[78] the intermediate such as in Wilkinson's catalyst used for the hydrogenation of alkenes,[79] to the more complex such as the carbene-containing second generation Grubbs' catalyst used for olefin metathesis (**Figure 2-5**).[80]

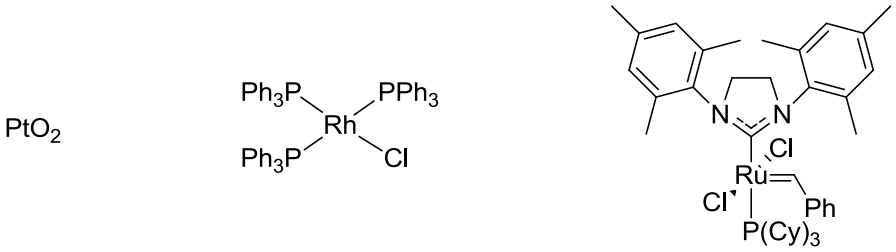

Figure 2-5 Adams' Catalyst (left), Wilkinson's Catalyst (centre), Grubbs' Catalyst (right)

The use of Cp* and Cp-like ligands with PGM have always been of particular interest in organometallic chemistry. This is because of the benefits gained when using π-ligands. Combining a Cp derivative with transition metals bestows the complex with stabilising properties which is an essential trait sought after in the design of catalysts. There are several important commercial catalysts that have either Cp or Cp* as one of their ligands.

The impact that metallocenes have had in the area of chemistry is profound. Several catalysts have become the cornerstone in the production of several chemicals. Their impact can be summarised in a handful of applications.

Schwartz's reagent (zirconocene hydrochloride) for example, is used in organic synthesis for hydrometallation reactions.[81] These reactions are invaluable in several industrial processes. The use of Schwartz's reagent in hydrometallation reactions is commonly termed as hydrozirconation. This reaction converts both alkenes and alkynes into their saturated forms. By reacting zirconocene hydrochloride with one of the substrates, an organozirconocene intermediate is generated. This intermediate can then be demetalated with the use of an electrophile such as hydrochloric acid or bromine yielding their corresponding alkane or bromoalkanes. Acid chlorides can also be employed as the electrophile this time yielding ketones as the product.

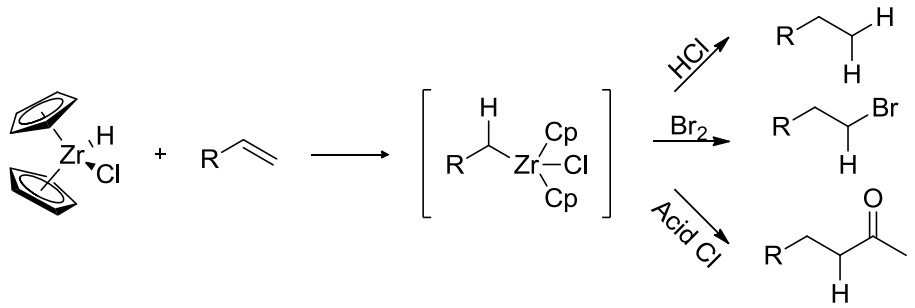

Figure 2-6 Hydrozirconation Process Using Schwartz's Reagent (left)

The Ziegler-Natta catalyst is yet another important metallocene catalyst and is used in industry for the polymerisation of olefins.[82] This catalyst is not limited to one metal and can be made of Zr, Hf or Ti. The catalyst when used in conjunction with the co-catalyst MAO (methylaluminoxane) is able to polymerise propylene to produce polypropylene.[83] Using the metallocene catalyst shown bellow (**Figure 2-7**), the atactic conformer is synthesised. By a slight modification of the π-ligand, both the isotactic and syndotactic conformers can also be synthesised. Metallocenes are used for the synthesis of many different polyolefins including polyethylene, polypropylene, polystyrene and ethylene-propylene-diene monomer rubber. Many different companies such as Exxon, Mobil, Mitsui Petrochemical, BASF, Dow-Dupont, Mitsubishi and BP Chemicals hold patents in the production of metallocene derived polyolefins.[84]

M = Zr, Hf, Ti

Figure 2-7 Kaminsky Catalysts for the Production of Polyolefins

These simple catalysts play a vital role in industrial applications. The use of Ziegler-Natta catalysts in homogenous reactions alone creates a volume of 45.1 megatonnes of polypropylene worth in the region of $65bn in 2007.[85]

While early transition metal metallocenes have become very important catalysts, the impact of half-sandwiched PGM catalysts has also been notable. The area of carbon-hydrogen bond activation properly began with the use of Cp* iridium complexes that are able to undergo oxidative addition with saturated hydrocarbons. Before then, C-H activation was thought a very difficult process with varying results that required very high temperatures. Through the use of a half-sandwiched Cp* iridium complex, the first fully successful activation of C-H bonds in fully saturated hydrocarbons was pioneered by R. G. Bergman.[86] This process involved the irradiation of the system with UV radiation (**Figure 2-8**).

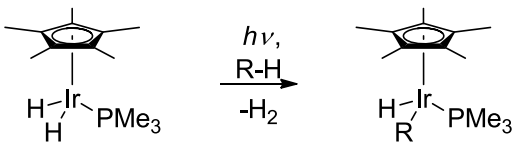

Figure 2-8 Bergman's Process

The activity of this complex was independently verified by W. A. G. Graham.[87] In his system he noticed the ability of Cp* iridium dicarbonyl complex to convert to a dihydrido complex with hydrocarbons (**Figure 2-9**).

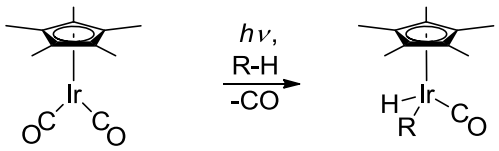

Figure 2-9 Graham's Process

While some metallocene-based catalysts are used in the multi-megatonne productions of hydrocarbons, others have a much more dedicated and specialised use and are important in the synthesis of natural products and have very specific reaction requirements. For example, the use of a ruthenium complex with a Cp derivative is able to conveniently and efficiently synthesise cyclic ethers from alcohols (**Figure 2-10**).[88]

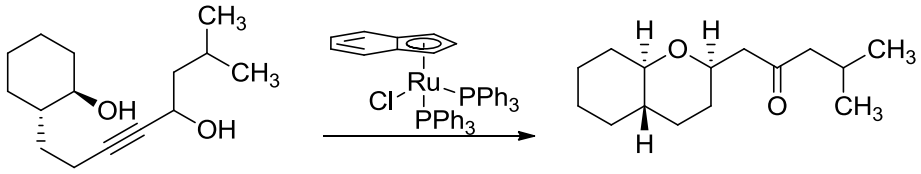

Figure 2-10 Cyclic Ether Catalysis

2.2 Aims

Herein a series of related complexes with dithiolato ligands were prepared. The bonding and structure of these three different ligands with Cp*Ir/Rh were studied. Three different dithiolato ligands have been explored; benzene-1,2-dithiol (**1**), naphthalene-1,2-dithiol (**2**) and biphenyl-2,2'-dithiol (**3**).

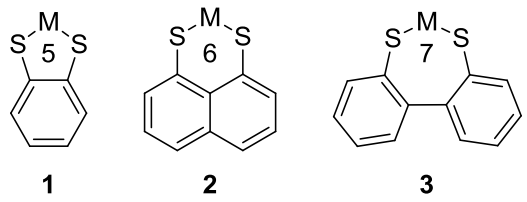

Figure 2-11 Ring Size Comparison when Coordinated

The three different ligands all have different backbones that when coordinated produce complexes with different ring size, varying intermolecular S…S distances, and different M…S bond lengths.

The different ring size induced by the three ligands will also have an effect on the C-S-M bond and torsion angle along with a differing geometry about the sulfur atoms. The intermolecular S…S distances will also show a change from the pro-ligand dithiol to the dithiolate ligand due to the different ring size. The pro-ligand thiol interatomic S…S distances for the three ligands is shown below in **Figure 2-12** .

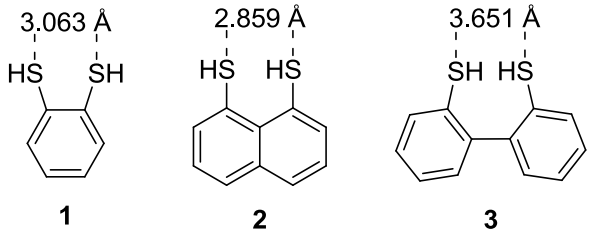

Figure 2-12 Thiol Intramolecular S**…**S Distance[89]

2.3 Results and Discussion

The iridium and rhodium complexes were prepared by the ligand replacement reactions between the chloride ligand of the metal and the thiol-hydrogen as shown (**Scheme 2-1**) in a 1 : 1.5 molar ratio with refluxing. The reaction is driven forward by the evolution of hydrochloric acid produced from the coupling reaction of the chloride and the hydrogen. Yields range from 20-60% after chromatography.

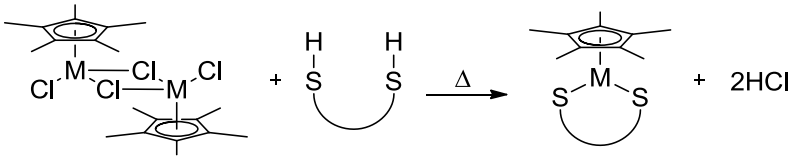

4 M=Ir, L=NaphS2
5 M=Rh, L=NaphS2
4B M=Ir, L=NaphS2 & PEt_3
5B M=Rh, L=NaphS2 & PEt_3
5NS M=Rh, L=NaphNS & Cl

6 M=Ir, L=BenzS2
7 M=Rh, L=BenzS2

9 M=Rh, L=BiphenS2
8B M=Ir, L=BiphenS2 & PEt_3
9B M=Rh, L=BiphenS2 & PEt_3

Scheme 2-1 Preparation of Cp*Ir/Rh Complexes

The Cp* ligand acts as a cap to one half of the metal atom, leaving the second half open for coordination. It was speculated that since all of the ligands used are bidentate and relatively planar (especially ligands **1** and **2**), the ligands will most likely be placed perpendicular to the plane of the Cp* ring (**Figure 2-13**). As for ligand **3**, the rotation about the phenyl ring link will most likely give a staggered configuration and not produce a perpendicular structure like that of **1** and **2** and possibly only leave one vacant coordination site available.

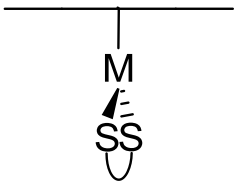

Figure 2-13 Proposed Structure of Cp* Dithiolate Complex

However, the replacement of the chloride ligands with a bidentate ligand will lead to the complex possessing a total of 16-electrons. This produces a complex that is coordinatively unsaturated (**Figure 2-14**). While 16-electron complexes are technically coordinatively unsaturated, they are common for d^8 tetrahedral and square planar complexes.

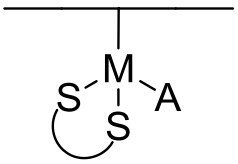

Figure 2-14 Proposed Structure with Empty Coordination Site (A).

Since the chloride ligands are unavailable to coordinate, it is possible for a second ligand to coordinate. This is avoided by controlling the ligand concentration. To comply with Langmuir's law,[90] a sulfur-donor atom is used as a neutral ligand, donating extra electron density to an adjacent metal centre and resulting in a dimer with each complex now possessing a total of 18-electrons (**Figure 2-15**).

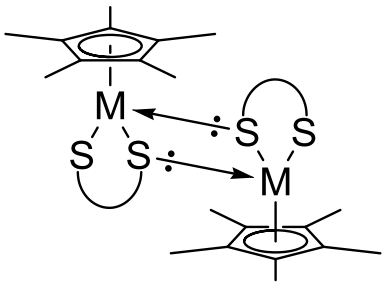

Figure 2-15 Dimerisation of Complexes Through Sulfur Donor

The ability of the complexes to dimerise was confirmed by single-crystal X-ray data for the solid state and electro-spray mass spectrometry for the solution state. The NMR data shows that while in solution, both sub-units are environmentally equivalent, producing NMR signals that correspond to a monomer.

In order to study the difference in bond lengths, as well as bond angles, between the monomeric and the dimeric conformations, the dimer was 'broken open' by a neutral ligand that preferentially binds to the metal over sulfur. Phosphines bind well to PGMs and a simple non-bulky phosphine (PEt_3) was chosen to occupy the empty coordination site (**Figure 2-16).** PEt_3 was chosen because of its high volatility which aids in the removal of any excess ligand. It was anticipated that when coordinated, the phosphine would increase the solubility of the compound and aid in the purification of the new compound. It was also chosen as this particular phosphine is non-bulky and would interact minimally with the ligands in question.

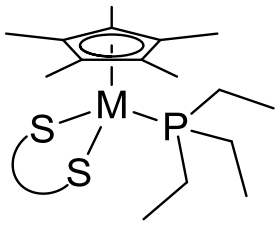

Figure 2-16 Monomeric Form of Complexes with PEt_3

All complexes stated above (**4** – **9B**) were obtained as pure products as evident from their NMR and mass spectra. Unfortunately, the elemental analysis results of **6**, **7** and **9** did not give agree with their theoretical percentage composition, possibly due to the absorption of solvent and/or water that could not be evaporated. However for the rest of the complexes, the elemental analysis agreed with the theoretical percentage composition within the accepted ±0.3% error margin. Single crystals for all were grown by either slow evaporation or by solvent diffusion.

2.3.1 Dimeric Ir & Rh Naphtho[1,8-*cd*]-1,2-dithiole Complexes

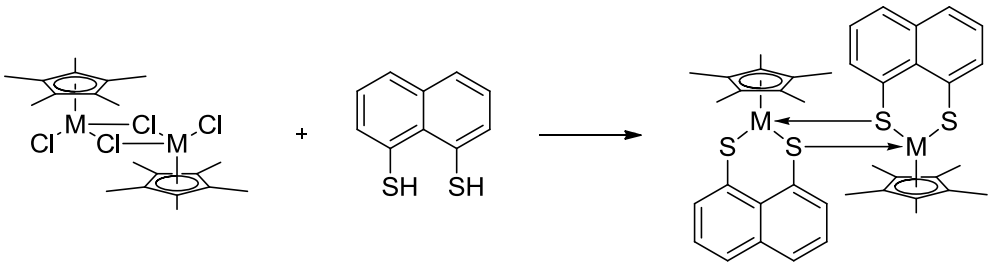

Scheme 2-2 Preparation of **4** and **5**

Naphtho-1,8-dithiole, along with other chalcogen and pnictogen *peri*-substituted naphthalenes, has been extensively studied in our group.[91] These compounds are interesting to study as the rigid naphthalene backbone places the two substituents in close proximity to each other producing strained conformations. They have been studied as possible sources of phosphine radicals and phosphine cations.[92]

Reaction of the naphthalenedithiol pro-ligand with that of the dimeric [Cp*Ir/$RhCl_2$] complex yielded complexes **4** and **5**.

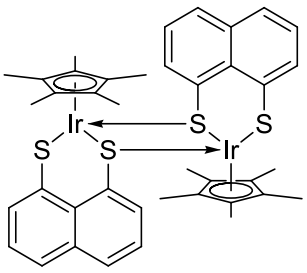

4

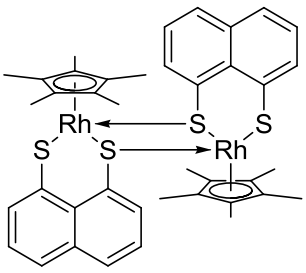

5

NMR studies of the Ir and Rh naphtho-1,2-dithiolato complexes (**4** & **5**) give straight-forward results. The results show that both Cp* groups along with both naphthalene groups of the dimer are in equivalent environments. This gives simple NMR signals close to 1.22 and 8.15-7.12 ppm for the Ir complexes, while the Rh complexes give similar, albeit slightly shifted, signals of 1.18 and 8.14-7.16 ppm. The ^{13}C NMR signal for the quaternary carbons of the Cp* for the Rh complex shows a small splitting (J = 6.13) due to the NMR active Rh, which has a nuclear spin of ½.

The ^{1}H NMR spectrum of **4** is shown below in **Figure 2-17** along with the peak assignments and relative integration. From the spectrum it can be seen that the two constituents of the dimer are in equivalent environments.

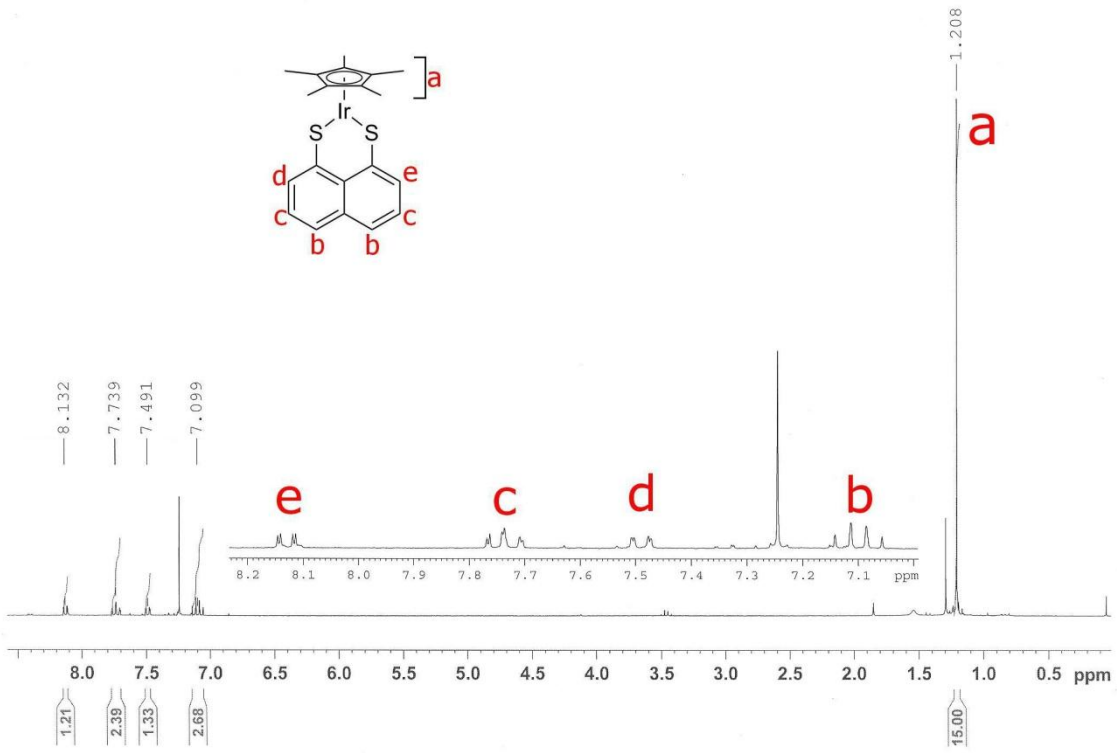

Figure 2-17 ^{1}H NMR Spectrum of **4**

The presence of a symmetric dimer is further confirmed in the solid state by the crystal structure data which show that there is a plane of symmetry though the middle of the dimer.

Crystals of **4** and **5** were grown from the slow evaporation of a saturated solution in dichloromethane. The structures elucidated were in agreement with the data previously presented on those two complexes and structurally were as expected i.e. a dimeric structure with formula of $[(Cp^*IrC_{10}H_6S_2)_2]$ for **4** and $[(Cp^*RhC_{10}H_6S_2)_2]$ for **5**. The data collected was of good quality with residual R1 factor of 4.4 and 8.2% respectively.

The geometry about the metal centre of both **4** & **5** is that of a typical piano stool structure. This kind of structure geometry is common for monometallic half-sandwiched compounds where the Cp* occupies the top half and resembles the seat and the three sulfur ligands resemble the three individual legs of the stool (**Figure 2-18**).

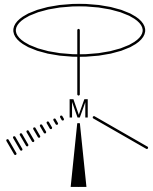

Figure 2-18 Piano Stool Structure

There are three principal planes present in 4 and 5, Cp* plane, M-S-S plane and the naphthalene plane. The M-S-S plane for **4** is hinged at an angle of 45.35° with respect to the naphthalene plane, while in **5**, this value has decreased marginally to 43.87°. Although both the Cp* and naphthlane seems to be parallel to each other, they are in fact ever so slightly angled at 12.96° for **4** and 12.87° for **5**.

Naphthalene-1,8-dithiol, the pro-ligand, exhibits an S…S distance of between 2.85 and 2.93 Å. The torsion angle of the naphthalene ring is 176.2°, while the torsion about the sulfur-sulfur

vector is 5.2°. The splay angle is 371.6°, an increase of 14.4° from the idealised sum of 360° which is that of naphthalene.

The torsion angle along with the splay angle (**Figure 2-19**), are two important measurements for compounds with substituents in close proximity to each other such as in *peri*-substituted naphthalenes. The splay angle is the summation of all angles between the heteroatoms. By comparing this measurement with that of an idealised system, such as that of the unsubstituted pro-compound, the degree of repulsion or attraction can be quantified. The torsion angle, on the other hand, is the amount of planarity (or lack thereof) of a compound and is used to quantify the degree by which the ring or substituents project above or below the plane.

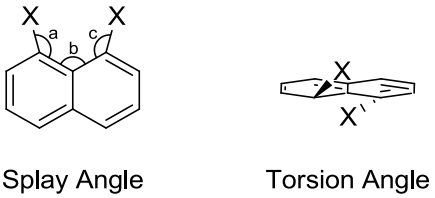

Figure 2-19 Splay and Torsion Angles

For compound **4**, the S…S distance has increased to 3.252 Å, while the splay angle is 381.4°, an increase of 10.3° from that of the pro-ligand. For the Rh analogue **5**, the respective measurements are 3.234 Å for the S…S distance, while the splay angle is 380.9°, an increase of 9.3° from that of the pro-ligand.

Normally, an increase in nucleons from 102 in Rh to 193 in Ir, along with the corresponding increase in electrons, would suggest that the radius of an Ir atom would be considerably larger than that of Rh. This should lead to the splay angle of the Ir complex being larger than that of the Rh. However, due to the lanthanide contraction, which is caused by the poor shielding of nuclear charge by the 4f electrons, the period-6 elements display almost identical radii to those in the fifth period.[33] Both Rh and Ir have approximately the same atomic radii of 2.10 and 2.13Å, and almost same covalent radii of 1.34 and 1.32 Å, respectively.[93] As such, the splay angles for **4** and **5** are almost identical.

Since the ligand has a rigid naphthalene backbone, forcing open the C-S bond angles by the insertion of the metal atom is not favourable. The least energetically demanding conformation that allows the insertion of the metal atom is by slightly moving the C-S bonds, leaving them slightly out of plane. This leaves one sulfur atom above the plane, while the second sulfur is below the naphthalene plane. This leads to a change in the torsion about the sulfur-sulfur vector of **4** and **5**. This change in torsion between the S(1)-C(1)-C(9)-S(2) can be seen to have increased dramatically between that of the pro-ligand and the coordinated ligand. Described above, the torsion of the pro-ligand is 5.2°, while the same torsion of the coordinated ligand has increased to 11° for both **4** and **5**.

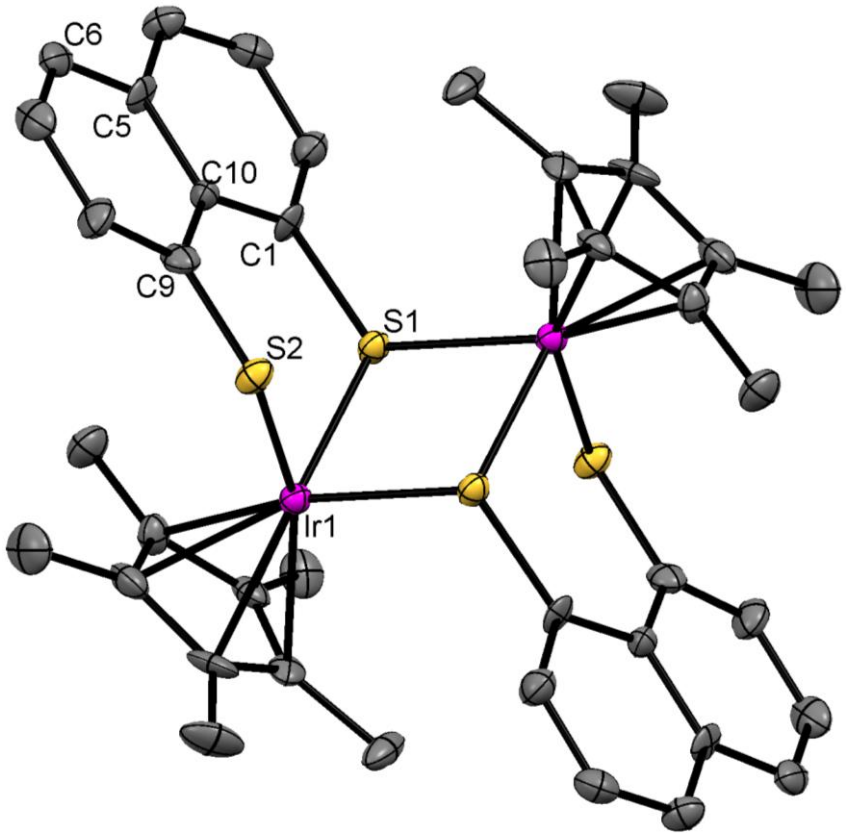

Figure 2-20 Crystal Structure of **4**

Bond Length (Å)		*Bond Angle (°)*		*Torsion Angle (°)*	
S(1)…Ir(1)	2.326(2)	**S(1)-Ir(1)-S(2)**	87.96(7)	**S(1)-C(1)-C(9)-S(2)**	11.0(5)
S(2)… Ir(1)	2.357(2)	**C(1)-S(1)-Ir(1)**	112.3(3)	**C(1)-C(10)-C(5)-C(6)**	176.3(7)
S(1)… Ir(1')	2.396(2)	**C(9)-S(2)-Ir(1)**	109.7(3)		
S(1)…S(2)	3.252(3)	**C(1)-S(1)-Ir(1')**	115.4(3)		
S(1)…C(1)	1.799(8)	**Ir(1)-S(1)-Ir(1')**	100.19(7)		
S(2)…C(9)	1.758(8)				

Table 2-1 Selected Bond Lengths for **4**

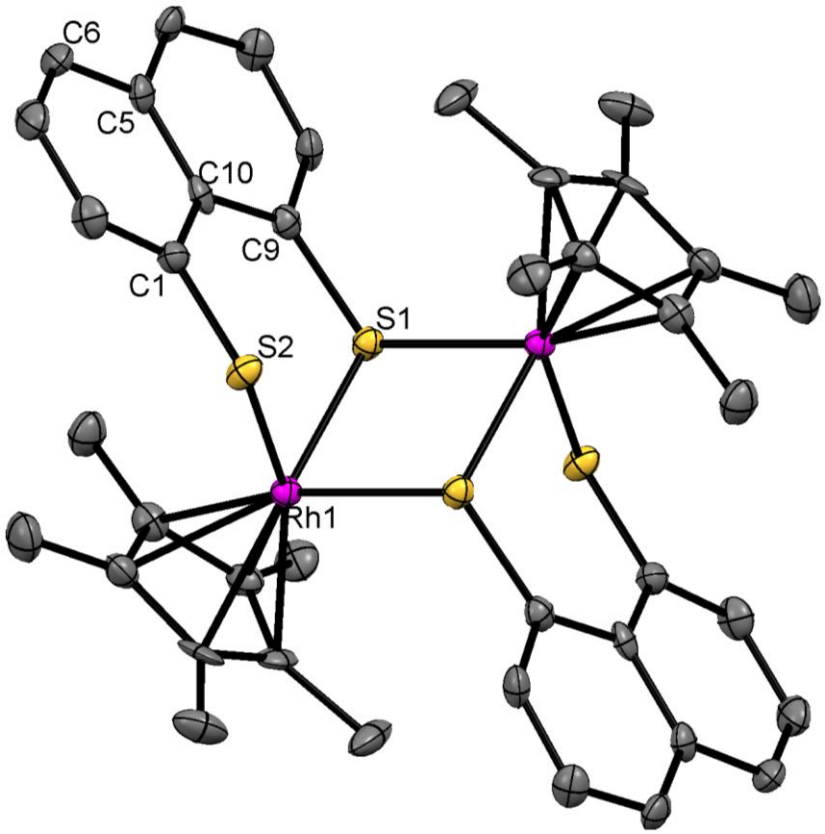

Figure 2-21 Crystal Structure of **5**

Bond Length (Å)		*Bond Angle (°)*		*Torsion Angle (°)*	
S(1)…Rh(1)	2.319(2)	**S(1)-Rh(1)-S(2)**	87.67(5)	**S(1)-C(1)-C(9)-S(2)**	11.1(4)
S(2)…Rh(1)	2.351(2)	**C(1)-S(1)-Rh(1)**	112.3(2)	**C(1)-C(10)-C(5)-C(6)**	179.6(6)
S(1)…Rh(1')	2.406(2)	**C(9)-S(2)-Rh(1)**	109.6(2)		
S(1)…S(2)	3.234(2)	**C(1)-S(1)-Rh(1')**	117.0(2)		
S(1)…C(1)	1.782(6)	**Rh(1)-S(1)-Rh(1')**	98.35(5)		
S(2)…C(9)	1.751(6)				

Table 2-2 Selected Bond Lengths for **5**

2.3.2 Monomeric Ir & Rh Naphtho[1,8-*cd*]-1,2-dithiole Complexes

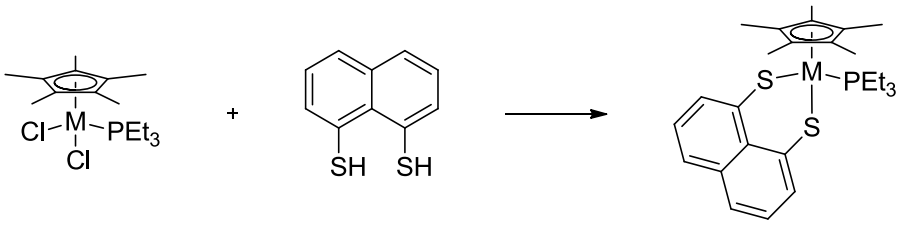

Scheme 2-3 Preparation of **4B** and **5B**

The monomeric forms of **4** and **5**, **4B** and **5B** were synthesised by the breaking open of the dimeric starting material with a neutral ligand giving the monomeric starting material shown above in **Scheme 2-3**. The ligand chosen was triethylphosphine. Although triphenylphosphine is generally chosen over other phosphines due to its stability and ease of use, the steric bulk of this phosphine would most likely incur conformational changes in the ligand which we are to study and would therefore not be suitable.

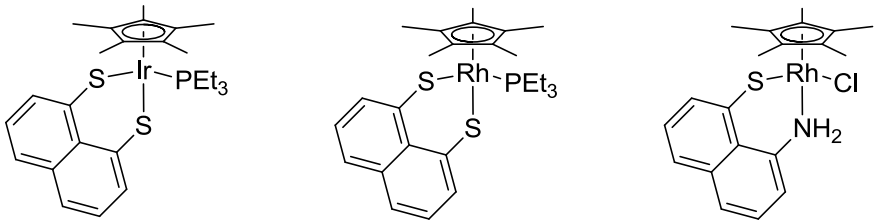

4B **5B** **5NS**

NMR studies of the complexes yield similar results to those previously mentioned, except with added signals due to the presence of PEt_3. These signals manifest themselves as an overlapping doublet-of-triplets and as a pseudo-pentet present at ~1 and ~2 ppm respectively. Their complex splitting is due to their proximity to the NMR active ^{31}P. The splitting effect of the phosphorus is also noticed in the Cp* signal, which has been split into a doublet with a coupling constant of ~1.9 Hz for Ir and ~2.8 Hz for Rh.

The ^{1}H NMR spectrum of **5B** is shown below (**Figure 2-22**). This representative NMR shows the complex splitting incurred by the hydrogens, in particularly when split by the phosphorus. Slight splitting can be seen for the peaks assigned as "f", these being split by the rhodium centre.

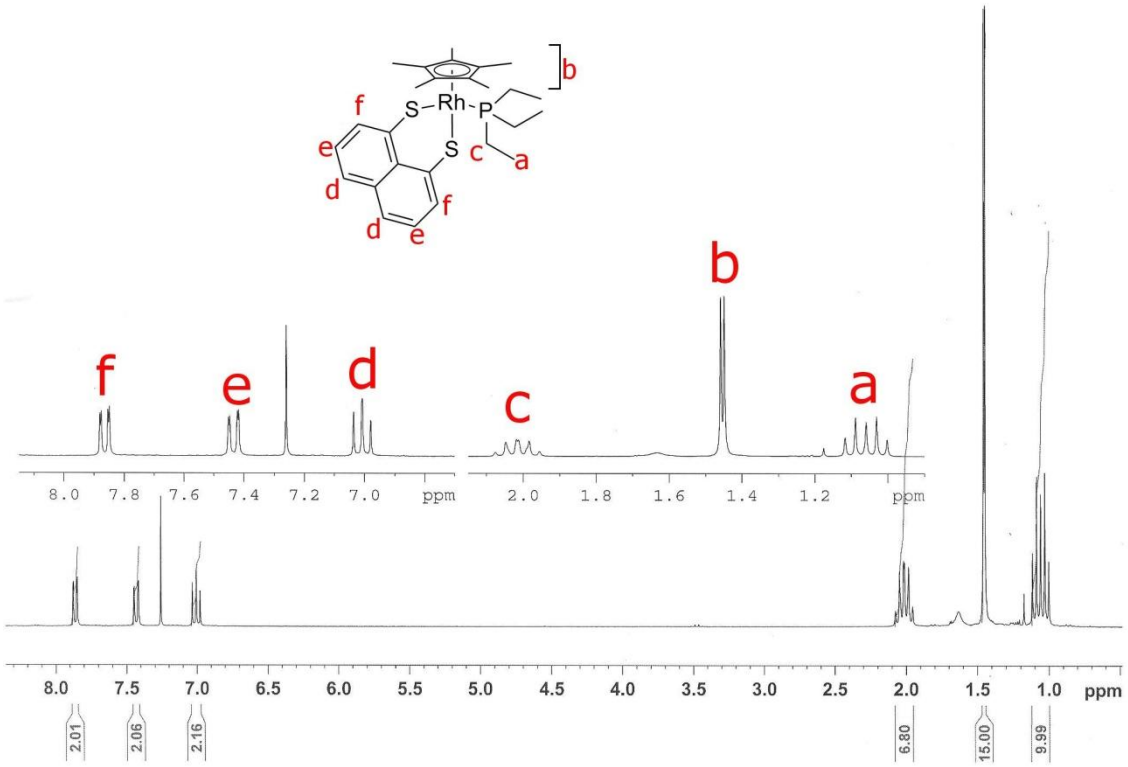

Figure 2-22 ^{1}H NMR Spectrum of **5B**

Crystals of **4B** and **5B** and **5NS** were also grown from the slow evaporation of a saturated solution in dichloromethane. The structures elucidated were in agreement with the data and were as expected. The phosphine ligand had indeed opened the dimeric structure yielding the monomeric forms with formula of [Cp*$IrC_{10}H_6S_2PEt_3$] for **4B** and [Cp*$RhC_{10}H_6S_2PEt_3$] for **5B** and [Cp*$RhC_{10}H_6SNH_2Cl$] for **5NS**. The data collected for these was of good quality with residual R1 factor of 7.0, 4.0. and 7.6% respectively.

The geometry about the metal centre of both these three is similar to those of **4** and **5** i.e. piano stool structure. There are three principal planes present in 4 and 5, Cp* plane, M-S-S plane and the naphthalene plane. The M-S-S plane for **4B** is hinged at an angle of 50.16° with respect to the naphthalene plane, while in **5B**, this value has increased marginally to 50.50°. When compared to **4** and **5**, the angle of the Cp* with respect to the naphthalene has reduced significantly and now measure 4.88° for **4B** and 4.87° for **5B**.

There are also subtle changes that can be seen between that of the monomer and that of the dimer. For iridium, the interatomic S…S distance has decreased from 3.252 Å in **4** to 3.190 Å in **4B**. This decrease is because there is no neighbouring metal atom stretching the sulfurs apart. This decrease is also seen in **5B**, where the interatomic S…S distance is 3.186 Å, down from 3.234 Å in **5**.

Another change that can be seen in the monomers is in the S…M bond length distance. For **4** and **5**, S(1) acted as a donor, donating a pair of electrons to M(2), producing the dimer. This leads to a loss of electron density about S(1) and thus a shortening of the S(1)…M(1) bond length. For the monomeric forms, **4B** and **5B**, the measurements of the S…M yield near equal lengths for both S(1) and S(2). This is expected as both sulfurs are identical, neither having donated electron density to form a dimer. Their respective measurements are 2.349 Å and 2.344 Å in **4B** and 2.334 Å and 2.350 Å in **5B.**

It is interesting to note that the splay angles have remained largely unchanged. The iridium splay angle has increased by 0.5° to 381.9°, while that of rhodium now totals 379.4, a decrease of 1.5°.

As expected from the coordination of the phosphine ligand, the torsion about S(1)-C(1)-C(9)-S(2) of both **4B** and **5B** have also changed. Since there no neutral donor acting as the bridge between the two monomers and no second metal centre forcing the sulfurs further apart, there is a relaxation of the torsion angle between the sulfurs. As such, they both decreased from 11 to 9° for the iridium complex and from 11 to 7.4° for rhodium complex.

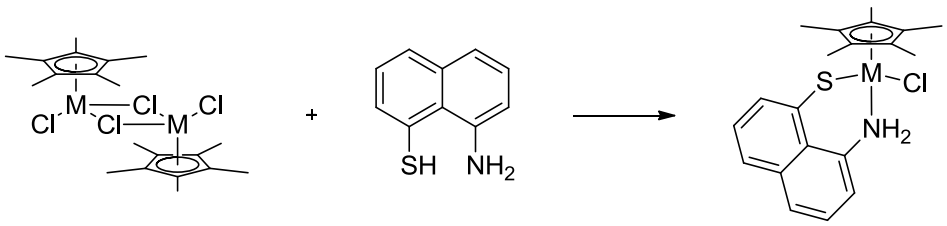

Scheme 2-4 Preparation of **5NS**

For a simple comparison, **5NS** was synthesised. The 1-aminonaphthalene-8-thiol ligand behaves very much like that of naphthalene-1,8-dithiol. From the crystal structure of **5NS**, the M-S-N plane is angled at 54.61° with respect to the naphthalene plane, while the angle between the Cp* and naphthalene planes is smaller at 3.76° when compared to **4B** and **5B**. The S…M bond length is 2.371 Å, compared to that of 2.334 Å in **5B**. The most significant change is obviously those related to the smaller size of the nitrogen. The interatomic S…N distance has reduced to 2.907 Å, while the S-M-N angle has been lowered to 79.8°, down from 85.2 from **5B**. The most obvious change that has occurred is not on the bonding geometry of **5NS**, but in its chemistry. Whereas **5B** formation proceeds by the complete substitution of both chlorides, for **5NS** only one is replaced. This is due the properties of the individual heteroatoms. Whereas thiols behave as weak acids (thiophenol pK_a = 8), amines (NH_2R) behave the exact opposite, as bases. The relatively high basicity (analine pK_b = 9.3) prevents the 1° amine releasing the hydrogen and thus acting as a negative donor, in turn becoming a neutral donor.

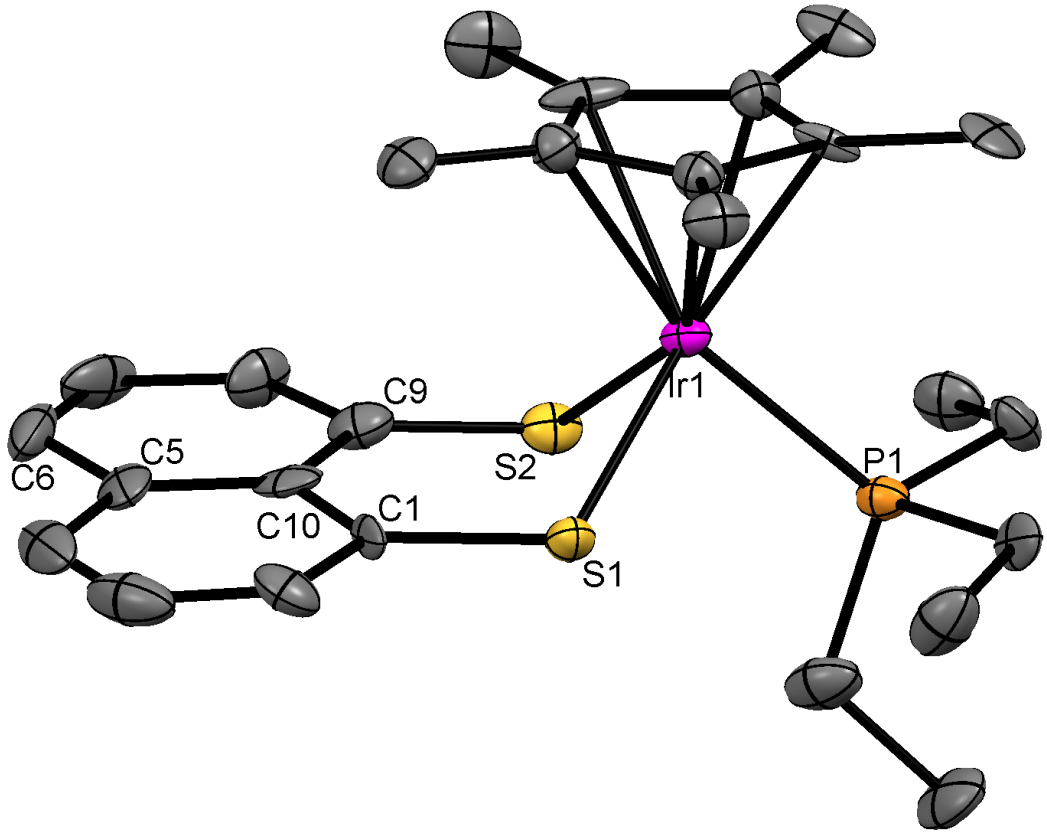

Figure 2-23 Crystal Structure of **4B**

Bond Length (Å)		*Bond Angle (°)*		*Torsion Angle (°)*	
S(1)…Ir(1)	2.349(4)	**S(1)-Ir(1)-S(2)**	85.6(1)	**C(1)-S(1)-C(9)-S(2)**	9.1(9)
S(2)…Ir(1)	2.344(3)	**C(1)-S(1)-Ir(1)**	105.5(6)	**C(1)-C(10)-C(5)-C(6)**	178.0(1)
Ir(1)…P(1)	2.278(3)	**C(9)-S(2)-Ir(1)**	109.8(5)		
S(1)…S(2)	3.190(5)				
S(1)…C(1)	1.710(2)				
S(2)…C(9)	1.790(1)				

Table 2-3 Selected Bond Lengths for **4B**

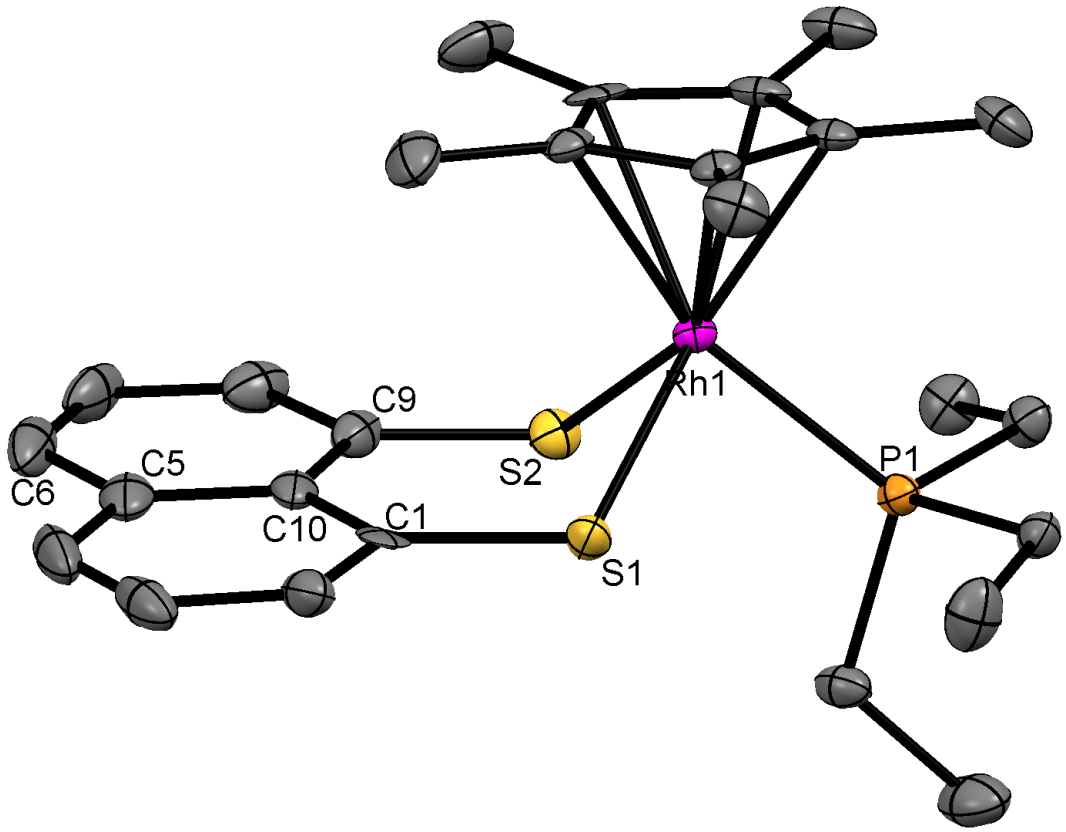

Figure 2-24 Crystal Structure for **5B**

Bond Length (Å)		*Bond Angle (°)*		*Torsion Angle (°)*	
S(1)…Rh(1)	2.334(1)	**S(1)-Rh(1)-S(2)**	85.9(2)	**C(1)-S(1)-C(9)-S(2)**	7.4(2)
S(2)…Rh(1)	2.350(1)	**C(1)-S(1)-Rh(1)**	107.4(1)	**C(1)-C(10)-C(5)-C(6)**	178.3(4)
Rh(1)…P(1)	2.301(1)	**C(9)-S(2)-Rh(1)**	109.8(1)		
S(1)…S(2)	3.186(1)				
S(1)…C(1)	1.779(5)				
S(2)…C(9)	1.787(4)				

Table 2-4 Selected Bond Lengths for **5B**

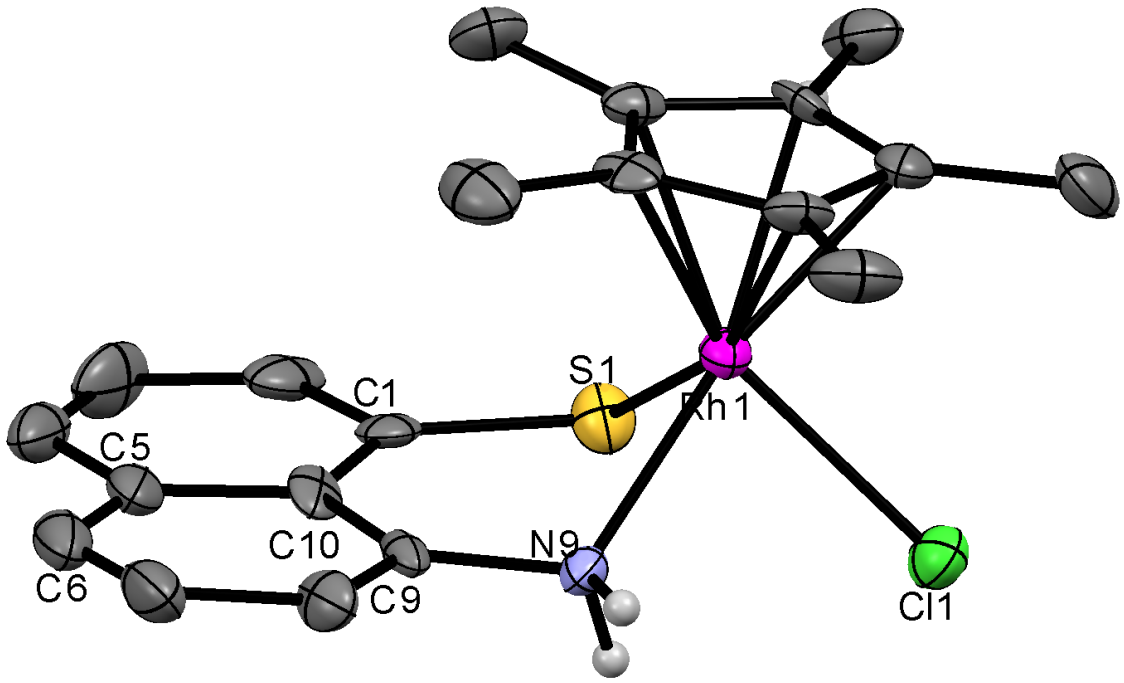

Figure 2-25 Crystal Structure for **5NS**

Bond Length (Å)		*Bond Angle (°)*		*Torsion Angle (°)*	
S(1)…Rh(1)	2.371(2)	**S(1)-Rh(1)-N(1)**	79.8(2)	**C(1)-S(1)-C(9)-S(2)**	4.7(6)
N(1)…Rh(1)	2.152(8)	**C(1)-S(1)-Rh(1)**	104.9(3)	**C(1)-C(10)-C(5)-C(6)**	176.4(9)
Rh(1)…Cl(1)	2.420(2)	**C(9)-N(1)-Rh(1)**	117.1(5)		
S(1)…N(1)	2.907(7)				
S(1)…C(1)	1.757(9)				
N(1)…C(9)	1.450(1)				

Table 2-5 Selected Bond Lengths for **5NS**

2.3.3 Ir & Rh Benzene1,2-dithiol Complexes

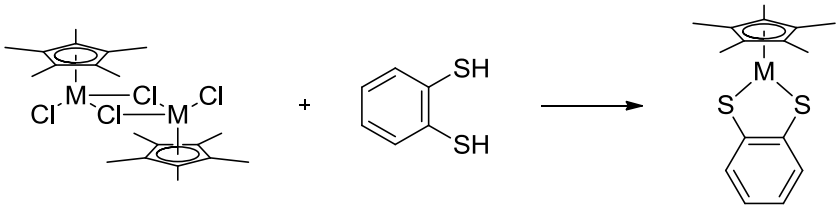

Scheme 2-5 Preparation of **6** and **7**

The use of benzene-1,2-dithiolate ligands has been studied since the 1960s due to their interesting bonding and magnetic properties in square planar complexes.[94,95] Complexes with BDT, and BDT-type ligands known as dithiolenes have also been extensively studied due to their interesting electrochemical behaviour.[96,97,98] Unsurprisingly, in many ways BDT is very similar to NaphS2. They are both planar ligands with an electron rich rigid backbone that have neighbouring sulfur atoms. Unlike **1**, the intermolecular S…S distance of 3.063 Å is just far enough that both sulfurs are unable to impart an appreciable repulsive effect upon each other, yielding a negligible torsion of just 1°, compared to the 5.2° for **1**.

Although **6** was previously recorded,[99] its Rh analogue (**7**) was not.

6 **7**

NMR studies of the Ir and Rh benzene-1,2-dithiolato complexes (**6** & **7**) yield very similar results to those of **4** & **5**. Two types of signals are observed. The Cp* methyls and the aromatic hydrogens which are present at 2.1 and 8.05-7.04 ppm respectively for **6**, and at 2.0 and 8.87-

7.11 ppm for **7**.The ^{13}C NMR signal for the quaternary carbons of the Cp* for the Rh complex shows a small splitting (*J* = 7.15) due to the NMR active Rh. Just like **4** and **5**, it was thought that the compounds **6** and **7** would exist as dimers, and would be proven by the crystal structure of these.

The ^{1}H NMR spectrum of **6** is shown below (**Figure 2-26**). This is shown in lieu of an acceptable elemental analysis to verify that the complex was isolated in its pure form. The peak assignments are shown in the diagram along with their corresponding integrations.

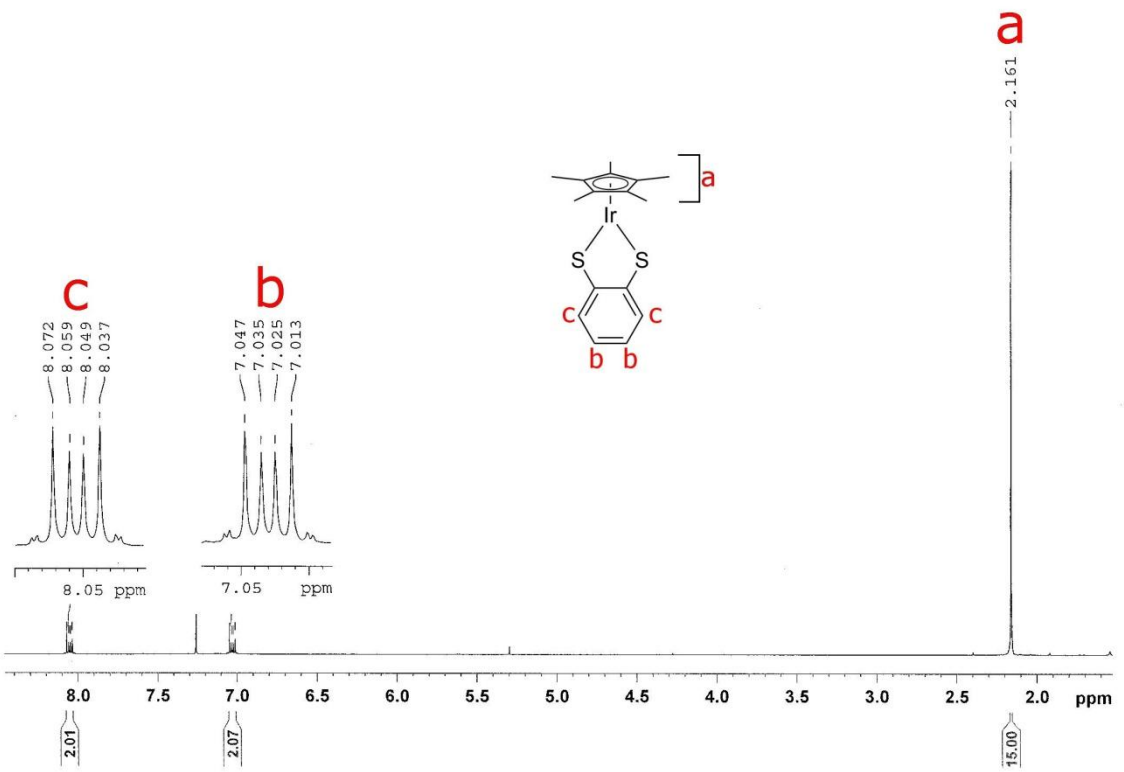

Figure 2-26 ^{1}H NMR Spectrum of **6**

Crystals of **6** and **7** were also grown from the slow evaporation of a saturated solution in dichloromethane. The quality of the data collected was not as good quality to those previously mentioned with residual R1 factor of 9.1, and 14.4% respectively. To our surprise, the crystal structure elucidated showed that these compounds do not dimerise like previously and had a formula of $[Cp^*IrC_6H_4S_2]$ for **6** and $[Cp^*RhC_6H_4S_2]$ for **7**.

The geometry of these is different to those previously discussed with these being termed as two-legged piano stool. The structure of **6** & **7**and are essentially T-shape structures with a slight buckling about the sulfur-sulfur . The M-S-S plane angle, with respect to the benzene ring plane is 8.12° for **6** and 9.08 for **7**. The Cp* plane and the benzene plane are essentially perpendicular. This is very different to the compounds previously discussed where they were virtually parallel. In the case of **6**, the angle of the Cp* plane to the benzene plane is 77.63°, while for **7**, this angle is 75.29°.

It is possible that the inability of these compounds to dimerise is due to several factors. In the solid state, the crystal packing diagram of these show that there is evidence of π-π stacking interactions (**Figure 2-27**). The average C…C distance between the Cp*and a neighbouring benzene ring is 3.66 Å, while the centroid to centroid distance is 3.59 Å. Normal π-π interactions range between 3.3-3.8 Å,[100] which is well within the distances measured in these compounds. The stacking of the π-orbitals of the Cp* and that of the benzene ring of the ligand possibly prevents another molecule getting close enough to create a bond between monomers preventing the two units from coalescing and yielding a dimer.

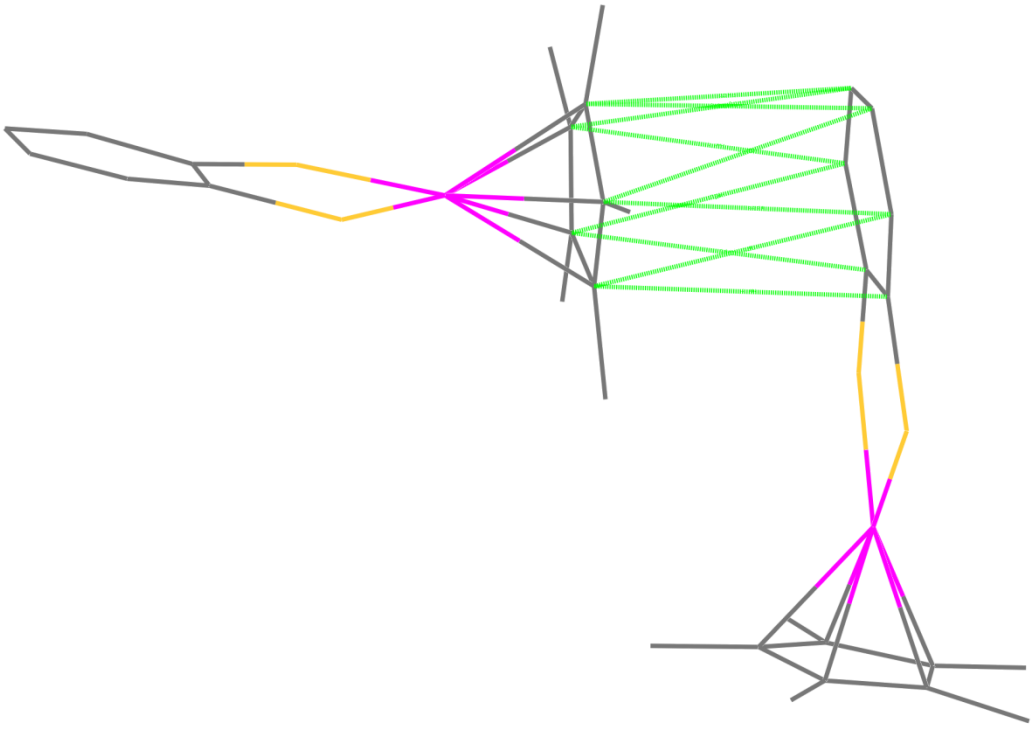

Figure 2-27 Packing Diagram of **6** & **7** Showing the Cp* and Benzene Ring π-π Stacking Interaction

It is also possible that the geometry about the sulfurs also creates an environment that is not conducive for the dimerisation of **6** and **7**. The structures of **4** and **5** show that the sulfurs point under the central metal leaving half of the metal exposed. This is due to the constraints imposed by the naphthalene ring with *peri* substitutions. This forces the sulfur lone pairs to lie above and below the naphthalene plane. In **6** and **7**, however, the geometry about the *peri* substituents of the benzene forces the sulfurs to adopt a different bonding geometry forcing the sulfur lone pairs to be coplanar with the ligand, inhibiting the formation of the dimer.

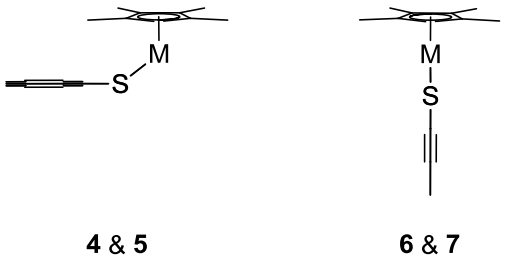

Figure 2-28 Different Sulfur-Metal Bond Geometry

The pro-ligand, benzene-1,2-dithiol, has an S…S distance of 3.063 Å, along with a torsion angle of 1°. As the ring is aromatic, and therefore planar, we can assume that the torsion about the ring is negligible. The splay angle has a total value of 244.14°, while the idealised value, that of benzene, is 240°.

For compound **6**, the interatomic S…S distance is 3.12 Å. The splay angle is 239°, an increase of 5° from the pro-ligand, while the torsion angle is 1°, a negligible amount. The respective measurements for **7**, the Rh analogue, are 3.14 Å and 234° for the splay, a 6° decrease.

As these structures were in the monomer form, we found no need to react these with a phosphine ligand. For comparison, however, the reaction was tried, but with failure. When the dithiol was added to $Cp^*MCl_2PEt_3$, unlike the previous work with **4B** and **5B** where only the chlorides are replaced, **6** and **7** proceed in replacing the chlorides as well as displacing the phosphine ligand from the complex, yielding the simple monomer.

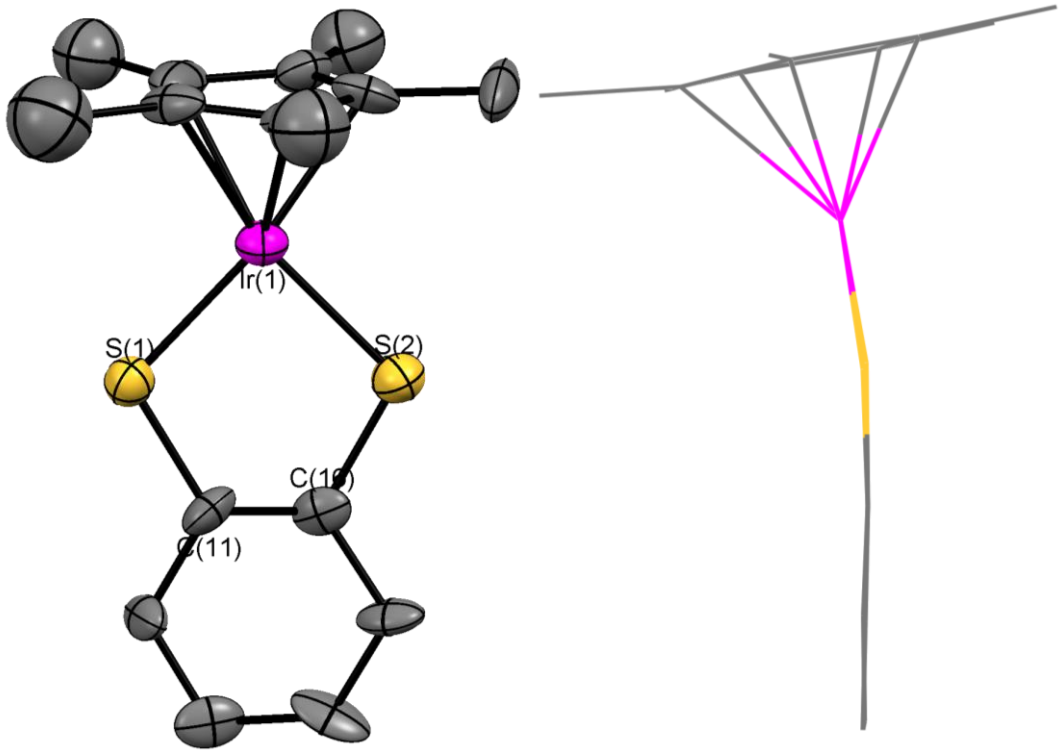

Figure 2-29 Crystal Structure of **6**

Bond Length (Å)		*Bond Angle (°)*		*Torsion Angle (°)*	
S(1)…Ir(1)	2.243(7)	**S(1)-Ir(1)-S(2)**	88.0(2)	**S(1)-C(11)-C(16)-S(2)**	1.00(3)
S(2)…Ir(1)	2.251(7)	**C(11)-S(1)-Ir(1)**	104.9(7)		
S(1)…S(2)	3.120(1)	**C(16)-S(2)-Ir(1)**	105.7(7)		
S(1)…C(11)	1.780(2)				
S(2)…C(16)	1.790(2)				

Table 2-6 Selected Bond Lengths for **6**

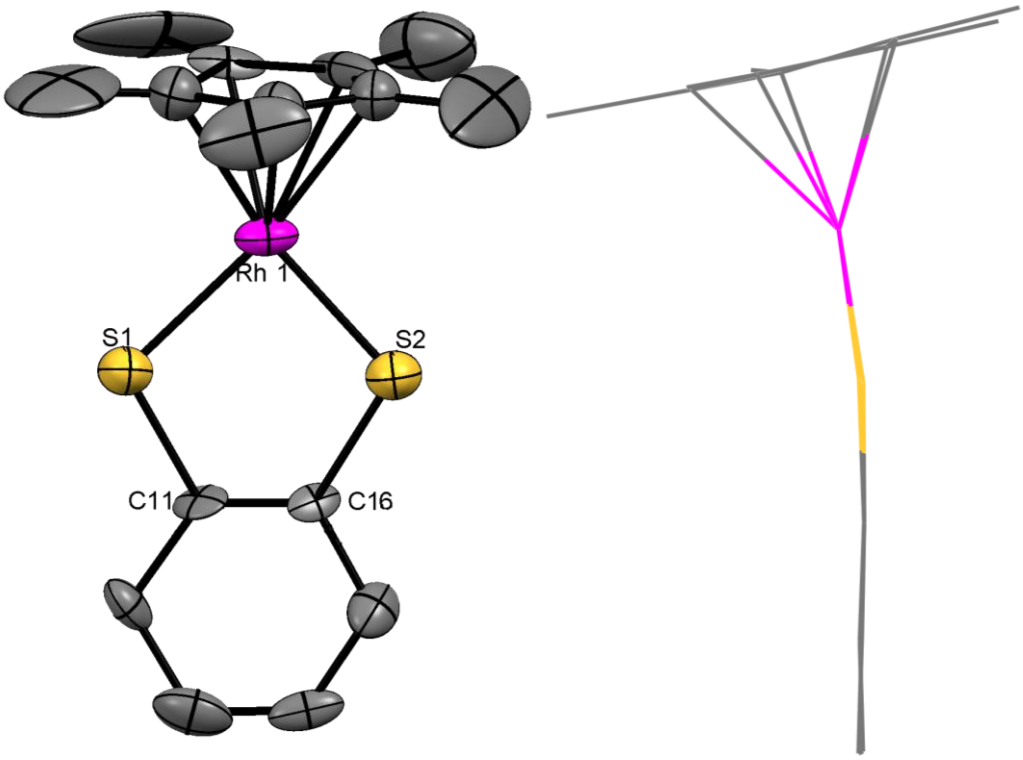

Figure 2-30 Crystal Structure of **7**

Bond Length (Å)		*Bond Angle (°)*		*Torsion Angle (°)*	
S(1)…Rh(1)	2.291(7)	**S(1)-Rh(1)-S(2)**	88.2(2)	**S(1)-C(11)-C(16)-S(2)**	2.00(2)
S(2)…Rh(1)	2.218(7)	**C(11)-S(1)-Rh(1)**	104.0(7)		
S(1)…S(2)	3.140(1)	**C(16)-S(2)-Rh(1)**	105.5(7)		
S(1)…C(11)	1.770(2)				
S(2)…C(16)	1.760(2)				

Table 2-7 Selected Bond Lengths for **7**

2.3.4 Ir & Rh Dibenzo[*c*,*e*]-1,2-dithiol Complexes

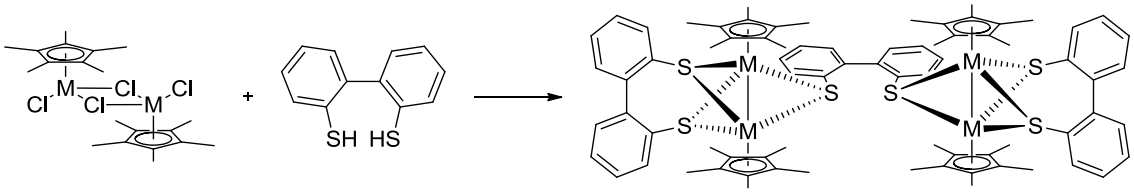

Scheme 2-6 Preparation of **9**

While the dibenzo[*c*,*e*]-1,2-dithiol ligand **3**, along with its analogues, is well known,[101] in coordination chemistry only a handful of complexes incorporating **3** have been reported.[102,103] The compounds described further expand knowledge on the coordination of this ligand, to include half-sandwich Ir and Rh complexes.

Dibenzo[*c*,*e*]-1,2-dithiol **3** is an interesting ligand with which to expand this series further. Unlike the other ligands dealt with in **Section 2.3.1** and **Section 2.3.3**, where the donor atoms contain aromatic backbones that are planar and are restricted in their movement, the biphenyl ligand is able to rotate freely about the phenyl link though. Complexes made with this ligand will be forced to adopt different bonding geometries to those of **1** and **2**. This is mainly due to the increased ring size when coordinated; a seven-membered ring, compared to five- and six-membered for **1** and **2** respectively.

Reaction of ligand **3** with Cp^*RhCl_2 gave different results to that of the Rh material. The reaction of **3** with Cp^*IrCl_2 yielded a precipitate that was insoluble in all but the most polar solvents such as DMSO. Unfortunately no solvent dissolved the compound well enough to get NMR or other data. The rhodium analogue, however, yielded an orange product (**9**) that was readily soluble in most chlorinated and polar solvents.

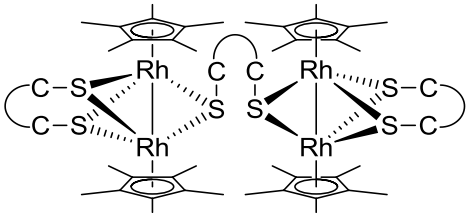

9

Figure 2-31 Structure of **9**

NMR data of **9** yielded different, yet interesting results to those of **4**-**7**. The aromatic signals of the ligand were as expected and similar to complexes of **1** and **2**. These aromatic signals were present between 9.16 and 7.4 ppm, along with the associated splitting. The non-aromatic region of the spectrum, however, was vastly different. Unlike those previously studied complexes where the Cp* methyl protons produced a single well defined and sharp singlet, the methyl region (1.4 to 0.94 ppm) of **9** was rather crowded, suggesting that it was impure. After further purification through chromatography and drying for several days, the same peaks were still observed.

Crystals of **9** were grown from the slow evaporation of a saturated solution in dichloromethane. The quality of the data collected was of good quality with residual R1 factor of 8.8%.

The geometry of **9** is markedly different to those previously discussed. The structure of **9** composes of four Cp*Rh subunits with piano stool like structure linked together by three biphenyl ligands (**Figure 2-31**).

X-ray diffraction of crystals grown from the isolated material showed that this ligand behaves differently to that of **1** and **2**. The structure elucidated shows that one ligand bridges two Cp*Rh metal centres (**Figure 2-32**). Another ligand bridges two of those units yielding a tetramer-like structure (**Figure 2-31**). In this example, ligand 3 acts as both a μ^2 and μ^4 bridge.

As there is free rotation about the C-C link joining the two benzene units of the ligand no plane angle can be described with respect to either the Cp* or M-S-S plane. There is however the rotation of the benzene units to each other with terminal biphenyl ligands possessing rotation of 33.86 and 36.12° and the central biphenyl ligand rotated by 56.73°

Depending on the angle between the two phenyl rings, there is a corresponding increase in the 2…2' interatomic distance. This varying distance is responsible for this ligand's ability to bridge the two and four metal centres in **9**. For the μ^2-ligand with a torsion angle of 38°, the S—S distance is 3.046, while for the μ^4-ligand with a torsion of 66°, the distance increases to 3.434 Å. That corresponds to an increase of 0.14 Å for every 10° increase of torsion.

The pro-ligand, dibenzo[*c*,*e*]-1,2-dithiol, has an interatomic S…S distance of 3.65 Å, along with a torsion angle of 90°. However, as the ligand is able to rotate freely about the phenyl link, comparing the measurements between the pro-ligand and that of the coordinated ligand is not helpful. The splay angle, on the other hand, is an important measurement. This will quantify the degree of change which the bond angles have incurred upon coordination, especially in the case of the μ^4-ligand, as this will have to change the most in order to accommodate the four metal centres.

The pro-ligand has a splay totalling 476.7°, while the μ^2- and μ^4-ligands have a splay of 520.6 and 497.3° respectively. For comparison, the splay angle of biphenyl is 494.1°.

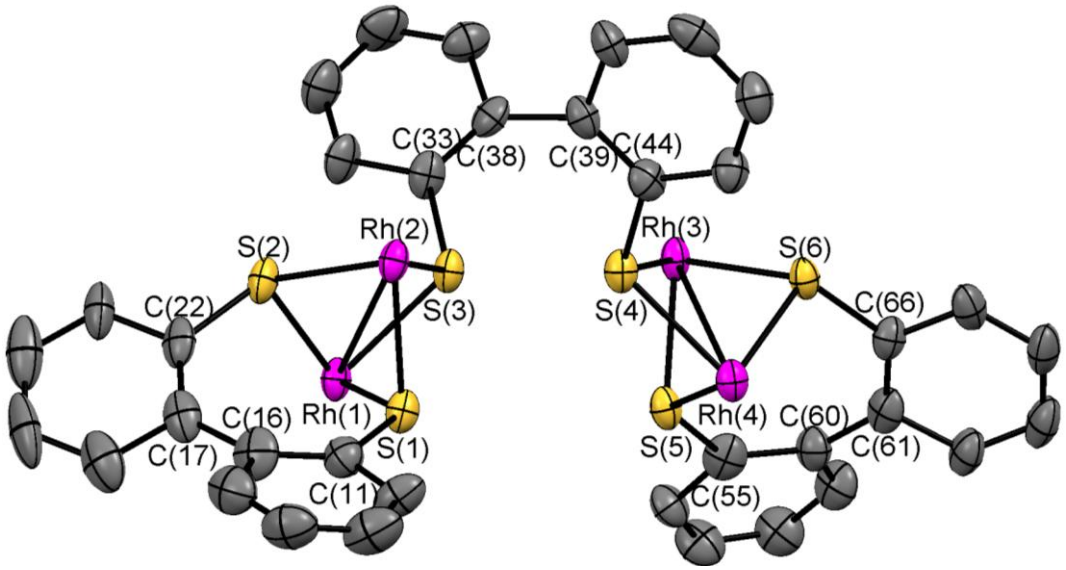

Figure 2-32 Crystal Structure of **9**
Cp* rings have been omitted for clarity

Bond Length(Å)		*Bond Angle (°)*		*Torsion Angle (°)*	
S(1)…Rh(1)	2.384(3)	**S(1)-Rh(1)-S(2)**	80.0(1)	**S(1)-C(11)-C(22)-S(2)**	21.8(5)
S(1)…Rh(2)	2.370(3)	**S(1)-Rh(2)-S(2)**	80.2(1)	**S(3)-C(33)-C(44)-S(4)**	68.8(5)
S(2)…Rh(1)	2.347(3)	**C(11)-S(1)-Rh(1)**	122.0(4)	**S(5)-C(55)-C(66)-S(6)**	17.8(5)
S(2)…Rh(2)	2.368(3)	**C(11)-S(2)-Rh(2)**	102.3(4)	**C(11)-C(16)-C(17)-C(22)**	38.0(2)
S(3)…Rh(1)	2.444(3)	**C(22)-S(2)-Rh(1)**	104.3(4)	**C(33)-C(38)-C(39)-C(44)**	66.0(2)
S(3)…Rh(2)	2.426(3)	**C(22)-S(2)-Rh(2)**	120.4(4)	**C(55)-C(60)-C(61)-C(66)**	38.0(2)
S(1)…S(2)	3.046(4)	**C(33)-S(3)-Rh(1)**	112.4(4)		
S(3)…S(4)	3.434(4)	**Rh(1)-S(1)-Rh(2)**	86.5(1)		
Rh(1)…Rh(2)	3.256(1)	**Rh(1)-S(2)-Rh(2)**	87.4(1)		
S(1)…C(11)	1.800(1)	**Rh(1)-S(3)-Rh(2)**	83.9(9)		
S(2)…C(22)	1.790(1)				
S(3)…C(33)	1.810(1)				
S(4)…S(44)	1.780(1)				

Table 2-8 Selected Bond Lengths for **9**

2.3.5 Monomeric Ir & Rh Dibenzo[*c*,*e*]-1,2-dithiol Complexes

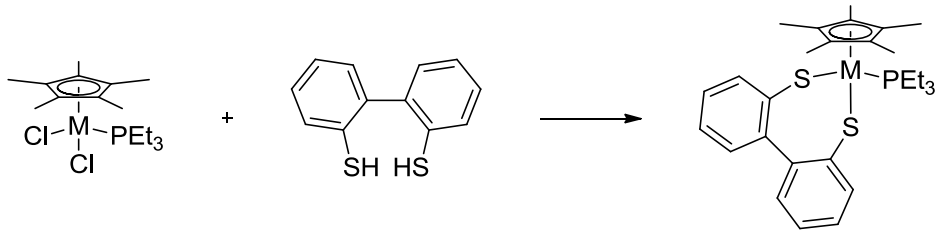

Scheme 2-7 Preparation of **8B** and **9B**

While the reaction of **3** with the rhodium pro-complex yielded the tetramer-like complex **9**, the iridium analogue produced an insoluble yellow material that could not be studied. In order to study the difference between Ir and Rh with ligand **3**, PEt_3 was coordinated giving a pro-complex which possessed markedly improved solubility. More importantly however, was that the phosphine occupied one coordination site, leaving only two empty sites, essentially inhibiting the possibility of synthesising polymeric complexes.

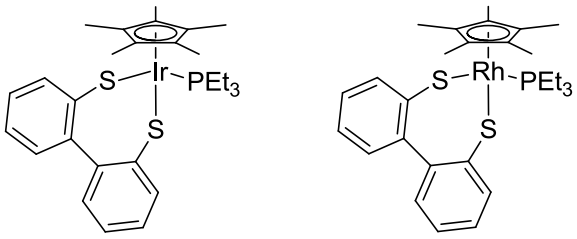

8B **9B**

NMR studies of **8B** and **9B** yield near identical results to those of **4B** and **5B**, except with the added signals due to the two extra protons in the above complexes. The PEt_3 signals also show up as overlapping doublet-of-triplets and a pseudo-pentet at ~1 and ~2 ppm respectively, with the extra splitting of the ethyl group due to the ^{31}P. In the ^{13}C NMR, the Cp* quaternary signals have also been split into a doublet, with coupling constants of 4 and 3.1 Hz.

The ^{1}H NMR spectrum of 9B is shown below (**Figure 2-33**). As it can be seen, there is complex splitting primarily from the ligand. This splitting is due to the spin active rhodium centre. There is also splitting encountered

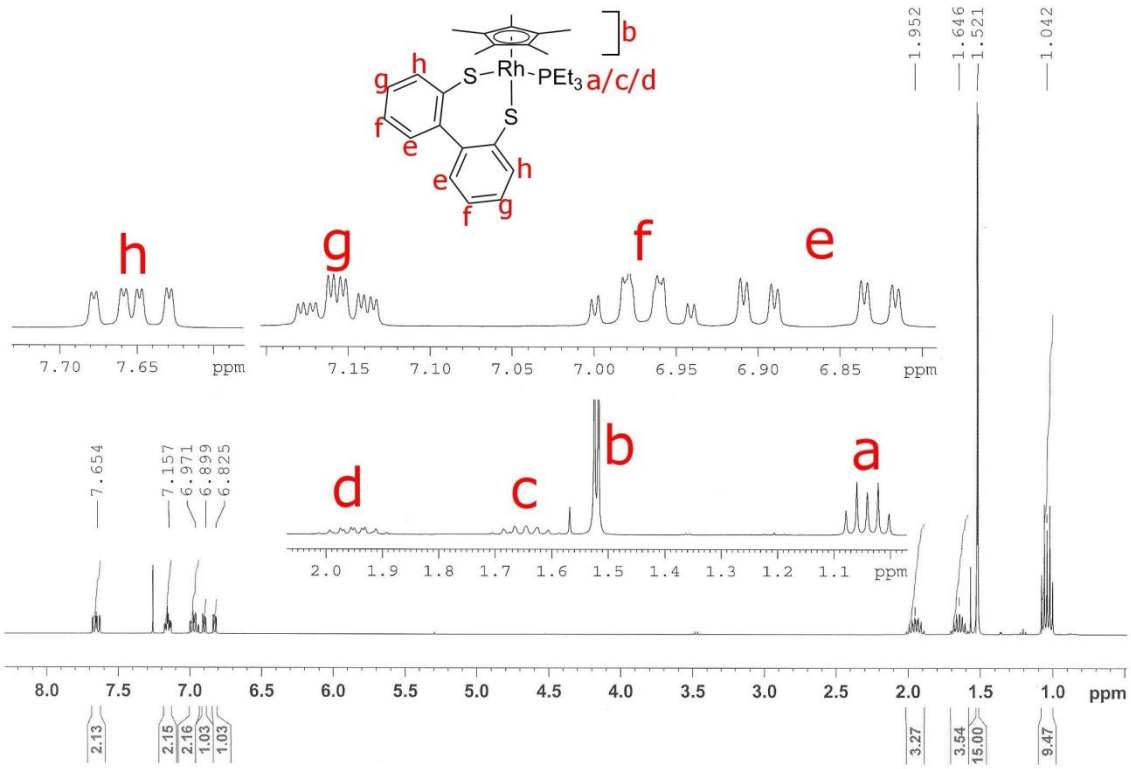

Figure 2-33 ^{1}H NMR Spectrum of **9B**

Crystals of **8B** and **9B** were grown from the slow evaporation of a saturated solution in dichloromethane. The crystals analysed provided data that possessed residual R1 factor of 10.8 and 7.6% respectively. The results obtained were as expected with structural formulae of $[Cp^*IrC_{12}H_8S_2PEt_3]$ for **8B** and $[Cp^*RhC_{12}H_8S_2PEt_3]$ for **9B**.

As mentioned for **9**, the ligand possesses a C-C link joining the two benzene subunits. This allows the ligand to rotate in order to minimise the contortion associated upon complexation. As such, no plane can be described with respects to either the Cp* plane or the M-S-S plane which has been discussed in previous complexes. The angle of the two benzene rings to each other can be described and has been calculated

The geometry of these is different to those previously discussed with these being termed as two-legged piano stool. The structure of **6** & **7**and are essentially T-shape structures with a slight buckling about the sulfur-sulfur . The M-S-S plane angle, with respect to the benzene ring plane is 8.12° for **6** and 9.08 for **7**. The Cp* plane and the benzene plane are essentially perpendicular. This is very different to the compounds previously discussed where they were virtually parallel. In the case of **6**, the angle of the Cp* plane to the benzene plane is 77.63°, while for **7**, this angle is 75.29°.

The crystallographic data shows that **8B** and **9B** differ only very slightly. The S…M bond length of the former is 2.417 Å and that of the latter is 2.378 Å. Little difference was observed in the angles, and only differ from each other by a maximum of 1°. The bonding of the ligand in **9** is very different to the bonding in **9B**, comparing the bonding and ligand geometries makes it difficult as they bear little resemblance to each other.

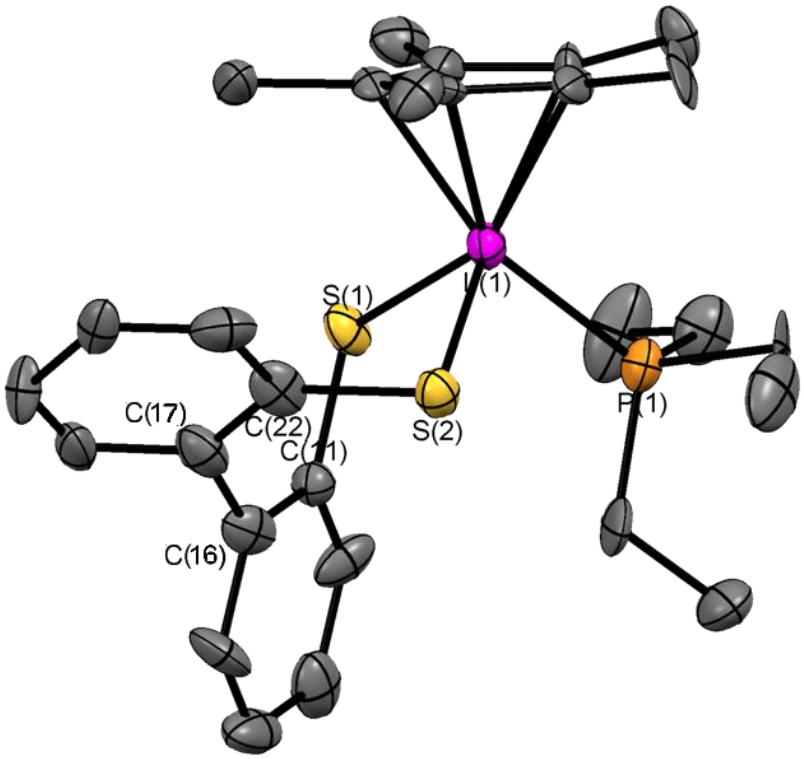

Figure 2-34 Crystal Structure of **8B**

Bond Length (Å)		*Bond Angles (°)*		*Torsion Angle (°)*	
S(1)…Ir(1)	2.417(5)	**S(1)-Ir(1)-S(2)**	92.1(1)	**S(1)-C(11)-C(22)-S(2)**	76.4(6)
S(2)…Ir(1)	2.412(5)	**C(1)-S(1)-Ir(1)**	116.7(5)	**C(11)-C(16)-C(17)-C(22)**	69.0(2)
Ir(1)…P(1)	2.320(6)	**C(9)-S(2)-Ir(1)**	104.3(5)		
S(1)…S(2)	3.476(7)				
S(1)…C(11)	1.790(1)				
S(2)…C(22)	1.800(2)				

Table 2-9 Selected Bond Lengths for **8B**

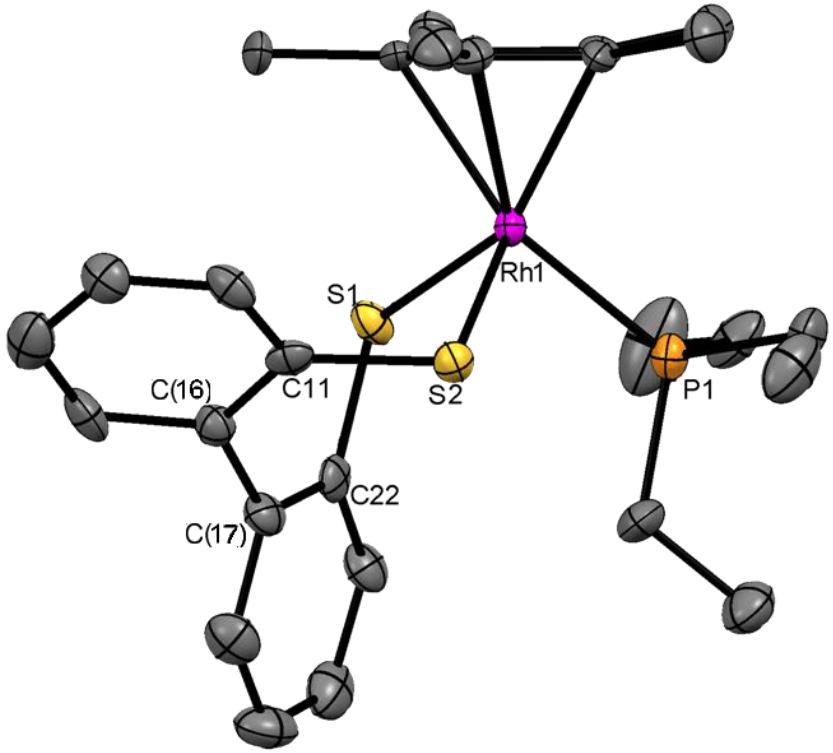

Figure 2-35 Crystal Structure of **9B**

Bond Length (Å)		*Bond Angles (°)*		*Torsion Angle (°)*	
S(1)…Rh(1)	2.378(2)	**S(1)-Rh(1)-S(2)**	92.73(7)	**S(1)-C(11)-C(22)-S(2)**	75.6(3)
S(2)…Rh(1)	2.380(2)	**C(1)-S(1)-Rh(1)**	115.8(3)	**C(11)-C(16)-C(17)-C(22)**	68.0(1)
Rh(1)…P(1)	2.294(2)	**C(9)-S(2)-Rh(1)**	105.0(3)		
S(1)…S(2)	3.444(3)				
S(1)…C(11)	1.740(1)				
S(2)…C(22)	1.800(1)				

Table 2-10 Selected Bond Lengths for **9B**

2.4 Experimental

General Procedures

Unless otherwise stated, all operations were performed under anaerobic conditions using a nitrogen atmosphere and standard Schlenk techniques. Dry and deoxygenated solvents were dispensed from an MBraun SPS-800 Solvent Purification System. Methanol and ethanol were dried by refluxing over their corresponding magnesium alkoxide salts and distilling under nitrogen. $IrCl_3 \cdot 3H_2O$ and $RhCl_3 \cdot 3H_2O$ were received from Johnson Matthey, Inc. All other reagents and chemicals were purchased from Sigma Aldrich, Alfa Aesar or Acros Organics. All chemicals/reagents were used as received without any further purification, unless otherwise stated. All NMR data was recorded using either a Jeol GSX Delta 270 or Bruker Avance 300, locked to external reference. Peaks are quoted as ppm, while coupling constants, if stated, are in Hz. Infrared spectra were recorded as KBr disks on a Perkin-Elmer FT-IR/Raman System 2000 spectrophotometer in the range of 4000-400 cm^{-1}. Mass spectra analyses were performed by the University of St Andrews Mass Spectrometry Service. Elemental analyses were performed by the Elemental Analysis service provided by London Metropolitan University.

The corresponding thiols were prepared by a slight modification to the published procedure.[104]

Syntheses of Starting Materials

2.4.1 Preparation of $[\eta^5\text{-Cp*IrCl}_2]_n$[105]

To a solution of $IrCl_3 \cdot 3H_2O$ (5 g, 14 mmol) in methanol (50 mL), 1,2,3,4,5-pentamethylcyclopentadiene (2.6 g, 20 mmol) was added. The mixture was then refluxed for 48 h. The solution was then cooled and the precipitate was filtered, washed with ethanol (3× 25 mL) and diethyl ether (3× 25 mL) and allowed to dry by air-stream. Yield 4.7 g, 85%.

2.4.2 Preparation of $[\eta^5\text{-Cp*RhCl}_2]_n$[105]

To a solution of $RhCl_3 \cdot 3H_2O$ (5 g, 21 mmol) in methanol (50 mL), 1,2,3,4,5-pentamethylcyclopentadiene (3 g, 22 mmol) was added. The mixture was then refluxed for 48 h. The solution was then cooled and the precipitate was filtered. The filtrate was condensed to ~25 mL, and cooled in an ice bath for 30 mins. Any precipitate formed was filtered over previous precipitate, washed with ethanol (3× 25 mL) and diethyl ether (3× 25 mL) and allowed to dry by air-stream. Yield 5.8 g, 90%.

2.4.3 Preparation of $[\eta^5\text{-Cp*Ir(PEt}_3)\text{Cl}_2]$

To a solution of $[\eta^5\text{-Cp*IrCl}_2]_2$ (0.2 g, 0.5 mmol) in THF (50 mL), PEt_3 (0.09 g, 0.75 mmol) was added and the solution was refluxed for 2 h. Once cooled, the solution was evaporated under Schlenk conditions to remove the solvent and any unreacted phosphine. Ether (25 mL) was added to the solid and stirred for 15 mins. The yellow solution was filtered off using a syringe capped off with filter paper and Teflon tape. This was repeated until the solution was near colourless. The combined solution was evaporated yielding a yellow crystalline powder. Yield 0.16 g, 62%.

2.4.4 Preparation of $[\eta^5\text{-Cp*Rh(PEt}_3)\text{Cl}_2]$

To a solution of $[\eta^5\text{-Cp*RhCl}_2]_2$ (0.2 g, 0.65 mmol) in THF (50 mL), PEt3 (0.15 g, 1.3 mmol) was added and the solution was refluxed for 2 h. Once cooled, the solution was evaporated under Schlenk conditions to remove the solvent and any unreacted phosphine. Ether (25 mL) was

added to the solid and stirred for 15 mins. The yellow solution was filtered off using a syringe capped off with filter paper and Teflon tape. This was repeated until the solution was near colourless. The combined solution was evaporated yielding a yellow crystalline powder. Yield 0.16 g, 80%.

2.4.5 Preparation of naphtho[1,8-*cd*]-1,2-dithiole[106]

Naphthalene (3.85 g, 30 mmol) was dissolved in hexane (45 mL). To it, *n*-butyllithium (120 mmol) and TMEDA (18 mL, 0.121 mol) was added. The solution was heated to 60° C. for 3 h. The brown suspension was cooled to -78 °C and THF (100 mL) was added. Sulfur flowers (8 g, 0.25 mol) was added with vigorous stirring and allowed to warm to RT. The mixture was washed with water (100 mL) and the organic layer was kept dried over $MgSO_4$ and evaporated under reduced pressure. Purification of the red-brown oil by column chromatography (silica gel, hexane) afforded red-brown powder which was washed with ethanol (1-2 mL), filtered and allowed to dry over suction. Yield: 2.1g, 36%.

The corresponding thiol was prepared by the slow addition of the dithiolate in THF into an ethanol suspension of $NaBH_4$ (2.5 eq.) at 0° C. Once the addition was complete, the solution was allowed to stir for 15 mins. The acidification of the solution with HCl (3 M) quenched the excess NaBH4 and acidified the thiolates to thiols. The solution was washed with diethyl ether and the organic layer was extracted and dried over $MgSO_4$. Evaporation of the solvent yielded an off white waxy material with a yield of ~80%.

2.4.6 Preparation of dibenzo[*c*,*e*]-1,2-dithiine[107]

Biphenyl (5 g, 32.4 mmol) was added in small portions to a solution of 2.5 M *n*-butyllithium (64.85 mmol) in hexane and TMEDA (9.72 mL, 64.85 mmol) at -15 °C over the course of an hour. The mixture was allowed to warm to RT overnight and sulfur flowers (2.28 g, 71.28 mmol) was added slowly with vigorous stirring over 3 h. The mixture was poured into water (300 mL) and the organic layer was extracted with DCM, dried over Na_2SO_4 and concentrated *in vacuo*. Column chromatography (silica gel, petroleum ether (40-60°) afforded a bright yellow powder which was subsequently washed with ethanol (1-2 mL) and filtered. Yield: 3.16 g, 45%.

The corresponding thiol was prepared by the slow addition of the dithiolate in THF into an ethanol suspension of $NaBH_4$ (2.5 eq.) at room temperature. Once the addition was complete, the solution was allowed to stir for 15 mins. The acidification of the solution with HCl (3 M) quenched the excess NaBH4 and acidified the thiolates to thiols. The solution was washed with diethyl ether and the organic layer was extracted and dried over $MgSO_4$. Evaporation of the solvent yielded a white waxy material with a yield of ~80%.

2.4.7 Preparation of 8-aminonaphthalene-1-thiol[108]

Lithium aluminium hydride (3 g, 80 mmol) was added to diethyl ether (100 mL). To it, 1,8-naphthosultam (4 g, 20 mmol) in THF (15 mL) was added dropwise to the suspension at -38 °C over 1 h. The mixture was then refluxed for 1 h, after which, the solution was cooled in an ice-salt bath, and the excess lithium aluminium hydride was quenched with the slow addition of water (10 mL). Sulfuric acid (100 mL, 2 M) was added. Any excess acid was neutralised with NaOH, and the product was extracted with ether, dried over $MgSO_4$ and evaporated to dryness. The product is air sensitive and is this stored under nitrogen. Yield: 2.41 g, 69%.

Synthesis of Complexes

2.4.8 Synthesis of $[\eta^5\text{-Cp*Ir}(\mu^2\text{-NaphS}_2)]_2$ (4)

To a solution of $[\eta^5\text{-Cp*IrCl}_2]_2$ (0.2 g, 0.52 mmol) in DCM (50 mL), naphthalene-1,8-dithiol (0.192 g, 1 mmol) was added in one portion. The solution was refluxed for 4 hrs, after which the solvent was evaporated. The solid material was washed with hexane (3× 50 mL) to remove excess ligand. Column chromatography (silica, toluene) yielded a yellow product. Yield 0.05 g, 10%. M. S. (ESI): *m/z* 517 (M^+, 100%). E. A. found (calculated, %) C: 46.29 (46.40), H: 4.13 (4.09). ^{1}H NMR ($CDCl_3$) δ: 1.22 (s, 15 H, C_5Me_5), 7.12 (q, *J* = 7.56 and 7.74, 2H, ArCH), 7.51 (d of d, *J* = 7.87 and 1.18, 1H, ArCH), 7.75 (m, 2H, ArCH), 8.15 (d of d, *J* = 7.29 and 1.35, 1H, ArCH). ^{13}C NMR ($CDCl_3$) δ: 7.7 (s, Cp*Me), 91.1 (s, q, Cp*), 113.5 (s, q, ArC), 127.4 (s, q, ArC), 123.2 (s, ArC), 124.0 (s, ArC), 125.0 (s, ArC), 128.4 (s, ArC), 129.3 (s, ArC), 130.2 (s, ArC).

2.4.9 Synthesis of [η⁵-Cp*Ir(μ²-NaphS₂)PEt₃] (4B)

To a solution of [η^5-Cp*Ir(PEt_3)Cl_2] (0.114 g, 0.22 mmol) in THF (50 mL), naphthalene-1,8-dithiol (0.06 g, 0.3 mmol) was added in one portion. The mixture was then refluxed for 2 hrs, after which the solvent was evaporated. The solid material was washed with hexane (3× 50 mL) to remove excess ligand. Purification via column chromatography (silica, DCM) yielded a yellow product. Yield 0.10 g, 90%. (ESI): *m/z* 637 (M^+, 100%). E. A. found (calculated, %) C: 49.07 (49.11), H: 5.65 (5.71). ^{1}H NMR ($CDCl_3$) δ: 1.0 (d of t, *J* = 7.6 and 7.9, 9H, CH_3), 1.50 (d, *J* = 1.9, 15H, Cp*Me_5), 2.09 (m, 6H, CH_2), 6.93 (t, *J* = 7.6, 2H, ArCH), 7.43 (d of d, *J* = 8.1, 2H, ArCH), 7.91 (d of d, *J* = 7.3, 2H, ArCH). ^{31}P NMR ($CDCl_3$) δ: -13.23 ppm (s, PEt_3). ^{13}C NMR ($CDCl_3$) δ: 6.9 (d, $J_{C\text{-}P}$ = 2.92, P(CH_2)CH_3), 8.3 (s, Cp*Me), 15.2 (d, $J_{C\text{-}P}$ = 35.6, PCH_2), 94.8 (s, q, $J_{C\text{-}P}$ = 2.8, Cp*), 123.9 (s, ArC), 124.3 (s, ArC), 127.3 (s, ArC), 133.5 (s, q, ArC), 136.5 (s, q, ArCH), 137.4 (d, q , $J_{C\text{-}P}$ = 4.8, ArC).

2.4.10 Synthesis of [η⁵-Cp*Ir(μ²-BenzS₂)] (6)

To a solution of [η^5-Cp*Ir(PEt_3)Cl_2] (0.12 g, 0.23 mmol) in THF (25 mL), benzene-1,2-dithiol (0.07 g, 0.46 mmol) was added and refluxed for 2 h during which the colour of the solution darkened. The solvent and excess ligand is removed under vacuo with heating for 4 hours. Purification via column chromatography (silica, DCM) yielded a brown/orange product. Yield 0.08 g, 73%. M. S. (ESI): *m/z* 490 (M^++Na). ^{1}H NMR ($CDCl_3$) δ: 2.2 (s, 15H, Cp*Me_5), 7.04 (d of d, *J* = 3.30 and 2.7, 2H, ArCH), 8.05 (d of d, *J* = 3.32 and 2.71, 2H, ArCH). ^{13}C NMR ($CDCl_3$) δ: 10.70 (s, Cp*Me), 91.99 (s, Cp*), 123.1 (s, ArC), 129.74 (s, ArC), 153.24 (s, ArC).

2.4.11 Synthesis of [η⁵-Cp*Ir(μ²-BiphenS₂)PEt₃] (8B)

To a solution of [η^5-Cp*Ir(PEt_3)Cl_2] (0.173 g, 0.34 mmol) in THF (50 mL), dibenzo[*c*,*e*]-1,2-dithiol (0.15 g, 0.7 mmol) was added in one portion. The solution was subsequently refluxed for 2 hrs, after which the solvent was evaporated. The solid material was washed with hexane (3× 50 mL) to remove excess ligand. Purification via column chromatography (silica, DCM) yielded an orange product. Yield 0.15 g, 83%. M. S. (ESI): *m/z* 685 (M^++Na). E. A. found (calculated, %) C: 50.72 (50.81), H: 5.79 (5.70). ^{1}H NMR ($CDCl_3$) δ: 1.0 (d of t, *J* = 7.6 and 7.9, 9H, CH_3), 1.55 (d, *J* = 2, 15H, Cp*Me_5), 1.7 (m, 3H, CH_2), 2.0 (m, 6H, CH_2), 6.8 (d of d, *J* = 7.6, 1H, ArCH), 6.9 (m, 3H, ArCH), 7.1 (m, 2H, ArCH), 7.6 (d of d, *J* = 7.6, 1H, ArCH), 7.6 (d of d, *J* = 7.6, 1H, ArCH). ^{31}P NMR

($CDCl_3$) δ: -14.9 (PEt3). ^{13}C NMR ($CDCl_3$) δ:7.75 (d, J_{C-P} = 3.5, P(CH_2)CH_3), 8.1 (s, Cp*Me), 16.1 (d, J_{C-P} = 33.6, PCH_2), 94.1 (d, q, J_{C-P} = 3.1, Cp*), 125.4 (s, ArC), 125.5 (s, ArC), 125.6 (s, ArC), 126.2 (s, ArC), 131.1 (s, ArC), 131.5 (s, ArC), 136.2 (s, ArC), 137.1 (s, ArC), 137.3 (s, q, ArC), 151.0 (s, q, ArC), 151.6 (s, q, ArC).

2.4.12 Synthesis of [η^5-Cp*Rh(μ^2-NaphS$_2$)]$_2$ (5)

To a solution of [η^5-Cp*RhCl$_2$]$_2$ (0.1 g, 0.32 mmol) in THF (25 mL), naphthalene-1,8-dithiol (0.1 g, 0.5 mmol) was added. The resulting mixture was refluxed for 2 hours. The colour of the solution did not change, but a precipitate was formed. The precipitate was filtered, washed with THF (20 mL) and diethyl ether (20 mL) and dried. The product was purified using column chromatography (silica, chloroform:ethanol (9:1)). 0.06 g, Yield 55%. M. S. (ESI): *m/z* 428 (M^+, 100%). E. A. found (calculated, %) C: 56.23 (56.07), H: 4.69 (4.94). ^{1}H NMR ($CDCl_3$) δ: 1.18 (s, 2H, Cp*Me), 7.16 (d of t, *J* = 7.58 and 6.94, 2H, ArCH), 7.51 (d of d, *J* = 8.06 and 1.17, 1H, ArCH), 7.71 (d of d, *J* = 8.06 and 1.17, 1H, ArCH), 7.79 (d of d, *J* = 7.32 and 1.38, 1H, ArCH), 8.14 (d of d, *J* = 7.32, 1.39, 1H, ArCH). ^{13}C NMR ($CDCl_3$) δ: 8.10 (s, Cp*Me), 96.61 (d, q, *J* = 6.13, Cp*), 123.36 (s, ArC), 124.84 (s, ArC), 125.00 (s, ArC), 129.29 (s, ArC), 129.37 (s, ArC), 130.52 (s, q, ArC), 132.04 (s, ArC), 135.60 (s, q, ArC), 136.21 (s, q, ArC).

2.4.13 Synthesis of [η^5-Cp*Rh(μ^2-NaphS$_2$)PEt$_3$] (5B)

To a solution of [η^5-Cp*Rh(PEt$_3$)Cl$_2$] (0.2 g, 0.47 mmol) in THF (50 mL), naphthalene-1,8-dithiol was added and heated at 70° for 2 hours. The solution was then evaporated and washed with hexane (3× 50 mL). Column chromatography (silica, DCM) yielded a dark yellow product. Yield 0.18, 81%. E. A. found (calculated, %) C: 57.21 (57.13), H: 6.58 (6.64). ^{1}H NMR ($CDCl_3$) δ: 1.06 (d of t, *J* = 7.62, 9H, P(CH2)*C*H3), 1.45 (d, *J* = 2.81, 15H, Cp*Me), 2.02 (m, 6H, P*C*H2), 7.01 (t, *J* = 7.63, 2H, ArCH), 7.43 (d of d, J = 8.17 and 1.21, 2H, ArCH), 7.86 (d of d, *J* = 7.23 and 1.28, 2H, ArCH). ^{13}C NMR ($CDCl_3$) δ: 7.52 (s, P(CH_2)CH_3), 8.86 (s, Cp*Me), 16.00 (d, J_{C-P} = 29.63, PCH2), 99.69 (s, q, Cp*), 123.77 (s, ArC), 124.85 (s, ArC), 128.32 (s, ArC), 134.28 (s, q, ArC), 136.40 (s, q, ArC), 139.82 (d, q, J_{C-Rh} = 4.15, ArC).

2.4.14 Synthesis of [η⁵-Cp*Rh(μ²-NaphNS)] (5NS)

To a solution of $[\eta^5\text{-Cp*RhCl}_2]_2$ (0.2 g, 0.52 mmol) in DCM (50 mL), 8-amminonaphthalene-1-thiol (0.16 g, 0.85 mmol) was added in one portion. The solution was refluxed for 2 hrs, after which the solvent was evaporated. The solid material was washed with ether (3× 50 mL) to remove excess ligand. Yield 0.05, 31%. M. S. (ESI): *m/z* 501 (M^+-Cl). ^{1}H NMR ($CDCl_3$) δ: 1.22 (s, 15 H, C_5Me_5), 7.12 (q, *J* = 7.56 and 7.74, 2H, ArCH), 7.51 (d of d, *J* = 7.87 and 1.18, 1H, ArCH), 7.75 (m, 2H, ArCH), 8.15 (d of d, *J* = 7.29 and 1.35, 1H, ArCH). ^{13}C NMR ($CDCl_3$) δ: 7.7 (s, Cp*Me), 91.1 (s, q, Cp*), 113.5 (s, q, ArC), 127.4 (s, q, ArC), 123.2 (s, ArC), 124.0 (s, ArC), 125.0 (s, ArC), 128.4 (s, ArC), 129.3 (s, ArC), 130.2 (s, ArC).

2.4.15 Synthesis of [η⁵-Cp*Rh(μ²-BenzS₂)] (7)

To a solution of $[\eta^5\text{-Cp*Rh(PEt}_3)\text{Cl}_2]$ (0.09 g, 0.21 mmol) in THF (25 mL), benzene-1,2-dithiol (0.07 g, 0.46 mmol) was added and refluxed for 2 h during which the colour of the solution turned purple. The solvent and excess ligand are removed under vacuo with heating for 4 hours. Purification via column chromatography (silica, DCM) yielded a purple product. Yield 0.04, 53%. M. S. (ESI): *m/z* 400 (M^++Na). ^{1}H NMR ($CDCl_3$) δ: 2.0 (s, 15H, Cp*Me_5), 7.11 (d of d, *J* = 3.30 and 2.7, 2H, ArCH), 8.87 (d of d, *J* = 3.30 and 2.77, 2H, ArCH). ^{13}C NMR ($CDCl_3$) δ: 10.88 (s, Cp*Me), 98.55 (d, J = 7.15, Cp*), 130.1 (d, J = 3.84, ArC), 152.7 (s, ArC).

2.4.16 Synthesis of [(η⁵-Cp*Rh)₄(μ²-BiphenS₂)₂(μ⁴-BiphenS₂)] (9)

To a solution of $[\eta^5\text{-Cp*RhCl}_2]_2$ (0.2 g, 0.65 mmol) in THF (50 mL), dibenzo[*c*,*e*]-1,2-dithiol (0.35 g, 1.6 mmol) was added. The resulting mixture was heated at 70° for 2 hours. The solvent was evaporated, and the solid material was washed with hexane and ether (3× 50 mL) to remove any remaining ligand. Column chromatography (silica, DCM) afforded a yellow product. Yield 0.11 g, 55%. M. S. (MALDI): *m/z* 1587 (M^+ -CH_3). ^{1}H NMR ($CDCl_3$) δ: 1.177 (m, 60H, Cp*Me), 7.386 (m, 5H, ArCH), 7.477 (m, 4H, ArCH), 7.525 (m, 5H, ArCH), 7.81 (t, J = 9.16, 4H, ArCH). ^{13}C NMR ($CDCl_3$) δ: 8.60 (m, Cp*Me), 98.82 (s, q, Cp*), 126.13 (s, ArC), 126.56 (s, ArC), 128.73 (s, ArC), 128.86 (s, ArC), 128.98 (s, ArC), 130.77 (s, ArC), 134.70 (s, ArC), 135.93 (s, ArC), 136.47 (s, ArC), 137.24 (s, ArC), 138.44 (s, ArC), 138.64 (s, ArC).

2.4.17 Synthesis of [η^5-Cp*Rh(μ^2-BiphenS$_2$)PEt$_3$] (9B)

To a solution of [η^5-Cp*Rh(PEt$_3$)Cl$_2$] (0.146 g, 0.34 mmol) in THF (50 mL), dibenzo[*c*,*e*]-1,2-dithiol (0.15 g, 0.68 mmol) was added and refluxed for 5 hours. The solution was then evaporated and washed with hexane (3× 50 mL). Column chromatography (silica, DCM) afforded a yellow product. Yield 0.14 g, 89%. E. A. found (calculated, %) C: 58.76 (58.73), H: 6.73 (6.69).^{1}H NMR ($CDCl_3$) δ: 1.04 (d of t, *J* = 7.53, 9H, P(CH_2)*C*H$_3$), 1.52 (d, *J* = 2.84, 15H, Cp*Me), 1.65 (m, 3H, P*C*H$_2$), 1.95 (m, 3H, P*C*H$_2$), 6.83 (d of d, *J* = 7.53 and 1.53, 1H, ArCH), 6.90 (d of d, *J* = 7.53 and 1.53, 1H, ArCH), 6.97 (q of d, J =8.30, 7.53 and 1.53, 2H, ArCH), 7.16 (t of q, *J* = 7.43, 3.06 and 1.31, 2H, ArCH), 7.65 (d of d, *J* = 7.64, 3.93 and 1.20, 2H, ArCH). ^{31}P NMR ($CDCl_3$) δ: 22.47 (d of d, $J_{Rh\text{-}P}$ = 150.24, PEt$_3$). ^{13}C NMR ($CDCl_3$) δ: 8.21 (d, $J_{C\text{-}P}$ = 3.95, P(CH_2)*C*H$_3$), 8.65 (s, Cp*Me), 16.31 (d, $J_{C\text{-}P}$ = 26.48, PCH_2), 99.27 (t, q, $J_{C\text{-}P}$ = 4.00, Cp*), 125.37 (s, ArC), 125.70 (s, ArC), 125.92 (s, ArC), 126.10 (s, ArC), 130.68 (s, ArC), 130.97 (s, ArC), 135.57 (s, ArC), 137.41 (s, ArC), 140.85 (s, q, ArC), 142.64 (s, q, ArC), 150.33 (s, q, ArC), 151.13 (s, q, ArC).

3 RUTHENIUM *bis*(2,2'-BIPYRIDINE) COMPLEXES WITH DITHIOLATO LIGANDS

3.1 Introduction

The homoleptic $[Ru(bpy)_3]^{2+}$ complex (**Figure 3-1**) is one of great importance and is responsible for the development of several areas of chemistry.

Since its initial synthesis in the 1930s,[41] and its first practical use by Paris and Brandt in 1959,[109] the complex was first studied for its use as a photosensitiser by Demas and Adamson. In their paper,[110] they found that the $[Ru(bpy)_3]^{2+}$ acted as a photosensitiser towards other metal complexes, leading to a reaction, for example, aquation. They also believed that it was the first example of a compound that exhibited energy transfer from a transition metal complex in room temperature solutions. In addition, it was found that the complex possessed unusual and interesting spectroscopic properties. The complex had a prominent absorption band λ_{max} at ~550 nm through spin-allowed charge-transfer (CT) processes, and emission through the lowest CT triplet state. It also possessed an extremely high molar extinction coefficient ($\varepsilon > 10^4$) due its metal-to-ligand CT. The complex was also found to be chemically and thermally stable. Through the results of their investigation, it was found that other analogous ruthenium complexes exhibited CT emissions and which could lead to their use as low energy sensitizers.

The Demas & Adamson paper led the way for great interest into d^6 polypyridine complexes due to their exceptional electrochemical and photochemical properties[111] and for their conversion of light energy to chemical energy.[112] The $[Ru(bpy)_3]^{2+}$ complex has also been examined as a photosensitiser for the splitting of water. A photosensitiser is a molecule that readily undergoes photoexcitation which then transfers its energy to another compound causing it to decompose or react further. Excitation through the absorption of a photon

converts the complex to the triplet state $[Ru(bpy)_3]^{2+}$*. The excited complex then transfers an electron to an oxidant resulting in $[Ru(bpy)_3]^{3+}$. This species is a powerful oxidising agent and is able to split water into O_2 and H_2 with the aid of a metal catalyst.[113]

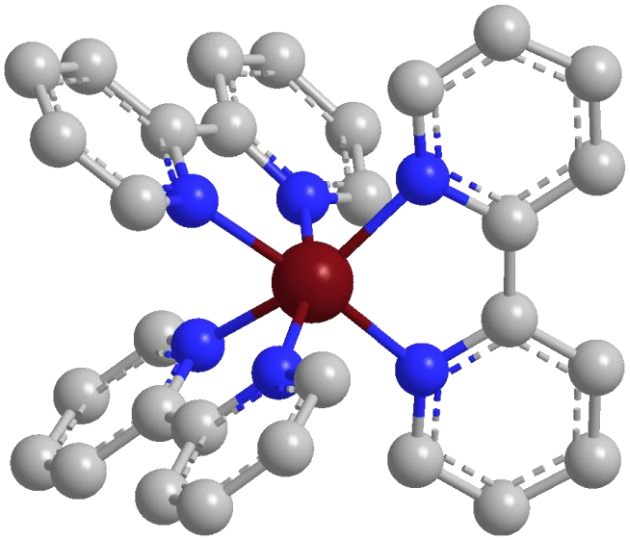

Figure 3-1 Ruthenium *tris*(Bipyridine)

Further potential uses for the $[Ru(bpy)_3]^{2+}$ complex are in the construction of more efficient displays using organic light emitting diodes (OLEDs). Its use in OLEDs could lead to more vivid colours, faster response times, and lower power requirements. $[Ru(bpy)_3]^{2+}$ and its derivatives have attracted the attention of many researchers due to the compounds possessing many important qualities such as chemical stability, redox properties, high extinction coefficient and exited state reactivity, all of which are important properties sought after in chemical research.

The *cis*-ruthenium(II) *bis*-bipyridine family of complexes (**Figure 3-2**) denoted $[Ru(bpy)_2LL]$ (where LL is two monodentate or one bidentate ligand) have been the centre of much study since the first syntheses in 1955,[114] and since then hundreds of complexes have been synthesised with various ligands such as amines, stilbenes, phosphines, oxides, halides, etc.[115] The $[Ru(bpy)_2LL]$ family of complexes has many properties like that of the parent compound $[Ru(bpy)_3]^{2+}$. It has been used as a starting material in order to incorporate many of the desired characteristics possessed by the $[Ru(bpy)_3]^{2+}$ complex, yet still allowing more properties to be added by the new ligand or ligands. One of the key properties that $[Ru(bpy)_2LL]$ complexes

exhibit is strong MLCT absorptions which can be tuned by differing the ligand(s) LL. The drive for the synthesis and study of these complexes is equally as varied. They have been studied for their potential uses in the solar energy industry, as oxidation catalysts in dye-sensitized solar cells, for the photolysis of water to produce dioxygen, and even as reduction catalysts in the electrochemical industry for the production of ethane or ethylene from acetylene.[116] They are also valuable for studying the electrochemistry, spectroscopy, electronic and magnetic behaviour of such complexes.

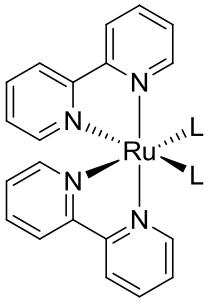

Figure 3-2 Ruthenium *bis*(Bipyridine)

Many of the potential uses for the complexes are due to the strong MLCT bands in the visible region displayed by compounds incorporating the $Ru(bpy)_2$ moiety. This absorption is responsible for potent coloured solutions due to a high extinction coefficient ($\varepsilon > 10^4$). This can be used in colorimetric tests. For example, an efficient sensor testing for the presence of acetate ions (AcO^-) has been created.[117] The 1,10-phenanthroline derived ligand (**Figure 3-3**) incorporates hydrazone into the $Ru(bpy)_2$ complex. It was found that once the complex was deprotonated, the complex can bind to the AcO^- ion and its presence could be detected visually by a change in the colour of the solution, without the need for any kind of instrumentation.

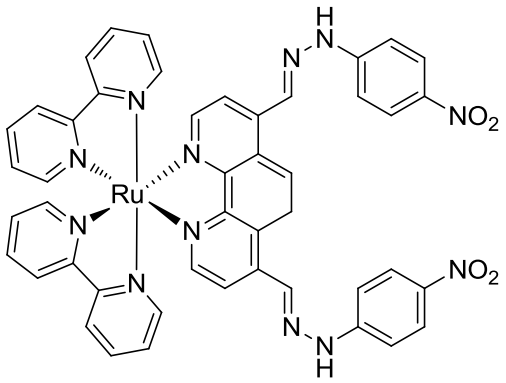

Figure 3-3 Ruthenium *bis*(Bipyridine) with 1,10-Phenanthroline Hydrone Ligand

3.1.1 Photochemistry

Many thousands of ruthenium polypyridyl complexes have been synthesised and studied due to their potential applications in areas such as catalytic synthesis, electrochemistry, photophysical chemistry, biosensors and solar cells.[41] As mentioned above, the realisation that ruthenium bipyridyl complexes were able to catalyse the splitting of water using sunlight,[118] led the way into the possible application of ruthenium polypyridyl complexes in the area of phototechemistry where the complexes act as photosensitizer. Photosensitisation is a process of transferring energy derived from electromagnetic irradiation to a molecular entity via a second molecular entity known as a photosensitizer.[13] The reason ruthenium bipyridyl complexes are used as photosensitizers is due to the fact that ruthenium *tris*-bipyridine and other related complexes when excited, exhibit remarkable properties due to the prolonged lifetime of the excited state. The excited state can then be quenched by several processes such as electron transfer, energy transfer and complex formation.[118] The former is most important as it opens the way for such complexes to be used in light-driven reactions used in energy conversion applications.[119] Research in polypyridyl photosensitizers is mainly dominated by the area of dye-sensitised solar cells (DSC) but is also found in the area of photodynamic therapy. In both cases the photosensitizer is excited by electromagnetic radiation which goes on and transfers the energy imparted to another molecular entity. In DSCs the excited electron is transfered from the photosensitizer to a TiO_2 layer connected to

the electrode, thus generating a current. In photodynamic therapy, however, the photosensitizer is used to transfer the energy to molecular oxygen generating singlet-state oxygen ($^1O_2$). This energetic molecule is then used to either destroy the malignant carcinoma cells or it can also be used to deliver a drug to a specific area.

Dye-Sensitised Solar Cells (DSC) are a class of solar cells developed by Grätzel and O'Regan.[120] Although the use of dyes to generate current through the irradiation of light had been known for several years prior,[121] it wasn't until the Grätzel-O'Regan design, the Grätzel Cell, that the possibilities of using DSC as a source of electricity were wholly realised. Modern DSC are made of several components sandwiched together to generate current. The first layer is that of the transparent anode which is made by doping tin dioxide with fluoride (SnO_2:F) and layering onto a transparent surface like glass. A layer of porous TiO_2 is then spread over the anode then dipped in a solution containing the molecular dye. This permanently bonds the dye and TiO_2. The iodine electrolyte which mediated electrons between the TiO_2 and the cathode is then added. The counter electrode, typically made out of platinum is the added and all the layers are then sandwiched together forming the cell (**Figure 3-4**).

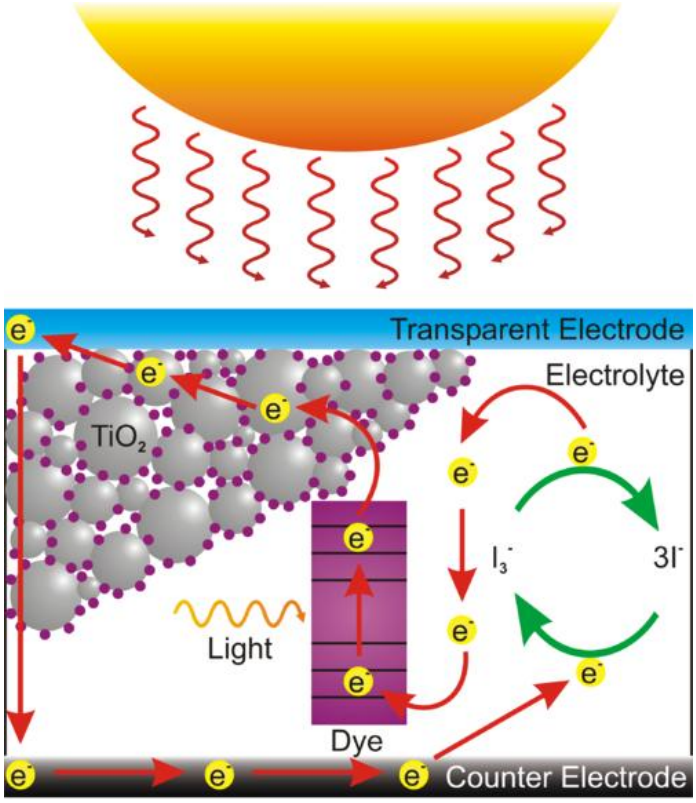

Figure 3-4 Schematic Representation of a Grätzel Cell

Source: www.energyer.com

The ability for DSC to generate an electron is solely due to the photosensitizer. This photosensitizing dye must be capable of absorbing the incident light and must be capable being easily promoted to an excited state. Several different families of dyes have been researched, from organic to inorganic and from complexes to quantum dots. Without a doubt, those that are best suited are polypyridyl complexes of osmium and ruthenium.[122] Of those, it is the complexes of ruthenium bis-(2,2'-bipyridyl-4,4'-dicarboxylic acid) with cyanide, thiocyanate, acetyl acetonate, thiocarbamate ligards that are most promising (**Figure 3-5**).[122]

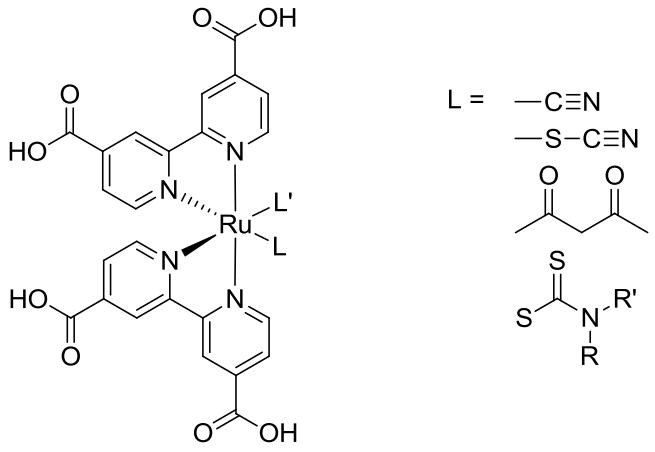

Figure 3-5 Promising Ru-based Dyes

In 2003, a new milestone was achieved by the Grätzel group with the introduction and publication of a DSC using a new dye known as Z-907 (**Figure 3-6**).[123] DSC using this dye as the photosensitizer have an efficiency of 8.2%.

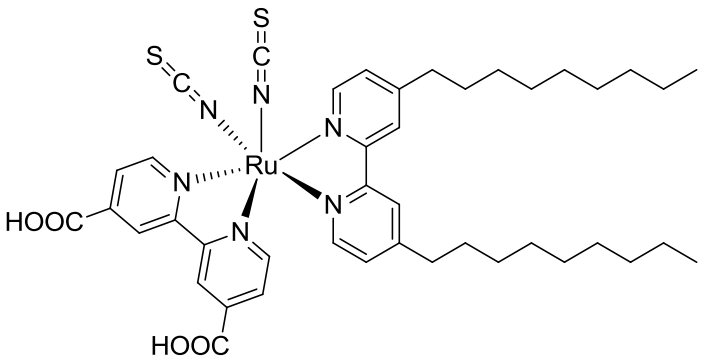

Figure 3-6 Z-907 Dye

The Ru dye known as N3 has become the standard by which all other dyes are tested. This dye, when part of a Grätzel-cell has an absorption maxima at 518 and 380 nm with an overall efficiency of 7.1 – 10% has only been surpassed by the recent dye known as "Black Dye" with an overall efficiency of 10.4%.[124]

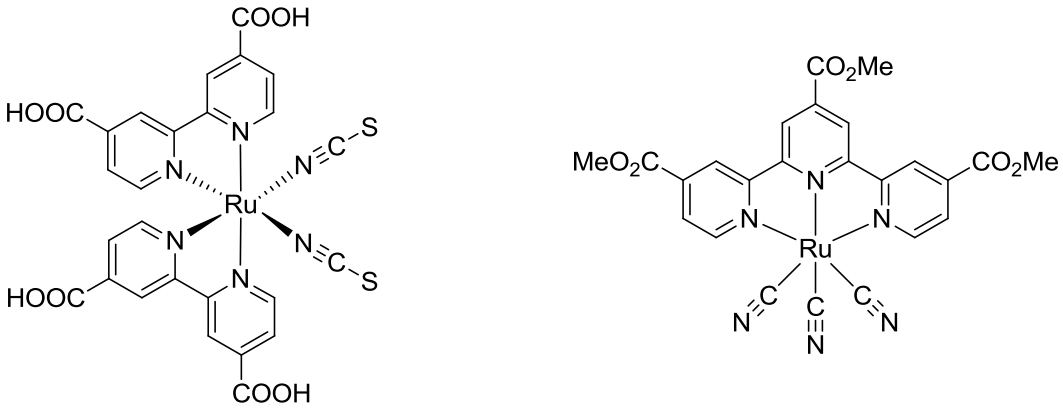

Figure 3-7 N3 Dye (left) and Black Dye (right)

Currently there are several factors affecting the widespread adoption of DSC. Dye stability is one of the largest factors. Generally, a photovoltaic device must possess a life cycle of 20 years if the device is to be deemed commercially viable. Although this has now been achieved with cells containing the N3 dye, other factors now hinder the widespread adoption of these devices. The stability of the N3 dye is due to the very rapid deactivation of the dye's excited state is eight orders of magnitude faster than any other competing process that could lead to spoiling of the cell.[122] Although the dye is stable in its ground, the oxidised dye ($N3^+$) exhibits problems and decomposition occurs with the loss of sulfur. In order to reduce the possibility of the oxidised state decomposing, reduction of the dye should therefore occur as speedily as possible. This is achieved by compressing all of the different parts of the cell tighter and by employing different electrolytes.

Recently researchers announced a solution to a problem that had plagued the traditional Grätzel cells.[125] In these traditional cells, the electrolyte is in a liquid state and consists of several volatile organic solvents. These show high temperature stability problems such as volatility and decomposition and also freeze in cold temperatures. The electrolyte is also prone to leakage or drying over prolonged used which leads to the destruction of the cell. The solution devised uses a cell with a solid electrolyte. This new solid electrolyte was achieved through nanotechnology and the use of fluorine doped $CsSnI_3$. The solid creates a semiconductor that is able to conduct electrons efficiently because of its high hole mobility of (μ_h) 585 $cm^2V^{-1}s^{-1}$ and low energy band gap of 1.3 eV. Hole mobility is a measure of how quickly an electron can move through a semiconductor. The conductor is also soluble in polar solvents and can therefore be spread evenly as a thin film over the dye. This new electrolyte negates the need for the I^-/I_3^- redox couple and thus prevents many of the problems associated with it.

Replacing the iodine redox couple makes the electron transfer process faster which could otherwise lead to decomposition pathways of oxidised or reduced entities.

Recently, a new record in efficiency has been achieved. Through the replacement of the I^-/I_3^- redox shuttle with a cobalt *tris*-bipyridyl complex, the efficiency of the cell was able to operate at the highest level yet, at 12.3%.[126]

Although research in the area of ruthenium polypyridyl complexes is dominated by their possible uses as dyes in DSC and as redox mediators in electrochemical cells, by no means is it limited to those, nor to the inorganic research areas.

The ability of $[Ru(bpy)_2LL]$ complexes to interact with DNA has recently been explored. The possible uses are as synthetic restriction enzymes, chemotherapeutic drugs and DNA foot printing agents due to their unique physical and chemical properties.[127,128,129] Although the binding geometries have as of yet eluded chemists, there is a clear consensus that certain compounds bind to different places in the DNA double helix. For example, the complex $[Ru(bpy)_2(dppz)]^{2+}$ (dppz = dipyrido[3,2-a:2',3'-c]-phenazine) (**Figure 3-8**) has been shown to intercalate between the base pairs of double helical DNA.

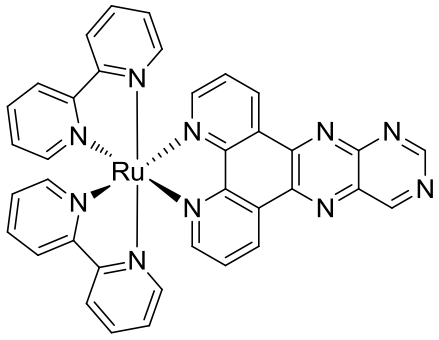

Figure 3-8 Ruthenium *bis*(Bipyridine) DPPZ Complex

Through careful small modifications to the ligand dppz, the molecule can intercalate through either the major or minor groove in the DNA (**Figure 3-9**).

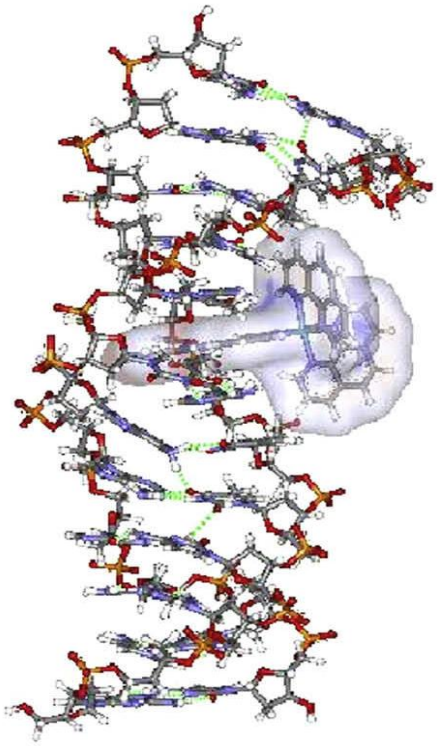

Figure 3-9 Intercalation of the DPPZ Complex Through the Major Grove[126]

3.2 Results and Discussion

Here the results of a number of ruthenium bis-bipyridine complexes with a series of bidentate dithiolato ligands are reported. The cyclic voltammograms of each are also shown, along with any other characterisation. A compound is deemed to be electrochemically viable for use as a redox mediator if its voltammogram exhibits reversible redox waves at an appropriately low potential.

All of the complexes synthesised herein were prepared by the reaction of $[Ru(bpy)_2Cl_2]$ and a dithiol pro-ligand in a 1:1.5 molar ratio with refluxing. The reaction produced HCl gas as a by-product.

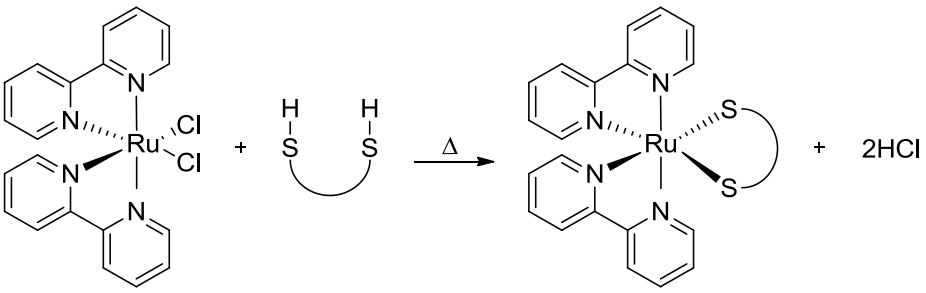

Scheme 3-1 Preparation of $[Ru(bpy)_2]$ Complexes

The purification of the complexes synthesised by column chromatography, whether by silica, alumina or BioBeads (size exclusion) could not be achieved. The products were permanently absorbed onto the stationary phase and could not be eluted with any solvent available to us, and as such, no complex could be completely purified. All complexes reported were purified by washing with various low dielectric constant (polarity) solvents to remove excess ligand, as well as precipitation with diethyl ether from a solution of DCM.

Initial ^{1}H NMR studies on the complexes synthesised proved unsuccessful. Results obtained provided few signals and those that were recorded were broad. Although theoretically the metal centre of the complexes synthesised should be Ru^{II}, single-crystal X-ray analysis confirmed, by the presence of a counter ion, the results obtained by NMR; that the metal centre had become oxidised by some process to Ru^{III}, and was, indeed, paramagnetic. This, unfortunately, coupled with the low purity of the compounds, left few methods of characterisation available. Mass spectrometry (MS) along with Infrared spectroscopy (IR) are thus the only two available methods for characterisation other than single crystal X-ray analysis. While the presence of the complex cannot be proven by either method alone, the combination of the two methods will corroborate as to the likely synthesis of the complex.

Complexes containing Ru are very convenient to characterise by MS. This is because Ru has seven stable isotopes (^{96}Ru 5.5%, ^{98}Ru 1.9%, ^{99}Ru 12.7%, ^{100}Ru 12.6%, ^{101}Ru 17.0%, ^{102}Ru 31.6%, ^{104}Ru 18.7%) and produces a distinctive pattern (**Figure 3-10**).

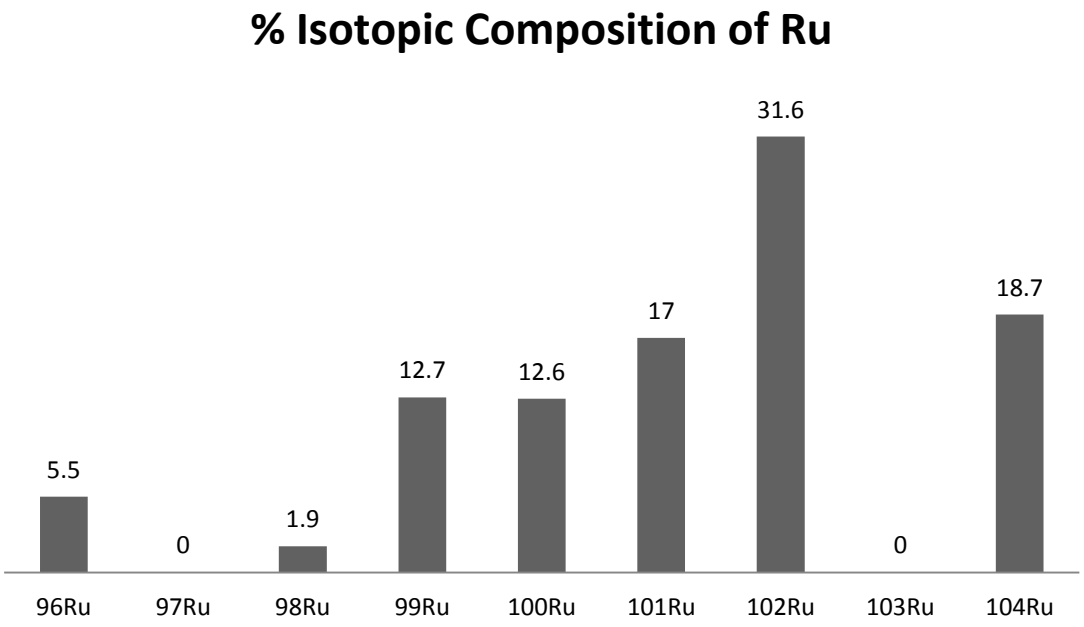

Figure 3-10 Percentage Isotopic Composition of Ruthenium

This 'fingerprint' is a convenient method for characterisation of Ru compounds, or indeed, for many other elements with multiple stable isotopes. This pattern known as the isotopic distribution can in turn be used to compare the experimental distribution pattern to that of a software generated theoretical distribution. If the experimental pattern corroborates with the theoretical pattern, a conclusion can be drawn that the correct complex has been synthesised. The theoretical data can therefore be used to corroborate the data observed experimentally. Obviously, if there are several elements with multiple stable isotopes in a compound, a more complex pattern is observed.

In the complexes synthesised herein, there are two elements that contain appreciable number of multiple stable isotopes; these being Ru with seven stable isotopes and S with 4 stable isotopes, of which only two are in high enough abundance to affect the distribution (^{32}S (95.2%) and ^{34}S (4.21%)). The other elements present (C, H and N) do not contain isotopes in large enough concentration to produce a difference to the distribution. The distribution of the percentage composition of such a compound is shown in **Figure 3-11**.

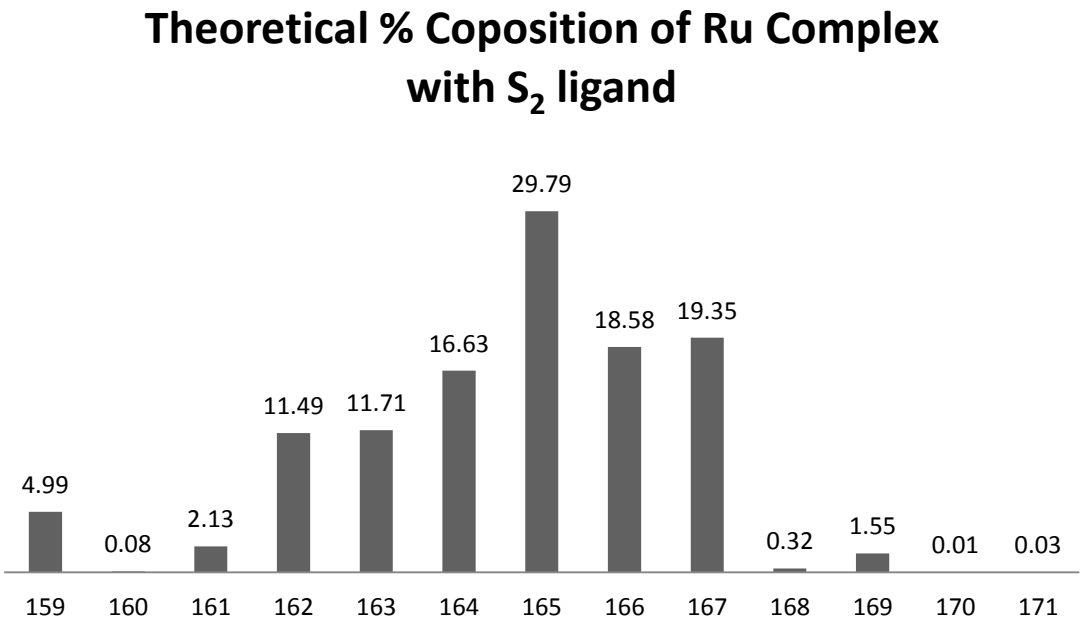

Figure 3-11 Theoretical Distribution of a Ruthenium Complex with Sulfur

For example, the MS results of compound **10** is shown below in **Figure 3-12**. This spectrum exhibits six signals from *m/z* = 550.85 to 555.83, each separated by one unit.

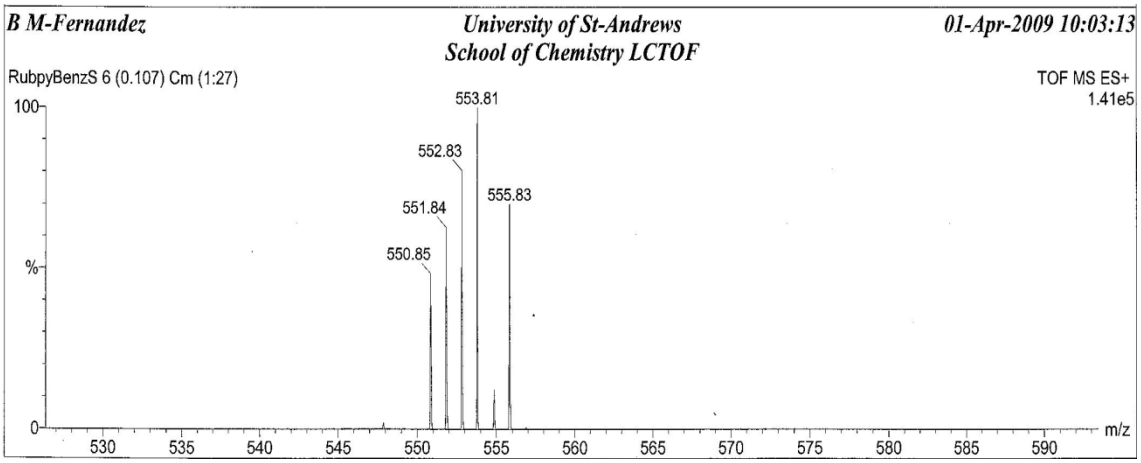

Figure 3-12 Isotopic Distribution of **10**

The theoretical distribution generated is shown below in **Figure 3-13**. This distribution was generated by the MS distribution software IsoPro version 3.1.

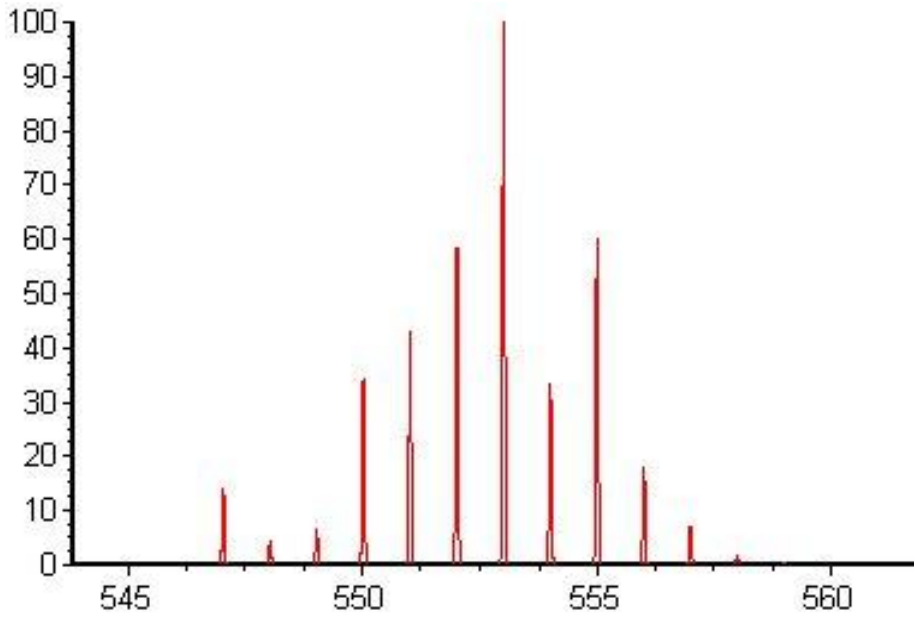

Figure 3-13 Theoretical Isotopic Distribution of **10** as Generated by IsoPro 3.1

By overlaying the theoretical spectrum upon the actual experimental spectrum, (**Figure 3-14**) it can be seen that both the experimental and the theoretical agree with each other. There are however some missing signals. The lack of these are attributed to the minimum threshold setup in the MS experiment.

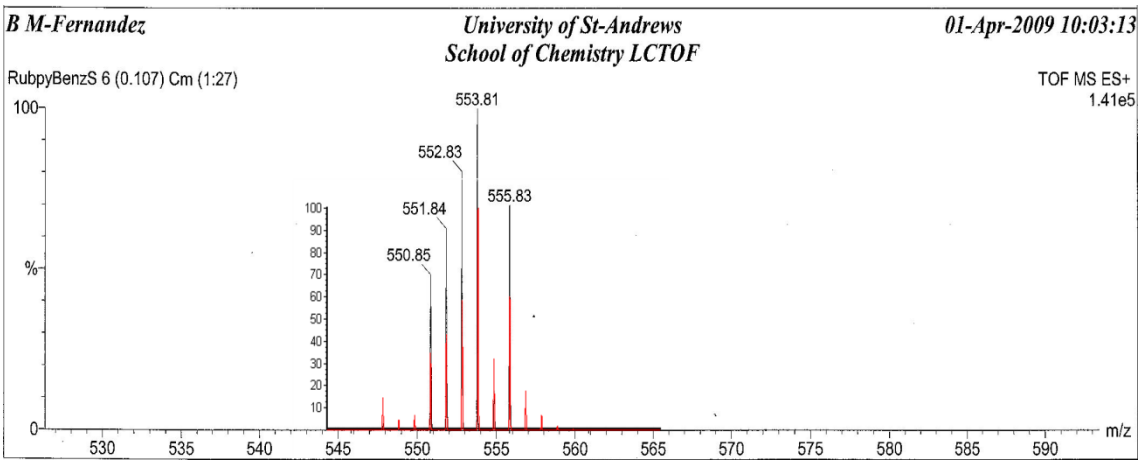

Figure 3-14 Overlaid Image of the Theoretical and Experimental Distribution of **10**

Only few major differences are expected in the IR spectrum of the product, the most important of these being the vibration of the new Ru-S bond. This vibration is reported to occur at the fringe of the common IR region at 401 cm^{-1}.[134] This vibration is very weak and rarely seen. The disappearance of the Ru-Cl would also be a key vibration of interest as the lack of this vibration would suggest replacement of these with the ligand. Unfortunately, this vibration occurs far below the conventional range of IR at ~290 cm^{-1}.[130]

A key feature which we have looked for closely is the disappearance of the thiol S-H vibration coupled with the remaining C-S vibration. C-S vibrations are found in the region of 750-570 cm^{-1}.[131] When bonded to a PGM, they exhibit a vibration at about 470 cm^{-1}.[132]

The main indicative clue that the product has been synthesised is in the disappearance of the thiol S-H stretching vibration along with the retention of the ligand's aromatic C-C and C-H vibrations. Other key absorptions that will also be used are the changes incurred to the aromatic C=C, C=N and C-H vibrations upon the replacement of the chloride ligands and coordination of the aromatic dithiol ligand. The addition of the aromatic ligand should also possess its own aromatic C=C and C-H vibrations, although sometimes overlapping with those of the bpy ligands. The key absorptions are listed below.

The presence of the Ru-S bond absorption in the IR would give, coupled with MS, an almost undeniable proof that the complex had been synthesised. Unfortunately, such absorption lies beyond the normal IR range of 4000 – 400 cm^{-1}, and is also very weak when visible. However, the disappearance of the thiol S-H stretch at ~2540 whilst still exhibiting the C-S stretch at 472 cm^{-1} is indicative of the synthesised complex. Coupled with this, aromatic dithiol ligands exhibit a characteristic C-H absorption at ~750 cm^{-1} due to the aromatic C-H wagging.[132] These three absorptions prove that the complex has been synthesised.

3.2.1 Synthesis of $[Ru(bpy)_2(BenzS_2)]$ (10)

A dark green material was isolated from the reaction of benzene-1,2-dithiol and $[Ru(bpy)_2Cl_2]$ in refluxing ethanol.

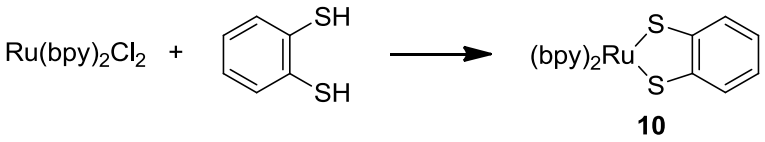

10

Scheme 3-2 Preparation of **10**

The mass spectrum (ES+) of complex **10** has one signal. This corresponds to the positive ($[M^+]$) ion of the complex with a mass-to-charge ratio (*m/z*) of 553.81. The base peak exhibits the characteristic isotopic distribution associated with ruthenium which has seven stable isotopes and is in inline with the theoretical isotopic distribution.

The key absorption bands of the IR spectrum of **10** are shown in **Table 3-1**. The pro-ligand exhibits a thiol S-H stretch at 2538 cm^{-1} while the aromatic C-H wag at 744 cm^{-1}.

The isolated material does not show any absorptions associated with a thiol S-H stretch, yet the ligand C-H wag is still present, although slightly shifted to 753 cm^{-1}. The M-C-S stretch is also present at 472 cm^{-1}.

Wavenumber (cm^{-1})	Assignment
3049	C-H (arom.) of bpy
2961 (+5)	C-H (arom.) of benzS2
2923 (+3)	C-H (arom.) of benzS2
1602 (+3)	C=N/C=C (arom.) of bpy
1565 (+7)	C=C (ring) of benzS2
1467 – 1438	C=C (ring) of bpy and benzS2
753 (+9)	C-H (arom.) of benzS2
472	M-(C-S)

Table 3-1. Key IR vibrations for **10.**
(Change in frequency is shown in parentheses)

The CV of **10** (**Figure 3-15**)exhibits a reversible oxidation at +0.14 V, while a second non-reversible oxidation is present at 0.61 V. Two waves are also present in the negative region and are attributed to the reduction of the bpy ligands to bpy^{-}. These are present at -1.5 and -1.9 V and have the usual reduction potential values.[133,134] **Figure 3-16** shows an overlay of the CV of **10** and the CV of **10** with ferrocene as an internal standard. This helps in assigning oxidation potentials relative to ferrocene, which can then be used to correct the oxidation potentials of the complexes synthesised relative to SHE. Note that the peaks in the CV are broad and display shoulders. As we shall see, this appears to be common for this type of complex and indicates slow electron transfer (broad peaks) and the shoulders on the peaks indicate possibly adsorption onto the electrode and/or peaks due to the products of rapid follow-up reactions. The slow electron transfer may indicate that the there is a large reorganisation energy associated with electron transfer, perhaps due to changes in the Ru-S bond lengths.

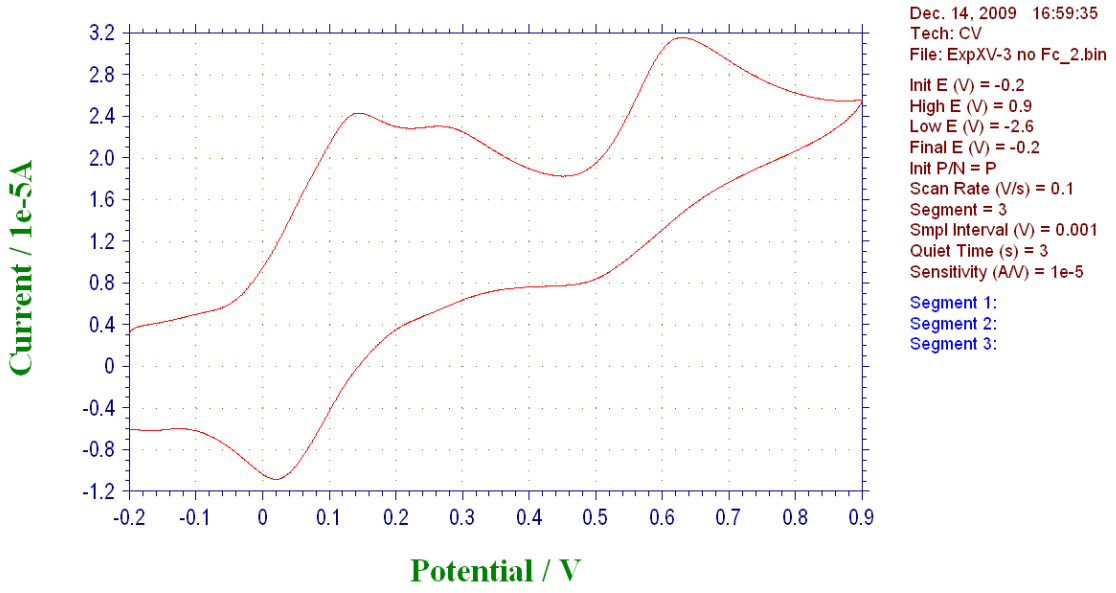

Figure 3-15. CV of **10**
3 mM conc. at 3 mm Glassy Carbon Working Electrode in DCM with
1 M TBAPF6 Electrolyte with Scan Rate of 0.1 V/s

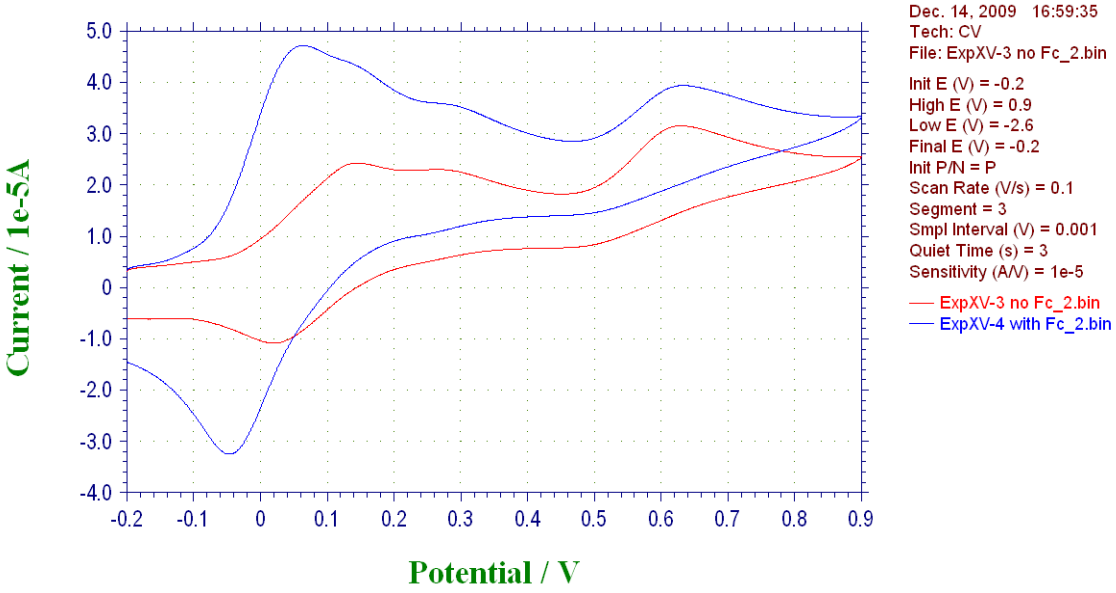

Figure 3-16. CV of **10** with 3 mM Fc (blue trace) and Without (red trace)
Conditions Same as Above

Crystals of **10** were grown through the slow diffusion of diethyl ether into a saturated solution of **10** in dichloromethane and kept in the dark. The structure elucidated differs from the proposed structure as it is the oxidised derivative of **10**, **10ox** shown below. The structure also shows that the oxidation is not limited to the sulfur, but to the metal centre as well as evident from the chloride counterion, suggesting that the ruthenium centre is has become oxidised from Ru(II) to Ru(III). The structure geometry is typical of an octahedral complex

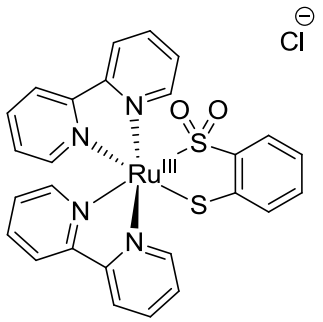

10ox

The complex exhibits sensitivity towards atmospheric oxygen, and as a result becomes, oxidised to the sulfhydryl monosulfinate form. The complex is doubly oxidised to SO_2·S rather than to the singly SO·S or SO·SO due to the greater stability of the former sulfur oxidation state (i.e. S^{VI} is more stable than S^{IV}). The double oxidised sulfur also exhibits a high steric hindrance upon the second unoxidised sulfur which leaves it unoxidised in ambient conditions. The M-S-S plane, with respect to the benzene plane, is hinged at an angle of 5.05°. The S…S distance in this complex is 3.186 Å. This length is slightly larger than those experienced by the other $BenzS_2$ containing complexes **6** & **7**, which has an S…S distance of 3.120 and 3.140 Å respectively. The torsion experienced by the ligand is larger at 7°, while in those of **6** & **7** are 1 and 2° respectively. The Ru…S distance differs between both sulfur by 0.13 Å with the Ru…S^{II}(3) distance at 2.353 Å and the Ru…S^{VI}(2) distance at 3.225 Å with the shortening of the bond due to the loss of the sulfur lone pairs.

Although the MS and X-ray results seem to contradict each other, this is due to the slow rate of oxidation exhibited by the complex. Concurrently with our investigations, Lever[134] published the synthesis of the complex, and gives, in some detail, the chemistry of this compound. The results found by Lever suggest that the complex is indeed air sensitive, but that the rate at which it is oxidised increases when the compound is in solution. It was also found that the rate at which it is oxidised is more rapid upon irradiation by white light ($\lambda > 400$ nm).[135] It is likely that the complex became oxidised as it was left to crystallise in non-deoxygenated solvents in daylight for several days.

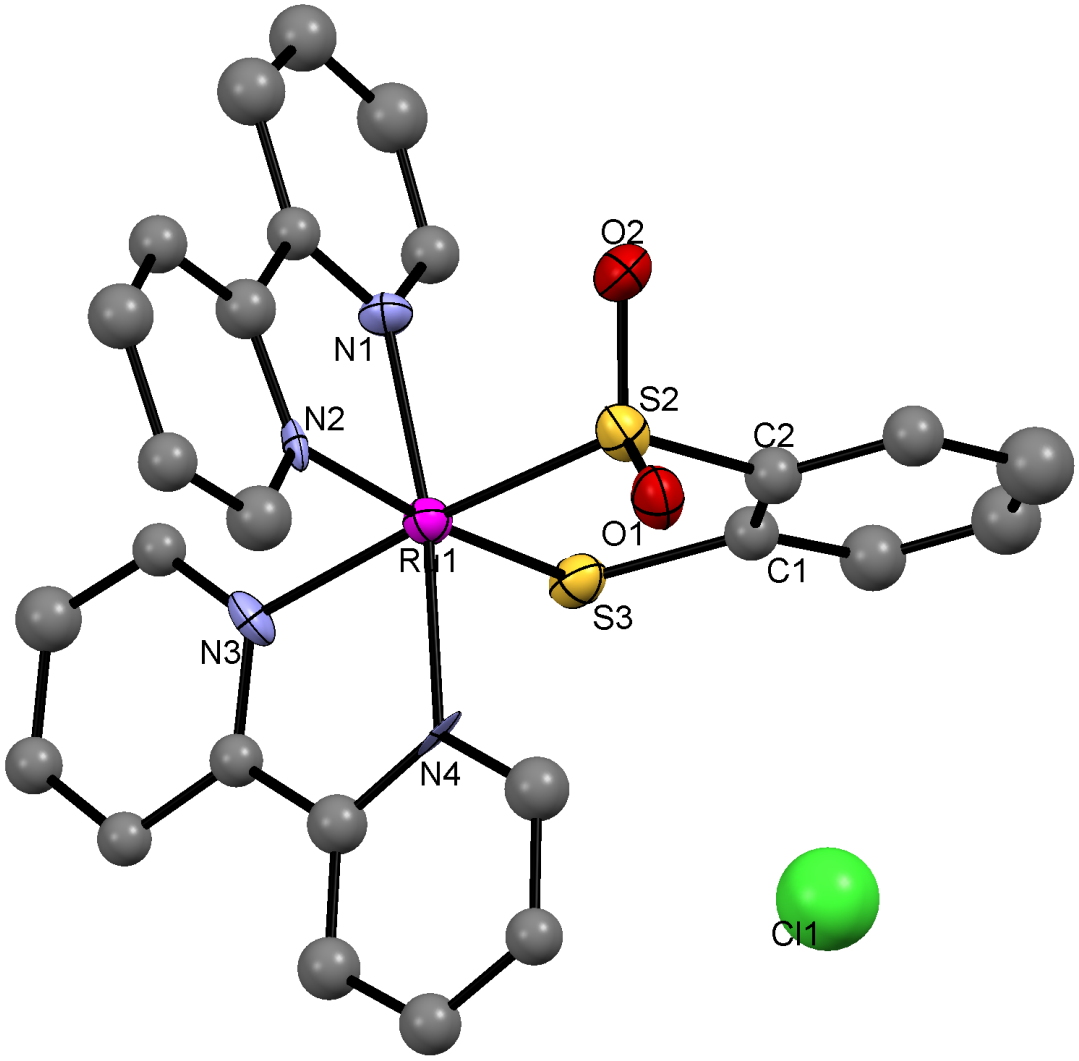

Figure 3-17 Crystal Structure of **10ox**

Bond Length (Å)		*Bond Angle (°)*		*Torsion Angle (°)*	
S(2)…Ru(1)	2.225(5)	**S(2)-Ru(1)-S(3)**	73.2(2)	**S(2)-C(2)-C(1)-S(3)**	7.00(2)
S(3)…Ru(1)	2.353(5)	**C(2)-S(2)-Ru(1)**	106.9(7)		
S(2)…S(3)	3.186(7)	**C(1)-S(3)-Ru(1)**	103.5(7)		
S(2)…O(1)	1.450(1)				
S(3)…O(2)	1.480(1)				

Table 3-2 Selected Bond Lengths for **10ox**

3.2.2 Synthesis of [Ru(bpy)$_2$(BDT)] (11)

A black precipitate was isolated from the reaction of benzene-1,2-dimethanethiol (BDT) and [Ru(bpy)$_2$Cl$_2$] in refluxing ethanol.

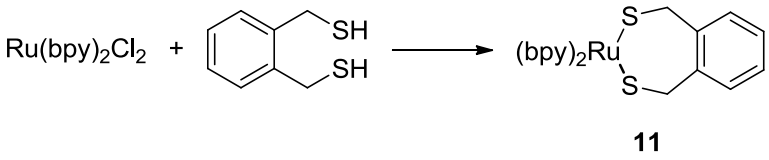

11

Scheme 3-3 Preparation of **11**

The mass spectrum (ES$^+$) of the isolated material recorded two signals. The first at *m/z* = 581.97 and a second at 446.98 (<30%). The first signal corresponds to the positive ion of the complex ([M]$^+$), while the second signal is due to the fragmentation of one of the chlorides from the starting material. The base peak exhibits the characteristic isotopic distribution associated with ruthenium with seven stable isotopes and is in line with the theoretical distribution.

The IR spectrum of **11** is shown in **Table 3-3**. The pro-ligand exhibits a thiol S-H stretch at 2565 cm^{-1}, which disappeared from the product after the reaction. Although the S-H stretch disappeared, the aromatic C-H wag of the BDT was still visible after the reaction.

Wavenumber (cm^{-1})	Assignment
2962 (+6)	C-H (arom.)
2927 (+7)	C-H (arom.)
2282 (+5)	C-H (alkyl)
2204 (+7)	C-H (alkyl)
1627 (+25)	C=N/C=C (arom.) of bpy
1543 (-29)	C=C (arom.) of BDT
1457 – 1384	C=C (arom.)
1279 – 1260	bpy and benzS2 C-H
770 (+5)	C-H (arom.) of BDT
474 (+4)	M-(C-S)

Table 3-3. Key IR vibrations for **11.**
(Change in frequency is shown in parentheses)

The CV of **11** (**Figure 3-18)** shows a non-reversible oxidation commencing at +0.45 V. The two bpy/bpy- reductions waves are also present (-1.8 and -2.0 V).

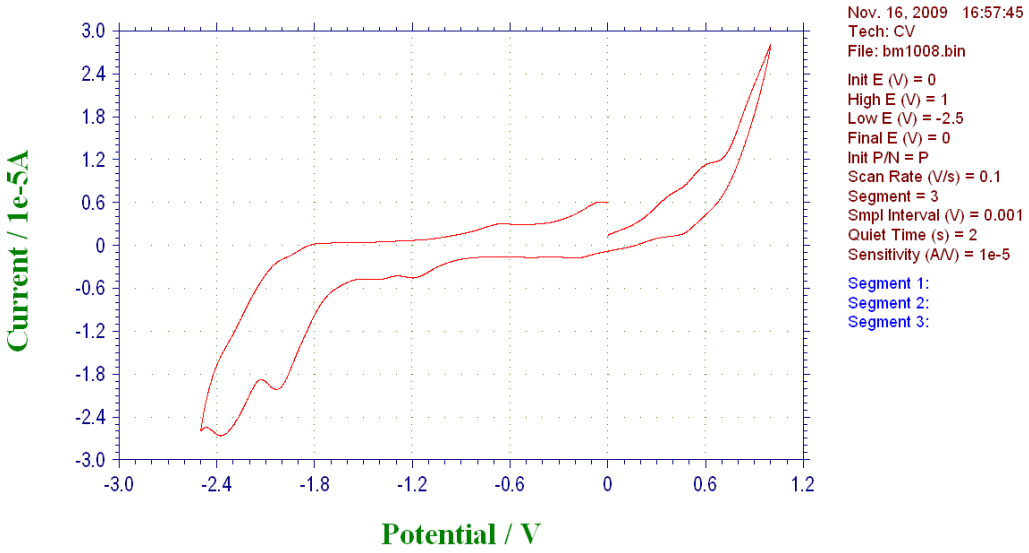

Figure 3-18. CV of **11**
3 mM conc. at 3 mm Glassy Carbon Working Electrode in DCM with
1 M TBAPF6 Electrolyte with Scan Rate of 0.1 V/s

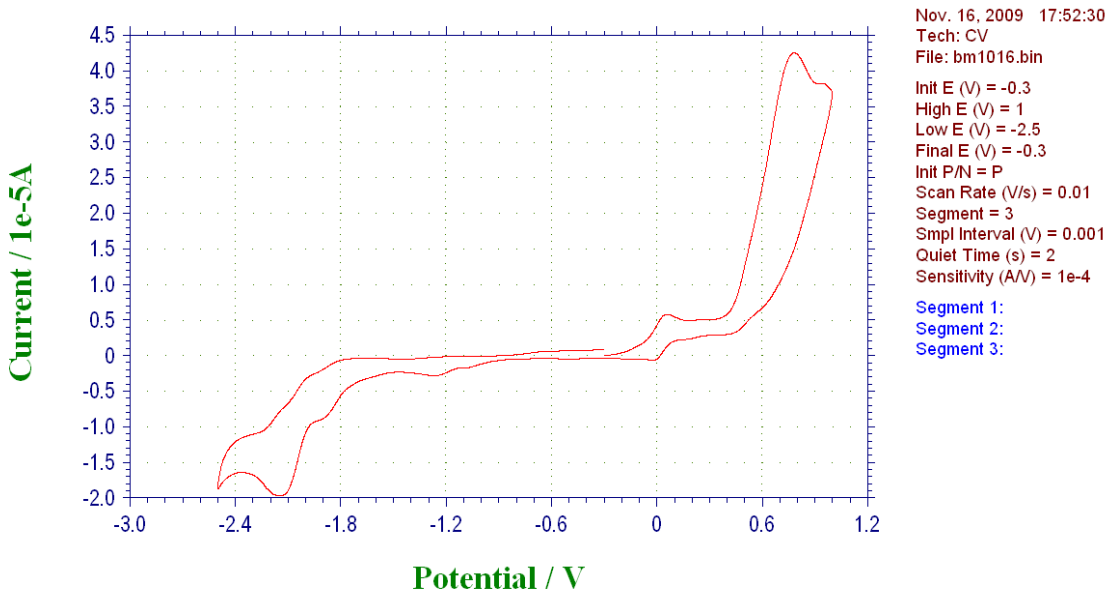

Figure 3-19. CV of **11** with 3 mM Fc
Conditions Same as Above

This compound shows that it is the electron rich backbone that promotes the redox capabilities of the ligands that we are looking at. The unconjugated tether between the benzene backbone and the sulfur prevents stabilisation of the charge by electron delocalisation onto the benzene ring and thus no reversible oxidation wave is observed.

Crystals of **11ox** were grown through the slow diffusion of diethyl ether into a saturated solution of **11** in dichloromethane and kept in the dark. The structure elucidated differs from the proposed structure as it contains two chloride atoms. This gives two possibilities. It is possible that both of the chlorides are anionic counter ions suggesting that the ruthenium centre is Ru(IV). The second possibility is that only one of the chlorides is anionic, while the second is simply HCl produced by the coupling reaction of a thiol hydrogen with a ruthenium chloride as shown in **Scheme 3-1**. The structure geometry is typical of an octahedral complex

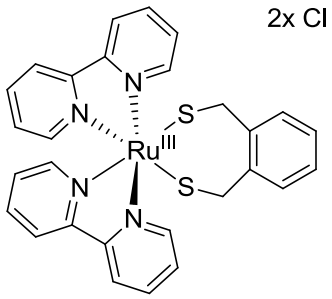

11ox

Unlike **10** which was crystallised with one sulfur doubly oxidised (**10ox**), **11** was isolated with both sulfurs unoxidised. It is likely that the close contact between the sulfurs and the electronegative phenyl ring in the ligand of **10** is capable of stabilising the high oxidation state of the sulfonic sulfur (S^{VI}). In the ligand of **11**, the stabilisation effect from the phenyl ring is disrupted by the CH_2 link and is unable to support the high oxidation state of the sulfur. This alkyl link prevents the oxidation of **11** by the delocalisation of extra electron density onto the benzene ring.

The M-S-S plane, with respect to the benzene plane, is hinged at an angle of 78.79°. This greater angle is due to presence of an alkyl carbon possessing sp3 bonding character. The S…S distance in this complex is greater than **10ox**, standing at 3.644 Å due to the bonding angles of the alkyl carbon forcing the sulfurs further apart, and therefore cannot be compared to another complex synthesised. The torsion experienced by the ligand is larger than **10ox** at 14°. This increased torsion is as a result in minimising the S-Ru-S bond angle which would have otherwise produced a wider angle. The Ru…S are virtually identical as neither of the sulfurs are oxidised which leads to a shortening of the Ru-S bond by the loss of electron density.

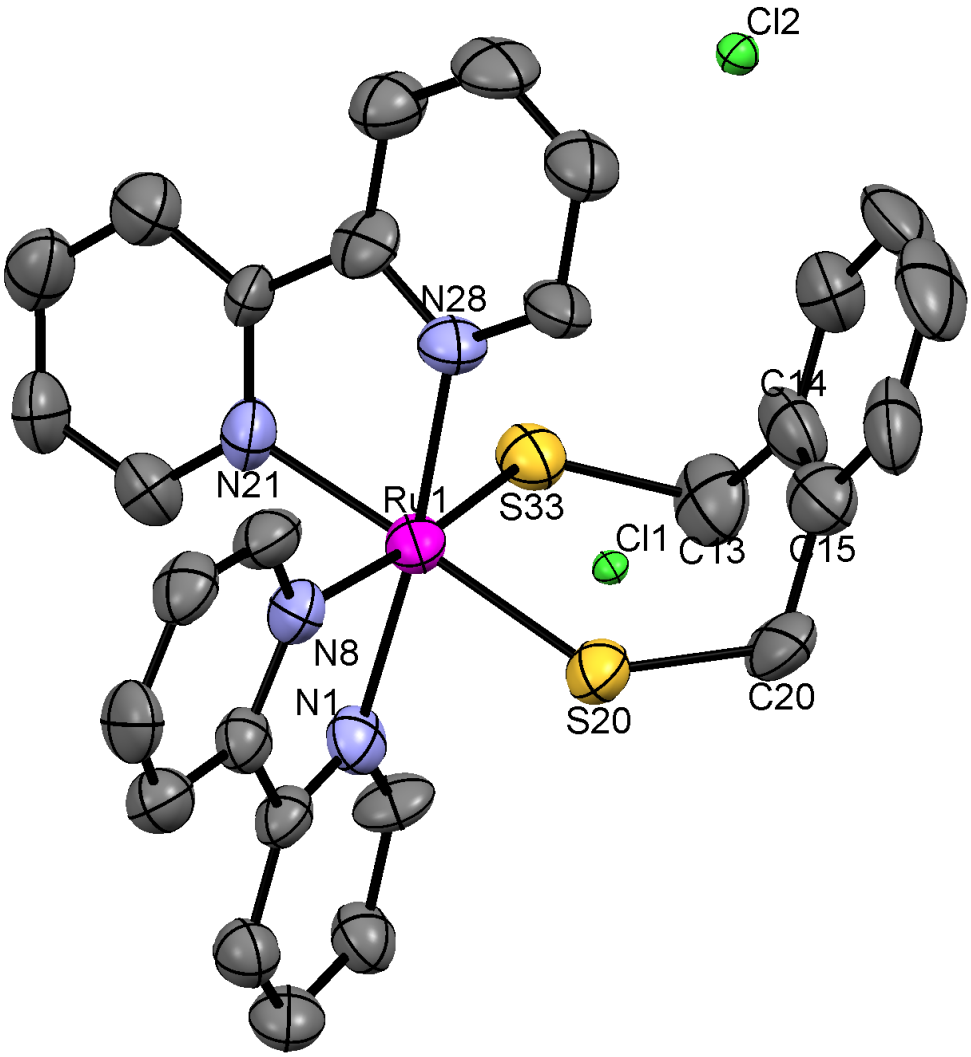

Figure 3-20 Crystal Structure of **11ox**

Bond Length (Å)		*Bond Angle (°)*		*Torsion Angle (°)*	
S(20)…Ru(1)	2.373(6)	**S(20)-Ru(1)-S(33)**	100.5(2)	**S(20)-C(20)-C(13)-S(33)**	14.0(1)
S(33)…Ru(1)	2.367(5)	**C(20)-S(20)-Ru(1)**	120.6(6)		
S(20)…S(33)	3.644(7)	**C(13)-S(33)-Ru(1)**	117.3(7)		
S(20)…C(20)	1.850(2)	**C(15)-C(20)-S(20)**	115.0(1)		
S(33)…C(13)	1.790(2)	**C(14)-C(13)-S(33)**	108.0(1)		

Table 3-4 Selected Bond Lengths for **11**

3.2.3 Synthesis of $[Ru(bpy)_2(NaphS_2)]$ (12)

A dark brown-green product was isolated from the reaction of the lithiated naphtho-[1,8-*cd*]-1,2-dithiole and $[Ru(bpy)_2Cl_2]$ in refluxing ethanol.

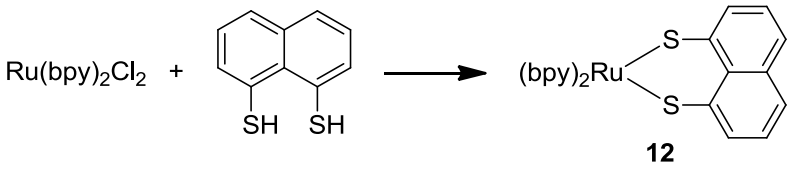

Scheme 3-4 Preparation of **12**

The mass spectrum (ES+) of the isolated material recorded a single signal at *m/z* = 603.61 ($[M^+]$) along with the characteristic isotopic distribution associated with ruthenium.

The IR spectrum of **12** is very much like the previous spectra recorded for this family of compounds, although as expected, it exhibits a greater number of aromatic C-H and C=C bond absorptions. The key absorptions are shown below in **Table 3-5**.

The pro-ligand exhibits two characteristic absorptions associated with it. The thiol S-H is present at 2520 cm^{-1}, while the aromatic C-H wag is present at 756 cm^{-1}. The disappearance of the former, while still retaining the latter, is a key indication of the reaction of the reactants. It is, of course, expected that the remaining C-H wag absorption will be shifted as it has been bonded to an electronegative metal centre.

Wavenumber (cm^{-1})	Assignment
3036 (-30)	C-H (arom.) of bpy
1597 (0)	C=N/C=C (arom.) of bpy
1527 (-19)	C=C (arom.) of naph
1460 (+3)	C=C (arom.) of bpy
1415 (-3)	C=C + C=N (arom.) of bpy
760 (+4)	C-H (arom.) of naph
463	M-S-C

Table 3-5. Key IR vibrations for **12.**
(Change in frequency is shown in parentheses)

The CV of **12** exhibits a reversible oxidation wave at +0.15 V, with peak separation of 0.07 V. This value is very similar to that of **10**, slightly higher but with a much smaller peak separation. This suggests that this complex possesses a greater heterogeneous electron transfer rate constant than that of **10**. This is possibly due to the more electron rich naphthalene ligand which is able to delocalise more electron density from the complex, yielding a faster process due to smaller reorganisation energy.

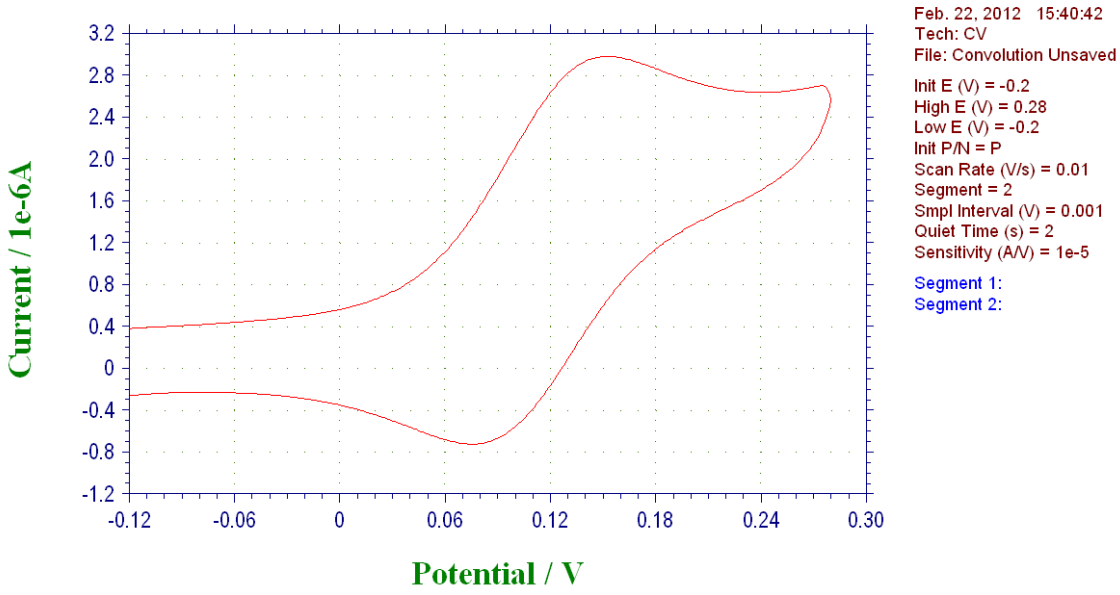

Figure 3-21. CV of **12**
3 mM conc. at 3 mm Glassy Carbon Working Electrode in DCM with
1 M TBAPF6 Electrolyte with Scan Rate of 0.1 V/s

The voltammogram bellow (**Figure 3-23**) displays an overlay of three voltammograms of **12** at three different scan rates. This plot is used to illustrate the presence or lack of electrochemical reversibility of a compound. Electrochemical reversibility differs from chemical reversibility in that instead of describing a process being reversible i.e. Red ↔ Ox + ne^-, electrochemical reversibility describes a process where the electron transfer is fast enough to maintain Nernstian equilibrium at the electrode.[136] Electron transfers can be termed as reversible where there is a corresponding backwards wave and irreversible where the is no backwards wave due to the dispersion of the charge. A third term known as quasi-reversible lies in between reversible and irreversible.

The reversibility can be measured using the standard heterogeneous rate constant, k_s and is calculated using the forward (k_f) and backwards (k_b) rate constants. Depending on the magnitude of k_s the electron transfer can be described as reversible if $k_s > 0.020$ cm/s, quasi-reversible if k_s lies between 0.020 and 5.0 x10^{-5}cm/s, and irreversible if $k_s > 5.0$ x10^{-5}cm/s.[137] An illustration is shown below (**Figure 3-22**) displaying the three terms.

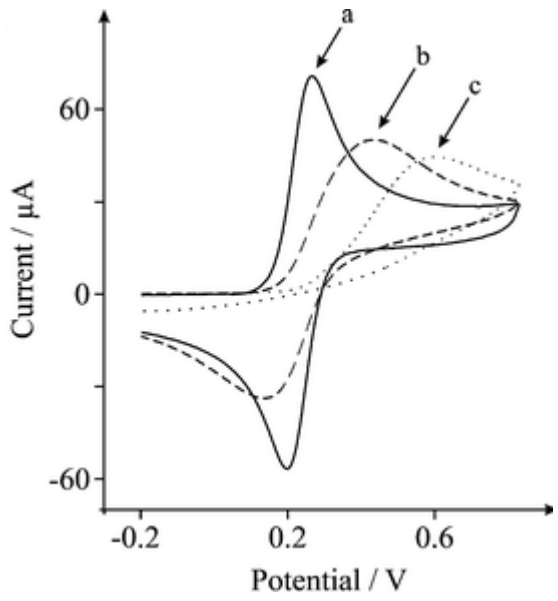

Figure 3-22 Voltammograms for Reversible (a), Quasi-Reversible (b) and Irreversible Electron Transfer.[138]

There are several other ways by which the presence or lack of reversibility of electron transfer can be measured.[137]

- In a reversible voltammogram, the peak-to-peak separation, ΔE_p, approximately equals 59/n mV, independent of scan rate. This, however is rarely the case in resistive solvents like DCM.
- The peak current, I_p, can be used to determine reversibility. If a linear relationship is calculated by plotting the maximum peak current versus square root of scan rate, the process can be deemed reversible. Normally done with five or more scan rates.
- If the peak current potential, E_p, is independent of scan rate, the reversibility of the process can be estimated.

From the voltammogram below of **12**, it is safe to assume that the process is reversible since the peak current potentials do not change with scan rate. The plot also fits other criteria which classifies it as electrochemically reversible including that I_{pa}/I_{pc} = 1. ΔE_p is >0.59/n mV, but as this was carried out in the resistive solvent, DCM, this does not apply. As the compound of this family are closely related, it is also safe to assume that the revesability holds true for all the $Ru(bpy)_2$ complexes synthesised herein.

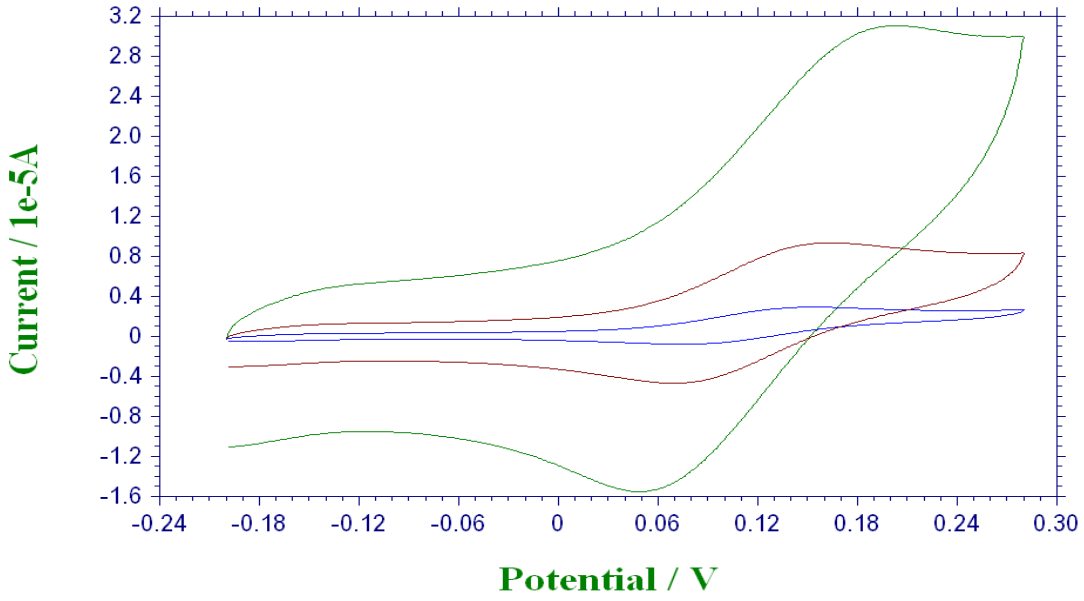

Figure 3-23 CV of **12** Run at Different Scan Rates
Green = 1 V/s, Red = 0.1 v/s and Blue = 0.01 V/s.
Other Conditions Same as Above

Crystals of **12ox** were grown through the slow diffusion of degassed diethyl ether into a saturated solution of **12** in degassed dichloromethane and kept under a nitrogen atmosphere in the dark. The structure shows that oxidation of the metal has occurred suggesting that the ruthenium centre is has become oxidised from Ru(II) to Ru(III). The structure geometry is typical of an octahedral complex

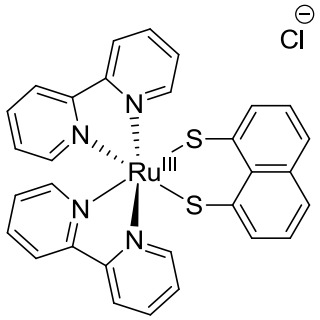

12ox

The complex exhibits sensitivity towards atmospheric oxygen and as a result becomes oxidised. Unlike **10**, however, the oxidation occurs doubly at both sulfurs. It is likely that wider S…S distance allows for both sulfurs to become oxidised simultaneously without experiencing steric hindrance. The oxidation of both sulfurs is possibly aided by the higher stabilising effects of the naphthalene ligand than that of benzene, allowing both sulfurs to oxidise simultaneously.

The M-S-S plane, with respect to the naphthalene plane, is hinged at an angle of 45.72°, the angle incurred by the bonding geometry of the sulfurs. The S…S distance in this complex is 3.120 Å. This length is shorter than those experienced by the other $NaphS_2$ containing complexes **4**, **4B**, **5** & **5B**, measuring 3.252, 3.190, 3. 234 and 3.186 Å respectively. While **4** & **5** cannot be compared directly and applied to **12ox** due to the stressed incurred through the formation of the dimer, **4B** & **5B**, have similar bonding and therefore similar S…S distances, albeit longer due to the different metal centre. The torsion experienced by the sulfurs is larger at 20°, while the torsion exhibited by the naphthalene backbone is 172°.

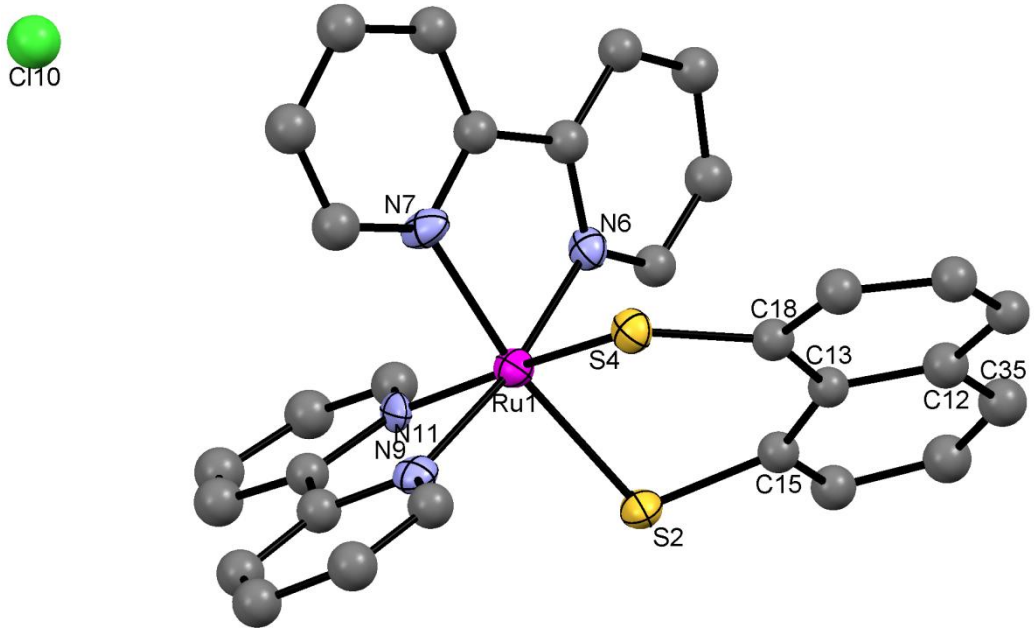

Figure 3-24 Crystal Structure of **12**

Bond Length (Å)		*Bond Angle (°)*		*Torsion Angle (°)*	
S(2)…Ru(1)	2.336(3)	**S(2)-Ru(1)-S(4)**	83.33(9)	**S(2)-C(15)-C(18)-S(4)**	20.0(6)
S(4)…Ru(1)	2.356(2)	**C(15)-S(2)-Ru(1)**	110.4(3)	**C(18)-C(13)-C(12)-C(35)**	172.5(9)
S(2)…S(4)	3.120(3)	**C(18)-S(4)-Ru(1)**	116.4(4)		
S(2)…C(15)	1.810(1)				
S(4)…C(18)	1.740(1)				

3.2.4 Synthesis of [Ru(bpy)$_2$(BiphenS$_2$)] (13)

A dark precipitate was isolated from the reaction of the lithiated dibenzo[*c*,*e*]-1,2-dithiine and [Ru(bpy)$_2$Cl$_2$] in refluxing ethanol.

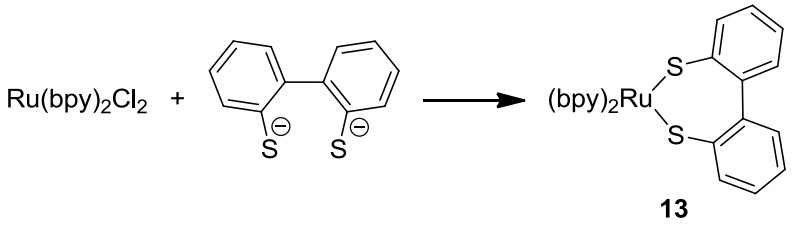

13

Scheme 3-5 Preparation of **13**

This complex was unstable in solution. After a few hours in solution, the blue-grey solution would change into a murky brown solution, regardless of solvent or conditions. As such, all characterisation involving the dissolving of the compound was completed as fast as possible.

The mass spectrum (MALDI) of the complex gives a single signal at *m/z* = 629.68. This corresponds to the molecular weight of the proposed complex. Furthermore, the isotopic distribution of the observed signal is in accordance with that of the theoretical isotopic distribution.

The IR spectrum of **13** is shown in **Table 3-6**. The pro-ligand has a thiol S-H stretch at 2559 cm^{-1}, along with a C-H wag at 752 cm^{-1}.

Wavenumber (cm^{-1})	Assignment
3036 (-30)	C-H (arom.)
1594 (-5)	C=N/C=C (arom.) of bpy
~1454	C=C (arom.) of bpy
1409	C=C (arom.) of bpy
1004	C=C (arom.)
746 (-8)	C-H (arom.) of biphen
483 (+13)	(M)-C-S

Table 3-6 Key IR vibrations for **13.**
(Change in frequency is shown in parentheses)

The CV of **13** (**Figure 3-25)** exhibits a reversible oxidation wave at +0.14 V with a peak separation of 0.07 V. There is also a reversible reduction wave present at -0.28 V with a peak separation of 0.1 V. Since the CV is that of a precipitated powder, rather than material isolated by precipitation with diethyl ether, the voltammogram produced is much clearer and well defined. The oxidation of the complex is in line with the previous set of results and has an oxidation potential close to that of **12**. As mentioned above, the CV of **13** is that of a precipitated powder that had been washed thoroughly in order to reduce the concentration of any impurities. It is then safe to assume that the reversible reduction present at -0.28 is due to the reduction of the complex, rather than the reduction of an impurity. Assuming the oxidation of the complex is a 1-electron process, the reduction here is either a 3 or 4-electron reduction. This is possibly attributed to the reduction of the BiphenS_2 ligand.

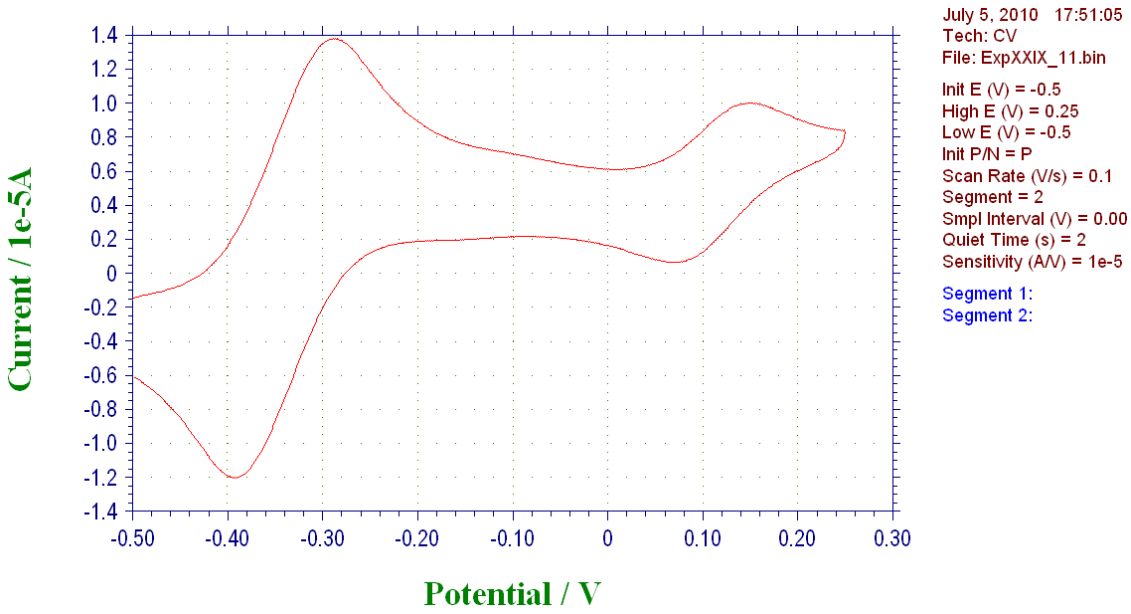

Figure 3-25. CV of **13**
3 mM conc. at 3 mm Glassy Carbon Working Electrode in DCM with
1 M TBAPF6 Electrolyte with Scan Rate of 0.1 V/s

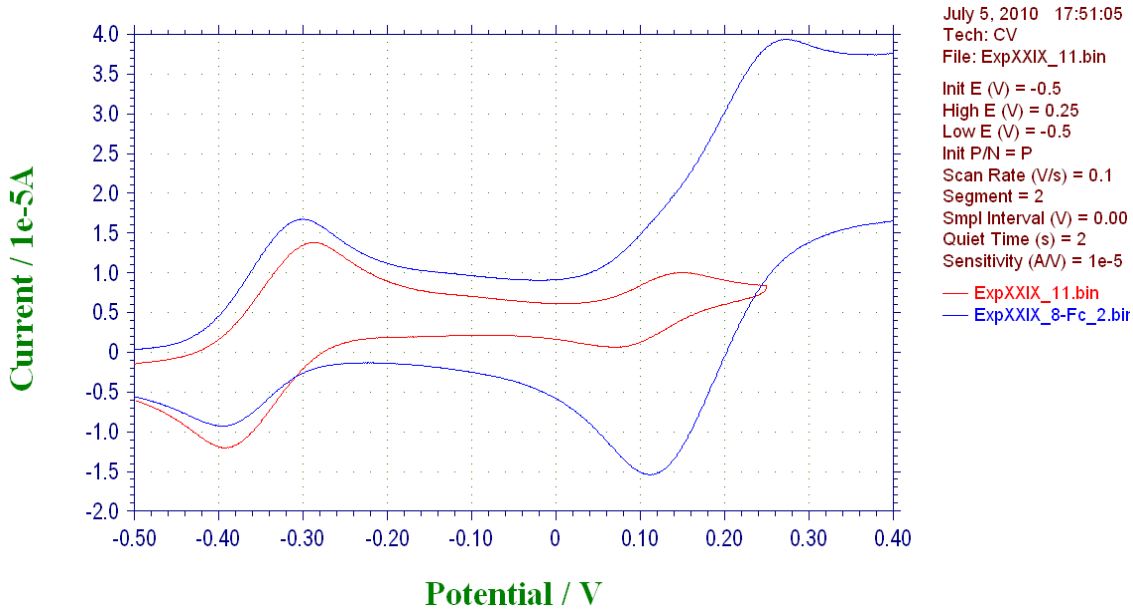

Figure 3-26. CV of **13** with 3 mM Fc (blue trace) and Without (red trace)
Conditions Same as Above

3.2.5 Synthesis of [Ru(bpy)$_2$(AcenaphS$_2$)] (14)

A dark green-brown material was isolated from the reaction of the lithiated 5,6-dihydroacenaphtho[5,6-*cd*]-1,2-dithiole and [Ru(bpy)$_2$Cl$_2$] in refluxing ethanol.

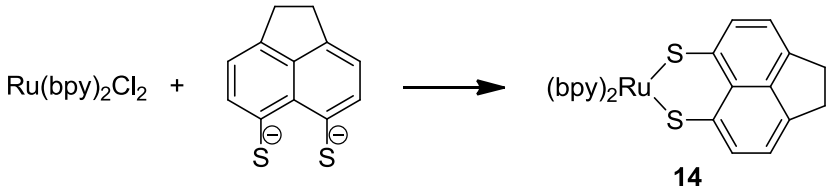

Scheme 3-6 Preparation of **14**

The MS (ESI) of **14** recorded a single peak at *m/z* = 629.69. This represents the positive ion of the complex. It also exhibits the isotopic distribution associated with the complex.

Key absorptions of the IR spectrum of **14** are shown below in **Table 3-7**. As expected, the IR spectrum is very similar to that of **13** except for the aliphatic C-H wag and C-C stretch.

As expected, the pro-ligand thiol S-H stretch at 2520 cm^{-1} has disappeared in the isolated product, yet the acenaphthene C-H wag is still present.

Wavenumber (cm^{-1})	Assignment
3058 (-10)	C-H (arom.) of acena
3034 (-7)	C-H (arom.) of bpy
2957	C-H (alkene) of acena
2907	C-H (arom.) of acena
1597 (-2)	C=N/C=C (arom.) of bpy
1460-1415	C=C (arom.)
1261 (+4)	C-(H)2 (aliph.) wag
800 (+4)	C-C (aliph.)
763	C-H (arom.) of acena
463	(M)-S-C

Table 3-7. Key IR vibrations for **14.**
(Change in frequency is shown in parentheses)

The CV of **14** is shown below in **Figure 3-27**. This complex exhibits a reversible oxidation wave at +0.13 V with a peak separation of 0.08 V. This value is very similar, yet slightly lower than that of **10** and **12**. It is likely that the presence of the alkyl bridge gives a ligand that is more electron rich and is able to promote the complex to oxidise at lower potentials.

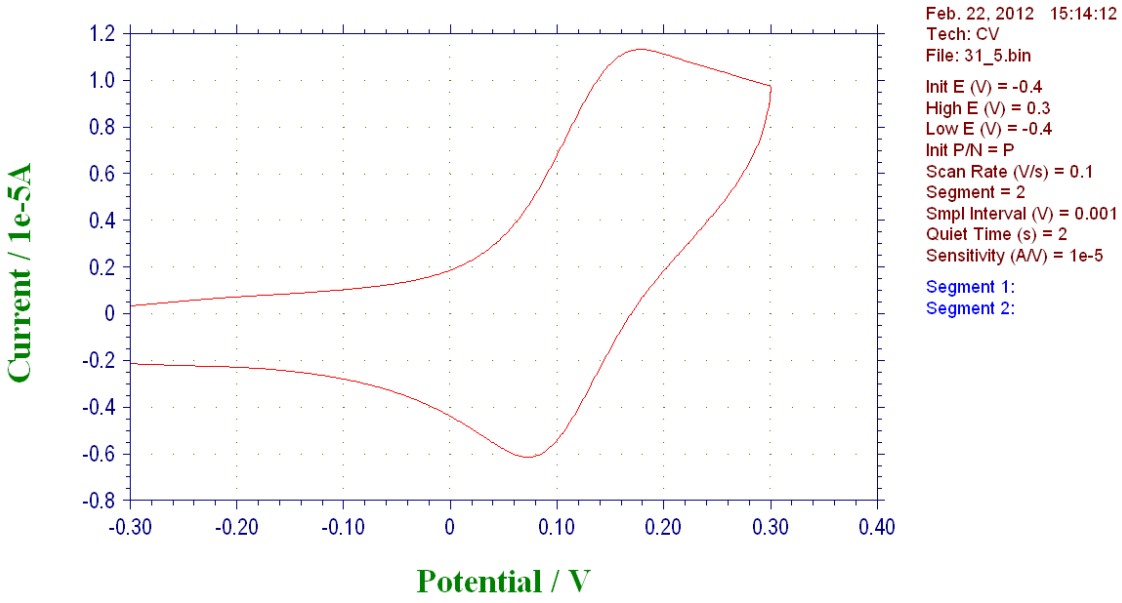

Figure 3-27. CV of **14**
3 mM conc. at 3 mm Glassy Carbon Working Electrode in DCM with
1 M TBAPF6 Electrolyte with Scan Rate of 0.1 V/s

3.2.6 Synthesis of [Ru(^{t}Bu-bpy)$_2$(NaphS$_2$)] (15)

A dark brown-green product was isolated from the reaction of the lithiated naphtho-[1,8-*cd*]-1,2-dithiole and [Ru(^{t}Bu-bpy)$_2$Cl$_2$] in refluxing ethanol.

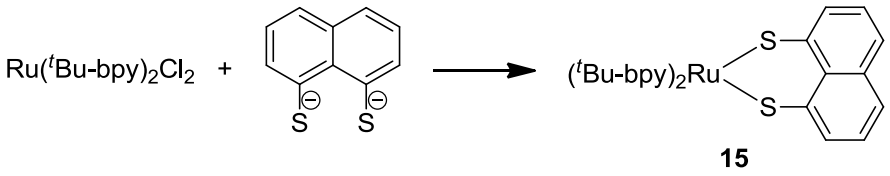

Scheme 3-7 Preparation of **15**

MS (ESI) of the isolated material showed one signal at *m/z* = 828.03, which corresponds to the cation of the proposed complex. The MS also shows the expected isotopic distribution.

The IR of the isolated material was very much like that of **13**, only with extra absorptions present due to the alkyl substituents on the bipyridine.

The pro-ligand exhibited the thiol S-H stretch at 2520 cm^{-1} and the naphthalene aromatic wag at 756 cm^{-1}. After the reaction, the former absorption has disappeared, but the aromatic wag was still present. The key absorptions are present below in table **Table 3-8**.

Wavenumber (cm^{-1})	Assignment
3049(-17)	C-H (arom.) of bpy
2959 (0)	C-H (aliph.) of bpy
2868 (0)	C-H (aliph.) of bpy
1612 (+13)	C-C (aliph) of bpy
1544 (-30)	C=N/C=C (arom.) of bpy
1479 (+13)	C=C (ring) of bpy
1411 (+8)	C=C & C=N in-plane vib.
1365 (0)	C-C (aliph.)
760 (+4)	C-H (arom.) of naph
463	M-S-C

Table 3-8. Key IR vibrations for **15.**
(Change in frequency is shown in parentheses)

The CV of **15** is as expected very similar to that of **12**. The reversible oxidation wave associated with the $Ru^{III/IV}$ has decreased by 0.03 V to +0.12 V. This shift is due to the change in the HOMO/LUMO of the complex promoted by the extra electron density of the *tert*-butyl substituents on the bipyridine ligands. This also has the effect of lowering the peak separation to 0.1 V, down from 0.15 V. There is also some shouldering present. This is likely due to the presence of an impurity that appears to be non-reversible.

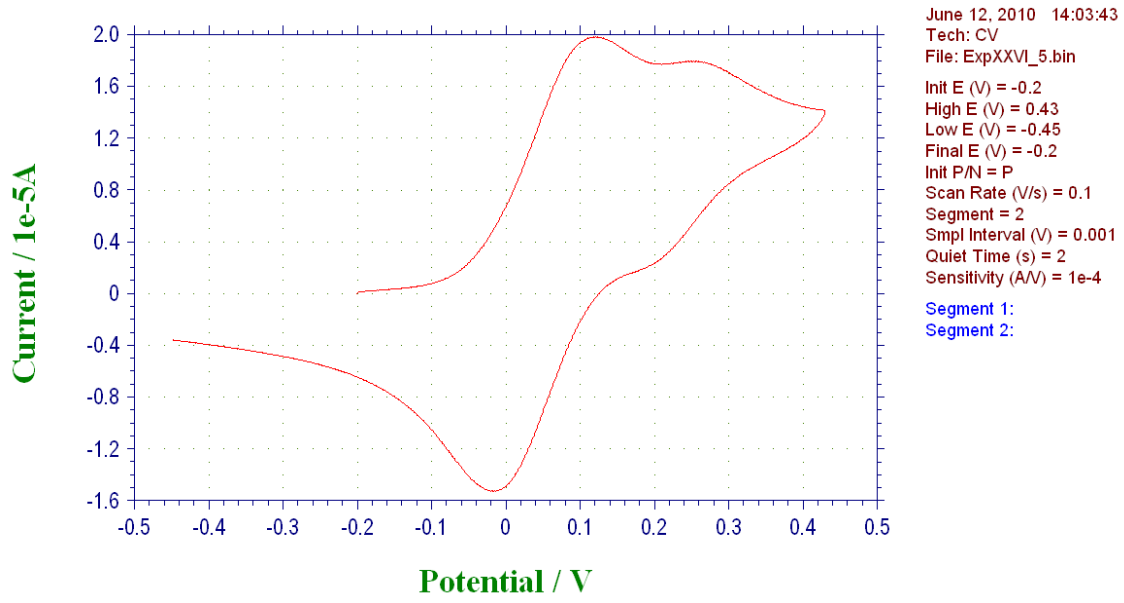

Figure 3-28. CV of **15**
3 mM conc. at 3 mm Glassy Carbon Working Electrode in DCM with
1 M TBAPF6 Electrolyte with Scan Rate of 0.1 V/s

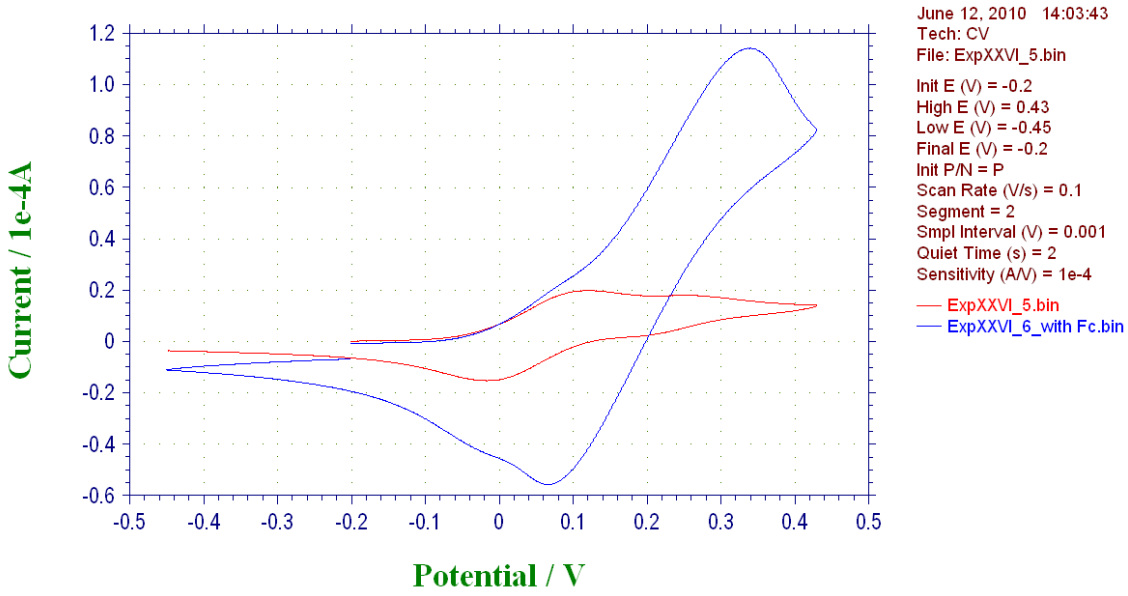

Figure 3-29. CV of **15** with 3 mM Fc (blue trace) and Without (red trace) Conditions Same as Above

3.2.7 Synthesis of [Ru(^{t}Bu-bpy)$_2$(BiphenS$_2$)] (16)

A dark grey-blue product was isolated from the reaction of the lithiated dibenzo[*c*,*e*]-1,2-dithiine and [Ru(^{t}Bu-bpy)$_2$Cl$_2$] in refluxing ethanol.

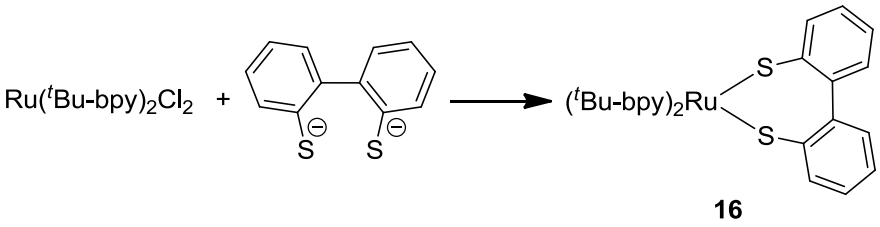

16

Scheme 3-8 Preparation of **16**

Unlike that of its analogue **13**, this complex was not isolated as a precipitate. It does however, still posses the same stability issues experienced with **13**. The complex, when in solution decomposes after a few hours. This complex was far more soluble and was therefore not isolated as a precipitate after the reaction, but rather as an induced precipitate by the addition of diethyl ether. As such, this material was not as pure as that of **13**.

The mass spectrum of this complex recorded several masses which are associated with the oxidation, decomposition of the complex along with the starting material. The proposed complex is present at *m/z*=854.20 ([M^+], 40%).

The key IR absorptions of **16** are shown below (**Table 3-9**). The pro-ligand exhibited the thiol S-H stretch at 2559 cm^{-1}, along with the C-H wag at 754 cm^{-1}, of which only the latter remained after the reaction.

Wavenumber (cm^{-1})	**Assignment**
3047 (-19)	C-H (arom.) of bpy
2957	C-H (aliph.) of bpy
2862	C-H (aliph.) of bpy
1608	C=C C=N (ring) of bpy
1535	C=C (ring) of bpy
1476	C=C (ring) of bpy
1412	C=C & C=N in-plane vib.
1365	C-C (aliph.)
746 (-8)	C-H (arom.) of naph

Table 3-9. Key IR vibrations for **16.**
(Change in frequency is shown in parentheses)

Similar to **13**, the CV of **16** (**Figure 3-30**) exhibits reversible oxidation and reduction waves. The oxidation wave occurs at +0.26 V, significantly higher than that of **13** with an increase of 0.12 V. The reduction wave has also shifted now with a reduction potential of 0.5 V, an increase of 0.23 V. This increase is most likely due to the oxidation of the sulfurs in the complex. This leads to a loss in electron density and the ability of the complex to donate it. This produces a higher HOMO and hence a higher redox potential.

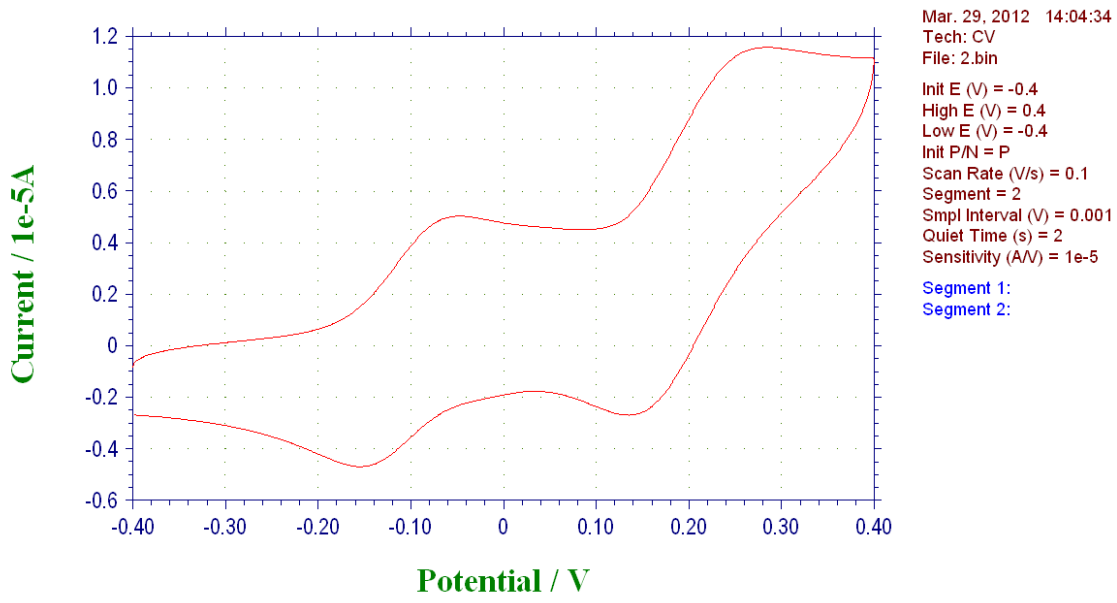

Figure 3-30. CV of **16**
3 mM conc. at 3 mm Glassy Carbon Working Electrode in DCM with
1 M TBAPF6 Electrolyte with Scan Rate of 0.1 V/s

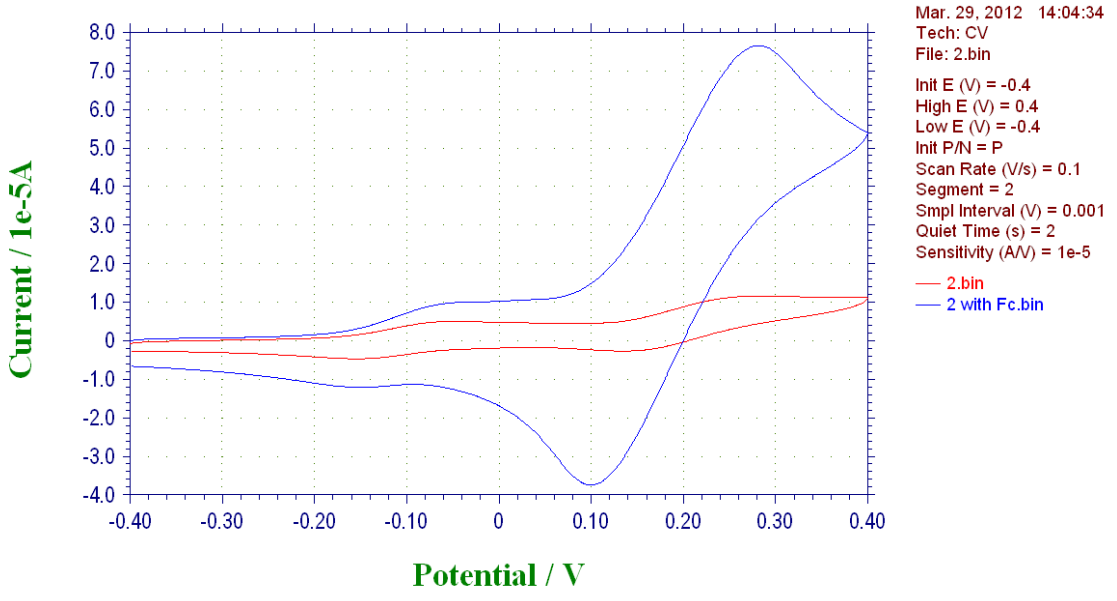

Figure 3-31. CV of **16** with 3 mM Fc (blue trace) and Without (red trace)
Conditions Same as Above

3.2.8 Synthesis of [Ru(^{t}Bu-bpy)$_2$(AcenaphS$_2$)] (17)

A dark green-brown product was isolated from the reaction of the lithiated 5,6-dihydroacenaphtho[5,6-*cd*]-1,2-dithiole and [Ru(^{t}Bu-bpy)$_2$Cl$_2$] in refluxing ethanol.

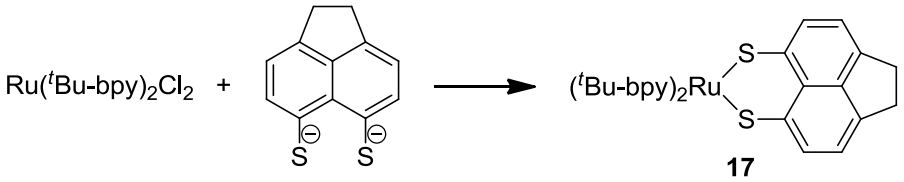

Scheme 3-9 Preparation of **17**

The MS (ESI) of the material isolated recorded the proposed complex at *m/z* = 854.19 ([M]$^+$) along with second signal at *m/z* = 886.13 ([M]$^+$+MeOH).

Key IR stretches of **17** are shown in **Table 3-10**. The pro-ligand thiol S-H stretch at 2520 cm^{-1} disappeared after the reaction, while the aromatic C-H wag at 750 cm^{-1} remained.

Wavenumber (cm^{-1})	Assignment
3057 (-10)	C-H (arom.) of bpy
2957	C-H (aliph.) of bpy
2862	C-H (aliph.) of bpy
1611	C=C C=N (ring) of bpy
1530	C=C (ring) of bpy
1479	C=C (ring) of bpy
1409	C=C & C=N in-plane vib.
1362	C-C (aliph.)
1258	CH2 wag (acena.)
802	C-C (alkene)
745 (-6)	C-H (arom.) of naph
464	(M)-S-C

Table 3-10. Key IR vibrations for **17.**
(Change in frequency is shown in parentheses)

The CV of **17** (**Figure 3-32**) is as expected, much like that of **14**. The reversible oxidation wave occurs at +0.11 V, while in comparison that of **14** occurs at +0.14 V. It is likely that the extra electron density from the *tert*-butyl substituents have promoted the complex's ability to become oxidised at a lower potential. Interestingly, the peak separation is 0.14 V, while that of **14** is 0.055 V, an increase of 0.8 V. The *tert*-butyl substituent are able to promote a lower redox potential with faster electron transfer rate.

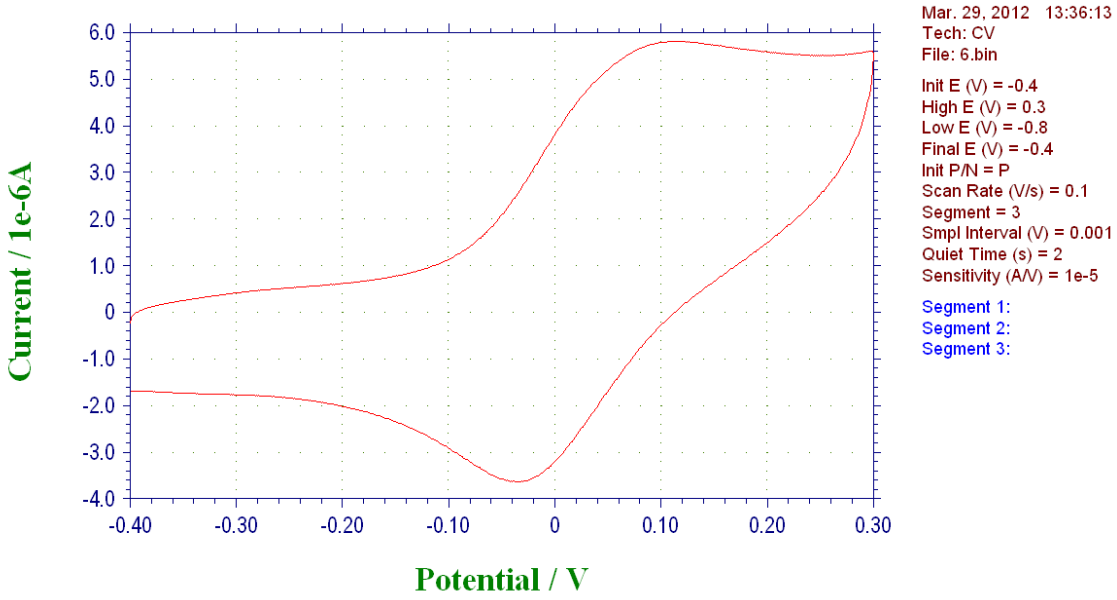

Figure 3-32. CV of **17**
3 mM conc. at 3 mm Glassy Carbon Working Electrode in DCM with
1 M TBAPF6 Electrolyte with Scan Rate of 0.1 V/s

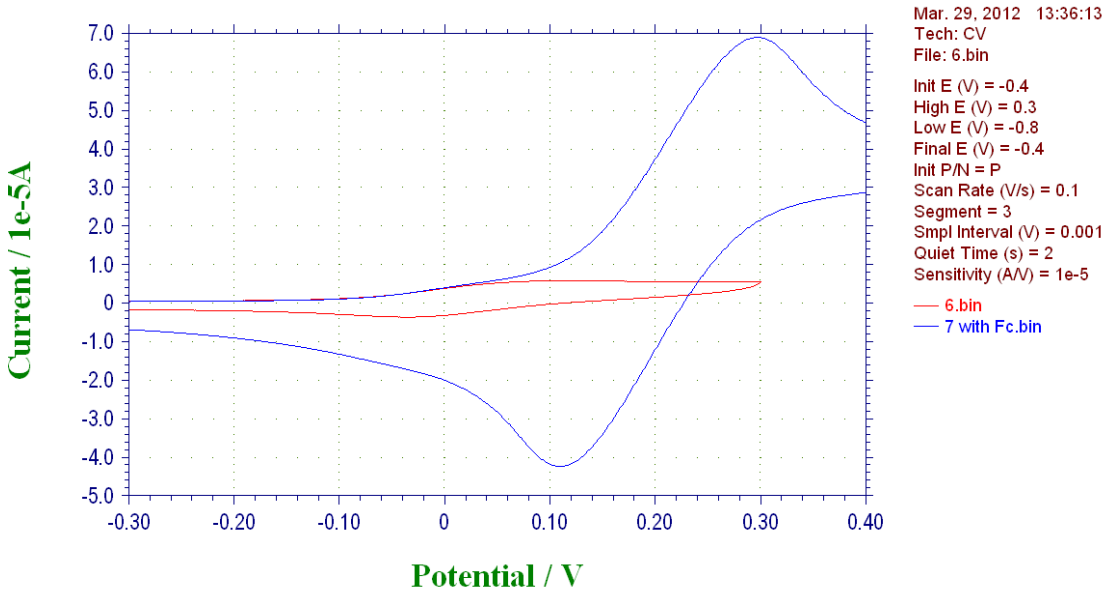

Figure 3-33. CV of **17** with 3 mM Fc (blue trace) and Without (red trace) Conditions Same as Above

3.3 Experimental

General Procedures

Unless otherwise stated, all operations were performed under anaerobic conditions using a nitrogen atmosphere and standard Schlenk techniques. Subsequent workup procedures and chromatographic purification were carried out in air. Dry and deoxygenated solvents were dispensed from an MBraun SPS-800 Solvent Purification System. Methanol and ethanol were dried by refluxing over their corresponding magnesium alkoxide salts and distilling under nitrogen. $RuCl_3 \cdot xH_2O$ was received from Ceimig Ltd. All other reagents and chemicals were purchased from Sigma Aldrich, Alfa Aesar or Acros Organics. All chemicals/reagents were used as received without any further purification, unless otherwise stated. All NMR data were recorded using either a Jeol GSX Delta 270 or Bruker Avance 300, locked to external reference. Coupling constants, if stated, are quoted in Hz. Infrared spectra were recorded as KBr disks on a Perkin-Elmer FT-IR/Raman System 2000 spectrophotometer in the range of 4000-400 cm^{-1}. Cyclic voltammetry was performed on a CH Instruments 600c Potentiostat with a Pt wire counter electrode and a Ag/Ag^+ reference electrode. Mass spectra analyses were performed by either the University of St Andrews Mass Spectrometry Service or by that of the EPSRC's Mass Spectrometry Centre. Elemental analyses were performed by the Elemental Analysis service provided by the London Metropolitan University.

Syntheses of Starting Materials

3.3.1 Preparation of *cis*-$[Ru(bpy)_2Cl_2]\cdot 2H_2O$[139]

$RuCl_3\cdot 3H_2O$ (1 g, 3.86 mmol), 2,2'-bipyridine (1.21 g, 7.77 mmol) and LiCl (1.44 g, 33.93 mmol) were dissolved in DMF (10 mL) and refluxed for 8 h. After cooling, acetone (50 mL) was added and the solution was allowed to cool overnight in a fridge. The dark purple precipitate was filtered, washed with water (3× 25 mL) and diethyl ether (3× 25 mL) and allowed to dry under vacuum. Yield: 1 g, 53.74%.

3.3.2 Preparation of *cis*-$[Ru(^t Bu\text{-}bpy)_2Cl_2]\cdot xH_2O$[140]

$RuCl_3\cdot 3H_2O$ (1 g, 3.82 mmol), 4,4'-di-*tert*-butyl-2,2'-bipyridine (2.05 g, 7.64 mmol), LiCl (1.44 g, 33.93 mmol) were dissolved in ethylene glycol (20 mL) and refluxed for 8h. The solution was allowed to cool and toluene (200 mL) was added and the product was extracted using a separation funnel. The toluene was then evaporated *in vacuo*. This process was repeated ten times yielding a deep purple product. Yield: 1.71 g, 63%.

3.3.3 Preparation of naphtho[1,8-*cd*]-1,2-dithiole[106]

Naphthalene (3.85 g, 30 mmol) was dissolved in hexane (45 mL). To it, *n*-butyllithium (120 mmol) and TMEDA (18 mL, 0.121 mol) was added. The solution was heated to 60° C. for 3 h. The brown suspension was cooled to -78 °C and THF (100 mL) was added. Sulfur flowers (8 g, 0.25 mol) was added with vigorous stirring and allowed to warm to RT. The mixture was washed with water (100 mL) and the organic layer was kept dried over $MgSO_4$ and evaporated under reduced pressure. Purification of the red-brown oil by column chromatography (silica gel, hexane) afforded red-brown powder which was washed with ethanol (1-2 mL), filter and allowed to dry over suction. Yield: 2.1g, 36%.

3.3.4 Preparation of dibenzo[*c*,*e*]-1,2-dithiine[107]

Biphenyl (5 g, 32.4 mmol) was added in small portions to a solution of 2.5 M *n*-butyllithium (64.85 mmol) in hexane and TMEDA (9.72 mL, 64.85 mmol) at -15 °C over the course of an hour. The mixture was allowed to warm to RT overnight and sulfur flowers (2.28 g, 71.28 mmol) was added slowly with vigorous stirring over 3 h. The mixture was poured into water (300 mL) and the organic layer was extracted with DCM, dried over Na_2SO_4 and concentrated *in vacuo*. Column chromatography (silica gel, petroleum ether (40-60°) afforded a bright yellow powder which was subsequently washed with ethanol (1-2 mL) and filtered. Yield: 3.16 g, 45%.

3.3.5 Preparation of 5,6-dihydroacenaphtho[5,6-*cd*]-1,2-dithiole[141]

To a solution of 5,6-dibromoacenaphtene (2g, 6.41 mmol) and TMEDA (0.52 mL, 12.82 mmol) in THF (120 mL), *n*-butillithium (6.5 mmol) was added dropwise at -78 °C over 1 h and left to stir for 15 mins thereafter. Sulfur flowers (0.205 g, 6.4 mmol) was added, allowed to warm to -35 °C and stirred for 2 h. The mixture was again cooled to -78 °C and *n*-butyllithium (6.5 mmol) was added and the procedure was repeated as above. The mixture was quenched with acetic acid (1.2 mL) followed by exposure to air stream for oxidation. The solution was concentrated and water (50 mL) was added and the organic layer was extracted with DCM (100 mL), dried over $MgSO_4$ and evaporated. Hexane (20 mL) was added and the precipitate was filtered off and washed with cold hexane (3× 5 mL) and the red-brown powder was left to dry under suction. Yield: 0.75 g, 55%.

Syntheses of Complexes

3.3.6 Synthesis of [Ru(bpy)$_2$(μ^2-BenzS_2)] (10)

Benzene-1,2-dithiol (0.17 g, 1.2 mmol) was added in one portion to a solution of $[Ru(bpy)_2Cl_2]$ (0.29 g, 0.6 mmol) in ethanol (20 mL). The mixture was refluxed under stirring for 3 hours. The resulting dark green solution was concentrated to a thick black liquid and was washed with

diethyl ether (3× 10 mL) to remove any excess ligand. The liquid was redissolved in ethanol (~5 mL) and diethyl ether was added dropwise. The precipitate formed was filtered and washed with diethyl ether. Yield 48%. Mass spec. (ESI): *m/z* 553(M^+, 100%). IR (KBr): ν_{max}/cm^{-1} 3049m, 2961m, 2923m, 1720m, 1637w, 1602s, 1565s, 1467s, 1438vs, 1313m, 1261m, 1243m, 1123m, 1096s, 1046w, 1039s, 802m, 753vs, 685s, 659m, 589m, 536m, 472m.

3.3.7 Synthesis of [Ru(bpy)$_2$(μ^2-BenzMethS$_2$)] (11)

Benzene-1,2-dimethanethiol (0.1 g, 0.6 mmol) was added in one portion to a solution of [Ru(bpy)$_2$Cl$_2$] (0.29 g, 0.6 mmol) in methanol (25 mL). The mixture was refluxed under stirring for 4 hours. The resulting dark brown solution was evaporated under vacuum and was washed with diethyl ether (3× 10 mL) to remove any excess ligand. The liquid was redissolved in ethanol (~5 mL) and diethyl ether was added dropwise. The precipitate formed was filtered and washed with diethyl ether. Yield 42%. Mass Spec. (ESI): *m/z* 581 (M^+ 100%), 446(29). IR (KBr) ν_{max}/cm^{-1}: 2962m, 2927m, 2228s, 2204s, 2066s, 1627s, 1543m, 1432s, 1384s, 1279m, 1260m, 1141s, 1105s, 1027s, 841m, 805m, 615m, 553m, 519s, 336m.

3.3.8 Synthesis of [Ru(bpy)$_2$(μ^2-NaphS$_2$)] (12)

Naphtho[1,8-*cd*]-1,2-dithiole (0.12 g, 0.6 mmol) was dissolved in THF (5 mL) and $LiEt_3BH$ (2.1 eq.) was added in one portion. Ethanol (20 mL) was added followed by [Ru(bpy)$_2$Cl$_2$] (0.15 g, 0.3 mmol) and refluxed for 2 hours. The resulting green-brown solution was evaporated, redissolved in the minimum amount of DCM and filtered through Celite to remove any LiCl. Yield (55%). Mass Spec. (ESI): *m/z* 603 (M, 100%). IR (KBr): ν_{max}/cm^{-1} 3036m, 1597m, 1527vs, 1460s, 1440s, 1415s, 1345s, 1306m, 1258s, 1191s, 1155m, 1116m, 1054m, 1006m, 981m, 878s, 805s, 760vs, 724s, 651m, 629m.

3.3.9 Synthesis of [Ru(bpy)$_2$(μ^2-BiphenS$_2$)] (13)

Dibenzo[*c*,*e*]-1,2-dithiine (0.13 g, 0.6 mmol) was dissolved in ethanol (10 mL) and $LiEt_3BH$ (2.1 eq.) was added in one portion. A further amount of ethanol (20 mL) was added along with [Ru(bpy)$_2$Cl$_2$] (0.29 g, 0.6 mmol). The solution was then refluxed for 2 hours where upon a precipitate was formed. The precipitate was filtered, and washed with ethanol (3× 10 mL).

Yield (87%). Mass Spec. (ESI): *m/z* 629 (M, 100%). IR (KBr): ν_{max}/cm^{-1} 3036s, 1594m, 1454s, 1409s, 1309m, 1255vs, 1152s, 1116s, 1057s, 1032s, 1004vs, 878m, 746vs, 721s, 648m, 483m, 416m.

3.3.10 Synthesis of [Ru(bpy)$_2$(μ^2-AcenaphS$_2$)] (14)

5,6-Dihydroacenaphtho[5,6-*cd*]-1,2-dithiole (0.13 g, 0.6 mmol) was dissolved in THF (5 mL) and LiEt3BH (2.1 eq.) was added in one portion. Ethanol (20 mL) was added followed by [Ru(bpy)$_2$Cl$_2$] (0.15 g, 0.3 mmol) and refluxed for 2 h. The resulting green-brown solution was evaporated to dryness, redissolved in the minimum amount of DCM and filtered through Celite to remove any LiCl. Yield (49%). Mass Spec. (ESI): *m/z* 629 (M, 100%). IR (KBr): ν_{max}/cm^{-1} 3058m, 2957m, 2907m, 1653w, 1636w, 1597m, 1460m, 1440m, 1415m, 1323m, 1261vs, 1096vs, 1096vs, 800vs, 763s, 727m, 637m.

3.3.11 Synthesis of [Ru(^{t}Bu-bpy)$_2$(μ^2-NaphS$_2$)] (15)

Naphtho[1,8-*cd*]-1,2-dithiole (0.12 g, 0.6 mmol) was dissolved in ethanol (10 mL) and LiEt3BH (2 eq.) was added in one portion. [Ru(^{t}Bu-bpy)$_2$Cl$_2$] (0.36 g, 0.5 mmol) was dissolved in ethanol (20 mL) and added to the reduced ligand and refluxed for 3 h. The resulting green-brown solution was evaporated, redissolved in the minimum amount of DCM, washed with water, dried over $MgSO_4$ and evaporated. The solid was washed with boiling hexane, which was discarded. The solid was the washed with boiling ethyl acetate which afforded a purple solution which was also discarded. This was repeated several times until the solution was colourless. Yield (49%). Mass Spec. (ESI): *m/z* 856 (M^+, 100%). IR (KBr): ν_{max}/cm^{-1} 3049m, 2959vs, 2868m, 1612vs, 1544vs, 1479vs, 1411vs, 1365s, 1320m, 1252m, 1200m, 1153m, 1128m, 1020m, 983m, 930w, 898w, 879m, 834m, 815s, 760vs, 720m, 604s, 553w.

3.3.12 Synthesis of [Ru(^{t}Bu-bpy)$_2$(μ^2-BiphenS$_2$)] (16)

Dibenzo[*c*,*e*]-1,2-dithiine (0.13 g, 0.6 mmol) was dissolved in THF (4 mL) and LiEt3BH (2.1 eq.) was added in one portion. Ethanol (20 mL) was added along with [Ru(^{t}Bu-bpy)$_2$Cl$_2$] (0.16 g, 0.3 mmol). The solution was refluxed for 2 hours. The grey-green-blue solution was evaporated to dryness, redissolved in the minimum amount of THF, and the product was precipitated by the

slow addition of diethyl ether. The precipitate was filtered and washed with diethyl ether. Yield (49%). Mass Spec. (ESI): *m/z* 854 (M, 40%). IR (KBr): ν_{max}/cm^{-1} 3047m, 2957vs, 2862m, 1608vs, 1535s, 1476s, 1454s, 1412vs, 1365vs, 1258vs, 1200s, 1090br, 1018s, 800s, 746vs, 696m, 660m, 601m, 584m, 475m, 401w.

3.3.13 Synthesis of [Ru(^{t}Bu-bpy)$_2$(μ^2-AcenaphS$_2$)] (17)

5,6-Dihydroacenaphtho[5,6-*cd*]-1,2-dithiole (0.13 g, 0.6 mmol) was dissolved in THF (5 mL) and LiEt3BH (2.1 eq.) was added in one portion. Ethanol (20 mL) was added followed by [Ru(^{t}Bu-bpy)$_2$Cl$_2$] (0.16 g, 0.3 mmol) and refluxed for 2 h. The resulting green-brown solution was evaporated to dryness, redissolved in the minimum amount of THF and filtered through Celite to remove any LiCl. Yield (49%). Mass Spec. (ESI): *m/z* 853 (M^+, 100%). IR (KBr): ν_{max}/cm^{-1} 3050m, 2957vs, 2862m, 1611vs, 1530m, 1538m, 1497s, 1409vs, 1362s, 1317m, 1258vs, 1138m, 1093vs, 1018vs, 836m, 802vs, 725m, 640s, 604s, 560m, 520m, 464s.

3.3.14 Synthesis of [Ru(bpy)$_2$(μ^2-NaphNS)]

[Ru(bpy)$_2$Cl$_2$] (0.29 g, 0.6 mmol) was dissolved in ethanol (50 mL) and 8-aminonaphthalene-1-thiol (0.21 g, 1.2 mmol) was added. The solution was refluxed for 2 hours, during which the colour of the solution changed from deep purple to brown-red. The solution was filtered through Celite and the filtrate was evaporated and the solid material was washed with THF (3× 10 mL). Mass Spec. (ESI): *m/z* 602 ($[M]^+$+O). IR (KBr): ν_{max}/cm^{-1} 3064m, 1622w, 1601m, 1562m, 1462m, 1443m, 1421m, 1311w, 1263m, 1157w, 1102w, 1062w, 1033w, 965m, 933m, 896m, 861m, 819m, 763vs, 728s, 695w, 658w, 629w, 595w, 565w, 532w, 502w, 467ws.

4 PENTAMETHYLCYCLOPENTADIENYL RUTHENIUM COMPLEXES WITH DITHIOLATO LIGANDS

4.1 Introduction

The chemistry and properties of the cyclopentadienyl ligand (Cp) and that of 1,2,3,4,5-pentamethylcyclopentadienyl (Cp*), have been dealt with and discussed in **Chapter 2**.

Complexes incorporating either of these ligands generally tend to be to more stable than complexes without π-ligands. One of the most distinguishing features in using these ligands is in that they both possess π and π* orbitals due to their conjugated unsaturation. This allows them to act as both π-donor and π-acceptor ligands, stabilising the overall complex.[142]

Cp, and its derivatives, are responsible for over 80% of known organometallic compounds.[143] Although there are other examples of multi-hapto aromatic organometallic complexes with π-bonds, the chemistry of Cp and Cp* is virtually unique. This is because unlike the other examples where the arene ligands are neutral, the Cp ligand is anionic, leading to more electron rich and more stable complexes. The other notable ligand is that of cycloheptatriene. This ligand, known as the tropylium ion, is cationic and becomes aromatic with the loss of a hydride using oxidants such as bromine or PCl_5.

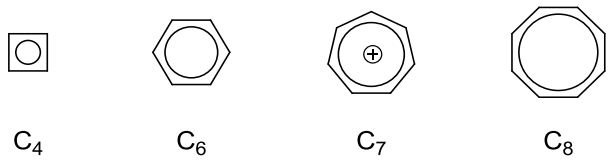

Figure 4-1 Other Examples of Multi-hapto Aromatic π-Complexes

The pro-ligand when deprotonated becomes aromatic and as a consequence when coordinated forms π-complexes. As the ligand is an aromatic arene, it can undergo many of the reactions associated with aromatic compounds such as Friedel-Crafts alkylation and acylation.

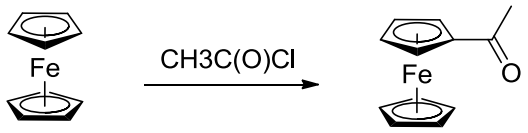

Figure 4-2 Friedel-Crafts Acylation of Ferrocene

Metallocenes can also become singly or doubly lithiated with the use of n-butyllithium. This yields a very versatile nucleophile in organometallic and phosphorus chemistry.

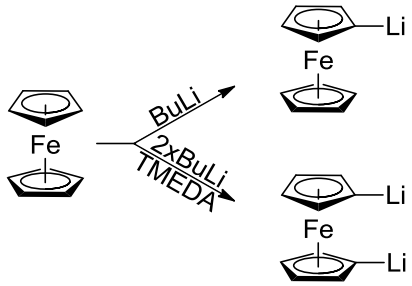

Figure 4-3 Lithiation of Ferrocene

Complex reactions involving one of the cyclopentadienyl ligands can also be carried out such as the recent synthesis of ferrocenestrone (**Figure 4-4**) which has more than 13 synthetic steps.[144]

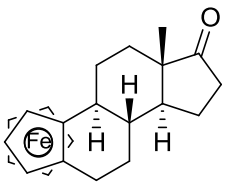

Figure 4-4 Complex Ferrocene Derivative Ferrocenestrone

Metal complexes with Cp or Cp* ligands show little charge separation between the metal and the ligand and so metallocenes generally override the requirement of the 18-electron rule with 14 to 16-electrons being common for half-sandwiched complexes.[142] The ligand is considered an electron rich ligand and is able to donate extra electron density to the metal centre. This lowers the oxidation potentials of these complexes since it is easier for the complex to donate electrons. For example, the use of ferrocene is very well documented in electrochemistry and has found an important use as an internal standard.[145] This is due to the fact that ferrocene undergoes a one-electron reversible oxidation at 0.641 V vs. SHE,[146] a relatively low value. Substituting the protons on the ligand with electron withdrawing (EWG) or donating groups (EDG) can alter the redox properties of ferrocene.[147] For example, the electron withdrawing carboxylic acid group changes the potential so that it becomes more positive. On the other hand, electron donating groups such as methyls donate extra electron density, and as a consequence, the complexes are easier to oxidise. For example, the redox potential of decamethylferrocene, $[Fe(Cp^*)_2]$, is -0.59 V lower than that of ferrocene itself.[146]

Cp or Cp* can be coordinated to virtually all the transition metal elements, but is generally limited to Ti, V, Cr, Fe, Co, Ni, Zr, Mo, Ru, Rh, Os, Ir and W. Many of these metallocenes are generally quite unstable as the Cp ligand is anionic and change in oxidation number is required for the metal. This leaves many metals in one of their least stable oxidation states or salts are produced which can be sparingly soluble. This makes the group 8 metals particularly well suited for coordination to Cp/Cp*. This group is known for the constituent elements exhibiting multiple stable oxidation states. Iron possesses ten possible oxidation states, with +2 and +3 being the most stable. Ruthenium has 8 oxidation states, with +3 and +4 being the most stable, while osmium has the most possible states with 11, with +4 being the most stable. This makes redox reactions, in particular electrochemical reactions, possible since the oxidised or reduced products are stable to decomposition or degradation.

For comparison, a list of common potentials for metallocenes are summarised in the table below.

Oxidation Couple	Potential vs. Fc.
$[Fe(C_5H_5)_2]^+$ / $[Fe(C_5H_5)_2]$	0 V
$[Fe(C_5Me_5)_2]^+$ / $[Fe(C_5Me_5)_2]$	-0.59
$[Co(C_5H_5)_2]^+$ / $[Co(C_5H_5)_2]$	-1.33[146]
$[Co(C_5Me_5)_2]^+$ / $[Co(C_5Me_5)_2]$	-1.94[146]
$[Rh(C_5H_5)_2]^+$ / $[Rh(C_5H_5)2]$	-1.79[148]
$[Rh(C_5Me_5)_2]^+$ / $[Rh(C_5Me_5)_2]$	-2.38[149]
$[Ir(C_5H_5)_2]^+$ / $[Ir(C_5H_5)_2]$	-2.65[150]

Table 4-1 Oxidation Potentials for Common Metallocenes

The other group 8 metallocenes have also been extensively researched.[151] As mentioned above, ferrocene undergoes a one-electron oxidation. Since Ru and Os are the two other group 8 metals, their electrochemical behaviour should be similar. This is indeed true for the osmium analogue, osmocene, which undergoes a one-electron oxidation at the potential of 0.25V relative to Fc. However for ruthenocene it is different. The electrochemical oxidation of ruthenocene proceeds via a two-electron oxidation at 0.41 V relative to Fc.[152] Recently, ruthenocene has been shown to oxidise via a one-electron process when weakly coordinating fluoroarylborate anions such as the tetrakis-(pentafluorophenyl)borate or the tetrakis[3,5-bis(trifluoromethyl)-phenyl]borate are employed.[153]

Due to the reactivity of the group 8 metallocenes being based upon and limited to substitution reactions on the cyclopentadienyl ligands, as well as simple reactions based on the metal centre e.g. oxidation and reduction, the chemistry of this class of compounds is quite limited.[154] By controlling the ligand excess, half-sandwiched complexes can be synthesised. When coordinated, the cyclopentadienyl ligands occupy three coordination sites leaving between 2 – 4 more sites available for coordination. This produces the characteristic geometry known as a piano stool-like structure.[155]

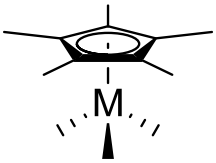

Figure 4-5 Three Legged Piano-Stool Structure

In contrast to the limited chemistry of the group 8 metallocenes, the half-sandwich group 8 complexes still exhibit considerable enhanced reactivity imparted and controlled by the cyclopentadienyl ligand, but largely governed by the remaining ligands coordinated to the metal centre.[154] These mono(cyclopentadienyl) complexes have applications ranging from C-X and C-C bond forming catalysis to the polymerisation of several commercially important products.[156]

Without a doubt, the largest studied group of half sandwich complexes belong to that of ruthenium.[154] The high thermal stability and excellent catalytic behaviour of the half-sandwich ruthenium complexes makes this class of compounds interesting to study.[157] Although the osmium analogue possesses similar chemistry and characteristics with slight enhanced redox properties, the limiting factor impacting the research of this metal is down to osmium, along with iridium, being the two least abundant metals on the planet. The natural abundance of the metal being in the region of 0.05 ppb,[158] limits the accessibility of this chemistry as well as its potential uses. At the time of writing, the price for a troy ounce of osmium was in the region of $400 while that of ruthenium is $114.

While there is still extensive research into the use of half-sandwich ruthenium compounds in the area of catalysis,[159] and photosensitisers,[160] recent research has also diversified and has included the biological role of these compounds. Arene-ruthenium complexes have been shown to inhibit the reproduction abilities of carcinoma cells.[161] Currently, there are a few ruthenium anti-cancer complexes in clinical trial. These include RAPTA, DW1/2 and ONOCO4417.[162]

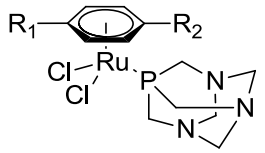

RAPTA

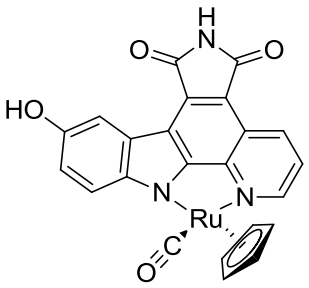

DW1/2

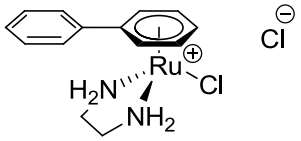

ONCO4417

To further understand the area of pentamethylcyclopentadienyl ruthenium chemistry and our research into redox mediators, we will expand it to include the bidentate dithiolato ligands used thus far. Complexes of this kind should possess interesting electrochemistry due to both the easily oxidised central metal atom and the electron rich ligand which will further lower the oxidation potentials of such complexes. They could prove to be viable redox mediators in glucose biosensors.

4.2 Results and Discussion

All of the complexes synthesised were prepared by the reaction of the pro-ligand, a dithiol, with the [Cp*$RuCl_2$] dimer in a 1:1.5 molar ratio with gentle heating in THF or toluene. The reaction produced HCl as a by-product from the coupling reaction of the thiol hydrogen and a chloride atom.

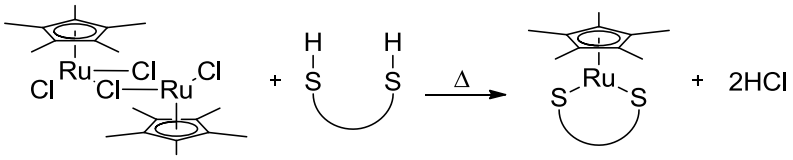

Scheme 4-1 Preparation of [Cp*Ru] Complexes

As with **Chapter 3**, the complexes synthesised were difficult to purify; all chromatographic methods proved unsuccessful. The products were permanently absorbed on to the stationary phase and could not be eluted with any solvent available to us. Therefore, all complexes reported were purified by washing with various low polarity solvents to remove any excess ligand present. The material used for the characterisation and CV was precipitated by the slow addition of diethyl ether to a solution of DCM containing the material.

NMR characterisation of these complexes was not carried out due to the paramagnetic nature of the central metal of the Ru^{3+}. Characterisation of the reported complexes will therefore be based on MS along with IR spectroscopy. As described in **Chapter 3**, complexes containing Ru are very convenient to characterise by MS. This is because Ru has seven stable isotopes (^{96}Ru 5.5%, ^{98}Ru 1.9%, ^{99}Ru 12.7%, ^{100}Ru 12.6%, ^{101}Ru 17.0%, ^{102}Ru 31.6%, ^{104}Ru 18.7%). These isotopes produce a characteristic isotopic distribution pattern, or a fingerprint which can be used to correctly identify the complex by comparing the data with the theoretical isotopic distribution.

A key feature which will be closely looked at in the IR data will be the disappearance of the thiol S-H vibration coupled with the remaining C-S vibration. C-S vibrations are found in the region of 750-570 cm^{-1}.[163] When bonded to a PGM, they exhibit a vibration at about 470 cm^{-1}.[164]

The presence of the Ru-S bond absorption in the IR would give, coupled with MS, an almost undeniable proof that the complex had been synthesised. Unfortunately, such absorption lies beyond the normal IR range of 4000 – 400 cm^{-1}, and is also very weak when visible. However, the disappearance of the thiol S-H stretch at ~2540 whilst still exhibiting the C-S stretch at 472 cm^{-1} is indicative of the synthesised complex. Coupled with this, aromatic dithiol ligands exhibit a characteristic C-H absorption at ~750 cm^{-1} due to the aromatic C-H wagging.[132] These three absorptions prove that the complex has been synthesised.

Another point raised in **Chapter 2** was that of the coordinative unsaturation of the complexes synthesised when using half-sandwich complexes with bidentate ligands. The metal centre would posses one or two possible empty coordination sites that could be possibly filled by the reaction of two monomers yielding a homodimer. Mass spectrometry, along with the crystallographic results shows that that is the case. As such, we employed the same neutral ligand triethylphosphine in an attempt to create a monomer.

4.2.1 Synthesis of $[Cp^*Ru(BenzS2)_2]$ (18)

A dark purple material was isolated from the reaction of benzene-1,2-dithiol and $[Cp^*RuCl_2]_2$ in THF. Although this complex has been synthesised previously, the CV associated with it has not been studied.[165]

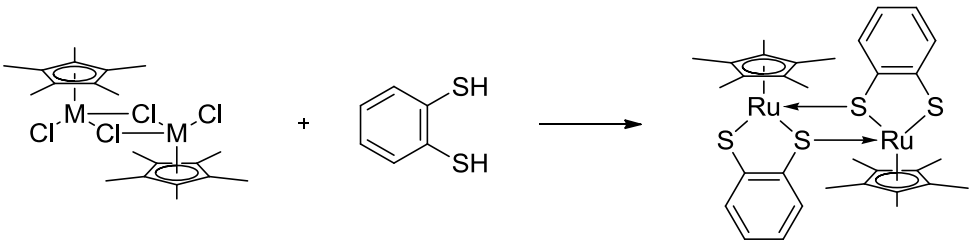

18

Scheme 4-2 Preparation of **18**

The mass spectrum (ES+) of complex **18** has one signal at *m/z* = 752.46, and corresponds to the positive ion of the complex ([M^+]). The signal also exhibits the characteristic isotopic distribution associated with a ruthenium metal centre and two sulfur atoms.

The key IR absorptions of **18** are shown below in **Table 4-2**. The pro-ligand exhibits a thiol S-H stretch at 2538 cm^{-1} and the aromatic C-H wag is at 744 cm^{-1}.

The isolated material does not show any absorptions associated with the S-H stretch, yet the ligand C-H wag is still present, although slightly shifted to 735 cm^{-1}. The M-C-S stretch is also present at 464 cm^{-1}.

Wavenumber (cm^{-1})	Assignment
3042 (-14)	C-H (arom.) of BenzS2
2963 (+21)	C-H (arom.) of Cp*
2901 (-9)	C-H (arom.) of Cp*
1536 (-6)	C=C (ring) of BenzS2
1370 (-5)	CH_3 symm. deform. Cp*
1018 (-4)	C-C (aliph.) of Cp*
735 (+11)	C-H (arom.) of BenzS2
472	M-(C-S)

Table 4-2 Key IR vibrations for **18.**
(Change in frequency is shown in parentheses)

The CV of **18** (**Figure 4-6**) exhibits a reversible one-electron oxidation at +0.1 V with a peak separation of 0.08 V. A reversible two-electron reduction is also observed at 0.24 V with a peak separation of 0.08 V. The microelectrode CV is also shown. Reducing the size of the working electrode's surface educes the current and therefore the iR drop which can lead to wave broadening in resistive solvents like DCM. Actually, at slow scan rates microelectrodes show plateau-like waves due to steady-state like currents arising from the increased mass flux. These plateaux can lead to a more precise calculation of the number of electrons transferred

(i=4nFDcr, where n is the number of electrons, F is Faraday's constant, D is the diffusion coefficient, c is the concentration and r is the radius of the microelectrode), and without the complication of additional electron transfer to follow-up products, since they diffuse away rapidly before they can undergo further electron transfer. From the microelectrode CV (**Figure 4-7**) it can be seen that there is a one-electron Ru(III)Ru(III)→Ru(III)Ru(IV) oxidation and a two-electron Ru(III)Ru(III)→Ru(II)Ru(II) reduction. Over time, the oxidation at +0.1 V decreases in intensity and eventually disappears. It is possible that this wave is due to the presence of a minor isomer which converts to the dimer.

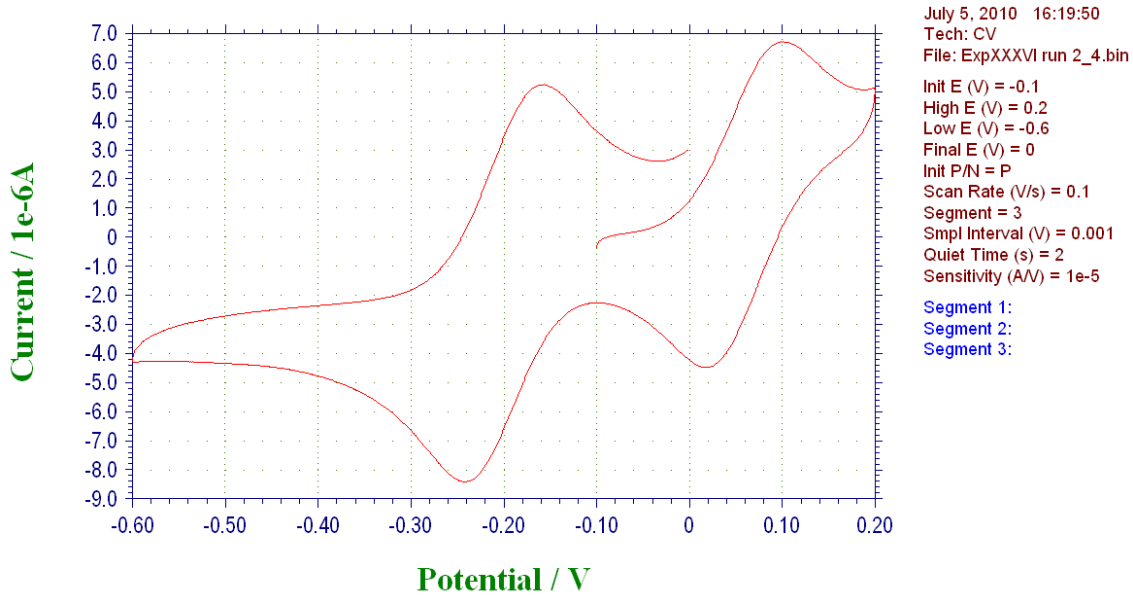

Figure 4-6 CV of **18**
3 mM conc. at 3 mm Glassy Carbon Working Electrode in DCM with
1 M TBAPF6 Electrolyte with Scan Rate of 0.1 V/s

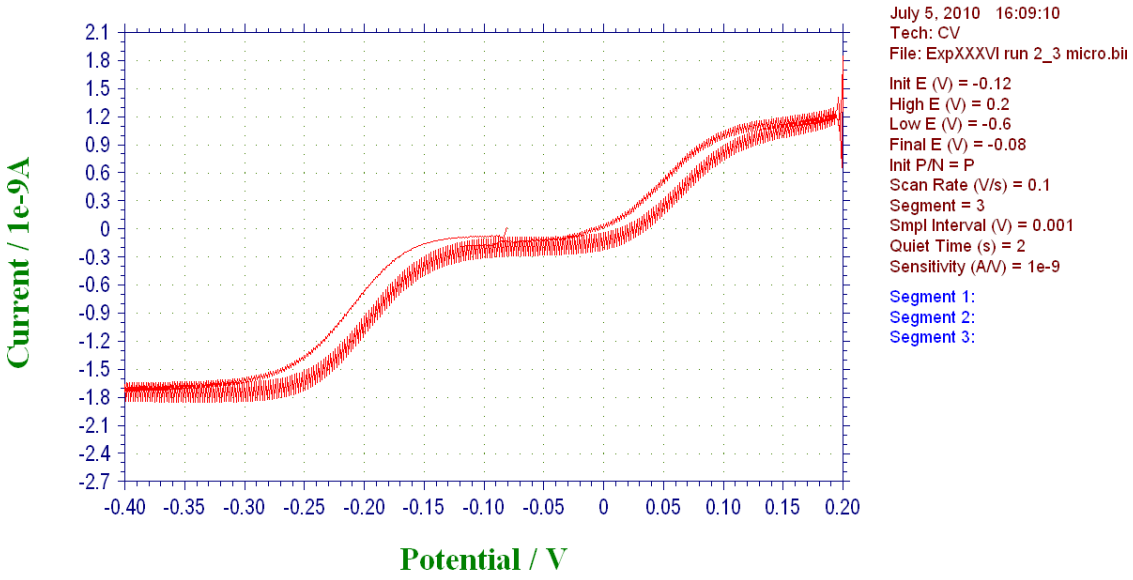

Figure 4-7 Microelectrode CV of **18**
Conditions Same as Above

The figure below (**Figure 4-8**) shows two voltammograms superimposed upon each other. This, as discussed in **Section 3.2.3**, serves to verify the electrochemical reversibility of the complex. As Ep is independent on scan rate, it is safe to assume that this family of complexes all behave in the same way and are all electrochemically reversible.

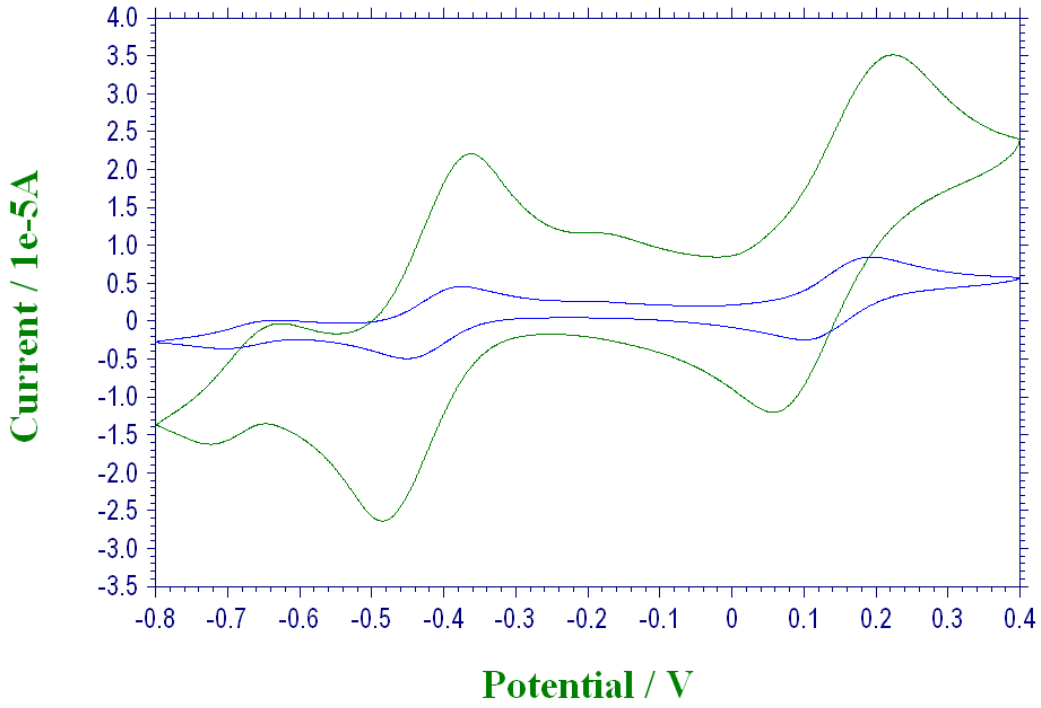

Figure 4-8 CV of **18** Run at Different Scan Rates
Green = 0.1 v/s and Blue =0.01 V/s.
Other Conditions Same as Above

Crystals of **18** were grown through the slow diffusion of diethyl ether into a saturated solution of **18** in dichloromethane and kept in the dark. The structure elucidated is that of a dimeric structure formed by the bonding of two subunits of 1**8** due to the coordinative unsaturation of the metal centre, as mentioned in **Chapter 2**. The electron configuration of the monomer ads up to a 15-electron species while the dimer is that of a 17-electron species. The two subunits of the dimer are typical of a two legged piano stool structure forming the three legged conformer upon dimerisation

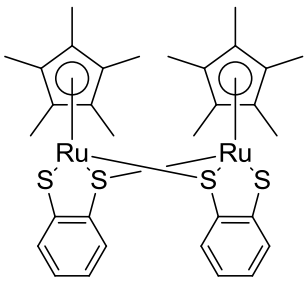

18

The M-S-S plane with respect to the benzene plane is hinged at an angle of 11.62°, an increase of roughly 6° from that of **10ox**. With respect to the Cp* plane, the M-S-S plane is angled at 43.25°. The S…S distance in this complex is shorter at 3.160 Å while that of **10ox** stands 3.186 Å. The torsion experienced by the ligand is virtually negligible at 1.8°, an angle very much like those experienced by **6** & **7** at 1 and 2° respectively. The Ru…S distance differs between both sulfur by 0.078 Å due to the loss of electron density experienced by S(1) through the formation of the dimer.

While the only structural difference between **18** and **6** & **7** is the metal centre, it is slightly perplexing that they have such different structures, **18** forming a dimer and the **6** & **7** maintaining themselves at monomers. This can be attributed by the greater bonding affinity of ruthenium towards sulfur than that of iridium of rhodium. The formation of the dimer is also facilitated by the electron count of the complexes with the monomeric ruthenium complex possessing 15 electron while the iridium/rhodium complex having 16 electrons.

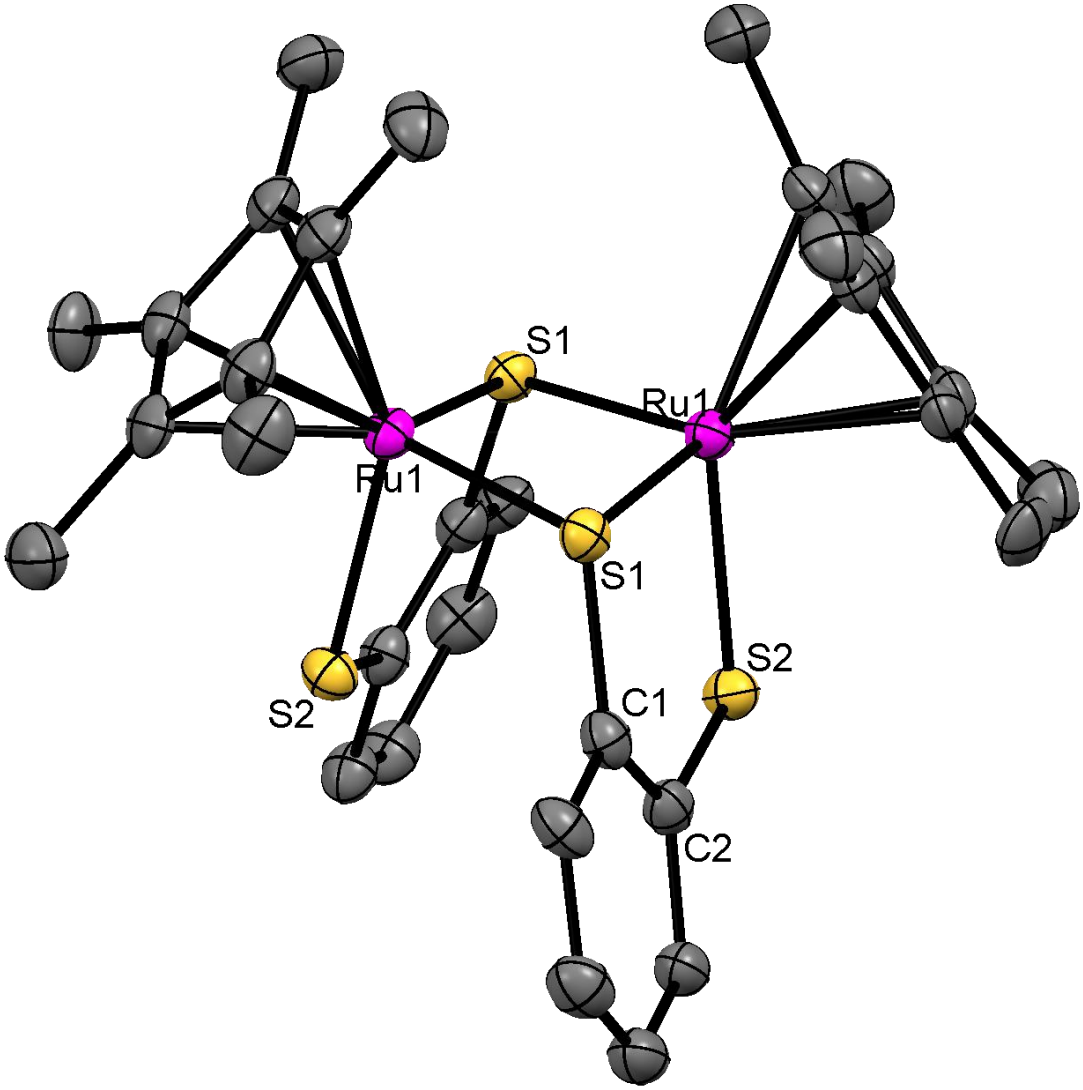

Figure 4-9 Crystal Structure of **18**

Bond Length (Å)		*Bond Angle (°)*		*Torsion Angle (°)*	
S(1)…Ru(1)	2.286(1)	**S(1)-M(1)-S(2)**	85.61(4)	**S(1)-C(1)-C(2)-S(2)**	1.8(5)
S(2)…Ru(1)	2.364(1)	**C(1)-S(1)-Ru(1)**	107.5(2)		
S(1)…S(2)	3.160(2)	**C(9)-S(2)-Ru(1)**	105.6(2)		
Ru(1)…Ru(1')	2.811(1)	**M(1)-S(1)-Ru(1')**	75.24(4)		
S(1)…C(1)	1.778(5)	**S(1)-Ru(1)-S(1')**	103.8(4)		
S(2)…C(2)	1.749(6)				

Table 4-3 Selected Bond Lengths for **18**

4.2.2 Synthesis of [Cp*Ru(BenzS2)PEt$_3$] (19)

As in **Chapter 2**, dimers were synthesised due to the coordinative unsaturation of the metal centre. The dimers were open by the use of a neutral ligand and triethylphosphine was chosen. The dimer of **18** was reacted with triethylphosphine to yield the monomer. This afforded a bright blue product that was stable in solution in most solvents, but not in chlorinated solvents.

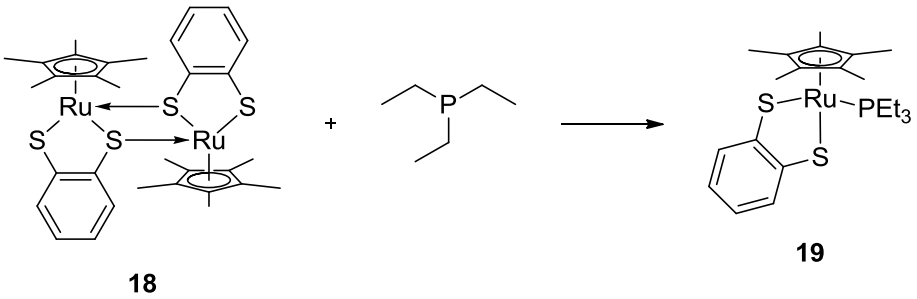

18 **19**

Scheme 4-3 Preparation of **19**

The mass spectrum (MALDI) of **19** recorded two signals that are indicative of the complex. The first signal at *m/z* = 135.09 (+H) is that of the oxidised triethylphosphine, while a second signal at *m/z* = 496.09 (M^++H) represents the monomeric form of **18.** The latter signal displays the corresponding isotopic distribution associated with the monomer and agrees with the theoretical pattern. Although the complex as a whole did not produce a corresponding signal, the combined presence of the monomer along with the oxidised triethylphosphine is an indication that complex **19** was synthesised. Moreover, the presence of the monomer, and not that of the dimmer, as in the results of **18**, adds to the supposition that **19** was successfully synthesised.

The key IR absorptions of **19** are shown below in **Table 4-4**. As this complex was synthesised from 18, there is an obvious similarity to the spectra. The main difference is in the presence of the characteristic alkyl bands along with the P-C stretch. The C-H wag is still present, although shifted to 781 cm^{-1}, while the M-C-S stretch is also present at 482 cm^{-1}.

Wavenumber (cm^{-1})	Assignment
2965 (+2)	C-H (arom.) of Cp*
2925 (+24)	C-H (arom.) of Cp*
2851	C-H (aliph.) of PEt_3
1544 (+8)	C=C (ring) of BenzS2
1413	P-CH_2-R CH_2 deform. vib
1378 (+8)	CH_3 symm. deform. Cp*
1029 (+8)	C-C (aliph.) of Cp*
781 (+46)	C-H (arom.) of BenzS2
714	P-C (aliph.)
482 (+10)	M-(C-S)

Table 4-4 Key IR vibrations for **19**
(Change in frequency from **18** is shown in parentheses)

The CV of **19** is shown below (**Figure 4-10**). It exhibits a reversible oxidation at 0.01 V with peak separation of 0.14 V. The extra electron density provided by the phosphine ligand lowers the energy of the oxidised form of the complex, and thus has a lower potential to that of **18**.

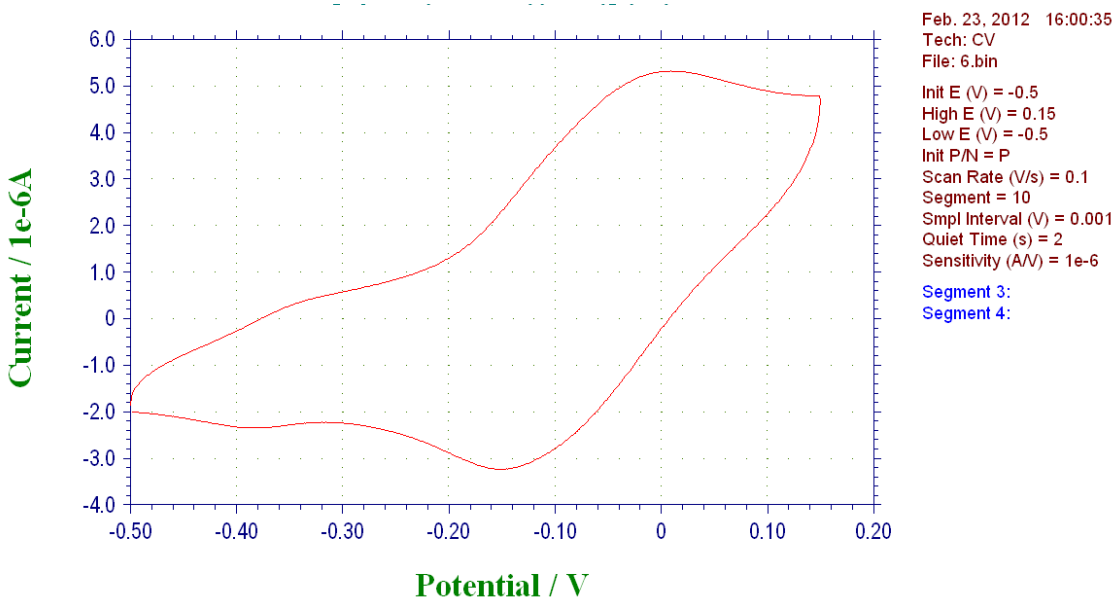

Figure 4-10 CV of **19**
3 mM conc. at 3 mm Glassy Carbon Working Electrode in DCM with
1 M TBAPF6 Electrolyte with Scan Rate of 0.1 V/s

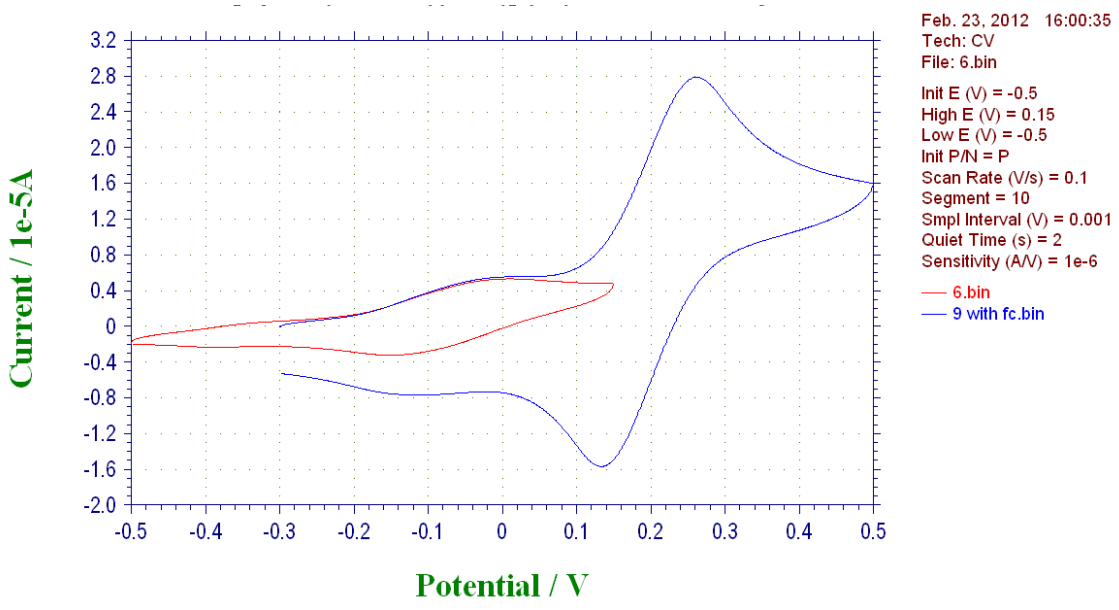

Figure 4-11 CV of **19** with 3 mM Fc (blue trace) and Without (red trace)
Conditions Same as Above

Crystals of **19** were grown by slowly cooling a saturated solution of **19** in hexane to -20° C. The crystallographic structure shows that the dimer of 18 has been opened by the reaction of triethylphosphine. The structure is that of a three legged piano stool structure typical of this family of compounds. Although several crystalisations were attempted, the quality of data obtained was of low quality and full refinement of the structure was not possible. This can be seen from the cube-like carbons instead of the typical thermal ellipsoid. Notwithstanding the low quality data, the overall structural details of interest can still be obtained.

The M-S-S plane with respect to the Cp* plane is hinged at an angle of 49.37°. The S…S distance in this complex is 3.212 Å, similar to the distance of **6** & **7**. The torsion experienced by the ligand is similar to 18 at 1.7°. Structurally, the bond lengths and angles of **19** are very similar to those of **18**, except clearly with the relaxation of the S(1)…Ru(1) bond length as the sulfur has not lost any electron density through the donation a pair of electrons to the second metal centre.

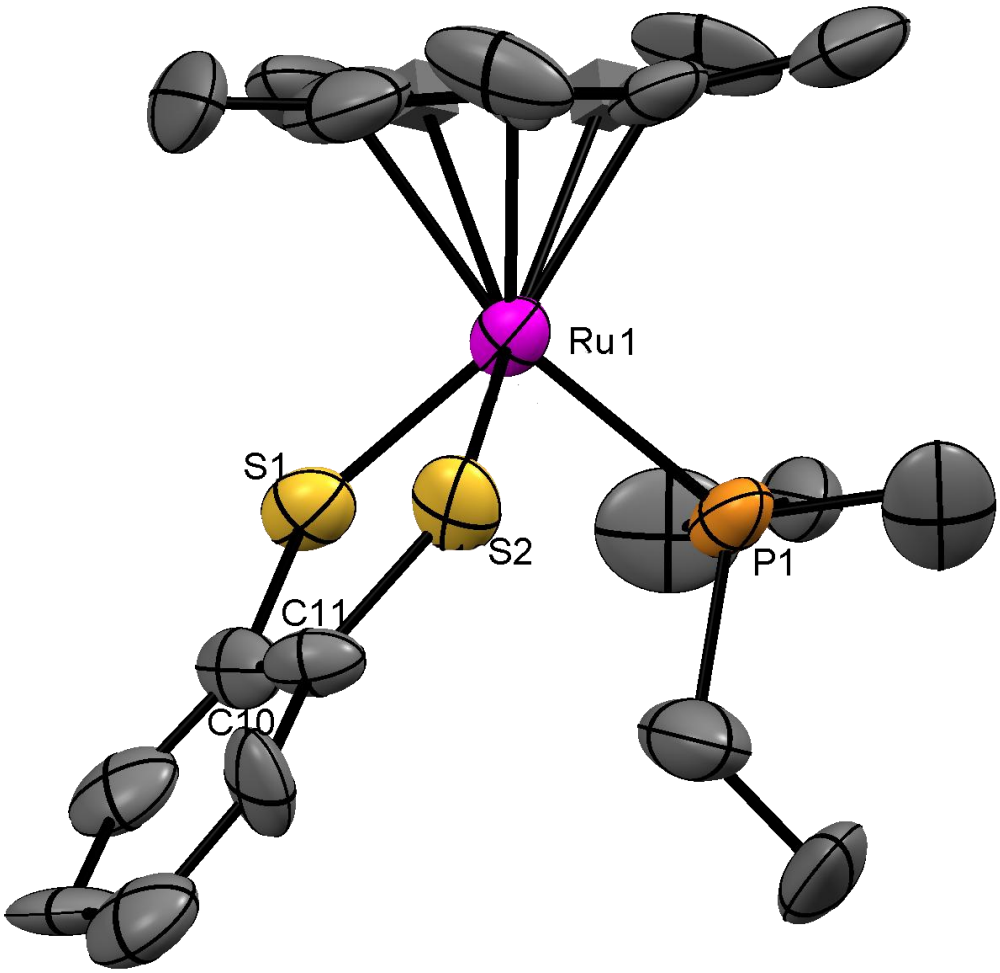

Figure 4-12 Crystal Structure of **19**

Bond Length (Å)		*Bond Angle (°)*		*Torsion Angle (°)*	
S(1)…Ru(1)	2.367(6)	**S(1)-Ru(1)-S(2)**	85.7(2)	**S(1)-C(10)-C(11)-S(2)**	2(2)
S(2)…Ru(1)	2.355(5)	**C(10)-S(1)-Ru(1)**	108.5(7)		
S(1)…S(2)	3.212(8)	**C(11)-S(2)-Ru(1)**	107.3(7)		
P(1)…Ru(1)	2.379(5)				
S(1)…C(10)	1.790(2)				
S(2)…C(11)	1.750(2)				

Table 4-5 Selected Bond Lengths for **19**

4.2.3 Synthesis of [Cp*Ru(NaphS$_2$)$_2$] (20)

Initially, this complex was synthesised employing the lithiated naphthodithiolate pro-ligand using naphtho[1,8-*cd*]-1,2-dithiole and Superhydride as the reducing agent. This led to a mixture of two products, **20** and **21** (**21** is discussed in **Section 4.2.4**). In an attempt to reduce or inhibit the synthesis of **21**, the dithiol analogue of the ligand was used in the synthesis of **20**. From the reaction of naphtho-1,8-dithiol and [Cp*RuCl$_2$]$_2$ in THF a dark green-brown material was isolated.

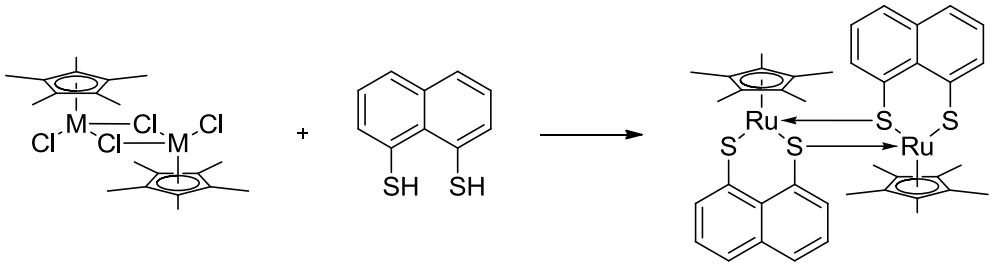

20

Scheme 4-4 Preparation of **20**

The mass spectrum (ES+) of complex **20** exhibits a single signal at *m/z* = 852.44 ([M]$^+$). It also exhibits the isotopic distribution that is associated with the ligand and fits into the theoretical model.

The key IR absorptions of **20** are shown below in **Table 4-2**. The pro-ligand exhibits a thiol S-H stretch at 2501 cm^{-1} and the aromatic C-H wag is at 756 cm^{-1}. The isolated material does not show any absorptions associated with the thiol S-H stretch, yet the ligand C-H wag is still present, although slightly shifted to 760 cm^{-1}. The M-C-S stretch is also present at 456 cm^{-1}.

Wavenumber (cm^{-1})	Assignment
3048 (0)	C-H (arom.) of NaphS2
2976 (-8)	C-H (arom.) of Cp*
2910 (-9)	C-H (arom.) of Cp*
1538 (-10)	C=C (ring) of NaphS2
1377 (+2)	CH_3 symm. deform. Cp*
1025 (+3)	C-C (aliph.) of Cp*
760 (+4)	C-H (arom.) of NaphS2
456	M-(C-S)

Table 4-6 Key IR vibrations for **20**.
(Change in frequency is shown in parentheses)

The CV of **20** exhibits a reversible oxidation at +0.55 V (**Figure 4-13**)with a peak separation of 0.12 V. A reversible reduction (**Figure 4-14**) is also observed at -0.88 V with a peak separation of 0.1 V. The oxidation at +0.55 V is that of Ru(III)→Ru(IV) process while the reduction is likely attributed to the Ru(III)→Ru(II) process.

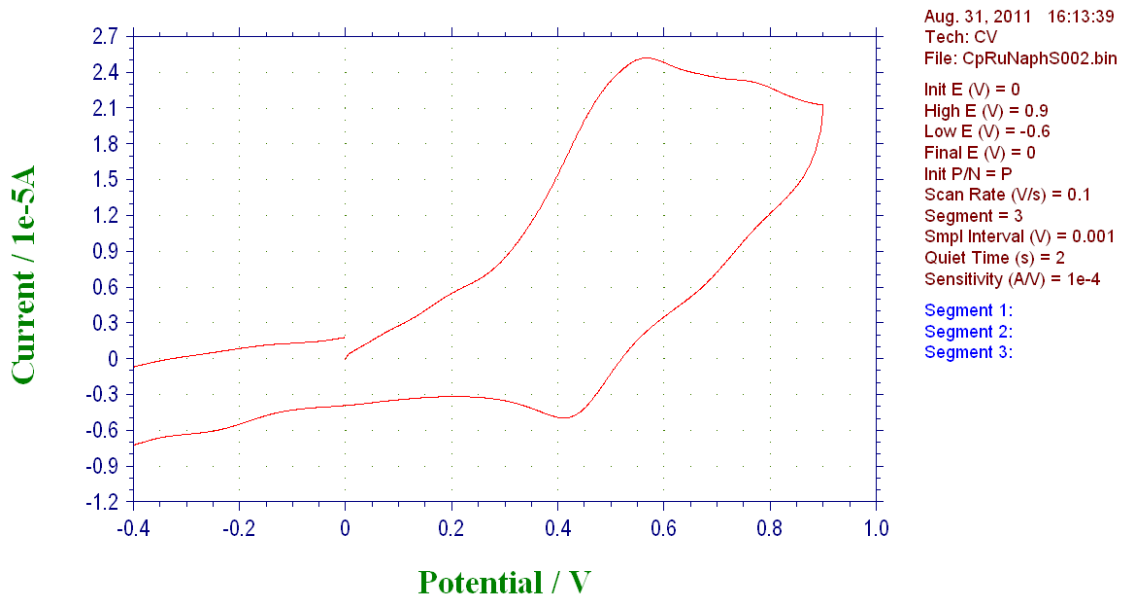

Figure 4-13 CV of **20**
3 mM conc. at 3 mm Glassy Carbon Working Electrode in DCM with
1 M TBAPF6 Electrolyte with Scan Rate of 0.1 V/s

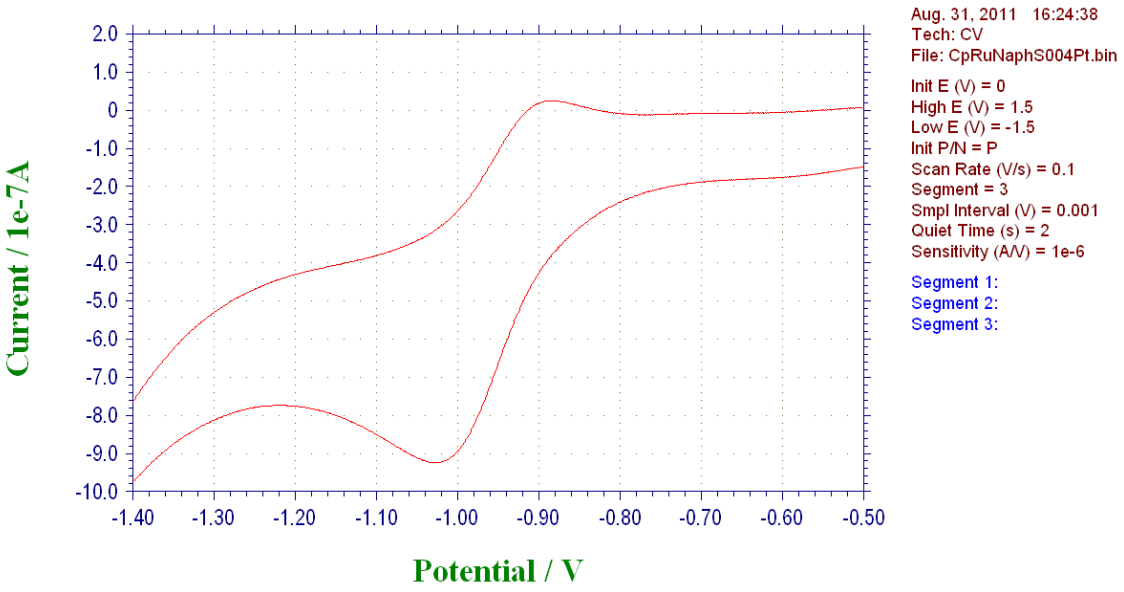

Figure 4-14 CV of **20** (2)
Conditions Same as Above

4.2.4 Synthesis of $[(Cp^*Ru)_2(\mu^2\text{-}NaphS_2)]$ (21)

Reaction of the lithiated naphtho[1,8-*cd*]-1,2-dithiole with $[Cp^*RuCl_2]_2$ yielded two different products as mentioned above in **Section 1.2.3**. Washing the crude material with hexanes afforded a green material. This type of complex where two [Cp*Ru] moieties are bridged by a single bidentate ligand has been previously reported with a related ligand.[165]

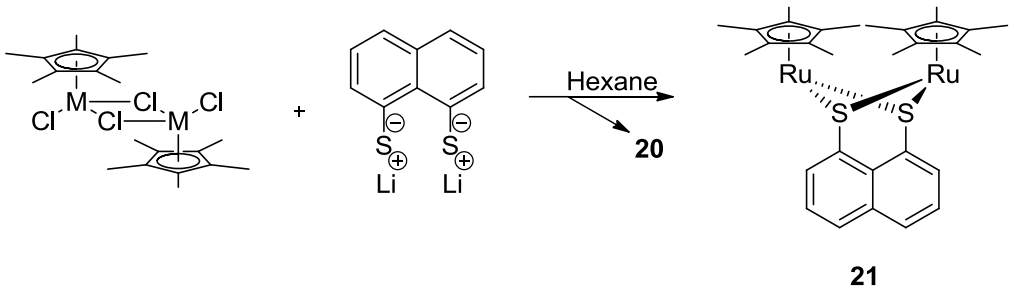

Scheme 4-5 Preparation of **21**

The mass spectrum (MALDI)of **21** gives at first glance a complicated spectrum of five different signals from *m/z* = 662.02 to 728.00, of which the former is due to **21**. However, upon further inspection, the five signals are separated from each other by 16, i.e. oxygen. This is due to the stepwise oxidation of the complex. Initially the complex is oxidised by one oxygen to give the sulfoxide-sulfide complex. The oxidation of the complex continues all the way to the double oxidation of both sulfurs giving the bisulfonic complex. The signal of **21** ([M+H]), exhibits isotopic distribution and fits in with the theoretical distribution. From the results it is evident that the complex experiences oxidation by air. However, it must be noted that the sample submitted for mass spec was that of one that had been left in solution for several hours. A second spectrum showing only one signal at *m/z* = 662.57 was also obtained, this one having been stored in nitrogen.

The key IR absorptions of **21** are shown below in **Table 4-7**. It is as predicted very similar to that of **20**. In fact, only very slight differences were noted in the wavenumbers.

The thiol S-H stretch is still absent, while the ligand's C-H wag has shifted by 756 to 803 cm^{-1}. The M-C-S stretch is also present at 469 cm^{-1}.

Wavenumber (cm^{-1})	Assignment
3058 (+10)	C-H (arom.) of NaphS2
2981 (+5)	C-H (arom.) of Cp*
2930 (+20)	C-H (arom.) of Cp*
1546 (+9)	C=C (ring) of NaphS2
1379 (+2)	CH_3 symm. deform. Cp*
1025 (+3)	C-C (aliph.) of Cp*
803 (+43)	C-H (arom.) of NaphS2
469 (+13)	M-(C-S)

Table 4-7 Key IR vibrations for **21**.
(Change in frequency from **20** is shown in parentheses)

The CV voltammetry of **21** was different to that of **20**. In the positive scan, irreversible oxidations were observed at +0.78 V. A reduction was noted at -0.1 V, with a peak separation of 0.1 V.

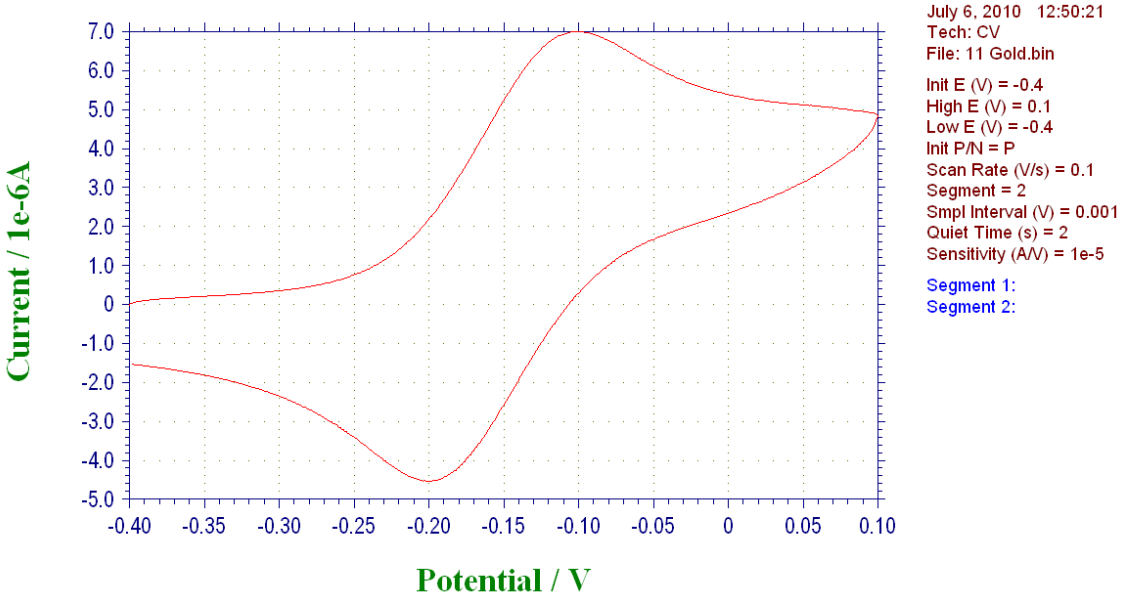

Figure 4-15 CV of **21**
3 mM conc. at 3 mm Glassy Carbon Working Electrode in DCM with
1 M TBAPF6 Electrolyte with Scan Rate of 0.1 V/s

4.2.5 Synthesis of [Cp*Ru(NaphS$_2$)PEt$_3$] (22)

The dimer of **20** was opened with the use of triethylphosphine. A red material was extracted with diethyl ether.

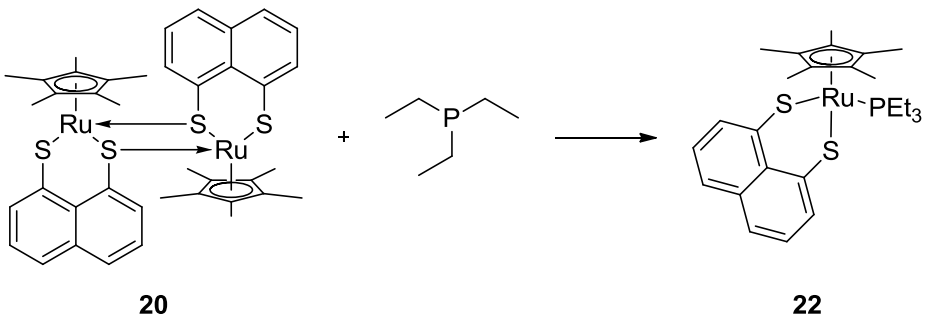

20 **22**

Scheme 4-6 Preparation of **22**

The mass spectrum of **22** is very similar to that of **19** in that two different signals were reported. The first signal is that of the sodium salt of triethylphosphine oxide at *m/z* = 157.29, while the second signal reported was that of the monomer of **20** at *m/z* = 426.39 ([M]).

The key IR absorptions of the spectrum of **22** are shown below in **Table 4-8**. Little difference is shown from **20**, except for the extra absorptions due to the alkyls C-C and C-H stretch. Change in the frequency of the P-C bond is also seen. The C-H wag is still present, although shifted to 781 cm^{-1}, while the M-S-C stretch is also present at 482 cm^{-1}.

Wavenumber (cm^{-1})	Assignment
2980 (+4)	C-H (arom.) of Cp*
2930 (+20)	C-H (arom.) of Cp*
2856	C-H (aliph.) of PEt_3
1544 (+8)	C=C (ring) of NaphS2
1426	P-CH_2-R CH_2 deform. vib
1387 (+10)	CH_3 symm. deform. Cp*
1036 (+11)	C-C (aliph.) of Cp*
801 (+41)	C-H (arom.) of NaphS2
717	P-C (aliph.)
467(+11)	M-(C-S)

Table 4-8 Key IR vibrations for **22**
(Change in frequency from **20** is shown in parentheses)

The CV of **22** is shown below (**Figure 4-16**). A reversible oxidation wave occurs at +0.12 V and has a peak separation of 0.12 V. Just like **19**, the extra electron density from the phosphine ligand promotes the lowering of the oxidation potential from the value observed for dimer **20**.

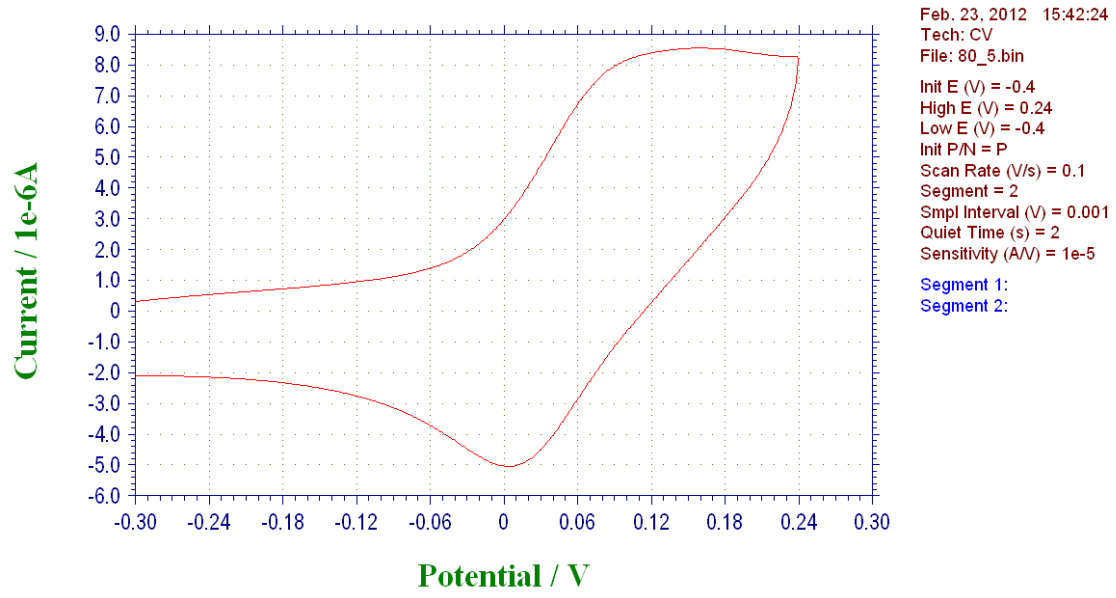

Figure 4-16 CV of **22**
3 mM conc. at 3 mm Glassy Carbon Working Electrode in DCM with
1 M TBAPF6 Electrolyte with Scan Rate of 0.1 V/s

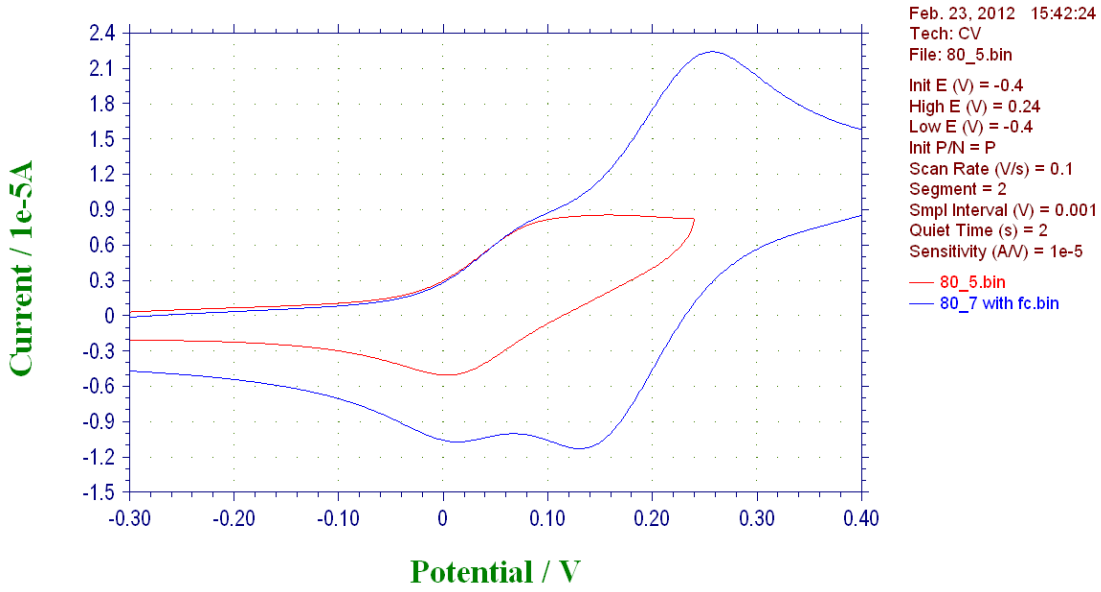

Figure 4-17 CV of **22** with 3 mM Fc (blue trace) and Without (red trace)
Conditions Same as Above

Crystals of **22ox** were grown from the slow evaporation of a saturated solution of **22** in dichloromethane. It can be seen from the crystal structure that not only has one of the sulfurs become doubly oxidised by oxygen, but the other has become ethylated. The ethylation is most likely through a reaction with ethanol, the solvent used during the reaction. The crystal structure shows that that the dimer opening reaction with triethylphosphine was successful and yielded a structure with formula of [Cp*$RuC_{10}H_6S_2PEt_3$]. The data collected was of good quality with residual R1 factor of 4.66%.

The geometry about the metal centre is a typical three legged piano stool structure and similar to those of **4B** and **5B**, the Ir and Rh analogues. The M-S-S plane with respect to the naphthalene is hinged at an angle of 65.22. an increase of ~15° when compared to **4B** and **5B**. The Cp* plane with respect to the naphthalene plane is angled at 13.22°.

The interatomic S…S distance stands at 2.937 Å is the shortest distance measured from all the complexes studied. This is likely brought about by a lessening of the lone pair repulsion exhibited by the *peri*-sulfurs. This lowering of repulsion between the sulfurs is due to the loss of electron density by bonding with oxygen and the ethyl substituent. The S…Ru bond lengths are 2.274 for the oxidised sulfur S(1) and 2.274 for the ethylated sulfur S(2). The former is shorter as it has two substituents reducing the overall electron density, while the latter only has one. The torsion exhibited by the ligand has reduced and is effectively planar with an angle of 1.5°.

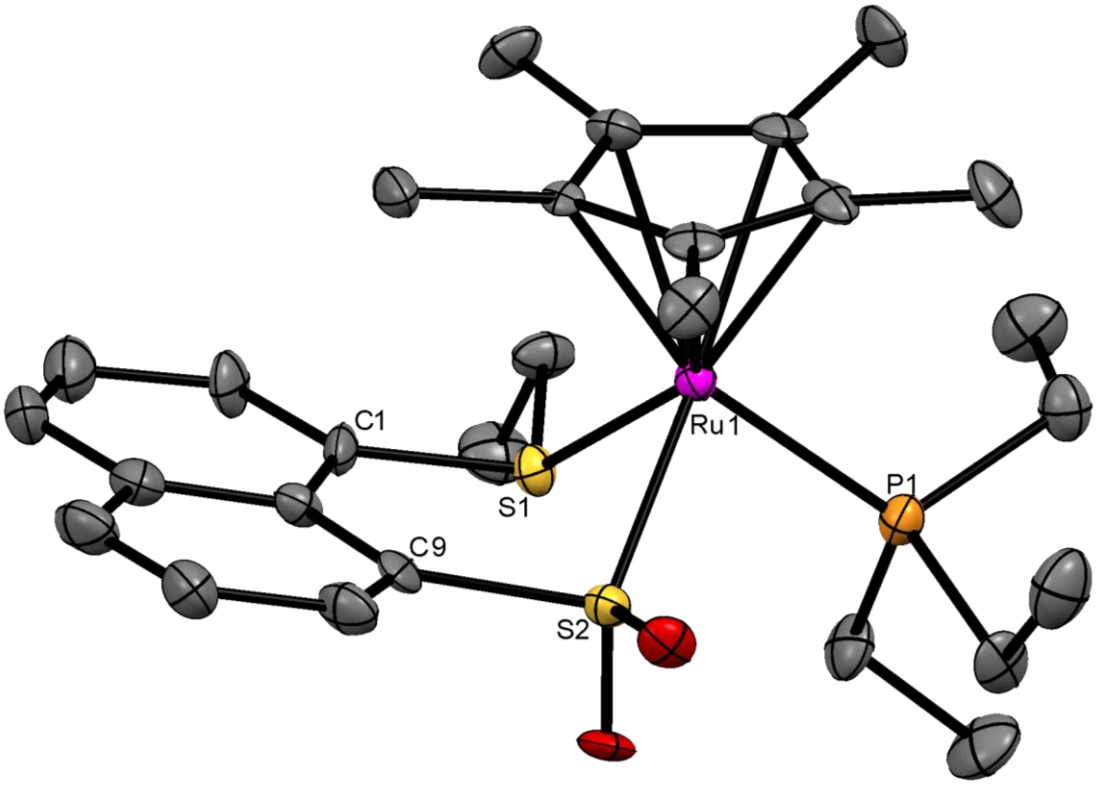

Figure 4-18 Crystal Structure of **22ox**

Bond Length (Å)		*Bond Angle (°)*		*Torsion Angle (°)*	
S(1)…Ru(1)	2.336(2)	**S(1)-Ru(1)-S(2)**	79.12(6)	**S(1)-C(1)-C(9)-S(2)**	1.5(3)
S(2)…Ru(1)	2.274(2)	**C(1)-S(1)-Ru(1)**	106.3(2)	**C(1)-C(10)-C(5)-C(6)**	177.2(6)
S(1)…S(2)	2.937(3)	**C(9)-S(2)-Ru(1)**	104.0(2)		
P(1)…Ru(1)	2.328(2)				
S(1)…C(1)	1.773(6)				
S(2)…C(9)	1.826(6)				

Table 4-9 Selected Bond Lengths for **22**

4.2.6 Synthesis of [Cp*Ru(μ²-NaphNS)Cp*RuCl] (23)

Reaction of $[Cp^*RuCl_2]_2$ with the mixed heteroatomic ligand 8-aminonaphthalene-1-thiol produced a bridged diruthenium complex. Unlike previous examples, the nitrogen of the amino group is the point of bridging between the two metal centres.

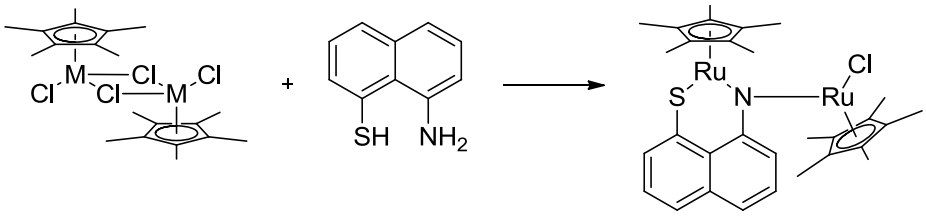

23

Scheme 4-7 Preparation of **23**

The MS (ESI) of **23** produced a single peak representative of the complex. The first at *m/z* = 645.07 represents the complex minus a chloride ligand ($[M - Cl]^+$), while the second at *m/z* = 680.03 ($[M^+]$) represents the complex with the chloride ligand still coordinated. They both exhibit their corresponding isotopic distribution and both fit within the theoretical model.

The key IR absorptions of **23** are shown in **Table 4-10** below. Unfortunately, the pro-ligand thiol S-H stretch that occurs at ~2520 cm^{-1} has been obscured by the combination of the N-H and S-H stretches giving several broad signals between 2754 and 2458 cm^{-1}. Nevertheless, the absence of the thiol stretch, yet still retaining the ligand's C-H wag at ~756 cm^{-1} would indicate that the complex had been synthesised. The isolated material did also not show any S-H or N-H stretch from the unreacted ligand. The ligand aromatic C-H wag has been sifted by several wavenumbers to 762 cm^{-1}. The C-S bond stretch is also present at 461 cm^{-1}.

Wavenumber (cm^{-1})	Assignment
3048 (-2)	C-H (arom.) of NaphSN
2987 (+3)	C-H (arom.) of Cp*
2912 (-11)	C-H (arom.) of Cp*
1569 (+8)	C=C (ring) of NaphSN
1377 (+2)	CH_3 symm. deform. Cp*
1022 (0)	C-C (aliph.) of Cp*
762 (+6)	C-H (arom.) of NaphSN
461	M-(C-S)

Table 4-10 Key IR vibrations for **23**
(Change in frequency is shown in parentheses)

The cyclic voltammetry of **23** shows no reversibility in the oxidative or reductive regions of the voltammogram. Two irreversible oxidations occur, the first at +0.73 V, with the second occurring at 1.63 V. The irreversible oxidation of this complex is most likely to be due to the presence of the amine group.

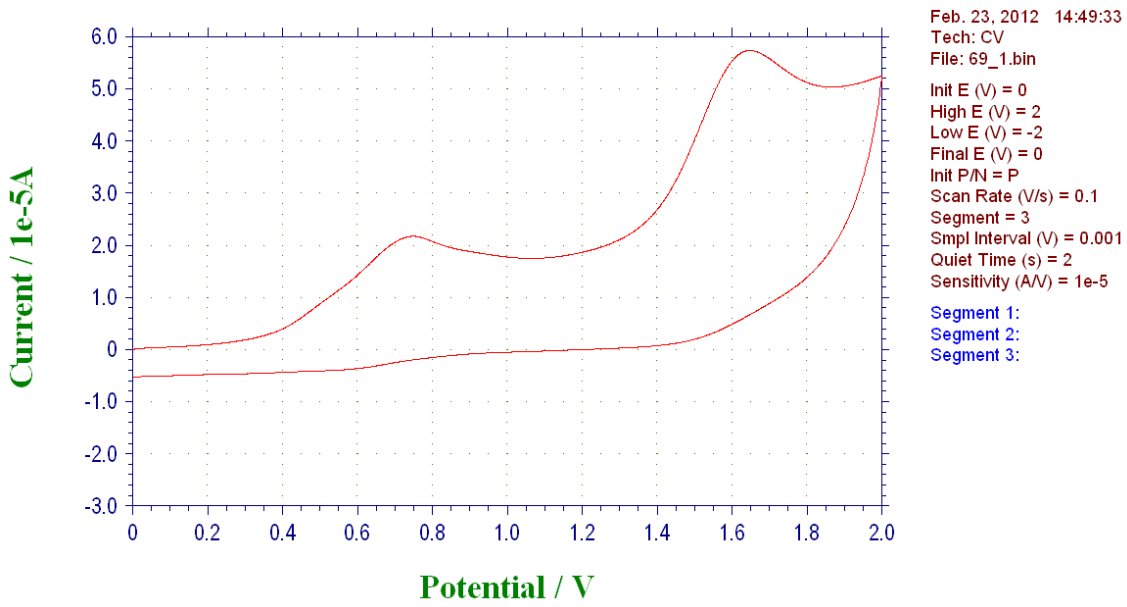

Figure 4-19 CV of **23**
3 mM conc. at 3 mm Glassy Carbon Working Electrode in DCM with
1 M TBAPF6 Electrolyte with Scan Rate of 0.1 V/s

This previous complex showed that the dithiolato ligand stabilises the oxidised complex, lowering the potential as a consequence. In this case, the replacement of a sulfur with a nitrogen creates a complex that is unstable when the metal is oxidised electronically. Amines with their high basicity (p*K*a aniline = 9.3) are known to be oxidised and easily succumb to electrochemical oxidation.

4.3 Experimental

General Procedures

Unless otherwise stated, all operations were performed under anaerobic conditions using a nitrogen atmosphere and standard Schlenk techniques. Subsequent work up procedures and chromatographic purification were carried out in air. Dry and deoxygenated solvents were dispensed from an MBraun SPS-800 Solvent Purification System. Methanol and ethanol were dried by refluxing over their corresponding magnesium alkoxide salts and distilling under nitrogen. $RuCl_3 \cdot xH_2O$ was received from Ceimig Ltd. All other reagents and chemicals were purchased from Sigma Aldrich, Alfa Aesar or Acros Organics. All chemicals/reagents were used as received without any further purification, unless otherwise stated. All NMR data were recorded using either a Jeol GSX Delta 270 or Bruker Avance 300, locked to external reference. Coupling constants, if stated, are quoted in Hz. Infrared spectra were recorded as KBr disks on a Perkin-Elmer FT-IR/Raman System 2000 spectrophotometer in the range of 4000-400 cm^{-1}. Cyclic voltammetry was performed on a CH Instruments 600c Potentiostat with a Pt wire counter electrode and a Ag/Ag^+ reference electrode. Mass spectra analyses were performed by either the University of St Andrews Mass Spectrometry Service or by that of the EPSRC's Mass Spectrometry Centre. Elemental analyses were performed by the Elemental Analysis service provided by the London Metropolitan University.

Syntheses of Starting Materials

4.3.1 Preparation of $[\eta^5\text{-Cp*RuCl}_2]_n$[166]

$RuCl_3 \cdot H2O$ (1.49 g, 6.62 mmol) was added to ethanol (25 mL). To this, 1,2,3,4,5-pentamethylcyclopentadiene (2.06 g, 15.1 mmol) was added and refluxed for 3h. The dark precipitate was filtered off and successively washed with ethanol (2× 5 mL) and diethyl ether (2× 5ml) and dried under reduced pressure. Yield 1.46 g, 72%.

4.3.2 Preparation of naphtho[1,8-*cd*]-1,2-dithiole[106]

Naphthalene (3.85 g, 30 mmol) was dissolved in hexane (45 mL). To it, *n*-butyllithium (120 mmol) and TMEDA (18 mL, 0.121 mol) was added. The solution was heated to 60° C. for 3 h. The brown suspension was cooled to -78 °C and THF (100 mL) was added. Sulfur flowers (8 g, 0.25 mol) was added with vigorous stirring and allowed to warm to RT. The mixture was washed with water (100 mL) and the organic layer was kept dried over $MgSO_4$ and evaporated under reduced pressure. Purification of the red-brown oil by column chromatography (silica gel, hexane) afforded red-brown powder which was washed with ethanol (1-2 mL), filter and allowed to dry over suction. Yield: 2.1 g, 36%.

4.3.3 Preparation of dibenzo[*c*,*e*]-1,2-dithiine[107]

Biphenyl (5 g, 32.4 mmol) was added in small portions to a solution of 2.5 M *n*-butyllithium (64.85 mmol) in hexane and TMEDA (9.72 mL, 64.85 mmol) at -15 °C over the course of an hour. The mixture was allowed to warm to RT overnight and sulfur flowers (2.28 g, 71.28 mmol) was added slowly with vigorous stirring over 3 h. The mixture was poured into water (300 mL) and the organic layer was extracted with DCM, dried over Na_2SO_4 and concentrated *in vacuo*. Column chromatography (silica gel, petroleum ether (40-60°) afforded a bright yellow powder which was subsequently washed with ethanol (1-2 mL) and filtered. Yield: 3.16 g, 45%.

4.3.4 Preparation of 5,6-dihydroacenaphtho[5,6-*cd*]-1,2-dithiole[141]

To a solution of 5,6-dibromoacenaphtene (2g, 6.41 mmol) and TMEDA (0.52 mL, 12.82 mmol) in THF (120 mL), *n*-butillithium (6.5 mmol) was added dropwise at -78 °C over 1 h and left to stir for 15 mins thereafter. Sulfur flowers (0.205 g, 6.4 mmol) was added, allowed to warm to -35 °C and stirred for 2 h. The mixture was again cooled to -78 °C and *n*-butyllithium (6.5 mmol) was added and the procedure was repeated as above. The mixture was quenched with acetic acid (1.2 mL) followed by exposure to air stream for oxidation. The solution was concentrated and water (50 mL) was added and the organic layer was extracted with DCM (100 mL), dried over $MgSO_4$ and evaporated. Hexane (20 mL) was added and the precipitate was filtered off and washed with cold hexane (3× 5 mL) and the red-brown powder was left to dry under suction. Yield: 0.75 g, 55%.

4.3.5 Preparation of 8-aminonaphthalene-1-thiol[108]

Lithium aluminium hydride (3 g, 80 mmol) was added to diethyl ether (100 mL). To it, 1,8-naphthosultam (4 g, 20 mmol) in THF (15 mL) was added dropwise to the suspension at -38 °C over 1 h. The mixture was then refluxed for 1 h, after which, the solution was cooled in an ice-salt bath, and the excess lithium aluminium hydride was quenched with the slow addition of water (10 mL). Sulfuric acid (100 mL, 2 M) was added. Any excess acid was neutralised with NaOH, and the product was extracted with ether, dried over $MgSO_4$ and evaporated to dryness. The product is air sensitive and is this stored under nitrogen. Yield: 2.41 g, 69%.

Syntheses of Complexes

4.3.6 Synthesis of $[\eta^5\text{-Cp*Ru}(\mu^2\text{-BenzS}_2)]_2$

To a solution of $[\eta^5\text{-Cp*RuCl}_2]_n$ (0.36 g, 1.2 mmol) in THF (50 mL), 1,2-benzenedithiol (0.26 g, 1.8 mmol) was added in one portion. An immediate colour change from dark orange to dark green occurred. The solution was stirred for a further 1 hour, after which the solvent was evaporated. The solid material was dissolved in DCM (10 mL) and washed with water. The

organic layer was dried over $MgSO_4$ and evaporated to dryness. Yield 85%. Mass spec. (ESI): *m/z* 752($[M]^+$, 100%). IR (KBr): ν_{max}/cm^{-1} 3042m, 2963s, 2901s, 1703w, 1563s, 1421vs, 1370vs, 1278m, 1233m, 1152m, 1085s, 1018s, 839w, 735vs, 662m, 612m, 584m, 537m, 464m, 436m, 411w.

4.3.7 Synthesis of $[\eta^5\text{-Cp*Ru}(\mu^2\text{-BenzS}_2)\text{PEt}_3]$

To a solution of $[\eta^5\text{-Cp*Ru}(\mu^2\text{-BenzS}_2)]_2$ (0.05 g, 0.13 mmol) in THF (25 mL) was added PEt_3 (0.025 mL, 0.13 mmol) and the solution was refluxed for 1 hour. The solvent was evaporated to remove solvent and volatile phosphine. Hexane (10 mL) was added and the blue solution was filtered off using a syringe and needle. Yield 85%. Mass spec. (ESI): *m/z* 496($[M +H -PEt_3]^+$, 30%), 135($[PEt_3 +O]^+$), 22%). IR (KBr): ν_{max}/cm^{-1} 2965s, 2952s, 2851m, 1656m, 1459s, 1413m, 1378m, 1261s, 1127m, 1101m, 1029s, 944w, 861w, 802s 781s, 714m, 660w, 622w, 579w, 531w, 482w, 453w.

4.3.8 Synthesis of $[\eta^5\text{-Cp*Ru}(\mu^2\text{-NaphS}_2)]_2$

Toluene (50 mL) was added to $[\eta^5\text{-Cp*RuCl}_2]_n$ (0.2 g, 0.6 mmol) and left to stir for 1 hour after which naphthalene-1,8-dithiol (0.35 g, 1.5 mmol). There was an instantaneous colour change from dark orange to green-brown. The solution was heated at 50° C. for 4 hours. The solution was filtered through celite and the filtrate was evaporated to dryness. The solid was washed with hexane (3× 25 mL) to remove excess ligand. Mass spec. (ESI): *m/z* 852($[M]^+$, 100%). IR (KBr): ν_{max}/cm^{-1} 3048m, 2976m, 2905s, 1638m, 1538s, 1490s, 1426m, 1377vs, 1184s, 1025s, 986m, 816m, 760vs, 724w, 600w, 585w, 547m, 468m, 456m.

4.3.9 Synthesis of $[(\eta^5\text{-Cp*Ru})_2(\mu^2\text{-NaphS}_2)]$

Toluene (50 mL) was added to $[\eta^5\text{-Cp*RuCl}_2]_n$ (0.2 g, 0.6 mmol) and left to stir for 1 hour after which naphthalene-1,8-dithiol (0.35 g, 1.5 mmol). There was an instantaneous colour change from dark orange to green-brown. The solution was heated at 50° C. for 1 hour. The solvent was evaporated and the solid was washed with hexane (3× 25 mL) to remove excess ligand. The solid material was washed several times with diethyl ether which afforded a green solution, which was discarded. The product was isolated using ethyl acetate and filtering off

the brown-green liquid with a blunt needle wrapped with filter paper. Mass spec. (ESI): *m/z* 662([M +H]$^+$, 50%). IR (KBr): ν_{max}/cm^{-1} 3058m, 2981m, 2930s, 1634m, 1546s, 1494s, 1431m, 1379vs, 1239m, 1166s, 1025s, 971m, 803m, 734w, 603w, 564w, 557w, 469m, 444w, 413w.

4.3.10 Synthesis of [η^5-Cp*Ru(μ^2-NaphS$_2$)PEt$_3$]

Toluene (50 mL) was added to [η ^{5}-Cp*Ru(μ^2-NaphS$_2$)]$_2$ (0.2 g, 0.66 mmol) and PEt$_3$ (1 mmol) was added in one portion and heated to 60° C. and then left to stir overnight. The solvent was evaporated and left under vacuum for an hour at 50° C. to evaporate any remaining ligand. The red product was extracted with diethyl ether. Mass spec. (ESI): *m/z* 426([M]$^+$, 90%), 157([PEt$_3$ +O +Na]$^+$, 100%). IR (KBr): ν_{max}/cm^{-1} 3044m, 2980m, 2930s, 2856m, 1638m, 1544s, 1481s, 1426m, 1426m, 1387vs, 1181s, 1114m, 1036s, 979m, 801m, 781vs, 717m, 609w, 579w, 467m, 424w.

4.3.11 Synthesis of [η^5-Cp*Ru(μ^2-NaphSN){η ^{5}-Cp*RuCl}]

To a solution of [η^5-Cp*RuCl$_2$]$_n$ (0.22 g, 0.7 mmol) in THF (50 mL), 8-amminonaphthalene-1-thiol (0.18 g, 1.05 mmol) was added in one portion. A precipitate formed, which was filtered off and washed with ether. Mass spec. (ESI): *m/z* 645([M -Cl]$^+$, 20%), 680([M]+), 20%). IR (KBr): ν_{max}/cm^{-1} 3050m, 2987m, 2912m, 1958w, 1619m, 1569s, 1490w, 1452s, 1377s, 1337w, 1275w, 1247w, 1200m, 1146w, 1076m, 1022vs, 822m, 762s, 615w, 526w, 461w.

5 CONCLUDING REMARKS

The synthesis and behaviour of a series of platinum group metal based complexes with electron rich dithiolato ligands has been reported. Two distinct areas have been covered. One exploring the chemistry of ruthenium based redox mediators, whilst the second explores the structure and bonding behaviour of iridium and rhodium complexes with dithiolato ligands.

5.1 Ruthenium Redox Mediators

The first class forms the main aim and aspect of this project. This is concerned with the synthesis of novel ruthenium based complexes incorporating electron rich dithiolato ligands. Their suitability to act as redox mediators in electrochemical cells was tested using cyclic voltammetry experiments.

Through an extensive review of past and current research in ruthenium based mediators, the area of redox mediators is generally divided and dominated by the two parent complexes $[Ru(bpy)_2]$ and [Cp*Ru] and analogues thereof (**Figure 5-1**). These two parent complexes have been extensively studied due to their interesting properties and are used in several technologies from redox mediators in electrochemical cells to dyes in dye-sensitised solar cells. Complexes of these possess low redox potentials, in part due to the low redox potential of the central metal atom, but mainly due to the electron rich ligands that coordinate onto the metal. They are noted in exhibiting remarkable stability in their oxidised or reduced forms as well as having remarkably high extinction coefficients and fast electron transfer processes.

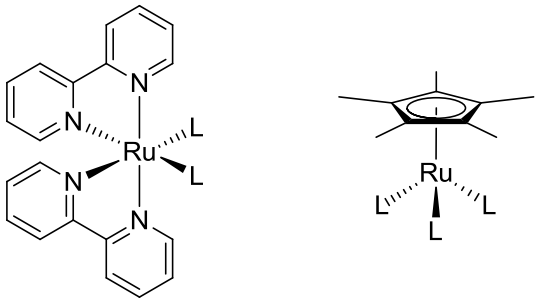

Figure 5-1 Most Common Parent Complexes Used as Redox Mediators

Whilst the area had been mostly unexplored, bar one recent example,[134] ruthenium complexes bearing dithiolato ligands with electron rich backbones should possess interesting properties that could be exploited. These sort of complexes should be electron rich and able to donate electrons to electrochemical processes due to both the electron rich amine, carbon and thiolate ligands as well as ruthenium's oxidation potential. These complexes will not be limited to oxidation processes but will also be able to accept electrons due to ruthenium exhibiting multiple stable oxidation states.

Although while in the solid state the complexes were shown to be oxygen stable only oxidising over prolonged periods when exposed to light, in solution, however, the oxidation occurred much more rapidly. The colour of the solutions changed over a matter of hours and oxides were produced. Through mass spec. and crystallographic data, it was noted that the oxidation of the sulfurs occurred doubly rather than singly yielding the thiolate sulfinate ($S{\cdot}SO_2$) form of the complex. This is presumably due to the higher stability of the S(VI) state compared to the S(IV). With time, the second sulfur would also become doubly oxidised to the disulfinate ($SO_2{\cdot}SO_2$) form. The lag in the formation of the tetroxide is likely due to the steric force created by the oxygens, the two oxygens inhibiting the oxidation of the second sulfur and only progressing slowly to form the tetroxide, helped perhaps also by the light.

Figure 5-2 Thiolate-Sulfinate Form (left), Disulfinate Form (right)

Chromatographic techniques for the purification of these compounds proved unsuccessful as the complexes were sparingly soluble in most solvents bar chlorinated solvents like DCM. The use of the 4,4'-*di-tert*-butyl-2,2'-bipyridine was intended to produce complexes that were more soluble and although did this occur and materials were more soluble in non-polar solvents, the oxygen sensitivity of the complexes yielded a column that did not elute as one band due to the ongoing oxidation of the complexes.

Notwithstanding the oxygen sensitivity and presence of impurities, all the complexes synthesised (**10** – **22**) performed well and exhibited reversible oxidations with potentials in the region of -0.1 to +0.2 V vs. Ag/Ag^{+}. Unfortunately, many of these reversible waves were not well defined due to adsorption, slow electron transfer and possibly follow up products. In addition, the presence and production of the sulfinate groups while in solution may have added to the ill-defined character of the redox wave.

Overall the Cp* subclass exhibited reversible oxidations at slightly lower potentials than those of *bis*(bipyridine), with the [$(Cp^*Ru)_2$NaphS] (**21**) complex having the lowest oxidation potential at -0.1 V and the [$Cp^*Ru(BenzS)PEt_3$] (**19**) having the second lowest oxidation potential at 0.01 V vs. Ag/Ag^{+}. The lowest oxidation potential achieved by the *bis*(bipyridine) series was that of the [$Ru(^{t}Bu\text{-}bpy)_2$AcenaphS] (**17**) complex exhibiting the lowest potential of the series at 0.11 V. The bis-bipyridine complexes, although having higher oxidation potentials than those of the Cp*, had smaller peak separation potentials which correspond to faster electron transfer process.

5.2 Structural Studies of Cp*Ir/Rh Complexes

The second area covered involved the synthesis and structural studies of a series of pentamethylcyclopentadienyl iridium and rhodium complexes with dithiolato ligands. As the ligands used were all bidentate, this left an empty coordination site. This site was filled though the dative bonding of an adjacent complex, though the sulfur lone pair, yielding a dimer. The structure and bonding of the complex while in the dimeric form would put a lot of strain upon

the ligand distorting it from its native form. In order to rectify this, the dimer was open up with a neutral donor. Triethylphosphine was chosen as is was employed in **Chapter 3**.

The NMR data of the complexes synthesised (**4**-**9**) was straightforward. The methyl protons of the Cp*showed up in the normal region of 1-2 ppm depending on the metal. The ligand protons were in the region of 6-8 ppm. In the case of the naphthalenedithiol ligand dimeric complexes (**4** & **5**), the NMR data showed that both sub-units of the dimer were in identical environments The NMR data of the pseudo-tetramer 9 showed that unlike 4 & 5, the Cp* methyl protons were in non-identical environments giving a signal that covered a region of 0.94 – 1.4 ppm.

Single crystal x-ray data showed that both the Ir…S and Rh…S bond lengths were relatively conventional and within expected parameters from published structures via the CDS. The smallest lengths were those of the benzenedithiol complexes and were calculated as 2.243 and 2.251 Å for **6** and .2.218 to 2.291 Å for **7**.

The naphthalenedithiol complexes (**4**, **4B**, **5** and **5B**) all exhibited normal bond lengths of ~2.350 Å. The dimeric structures did show that there was some distortion attributed with the dimerisation, but this was largely confined to the splay angle of the ligand due of the stretching force acted upon the sulfur atom acting as the anchor. This also shorted the M…S bond lengths of the sulfur in question. The M…S bond lengths for these sulfurs were calculated as 3.326 for **4** and 3.319 for **5**.The bond lengths for the non-anchoring sulfurs of the same ligand were 2.357 and 2.351, respectively. The formation of the adduct leads to a loss of electron density and thus leads to a shortening of the M…S bond.

The M…S bond lengths for the biphenyldithiol complexes (**8B**, **9**, **9B**) were comparable to those of the naphthalenedithiol complexes. The monomeric complexes had M…S bond lengths of 2.417 and 2.412 for **8B** and 2.378 and 2.380 Å for **9B**. The teramer-like complex (**9**) also showed slight shortening of the Rh…S bond lengths and can be explained as above. The average Rh…S bond length for 9 was in the region of 2.36 Å.

While for the most part the structural studies of the complexes yielded results that were not unprecedented in terms of bond lengths, it did show some unexpected results for two of the complexes synthesised. The crystal structure of complexes **6** and **7** showed that unlike the

others, these did not dimerise. This is somewhat perplexing as the ligand used in **6** and **7** is the smallest and should therefore inhibit the production of the dimer the least. This result might be explained by one of two observations, or possibly by a combination of both.

It is possible that there is some π-stacking-like interaction between the benzene ring of the ligand and that of the Cp* that inhibits the formation of the dimer. This is shown in the packing diagram in **Figure 2-27**. This shows that the two adjoining structures are perpendicular to each other yet align themselves so that rings meet face-to-face. The centroid to centroid distance is 3.59 Å which is well within the normal π-π interactions limits of 3.3-3.8 Å.

It is also possible that the geometry about the sulfur prevents the formation of the dimer. In the naphthalenedithiol complexes, the sulfur atom has a different orientation to the metal when compared to that of the benzenedithiol complexes (**Figure 2-28**). This leaves the lone pairs of the sulfur in a different orientation and creates steric repulsion between the Cp* and the benzene ring that stops the formation of the dimer.

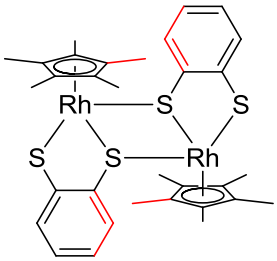

Figure 5-3 Steric Repulsion Inhibiting Dimerisation

6 BIBLIOGRAPHY

[1] P. T. Kissinger, *Biosensors and Bioelectronics*, 2005, **20**, 2512.
[2] L. C. Clark, C. Lyons, *Ann. N. Y. Accad. Sci.*, 1962, **102**, 29.
[3] Y. Nakabayashi, Y. Hirosaki, O. Yamauchi, *Bioelectrochem.*, 2006, **69**, 216.
[4] J. C. Vidal, E. Garcia Ruiz, *Microchim. Acta*, 2003, **143**, 93.
[5] A. Bentley, A. Atkinson, *Toxicol. Vitro*, 2001, **15**, 469.
[6] M. A. Arnold, M. F. Meyerhoff, *CRC Crit. Rev. Anal. Chem.*, 1998, **20**, 149.
[7] B. R. Eggins, *Chemical Sensors and Biosensors*, 2002, Wiley.
[8] A. P. F. Turner, *Science*, 2000, **290**, 1315.
[9] J. Castillo, S. Gaspar, S. Leth, M. Niculescu, A. Mortari, I. Bontidean, V. Soukharev, S. A. Dorneanu, A. D. Ryabov, E. Csoregi, *Sensors and Actuators B*, 2004, **103**, 179.
[10] L. Gorton, A. Lindgren, *Anal. Chim. Acta*, 1999, **400**, 91.
[11] R. M. Marcus, N. Sutin, *Biochim. Biophys. Acta*, 1985, **81**, 265.
[12] W. Schumann, T. J. Ohara, H-L. Schmidt, A. Heller, *J. Am. Chem. Soc.*, 1991, **113**, 1394.
[13] Compendium of Chemical Terminology (Gold Book), 2nd Ed., IUPAC.
[14] H. J. Hecht, H. M. Kalisz, *J. Mol. Biol*., 1993, **229**, 153.
[15] A. E. G. Cass, G. Davis, G. D. Francis, A. O. Hill, W. J. Aston, I. J. Higgins, E. V. Plotkin, L. D. L. Scott, A. P. F. Turner, *Anal. Chem.*, 1984, **56**, 4, 667.
[16] A. P. F. Turner, I. Kraube, G. S. Wilson, *Biosensors. Fundamentals and Applications*, 1987, Oxford University Press.
[17] E. V. Ivanova, V. S. Sergeeva, J.Oni, C. Kurzawa, A. D. Ryabov, W. Schuhmann, *Bioelectrochem.*, 2003, **60**, 65.
[18] R. A. Marcus, *Angew. Chem. Int. Ed.*, 1993, **32**, 8, 1111.
[19] J-D. Qiu, W-M. Zhou, J. Guo, *Anal. Biochem.*, 2009, **385**, 264.
[20] G. Sittampalam, G. S. Wilkinson, *J. Chem. Ed*., 1982, **59**, 70.
[21] D. R. Thevenot, R. Sterberg, P. R. Coulet, J. Laurent, *Anal. Chem*., 1979, **51**, 96.
[22] A. Chaubey, B. D. Maltora, *Biosens. Bioelectron.*, 2002, **17**, 411.
[23] N. G. Wilson, T. McGreedy, G. M. Greenway, *Analyst*., 2000, **125**, 237.
[24] B. Kiu, R. Hu, J. Deng, *Analyst*., 1997, **122**, 821.
[25] A. D. Ryabov, A. Amon, *J. Phys. Chem*., 1995, **99**, 14072.
[26] A. D. Ryabov, V. N. Goral, *J. Biol. Inorg. Chem*., 1997, **2**, 182.
[27] J-R. Mor, R. Guarnaccia, *Anal. Biochem.*, 1977, **79**, 319.
[28] D. L. Williams, A. R. Doig, Jr., A. Korosi, *Anal. Chem.*, 1970, **42**, 118.
[29] a) G. Marko-Varga, R. Appelqvist, L. Gorton, *Anal. Chim. Acta*, 1986, **179**, 371.
b) H. Liu, X. Zhang, J. Wei, X. Wu, D. Qi, Y. Liu, M. Dai, T. Yu, J. Dneg, *Anal. Chim. Acta*, 1996, **329**, 97.
[30] C. Zhang, T. Haruyamba, M. Aizawa, *Anal. Chim. Acta*, 2000, **408**, 225.
[31] a) M. Wang, N. Chamberland, L. Breau, JE. Mosser, R. Humphry-Baker, B. Marsan, S. M. Zakeeruddin, M. Gratzel, *Nature Chem.*, 2010, **2**, 385.
b) H. R. Zare, N. Nasirizadeh, M. Aradakin, *J. Electroanal. Chem.*, 2005, **577**, 25.
[32] E. A. Seddon, K. R. Seddon, *The Chemistry of Ruthenium*, 1984, Elsevier Science.
[33] F. A. Cotton, G. Wilkinson, *Advanced Inorganic Chemistry*, 6th Ed., Wiley-Interscience.
[34] G. Wilkinson, *Comprehensive Coordination Chemistry*, 1987**,** Pergamon.
[35] C. F.J. Barnard, S. C. Bennett, *Platinum Metals Rev.*, 2004, **48**, 4, 157.

[36] J. R. Schoonover, C. A. Bignozzi, T. J. Meyer, *Coord. Chem. Rev*., 1997, **166**, 121.
[37] M. Gratzel, B. O'Regan, *J. Photochem. Photobiol. A*, 2007, **185**, 2, 331.
[38] T. J. Meyer, *Pure Appl. Chem.*, 1990, **62**, 1003.
[39] S. M. Zakeeruddin, D. M. Fraser, M-K. Naseerudium, M. Gratzel, *J. Electroanal. Chem.*, 1992, **337**, 243.
[40] D.M. Frazer, S. M. Zakeeruddin, M. Gratzel, *J. Electroanal. Anal.*, 1993, **359**, 125.
[41] J. G. Vos, J. M. Kelly, Dalton Trans., 2006, 4869.
[42] C. Kaes, A. Katz, M. W. Hosseini, *Chem. Rev.*, 2000, **100**, 3553.
[43] W. B. Heuer, H.-L. Xia, W. Ward, W. H. Pearson, M. A. Siegler, A. A. N. Sarjeant, M. Abrahamsson, G. J. Meyer, *Inorg. Chem.*, 2012, **51**, 3981.
[44] M. D. Ward, F. Barigelletti, *Coord. Chem. Rev.*, 2001, **216-217**, 127.
[45] K. Westerlund, B.W. Berry, H. K. Privett, C. Tommos, *Biochim. Biophys. Acta – Bioenergetics*, 2005, **1707**, 1, 103.
[46] D. Ivnitski, P. Atanassov, B. Branch, C. Apblett, V. Shapovalov, *NATO Science for Peace and Security Series – E: Human and Societal Dynamics*, 2007, Springer.
[47] K. A. Fackelmann, *Sci. News*, 1993, **143**, 388
[48] T. J. Ohara, *Platinum Metals Rev.*, 1995, **39**, 2, 54.
[49] M. S. Vreeke, P. Rocca, A. Heller, *Anal. Chem.*, 1995, **6**, 303.
[50] P. Ugo, L. Moretto, S. Bellomi, V. Menon, C. Martin, *Anal. Chem.*, 1996, **68**, 4160.
[51] S. Rubin, J. T. Chow, J. P. Ferraris, T. A. Zawodzinski, *Langmuir*, 1996, **12**, 2, 363.
[52] I. Willner, A. Riklin, B. Shoham, D. Rivenzon, E. Katz, *Adv. Mater.*, 1993, **12**, 912.
[53] S. Xu, G. Tu, B. Peng, X. Han, *Anal. Chim. Acta*, 2006, **570**, 2, 151.
[54] Y. Degani, A. Heller, *J. Phys. Chem.*, 1987, **91**, 6, 1285.
[55] A. Heller, *Biosensors: A Practical Approach*, 2nd Ed., Oxford University Press.
[56] T. J. Ohara, R. Rajagopalan. A. Heller, *Anal. Chem.*, 1993, **65**, 3512.
[57] A. Heller, B. Feldman, *Acc. Chem. Res.*, 2010, **43**, 7, 963.
[58] F. Mao, N. Mano, A. Heller, *J. Am. Chem. Soc.*, 2003, **125**, 4951.
[59] M. N. Zafar, F. Tasca, S. Boland, M. Kujawa, I. Patel, C. K. Peterbauer, D. Leech, L. Gorton, *Bioelectrochem.*, 2010, **80**, 38.
[60] A. Badura, D. Guschin, B. Esper, T. Kothe, S. Neugebauer, W. Schumann, M. Rogner, *Electroanalysis*, 2008, **20**, 10, 1043.
[61] K. Matsumoto, T. Matsumoto, M. Kawano, *J. Am. Chem. Soc.*, 1996, **118**, 3597
[62] *Encyclopedia of Inorganic Chemistry*, Vol. 7, 1994, Wiley Interscience.
[63] R. Prasad, *Polyhedron*, 1995, **14**, 15-16, 2151.
[64] a) M. A. Haga, E. S. Dodsworth, A. B. P. Lever, *Inorg. Chem.*, 1986, **25**, 447.
b) A. B. P. Lever, P. R. Auburn, E. S. Dodsworth, M. Haga, M. Melnik, W. A Nevin, *J. Am. Chem. Soc.*, 1988, **110**, 8076.
c) H. Masui, P. R. Auburn, A. B. P. Lever, *Inorg. Chem.*, 1991, **30**, 2402.
d) A. B. P Lever, H. Masui; R. A. Metcalfe, D. J. Stufkens, E. S. Dodsworth, P. R. Auburn, *Coord. Chem. Rev.*, 1993, **125**, 317.
e) H. Masui, E. S. Dodsworth, A. B. P. Lever, *Inorg. Chem.*, 1993, **32**, 258.
f) M. Ebadi, A. B. P. Levr, *Inorg. Chem.*, 1999, **38**, 467.
[65] R. A.Begum, A. A. Farah, H. N. Hunter, A. B. P. Lever, *Inorg. Chem.*, 2009, **48**, 2018.
[66] P. J. Vergamini, G. J. Kubas, Prog. *Inorg. Chem.*, 1976, **21**, 261.
[67] S. D. Robertson, A. M. Z Slawin, J. D. Woollins, *Eur. J. Inorg. Chem.*, 2007, 247-253.
[68] C. Janiak, H. Schumann, *Adv. Organomet. Chem.*, 1992, **33**, 291.
[69] M. L. H. Green, *J. Organomet., Chem.*, 1995, **500**, 127.
[70] D. E. Bean, P. W. Fowler, M. J. Morris, *J. Organomet. Chem.*, 2011, **696**, 10, 2093.
[71] T. J. Kealy and P. L. Pauson, *Nature*, 1952, **168**, 1039.
[72] P. L. Pauson, *Quart. Rev., Chem. Soc.*, 1955, **4**, 391.
[73] E. O. Fischer and H. P. Fritz, *Advan. Inorg. Chem. Radiochem.*, 1959, **1**, 55.
[74] G. Wilkinson and F. A. Cotton, *Prog. Inorg. Chem.*, 1959, **1**, 1.
[75] J. Birmingham, *Advan. Organometal. Chem.*, 1964, **2**, 365.
[76] R. B. King and M. B. Bisnette, *J. Organomet. Chem.*, 1967, **8**, 2, 287.
[77] B. L. Hunt, F. M. Lever, *Platinum Metals Rev.*, 1969, **13**, 4, 126.
[78] V. Voorhees, R. Adams, *J. Am. Chem. Soc.*, 1922, **44**, 6, 1397.
[79] J. A. Osborn, F. H. Jardine, J. F. Young, G. Wilkinson, *J. Chem. Soc. A*, 1996, **0**, 1711.

[80] M. Scholl, S. Ding, C. W. Lee, R. H. Grubbs, *Org. Lett.*, 1999, **1**, 6, 953.
[81] D. W. Hart, J. Schwartz, *J. Am. Chem. Soc.*, 1974, **96**, 26, 8115.
[82] H. G. Alt, A. Koppl, *Chem. Revs.*, 2000, **100**, 1205.
[83] W. Kaminsky, A. Laban, *Appl. Catl. A*, 2001, **222**, 47.
[84] C. Dhury, K. Foughy, A. Shanley, *Chem. Eng.*, 1996, **2**, 35.
[85] Market Study: Polypropylene. Ceresana Research.
http://www.ceresana.com/en/market-studies/plastics/polypropylene (12 July 2012)
[86] A. H. Janowicz, R. G. Bergman, *J. Am. Chem. Soc.*, 1982, **104**, 352.
[87] J. K. Hoyano, W. A. G. Graham, *J. Am. Chem. Soc.*, 1982, **104**, 3723.
[88] B.M. Trost, A. C. Gutierrez, R. C. Livingston, *Org. Lett.*, 2009, **11**, 12, 2539
[89] ConQuest, The Cambridge Structural Database
[90] I. Langmuir, *Science*, 1921, **54**, 59.
[91] a) S. D. Robertson, A. M. Z. S. Slawin, J. D. Woollins, *Eur. J. Inorg. Chem.*, 2007, **2**, 247.
b) F. R. Knight, A. L. Fuller, A. M. Z. S. Slawin, J. D. Woollins, *Dalton. Trans.*, 2009, **40**, 8476.
c) F. R. Knight, A. L. Fuller, A. M. Z. S. Slawin, J. D. Woollins, *Polyhedron*, 2010, **29**, 8, 1956.
d) F. R. Knight, A. L. Fuller, M. Buhl, A. M. Z. S. Slawin, J. D. Woollins, *Chem. Eur. J.*, 2010, **16**, 25, 7503.
e) F. R. Knight, A. L. Fuller, M. Buhl, A. M. Z. S. Slawin, J. D. Woollins, *Chem. Eur. J.*, **16**, 25, 7617.
f) F. R. Knight, K.S. Athukorala Arachchige, R. A. M. Randall, Buhl, A. M. Z. S. Slawin, J. D. Woollins, *Dalton Trans.*, 2012, **41**, 11, 3154.
g) P. Kilian, A. M. Z. S. Slawin. J. D. Woollins, *Eur. J. Inorg. Chem.*, 1999, 12, 2327.
h) P. Kilian, A. M. Z. S. Slawin. J. D. Woollins, *Chem. Eur. J.*, 2003, **9**, 1, 215.
i) P. Kilian, A. M. Z. S. Slawin. J. D. Woollins, *J. Chem. Soc. Dalton Trans.*, 2003, **20**, 3876.
j) P. Kilian, A. M. Z. S. Slawin. J. D. Woollins, *Inorg. Chim. Acta*, 2005, 358, 5, 1719.
k) M. R. S. J. Foreman, J Novosad, A. M. Z. S. Slawin, J. D. Woollins, *J. Chem. Soc. Dalton Trans.*, 1997, **8**, 2302.
l) S. M. Aucott, H. L. Milton, A. M. Z. S. Slawin, J. D. Woollins, *Phosphorus, Sulfur Silicon Relat. Elem.*, 2004, **179**, 4-5, 985.
m) S. M. Aucott, S. D. Robertson, H. L. Milton, A. M. Z. S. Slawin, J. D. Woollins, *Chem. Eur. J.*, 2004, **10**, 7, 1666.
n) S. M. Aucott, P. Kilian, H. L. Milton, S. D. Robertson, A. M. Z. S. Slawin, J. D. Woollins, *Inorg. Chem.*, 2005, **44**, 8, 2710.
o) L. K. Aschenbach, F. R. Knight, R. A. M. Randall, D. B. Cordes, A. Baggott, M. Bühl, A. M. Z. S. Slawin, J.D. Woollins, *Dalton Trans.*, 2012, **41**, 11, 3141.
p) A. L. Fuller, F. R. Knight, A. M. Z. S. Slawin, J. D. Woollins, *Eur. J. Inorg,. Chem.*, 2010, 25, 4034.
[92] D. M. Upulani K. Somisara, M. Buhl, T. Lebl, N. V. Richardson, A. M. Z. S. Slawin, J. D. Woollins, P. Kilian, *Chem. Eur. J.*, 2011, **17**, 2666.
[93] The CRC Handbook of Chemistry and Physics, 92nd Ed., CRC Press.
[94] M. J. Baker-Hawkes, E. Billing, H. B. Gray, *J. Am. Chem. Soc.*, 1966, **88**, 4870.
[95] N. Robertson, L. Cronin, *Coord. Chem. Rev.*, 2002, **227**, 93.
[96] M. Nomura, T. Sasao, T. Sugiyama, M. Kajitani, *Inorg. Chim. Acta*, 2010, **363**, 3647
[97] D. Sellmann, M. Geck, F. Knoch, G. Ritter, J. Dengler, *J. Am. Chem. Soc.*, 1991, **113**, 3819.
[98] M. Fourmigue, *Coord. Chem. Rev.*, 1998, **178-180**, 823.
[99] R. Xi, M. Abe, T. Suzuki, T. Nishioka, K. Isobe, *J. Organomet. Chem.*, 1997, **549**, 117.
[100] C. Janiak, *J. Chem. Soc., Dalton Trans.*; 2000, **21**, 3885.
[101] a) W. Schroth, E. Hintzsche, H. Jordan, R. Spitzner, I. Thorndorf, *Tetrahedron*, 1997, **53**, 22, 7509.
b) M. Hamaguchi, T. Misumi, T. Oshima, *Tet. Lett.*, 1998, **39**, 39, 7113.
c) S. Cossu, G. Delogu, O. De Lucchi, D. Fabbri, M. P. Fois, *Synth. Commun.*, 1989, **19**, 20, 3431.
d) T. Fujii, H. Kusanagi, O. Takahashi, E. Horn, N. Furukawa, *Tetrahedron*, 1999, **55**, 5027.
e) B. Dakova, A. Walcarius, L. Lamberts, M. Evers, *Electrochem. Acta*, 2001, **46**, 1259.
[102] S. M. Aucott, P. Kilian, H. L. Milton, S. D. Robertson, A. M. Z. Slawin, J. D. Woollins, *Inorg. Chem.*, 2005,
44, 2719.
[103] S. M. Aucott, P. Kilian, H. L. Milton, S. D. Robertson, A. M. Z. Slawin, J. D. Woollins, *Chem. Eur. J.*, 2006,
12, 895.
[104] K. Yui, Y. Asho, T. Otsubo and F. Ogura, *Chem. Bull. Soc. Jpn.*, 1988, **61**, 953.

[105] C. White, A. Yates, P. M. Maitlis, *Inorg. Synth.*, 1992, **29**, 1161.
[106] A. J. Ashe, III, J. W. Kampf and P. M. Savla, *Heteroatom Chem.*, 1994, **5**, 2, 113.
[107] S. Cossu, G. Delogu, D. Fabbri and P. Maglioli, *Org. Perp. and Proc. Int.*, 1991, **23**, 4, 455.
[108] J. D. Wallis, R. J. C. Easton and J. D. Munitz, *Helv. Chim. Acta*, 1993, **76**, 1141.
[109] J. P. Paris, W. W. Brandt, *J. Am. Chem. Soc.*, 1959, **81**, 5001.
[110] J. N. Demas, A. W. Adamsson, *J. Am. Chem. Soc.*, 1971, **93**, 1800.
[111] T. B. Hadda, H. Le Bozec, *Polyhedron*, 1988, **7**, 7, 575.
[112] K. Kalyanasundaram, *Coord. Chem. Rev.*, 1982, **46**, 159.
[113] A. J. Bard, M. A Fox, *Acc. Chem. Res.*, 1995, **28**, 3, 141.
[114] R. R. Miller, W. W. Brandt, *J. Am. Chem. Soc.*, 1955, **77**, 3178.
[115] M. A. Greany, C. L.Coyle, E. I. Stiefel, *Inorg. Chem.*, 1989, **28**, 912.
[116] K. Tanaka, M. Morimoto, T. Tanaka, *Inorg. Chim. Acta*, 1981, **56**, L61.
[117] Xudong Yu, Hai Lin, Zunsheng Caia, Huakuan Lina, *Tetrahedron Lett.*, 2007, **48**, 8615.
[118] G. Sprintschnik, H. W. Sprintschnik, P. P. Kirsch, D. G. Whitten, *J. Am. Chem. Soc.*, 1977, **99**, 4947.
[119] V. Balzani, L.Moggi, M. F. Manfrim, F. Bolletta, M. Gleria, *Science*, 1975, **189**, 852.
[120] B. O'Regan. M. Gratzel, *Nature*, 1991, **353**, 737.
[121] H. Greischer, M. Michel-Beyerle, E. Rebentrost, H. Tributsch, *Electrochim. Acta*, 1968, **13**, 1509. H. Tributsch, *Photochem. Photobiol.*, 1972, **16**, 261.
[122] M. Gratzel, *J. Photochem.Photobiol C: Photochem. Revs.*, 2003, **4**, 145.
[123] P. Wang, S. M. Zakeeruddin, J. E. Moser, M. K. Nazeeruddin, T. Sekiguchi, M. Gratzel, *Nature Materials*, 2003, **2**, 402.
[124] M. K. Nazeeruddin, I. Kay, A. Rodicio, R. Humphry-Baker, E. Müller, P. Liska, N. Vlachopouloss, M. Grätzel, *J. Am. Chem. Soc.*, 1993, **115**, 6382.
[125] I. Chung, B. Lee, J. He, R. P. H. Chang, M. G. Kanatzidis, *Nature*, 2012, **485**, 486.
[126] A. Yella, H-W. Lee, H. N. Tsao, A. K. Chandiran, M. K. Nazeeruddin, E. W-G. Diau, C-Y. Yeh, S. M. Zakeeruddin, M. Gratzel, *Science*, 2011, **334**, 6056, 629.
[127] K.E. Erkkila, D.T. Odom, J.K. Barton, *Chem. Rev.*, 1999, **99**, 2777.
[128] L-F. Tan, F. Wang, H. Chao, Y-F. Zhou, C. Weng, *J. Inorg. Biochem.*, 2007, **101**, 700.
[129] D. Lawrence Arockiasamy, S. Radhika, R. Parthasarathi, B. U. Nair, *E. J. Med. Chem.*, 2009, **44** 2044.
[130] H. G. M. Edwards, I. R. Lewis, *Inorg. Chim. Acta.*, 1994, 216, 191.
[131] G. Socrates, *Infrared and Raman Characteristic Group Frequencies: Tables and Charts*, 3rd Ed. Wiley.
[132] C. Makedonas, C. A. Mitsopoulou, *Spectrochim. Acta Part A*, 2006, **64**, 918.
[133] A. Juris, V. Balzani, F. Barigelletti, S. Campagna, P. Belser, A. von Zelewsky, *Coord. Chem Rev.*, 1988, **84**, 85.
[134] R. A. Begum, A. A. Farah, H. N. Hunter, A. B. P. Lever, *Inorg. Chem.*, 2009, **48**, 2018.
[135] E. A. Seddon, K. R. Seddon, *The Chemistry of Ruthenium*, **1984**, Elsevier.
[136] D. H. Evans, K. M. O'Connell, R. A. Petersen, M. J. Kelly, *J. Chem. Ed.*, 1983, **60**, 290. P. T. Kissinger, W. R. Heineman, *J. Chem. Ed.*, 1983, **60**, 702.
[137] Southampton Electrochemistry Group, *Instrumental Methods in Electrochemistry*, **2001**, Woodhead Publishing.
[138] D. A. C. Brownson, D. K. Kampouris and C. E. Banks, *Chem. Soc. Rev.*, 2012, **41**, 6944.
[139] B. P. Sullivan, D. J. Salmon, T. J. Meyer, *Inorg. Chem.*, 1978, **17**, 3334.
[140] T. B. Hadda, H. LeBozec, *Polyhedron*, 1988, **7**, 7, 575.
[141] Y. Aso, K. Yui, T. Miyoshi, T. Otsubo, F. Ogura and J. Tanaka, *Chem. Bull. Soc. Jpn.*, 1988, **61**, 2013.
[142] M. Bochman, *Organometallics 2*, OCP, 1999.
[143] C. Janiak, H. Schumann, *Adv. Organomet. Chem.*, 1992, **33**, 291.
[144] F. Hessler, I. Cisarova, D. Sedlak, P. Bartunek, M. Kotora, Chem. Eur. J., 2012, 18, 5515.
[145] R. R. Gagne, C. A. Koval, G. C. Linesky, *Inorg. Chem.*, 1980, **19**, 9, 2854.
[146] N. G. Connelly, W. E. Geiger, *Chem. Rev.*, 1996, **2**, 877.
[147] S. M. Batterjee, M. I. Marzouk, M. E. Aazab, M. A. El-Hashash, *App. Organomet., Chem.*, 2003, **17**, 291.
[148] N. El Murr, J.E. Sheats, W. E. Geiger, J. D. L. Holloway, *Inorg. Chem.*, 1979, **18**, 6, 1443.
[149] O.V. Gusev, L. I. Denisovich, M. G. Peterleitner, A. Z. Rubenzhov, N. A. Unstynyuk, P. M. Maitlis, *J. Organomet. Chem.*, 1993, **452**, 1-2, 219
[150] O.V. Gusev, M. G. Peterleitner, M. A. Ievlev, A. M. Kal'sin, P. V. Petrovskii, L. I. Denisovich, N. A. Ustynyuk, *J. Organomet. Chem.*, 1997, **531**, 1-2, 95.

[151] T.P. Smith, K. S. Kwan, H. Taube, A. Bino, S. Cohen, *Inorg. Chem.*, 1984, **23**, 13, 1943.
[152] J. C. Swarts, A.Nafady, J. H. Roudebush, S. Trupia, W. E. Geiger, *Inorg. Chem.*, 2009, **48**, 2156.
[153] W. E. Geiger, F. Barrière, *Acc. Chem. Res.*, 2010, **43**, 7, 1030.
[154] M. O. Albers, D. J. Robinson, E. Singleton, *Coord. Chem. Rev.*, 1987, **79**, 1.
[155] R. H. Crabtree, *The Organometallic Chemistry of the Transition Metals*, **2001**, Wiley Interscience.
[156] S. Arndt, J. Okuda, *Chem. Rev.*, 2001, **102**, 1953.
[157] S. G. Davies, J. P. McNally, A. J. Smallridge, *Adv. Organomet. Chem.*, 1990, **30**, 1.
[158] K. H. Wedepohl, *Geochim. et Cosmochim. Acta*, 1995, **59**, 7, 1217.
[159] a) C. Bruneau, M. Achard, *Coord. Chem. Rev.*, 2012, **256**, 525.
b) Z-J. Yao, B. Xu, G. Su, G-X. Jin, *J. Organomet. Chem.*, 2012, XXX, 1. *in press*
c) P. Singh, G. Mukherjee, A. K. Singh, *J. Organomet. Chem.*, 2012, XXX, X. *in press*
d) M. Ulaganatha, R. Ramesh, *J. Organomet. Chem.*, 2012, **699**, 5.
e) B. Milde, T. Ruffer, H. Lang, *Inorg. Chim. Acta*, 2012, **387**, 338.
f) M. J. Calhorda, P. J. Costa, K. A. Kirchner, *Inorg. Chim. Acta*, 2011, **374**, 1, 24.
g) A. McGibbon, M. Nieuwenhuyzeni, G. C. Saunders, J. Fluorine Chem., 2011, **132**, 7, 495.
h) G. Albertin, S. Antoniutti, J. Castro, *J. Organomet. Chem.*, 2012, **697**, 6.
i) A. Valente, P. Zink, A. Mortreux, M. Visseaux, P. J. G. Mendes, T. J. L. Silva, M. H. Garcia, *J. Molec. Cat. A: Chemical*, 2011, **346**, 102.
[160] a) J. Freudenreich, J. Furrer, G. Suss-Fink, B. Therrien, *Organomet.*, 2011, **30**, 942.
b) S. Betanzos-Lara, L. Salassa, A. Habtermariam, O. Novakova, A. M. Pizzaro, G. J. Clarkson, B. Liskova, V. Brabec, P. J. Sadler, *Organomet.*, 2012, **31**, 3466.
c) Md. K. Nazeeruddin, S. M. Zakeeruddin, J-J. Lagref, P. Liska, P. Comte, C. Barolo, G. Viscardi, K. Schenk, M. Gratzel, *Coord. Chem. Rev.*, 2004, **248**, 1317.
d) Md. K. Nazeeruddin, C. Klein, P.Liska, M. Gratzel, *Coord. Chem. Rev.*, 2005, **249**, 1460.
e) P. Utaj, F. Lefebvre, *Coord. Chem. Rev.*, 2011, **255**, 1642.
[161] a) J. G. Malecki, *Transition Met. Chem.*, 2010, **35**, 801, and references therein.
b) G. E. Atilla-Gokcumen, L. Di Costnzo, E. Meggers, *J. Biol. Inorg. Chem.*, 2011, **16**, 45.
c) A. M. Pizzaro, A. Habtemariam, P. J. Sadler, *Top. Organomet. Che.*, 2010, **32**, 21.
d) S. H. Van Rijt, A. F. A. Peacock, P. J. Sadler, *Platinum and Other Heavy Metal Compounds in Cancer Chemotherapy*, 2009, **1**, 73, Humana Press.
e) L. Ronconi, P. Sadler, *Coord. Chem. Rev.*, 2007, **251**, 1633.
f) W. H. Ang, A. Casini, G. Sava, P. J. Dyson, *J. Organomet. Chem.*, 2011, **696**, 5, 989.
g) I. Bratsos, E. Mitri, F. Ravalico, E. Zangrando, T. Gianferrara, A. Bergamo, E. Alessio, *Dalton Trans.*, 2012, **41**, 7358.
[162] E. S. Antonarakis, A. Emadi, *Cancer Chemother. Pharmacol.*, 2010, **66**, 1.
[163] G. Socrates, *Infrared and Raman Characteristic Group Frequencies: Tables and Charts*, 3rd Ed. Wiley.
[164] C. Makedonas, C. A. Mitsopoulou, *Spectrochim. Acta Part A*, 2006, **64**, 918.
[165] A. Horning, U. Englert, U. Kolle, *J. Organomet. Chem.*, 1994, **464**, C25.
[166] N. Oshima, H. Suzuki and Y. Moro-Oka, *Chem. Lett.*, 1984, 1161.

7 CRYSTAL STRUCTURE APPENDIX

7.1 EXPERIMENTAL DETAILS 4

A. Crystal Data

Empirical Formula	$C_{20}H_{21}IrS_2$
Formula Weight	517.73
Crystal Color, Habit	orange, prism
Crystal Dimensions	0.120 X 0.120 X 0.120 mm
Crystal System	monoclinic
Lattice Type	Primitive
Lattice Parameters	a = 9.823(3) Å b = 16.203(5) Å c = 10.859(3) Å β = 90.467(8) ^{o} V = 1728.3(9) Å^3
Space Group	$P2_1/n$ (#14)
Z value	4
D_{calc}	1.990 g/cm^3
F_{000}	1000.00
μ(MoKα)	79.847 cm^{-1}

B. Intensity Measurements

Diffractometer	Mercury70
Radiation	MoKα (λ = 0.71075 Å)
Temperature	-180.0^{o}C
Detector Aperture	70 x 70 mm
ω oscillation Range	0.0 - 0.0^o
Exposure Rate	0.0 sec./^{o}
Detector Swing Angle	0.00^o
Detector Position	0.00 mm
Pixel Size	0.068 mm
$2\theta_{max}$	50.7^o
No. of Reflections Measured	Total: 10499 Unique: 3031 (R_{int} = 0.0941)
Corrections	Lorentz-polarization

C. Structure Solution and Refinement

Structure Solution	Direct Methods
Refinement	Full-matrix least-squares on F^2
Function Minimized	Σ w (Fo^2 - Fc^2)^2

Least Squares Weights	$w = 1/ [\sigma^2(Fo^2) + (0.0575 \cdot P)^2 + 1.0012 \cdot P]$ where $P = (Max(Fo^2,0) + 2Fc^2)/3$
$2\theta_{max}$ cutoff	50.0^o
Anomalous Dispersion	All non-hydrogen atoms
No. Observations (All reflections)	3031
No. Variables	213
Reflection/Parameter Ratio	14.23
Residuals: R1 (I>2.00σ(I))	0.0446
Residuals: R (All reflections)	0.0546
Residuals: wR2 (All reflections)	0.1215
Goodness of Fit Indicator	1.082
Max Shift/Error in Final Cycle	0.005
Maximum peak in Final Diff. Map	$2.13\ e^-/Å^3$
Minimum peak in Final Diff. Map	$-1.61\ e^-/Å^3$

7.2 EXPERIMENTAL DETAILS 4B

A. Crystal Data

Empirical Formula	$C_{26}H_{36}IrPS_2$
Formula Weight	635.88
Crystal Color, Habit	yellow, prism
Crystal Dimensions	0.150 X 0.030 X 0.030 mm
Crystal System	monoclinic
Lattice Type	Primitive
Lattice Parameters	a = 8.140(3) Å b = 15.563(4) Å c = 19.815(6) Å β = 98.175(7) ^{o} V = 2484.6(11) Å^3
Space Group	$P2_1/n$ (#14)
Z value	4
D_{calc}	1.700 g/cm^3
F_{000}	1264.00
μ(MoKα)	56.328 cm^{-1}

B. Intensity Measurements

Diffractometer	Mercury70
Radiation	MoKα (λ = 0.71075 Å)
Voltage, Current	50kV, 16mA
Temperature	0.0^{o}C
Detector Aperture	70 x 70 mm
Detector Position	0.00 mm
Pixel Size	0.068 mm
$2\theta_{max}$	50.7^o
No. of Reflections Measured	Total: 14915 Unique: 4478 (R_{int} = 0.0946)
Corrections	Lorentz-polarization Absorption (trans. factors: 0.412 - 0.845)

C. Structure Solution and Refinement

Structure Solution	Direct Methods
Refinement	Full-matrix least-squares on F^2
Function Minimized	Σ w (Fo^2 - Fc^2)^2
Least Squares Weights	w = 1/ [σ^2(Fo^2) + (0.1961 · P)^2 + 8.2456 · P] where P = (Max(Fo^2,0) + 2Fc^2)/3
$2\theta_{max}$ cutoff	50.7^o
Anomalous Dispersion	All non-hydrogen atoms
No. Observations (All reflections)	4478
No. Variables	271
Reflection/Parameter Ratio	16.52

Residuals: R1 (I>2.00σ(I))	0.0703
Residuals: R (All reflections)	0.1222
Residuals: wR2 (All reflections)	0.2870
Goodness of Fit Indicator	1.031
Max Shift/Error in Final Cycle	0.046
Maximum peak in Final Diff. Map	5.73 $e^-/Å^3$
Minimum peak in Final Diff. Map	-6.26 $e^-/Å^3$

7.3 EXPERIMENTAL DETAILS FOR 5

A. Crystal Data

Empirical Formula	$RhS_2C_{20}H_{21}$
Formula Weight	428.41
Crystal Color, Habit	orange, prism
Crystal Dimensions	0.15 X 0.09 X 0.02 mm
Crystal System	monoclinic
Lattice Type	Primitive
Lattice Parameters	a = 9.9532(19) Å b = 16.363(3) Å c = 10.855(2) Å β = 90.724(6) ^{o} V = 1767.7(6) Å^3
Space Group	$P2_1/n$ (#14)
Z value	4
D_{calc}	1.610 g/cm^3
F_{000}	872.00
μ(MoKα)	11.965 cm^{-1}

B. Intensity Measurements

Diffractometer	Rigaku Mercury275R CCD (SCX mini)
Radiation	MoKα (λ = 0.71075 Å) graphite monochromated
Voltage, Current	50kV, 40mA
Temperature	-148.0^{o}C
Detector Aperture	75 mm (diameter)
Data Images	540 exposures
ω oscillation Range (χ=54.0, ϕ=0.0)	-120.0 - 60.0^o
Exposure Rate	40.0 sec./^{o}
Detector Swing Angle	-30.10^o
ω oscillation Range (χ=54.0, ϕ=120.0)	-120.0 - 60.0^o
Exposure Rate	40.0 sec./^{o}
Detector Swing Angle	-30.10^o
ω oscillation Range (χ=54.0, ϕ=240.0)	-120.0 - 60.0^o
Exposure Rate	40.0 sec./^{o}
Detector Swing Angle	-30.10^o
Detector Position	50.00 mm
Pixel Size	0.146 mm
$2\theta_{max}$	54.9^o
No. of Reflections Measured	Total: 14831 Unique: 3998 (R_{int} = 0.2075)
Corrections	Lorentz-polarization Absorption (trans. factors: 0.670 - 0.976)

C. Structure Solution and Refinement

Structure Solution	Direct Methods
Refinement	Full-matrix least-squares on F^2
Function Minimized	Σ w $(Fo^2 - Fc^2)^2$
Least Squares Weights	$w = 1/ [\sigma^2(Fo^2) + (0.0847 \cdot P)^2 + 11.8898 \cdot P]$ where $P = (Max(Fo^2,0) + 2Fc^2)/3$
$2\theta_{max}$ cutoff	54.9^o
Anomalous Dispersion	All non-hydrogen atoms
No. Observations (All reflections)	3998
No. Variables	208
Reflection/Parameter Ratio	19.22
Residuals: R1 (I>2.00σ(I))	0.0820
Residuals: R (All reflections)	0.1607
Residuals: wR2 (All reflections)	0.2026
Goodness of Fit Indicator	0.923
Max Shift/Error in Final Cycle	0.000
Maximum peak in Final Diff. Map	0.78 $e^-/Å^3$
Minimum peak in Final Diff. Map	-0.78 $e^-/Å^3$

7.4 EXPERIMENTAL DETAILS 5B

A. Crystal Data

Empirical Formula	$C_{26}H_{36}PRhS_2$
Formula Weight	546.57
Crystal Color, Habit	orange, prism
Crystal Dimensions	0.100 X 0.030 X 0.030 mm
Crystal System	monoclinic
Lattice Type	Primitive
Lattice Parameters	a = 8. 143(4) Å b = 15. 485(8) Å c = 20.07(1) Å β = 98.27(2) ^{o} V = 2504 (2) Å^3
Space Group	$P2_1/n$ (#14)
Z value	4
D_{calc}	1.449 g/cm^3
F_{000}	1136.00
μ(MoKα)	9.225 cm^{-1}

B. Intensity Measurements

Diffractometer	Mercury70
Radiation	MoKα (λ = 0.71075 Å)
Voltage, Current	50kV, 16mA
Temperature	-180.0^{o}C
Detector Aperture	69 x 69 mm
Data Images	278 exposures
ω oscillation Range (χ=0.0, ϕ=0.0)	0.0 – 180.0^o
Exposure Rate	5.0 sec./^{o}
Detector Swing Angle	-10.00^o
Detector Position	40.00 mm
Pixel Size	0.136 mm
$2\theta_{max}$	50.7^o
No. of Reflections Measured	Total: 16013 Unique: 4521 (R_{int} = 0.0877)
Corrections	Lorentz-polarization Absorption (trans. factors: 0.484 - 0.973)

C. Structure Solution and Refinement

Structure Solution	Direct Methods
Refinement	Full-matrix least-squares on F^2
Function Minimized	Σ w (Fo^2 - Fc^2)^2
Least Squares Weights	w = 1/ [$\sigma^2(Fo^2)$ + (0.0838 · P)^2 + 22.2564 · P] where P = (Max(Fo^2,0) + 2Fc^2)/3

$2\theta_{max}$ cutoff	50.7^{o}
Anomalous Dispersion	All non-hydrogen atoms
No. Observations (All reflections)	4521
No. Variables	271
Reflection/Parameter Ratio	16.68
Residuals: R1 (I>2.00σ(I))	0.0400
Residuals: R (All reflections)	0.0572
Residuals: wR2 (All reflections)	0.0885
Goodness of Fit Indicator	1.002
Max Shift/Error in Final Cycle	0.002
Maximum peak in Final Diff. Map	0.56 $e^{-}/Å^{3}$
Minimum peak in Final Diff. Map	-0.51 $e^{-}/Å^{3}$

7.5 EXPERIMENTAL DETAILS FOR 5NS

A. Crystal Data

Empirical Formula	$RhSC_{20}H_{23}NCl$
Formula Weight	447.83
Crystal Color, Habit	orange, prism
Crystal Dimensions	0.05 X 0.05 X 0.02 mm
Crystal System	monoclinic
Lattice Type	Primitive
Lattice Parameters	a = 8.3719(12) Å b = 15.455(2) Å c = 14.527(2) Å β = 102.254(7) ^{o} V = 1836.8(5) $Å^3$
Space Group	$P2_1/c$ (#14)
Z value	4
D_{calc}	1.619 g/cm^3
F_{000}	912.00
μ(MoKα)	11.877 cm^{-1}

B. Intensity Measurements

Diffractometer	Rigaku Mercury275R CCD (SCX mini)
Radiation	MoKα (λ = 0.71075 Å) graphite monochromated
Voltage, Current	50kV, 40mA
Temperature	-100.0^{o}C
Detector Aperture	75 mm (diameter)
Data Images	540 exposures
ω oscillation Range (χ=54.0, ϕ=0.0)	-120.0 - 60.0^o
Exposure Rate	40.0 sec./^{o}
Detector Swing Angle	-30.10^o
ω oscillation Range (χ=54.0, ϕ=120.0)	-120.0 - 60.0^o
Exposure Rate	40.0 sec./^{o}
Detector Swing Angle	-30.10^o
ω oscillation Range (χ=54.0, ϕ=240.0)	-120.0 - 60.0^o
Exposure Rate	40.0 sec./^{o}
Detector Swing Angle	-30.10^o
Detector Position	50.00 mm
Pixel Size	0.146 mm
$2\theta_{max}$	55.0^o
No. of Reflections Measured	Total: 15124 Unique: 3215 (R_{int} = 0.1777)
Corrections	Lorentz-polarization Absorption (trans. factors: 0.729 - 0.977)

C. Structure Solution and Refinement

Structure Solution	Direct Methods
Refinement	Full-matrix least-squares on F^2
Function Minimized	Σ w $(Fo^2 - Fc^2)^2$
Least Squares Weights	$w = 1/ [\sigma^2(Fo^2) + (0.0423 \cdot P)^2 + 0.5740 \cdot P]$ where $P = (Max(Fo^2,0) + 2Fc^2)/3$
$2\theta_{max}$ cutoff	50.0^o
Anomalous Dispersion	All non-hydrogen atoms
No. Observations (All reflections)	3215
No. Variables	217
Reflection/Parameter Ratio	14.82
Residuals: R1 (I>2.00σ(I))	0.0760
Residuals: R (All reflections)	0.1321
Residuals: wR2 (All reflections)	0.1392
Goodness of Fit Indicator	1.109
Max Shift/Error in Final Cycle	0.001
Maximum peak in Final Diff. Map	0.72 $e^-/Å^3$
Minimum peak in Final Diff. Map	-0.68 $e^-/Å^3$

7.6 EXPERIMENTAL DETAILS FOR 6

A. Crystal Data

Empirical Formula	$C_{16}H_{19}IrS_2$
Formula Weight	467.67
Crystal Color, Habit	orange, platelet
Crystal Dimensions	0.15 X 0.10 X 0.02 mm
Crystal System	monoclinic
Lattice Type	Primitive
Lattice Parameters	a = 8.37(2) Å b = 13.82(4) Å c = 13.72(4) Å β = 91.52(4) ^{o} V = 1588(8) Å^3
Space Group	$P2_1/n$ (#14)
Z value	4
D_{calc}	1.956 g/cm^3
F_{000}	896.00
μ(MoKα)	86.802 cm^{-1}

B. Intensity Measurements

Diffractometer	Rigaku Mercury275R CCD (SCX mini)
Radiation	MoKα (λ = 0.71075 Å)
Voltage, Current	50kV, 40mA
Temperature	-148.0^{o}C
Detector Aperture	75 mm (diameter)
ω oscillation Range (χ=0.0, ϕ=0.0)	1.0 - 0.0^o
Exposure Rate	0.0 sec./^{o}
Detector Swing Angle	0.00^o
Detector Position	0.00 mm
Pixel Size	0.073 mm
$2\theta_{max}$	50.7^o
No. of Reflections Measured	Total: 13685 Unique: 2884 (R_{int} = 0.2893)
Corrections	Lorentz-polarization Absorption (trans. factors: 0.387 - 0.841)

C. Structure Solution and Refinement

Structure Solution	Direct Methods
Refinement	Full-matrix least-squares on F^2
Function Minimized	Σ w (Fo^2 - Fc^2)^2
Least Squares Weights	w = 1/ [σ^2(Fo^2) + (0.0309 · P)^2 + 0.0000 · P] where P = (Max(Fo^2,0) + 2Fc^2)/3
$2\theta_{max}$ cutoff	50.7^o
Anomalous Dispersion	All non-hydrogen atoms

No. Observations (All reflections)	2884
No. Variables	172
Reflection/Parameter Ratio	16.77
Residuals: R1 (I>2.00σ(I))	0.0908
Residuals: R (All reflections)	0.1875
Residuals: wR2 (All reflections)	0.1957
Goodness of Fit Indicator	1.024
Max Shift/Error in Final Cycle	0.000
Maximum peak in Final Diff. Map	2.34 $e^-/Å^3$
Minimum peak in Final Diff. Map	-1.63 $e^-/Å^3$

7.7 EXPERIMENTAL DETAILS FOR 7

A. Crystal Data

Empirical Formula	$C_{16}H_{19}RhS_2$
Formula Weight	378.35
Crystal Color, Habit	blue, platelet
Crystal Dimensions	0.15 X 0.15 X 0.02 mm
Crystal System	monoclinic
Lattice Type	Primitive
Lattice Parameters	a = 8.325(4) Å b = 13.834(7) Å c = 13.791(7) Å β = 90.0000 ^{o} V = 1588.3(14) Å^3
Space Group	$P2_1/n$ (#14)
Z value	4
D_{calc}	1.582 g/cm^3
F_{000}	768.00
μ(MoKα)	13.198 cm^{-1}

B. Intensity Measurements

Diffractometer	Rigaku Mercury275R CCD (SCX mini)
Radiation	MoKα (λ = 0.71075 Å) graphite monochromated
Voltage, Current	50kV, 40mA
Temperature	-148.0^{o}C
Detector Aperture	75 mm (diameter)
Data Images	540 exposures
ω oscillation Range (χ=54.0, ϕ=0.0)	-120.0 - 60.0^o
Exposure Rate	60.0 sec./^{o}
Detector Swing Angle	-30.10^o
ω oscillation Range (χ=54.0, ϕ=120.0)	-120.0 - 60.0^o
Exposure Rate	60.0 sec./^{o}
Detector Swing Angle	-30.10^o
ω oscillation Range (χ=54.0, ϕ=240.0)	-120.0 - 60.0^o
Exposure Rate	60.0 sec./^{o}
Detector Swing Angle	-30.10^o
Detector Position	50.00 mm
Pixel Size	0.146 mm
$2\theta_{max}$	55.0^o
No. of Reflections Measured	Total: 11304 Unique: 2790 (R_{int} = 0.2810)
Corrections	Lorentz-polarization Absorption (trans. factors: 0.614 - 0.974)

C. Structure Solution and Refinement

Structure Solution	Direct Methods
Refinement	Full-matrix least-squares on F^2
Function Minimized	Σ w $(Fo^2 - Fc^2)^2$
Least Squares Weights	$w = 1/ [\sigma^2(Fo^2) + (0.1612 \cdot P)^2 + 5.1891 \cdot P]$ where $P = (Max(Fo^2,0) + 2Fc^2)/3$
$2\theta_{max}$ cutoff	50.0^o
Anomalous Dispersion	All non-hydrogen atoms
No. Observations (All reflections)	2790
No. Variables	172
Reflection/Parameter Ratio	16.22
Residuals: R1 (I>2.00σ(I))	0.1441
Residuals: R (All reflections)	0.2459
Residuals: wR2 (All reflections)	0.3690
Goodness of Fit Indicator	1.106
Max Shift/Error in Final Cycle	0.000
Maximum peak in Final Diff. Map	3.90 $e^-/Å^3$
Minimum peak in Final Diff. Map	-0.93 $e^-/Å^3$

7.8 EXPERIMENTAL DETAILS FOR 8B

A. Crystal Data

Empirical Formula	$C_{28}H_{38}IrPS_2$
Formula Weight	661.92
Crystal Color, Habit	orange, prism
Crystal Dimensions	0.14 X 0.11 X 0.06 mm
Crystal System	monoclinic
Lattice Type	Primitive
Lattice Parameters	a = 10.688(19) Å b = 19.57(3) Å c = 13.16(2) Å β = 95.43(2) ^{o} V = 2740(8) Å^3
Space Group	$P2_1/n$ (#14)
Z value	4
D_{calc}	1.604 g/cm^3
F_{000}	1320.00
μ(MoKα)	51.105 cm^{-1}

B. Intensity Measurements

Diffractometer	Rigaku Mercury275R CCD (SCX mini)
Radiation	MoKα (λ = 0.71075 Å)
Voltage, Current	50kV, 40mA
Temperature	-148.0^{o}C
Detector Aperture	75 mm (diameter)
ω oscillation Range (χ=0.0, ϕ=0.0)	1.0 - 0.0^o
Exposure Rate	0.0 sec./^{o}
Detector Swing Angle	0.00^o
Detector Position	0.00 mm
Pixel Size	0.073 mm
$2\theta_{max}$	51.4^o
No. of Reflections Measured	Total: 23187 Unique: 4823 (R_{int} = 0.2243)
Corrections	Lorentz-polarization

C. Structure Solution and Refinement

Structure Solution	Direct Methods
Refinement	Full-matrix least-squares on F^2
Function Minimized	Σ w (Fo^2 - Fc^2)^2
Least Squares Weights	w = 1/ [σ^2(Fo^2) + (0.0264 · P)^2 + 18.1585 · P] where P = (Max(Fo^2,0) + 2Fc^2)/3
$2\theta_{max}$ cutoff	50.0^o
Anomalous Dispersion	All non-hydrogen atoms
No. Observations (All reflections)	4823
No. Variables	289

Reflection/Parameter Ratio	16.69
Residuals: R1 (I>2.00σ(I))	0.0895
Residuals: R (All reflections)	0.1221
Residuals: wR2 (All reflections)	0.2076
Goodness of Fit Indicator	1.164
Max Shift/Error in Final Cycle	0.000
Maximum peak in Final Diff. Map	2.92 $e^-/Å^3$
Minimum peak in Final Diff. Map	-1.70 $e^-/Å^3$

7.9 EXPERIMENTAL DETAILS FOR 9

A. Crystal Data

Empirical Formula	$C_{76}H_{84}S_6Rh_4O$
Formula Weight	1617.48
Crystal Color, Habit	orange, prism
Crystal Dimensions	0.10 X 0.03 X 0.03 mm
Crystal System	monoclinic
Lattice Type	Primitive
No. of Reflections Used for Unit Cell Determination (2θ range)	50748 (6.2 - 50.8^o)
Omega Scan Peak Width at Half-height	0.00^o
Lattice Parameters	a = 21.7232(7) Å b = 15.5777(5) Å c = 24.8693(17) Å β = 102.424(7) ^{o} V = 8218.6(7) Å^3
Space Group	$P2_1/n$ (#14)
Z value	6
D_{calc}	1.961 g/cm^3
F_{000}	4944.00
μ(MoKα)	14.654 cm^{-1}

B. Intensity Measurements

Diffractometer	Rigaku Saturn70 CCD
Radiation	MoKα (λ = 0.71075 Å)
Take-off Angle	2.8^o
Detector Aperture	2.0 - 2.5 mm horizontal 2.0 mm vertical
Crystal to Detector Distance	21 mm
Voltage, Current	50kV, 16mA
Temperature	-180.0^{o}C
Scan Type	ω
Scan Rate	0.0^o/min (in ω) (up to 0 scans)
Scan Width	(0.00 + 0.00 tan θ)^o
$2\theta_{max}$	50.7^o
No. of Reflections Measured	Total: 81027 Unique: 15009 (R_{int} = 0.0892)
Corrections	Lorentz-polarization Absorption (trans. factors: 0.788 - 0.957)

C. Structure Solution and Refinement

Structure Solution	Direct Methods
Refinement	Full-matrix least-squares on F^2
Function Minimized	Σ w (Fo^2 - Fc^2)^2

Least Squares Weights	$w = 1/ [\sigma^2(Fo^2) + (0.1498 \cdot P)^2 + 98.0757 \cdot P]$ where $P = (Max(Fo^2,0) + 2Fc^2)/3$
$2\theta_{max}$ cutoff	50.7^o
Anomalous Dispersion	All non-hydrogen atoms
No. Observations (All reflections)	15009
No. Variables	811
Reflection/Parameter Ratio	18.51
Residuals: R1 ($I>2.00\sigma(I)$)	0.0878
Residuals: R (All reflections)	0.1251
Residuals: wR2 (All reflections)	0.2788
Goodness of Fit Indicator	1.033
Max Shift/Error in Final Cycle	0.004
Maximum peak in Final Diff. Map	3.30 $e^-/Å^3$
Minimum peak in Final Diff. Map	-0.74 $e^-/Å^3$

7.10 EXPERIMENTAL DETAILS 9B

A. Crystal Data

Empirical Formula	$RhS_2PC_{28}H_{38}$
Formula Weight	572.61
Crystal Color, Habit	orange, chip
Crystal Dimensions	0.12 X 0.11 X 0.07mm
Crystal System	monoclinic
Lattice Type	Primitive
Lattice Parameters	a = 10.5523(15) Å b = 19. 412(3) Å c = 13.0520(19) Å β = 95.555(7) ^{o} V = 2661.0(7) Å^3
Space Group	$P2_1/n$ (#14)
Z value	1
D_{calc}	0.357 g/cm^3
F_{000}	298.00
μ(MoKα)	2.180 cm^{-1}

B. Intensity Measurements

Diffractometer	Rigaku Mercury275R CCD (SCX mini)
Radiation	MoKα (λ = 0.71075 Å)
Voltage, Current	50kV, 40mA
Temperature	-148.0^{o}C
Detector Aperture	75 mm (diameter)
ω oscillation Range (χ=54.0, ϕ=0.0)	-120.0 - 60.0^o
Exposure Rate	50.0 sec./^{o}
Detector Swing Angle	30.10^o
Detector Position	50.00 mm
Pixel Size	0.146 mm
$2\theta_{max}$	55.0^o
No. of Reflections Measured	Total: 26677 Unique: 6094 (R_{int} = 0. 1828)
Corrections	Lorentz-polarization Absorption (trans. factors: 0.745 - 0.984)

C. Structure Solution and Refinement

Structure Solution	Direct Methods
Refinement	Full-matrix least-squares on F^2
Function Minimized	Σ w (Fo^2 - Fc^2)^2
Least Squares Weights	w = 1/ [σ^2(Fo^2) + (0.0698· P)^2 + 13.7398· P] where P = (Max(Fo^2,0) + 2Fc^2)/3
$2\theta_{max}$ cutoff	55.0^o
Anomalous Dispersion	All non-hydrogen atoms

No. Observations (All reflections)	6094
No. Variables	297
Reflection/Parameter Ratio	20.52
Residuals: R1 (I>2.00σ(I))	0.0756
Residuals: R (All reflections)	0.1532
Residuals: wR2 (All reflections)	0.1734
Goodness of Fit Indicator	0.921
Max Shift/Error in Final Cycle	0.001
Maximum peak in Final Diff. Map	1.10 $e^-/Å^3$
Minimum peak in Final Diff. Map	-0.63 $e^-/Å^3$